UNIVERSITY OF TECHNOLOGY SYDNEY

MECHANISTIC STUDY OF ANTIBIOTICS AND ENDOCRINE DISRUPTORS REMOVAL BY WOOD-DERIVED BIOCHAR, FUNCTIONALIZED BIOCHAR AND BIOCHAR COMPOSITE

By
MOHAMMAD BOSHIR AHMED

A Dissertation
Submitted in Fulfilment for the Degree of
DOCTOR of PHILOSOPHY
in
Environmental Engineering

University of Technology Sydney
New South Wales, Australia

June 2018

CERTIFICATE OF ORIGINAL AUTHORSHIP

I, MOHAMMAD BOSHIR AHMED, certify that my research work in this thesis has not previously been submitted anywhere for a degree nor has it been submitted as part of requirements for a degree except as part of the collaborative doctoral degree and/or fully acknowledged within the text.

I also certify that the thesis has thoroughly been written by me. Any kind of help that I have received during my research activities and the preparation of the thesis itself has been acknowledged. Furthermore, I also certify that all information sources and literatures used are indicated in the thesis in the reference section.

Production Note:
Signature removed prior to publication.

SIGNATURE OF STUDENT:
MOHAMMAD BOSHIR AHMED

ACKNOWLEDGMENT

First of all, I owe my deepest gratitude to my principal supervisor, Prof. JOHN L. ZHOU for his continuous supports, guidance, time, patience and inspiration throughout my PhD study. I have learnt a lot from his ideas, critical review of my study plans and papers, knowledge and motivation that encouraged me to overcome many difficulties in the research as well as other aspects of life to achieve this milestone. I also would like to thank my supervisory committee, Prof. HUU HAO NGO for his mentor supports, papers revising and useful comments on this thesis. I would also like to give special thanks to Dr. WENSHAN GUO and Dr. ABU HASAN JOHIR for their contribution for papers revising and useful suggestions on this dissertation.

I gratefully acknowledge the UNIVERSITY OF TECHNOLOGY SYDNEY (UTS) for awarding me the "INTERNATIONAL RESEARCH SCHOLARSHIP" and "FACULTY OF ENGINEERING AND INFORMATION TECHNOLOGY" Scholarships. The financial support from "CENTRE FOR TECHNOLOGY IN WATER AND WASTEWATER" and "BLUE SKY SCHOLARSHIP" is also grateful.

The technical supports and guidance from Dr. ABU HASAN JOHIR, the environmental engineering laboratories, UTS are greatly appreciated. Also, I would like to thank RAMI HADDAD, the manager in civil and environmental engineering laboratories, UTS. Many thanks go to KATIE, HERBERT, MARK and other staff at Microstructure Analysis Unit, UTS. I would like to give special thanks to RONALD SHIMMON, for providing me training to run ^{1}H NMR in science lab, UTS. I would like to express my appreciation to Kireesan for his technical assistances and useful discussion. I am thankful to my colleagues Ali, Atique, Mahmud, Nawshad Akther, Ben, Lijuan, Dorji, and Nireen for their supports and contributions.

Finally, I am hugely indebted to all my family, colleagues and friends for their emotional supports, unconditional love and guidance.

DEDICATION

This thesis is deeply dedicated to the following people:

To my respective parents, LATE MOHAMMAD NORUL ISLAM & REHENA BEGUM

For their sacrifices, endless love, hard work and inspiration

To my wonderful wife, JASMIN KHTUN

For her constant love, supports and caring

To my lovely uncle and aunt, MD. BELAYET HOSSAIN & SALMA BEGUM

For giving me inspiration, help and hope.

CONTENTS

TABLE OF CONTENTS

MECHANISTIC STUDY OF ANTIBIOTICS AND ENDOCRINE DISRUPTORS REMOVAL BY WOOD-DERIVED BIOCHAR, FUNCTIONALIZED BIOCHAR AND BIOCHAR COMPOSITE i

CERTIFICATE OF ORIGINAL AUTHORSHIP ii

ACKNOWLEDGMENT iii

DEDICATION iv

CONTENTS 1

NOMENCLATURES 6

LIST OF FIGURES 11

LIST OF TABLES 11

LIST OF PUBLICATIONS 26

AWARDS 30

ABSTRACT 31

CHAPTER ONE: INTRODUCTION 37

1.1. Background 37

1.1.1. Adverse Effects of Antibiotic Residues 37

1.1.2. Adverse Effects of EDCs 38

1.1.3. Removal Technologies of Antibiotics and EDCs 39

1.1.4. Removal of Antibiotics and EDCs by Biochar, Functionalized Biochar and Their Composite 40

1.2. Research Hypothesis 41

1.3. Objectives 42

1.4. Research significance 43

1.5. Thesis Outline 43

CHAPTER TWO: LITERATURE REVIEW 46

2.1. Introduction 46

2.2. Antibiotics and EDCs in the Aquatic Environment 47

2.2.1. Definition, Characteristics, Source, Occurrence and Pollution of Antibiotics in the Aquatic Environment 47

2.2.2. Definition, Characteristics, Source, Occurrences and Pollution of EDCs in the Aquatic Environment 53

2.2.3. Relevant Regulations for Antibiotics and EDCs Residues 59

2.3. Antibiotics and EDCs Removal Technologies 60

2.3.1. Biological Treatment Technologies 61

2.3.2. Chemical Treatment Technologies 78

2.3.3. Physical Treatment Technologies 94

2.3.4. Hybrid Technologies 97

2.4. Biochar and Functionalized Biochar 100

2.5. Adsorption of Antibiotics and EDCs Using Biochar and fBC 102

2.6. Sorption and Reduction of Chloramphenicol Antibiotics Using ZVI and Its Composites 103

2.7. Conclusions and Research Gaps 104

CHAPTER THREE: MATERIALS AND METHODS 108

3.1. Materials 108

3.1.1. Experimental Materials 108

3.1.2. Woody Biomass Collection and Processing 108

3.1.4. Stock Solutions of Antibiotics and EDCs 109

3.1.5. Furnace and Reactor for Biochar & Functionalized Biochar Preparation 109

3.1.6. Synthetic Wastewater, MBR Sewage Effluent and Lake Water 109

3.2. Methods 110

3.2.1. *Preparation and Functionalization of Adsorbents, Synthesis of ZVI & Preparation of Composite* 110

3.2.2. Characterization Methods 112

3.2.3. Batch Adsorption Experiments for Removing Antibiotics and EDCs 114

3.2.4. The Analytical Method of the Antibiotic and EDCs Concentrations 115

CHAPTER FOUR: ANTIBIOTICS REMOVAL FROM WATER AND WASTEWATER: MECHANISMS AND APPLICATIONS 118

4.1. Single and Competitive Sorption Properties and Mechanism of Functionalized Biochar for Removing Sulfonamide Antibiotics from Water 118

4.1.1. Introduction 118

4.1.2. Experimental Section 120

4.1.3. Results and Discussion 125

4.1.4. Concluding Remarks 150

4.2. Competitive Sorption Affinity of Sulfonamides and Chloramphenicol Antibiotics toward Functionalized Biochar for Water and Wastewater Treatment 151

4.2.1. Introduction 151
4.2.2. Materials and Methods 152
4.2.3. Results and Discussion 155
4.2.4. Concluding Remarks 167
4.3. Chloramphenicol Interaction with Functionalized Biochar in Water: Sorptive Mechanism, Molecular Imprinting Effect and Repeatable Applications 168
4.3.1. Introduction 168
4.3.2. Materials and Methods 169
4.3.3. Results and Discussion 174
4.3.4. Concluding Remarks 193
4.4. Nano-Fe^0 immobilized onto Functionalized Biochar Gaining Excellent Stability During Sorption and Reduction of Chloramphenicol via Transforming to Reusable Magnetic Composite 195
4.4.1. Introduction 195
4.4.2. Materials and Methods 197
4.4.3. Results and Discussion 200
4.4.4. Concluding Remarks 222

CHAPTER FIVE: ENDOCRINE DISRUPTORS REMOVAL BY FUNCTIONALIZED BIOCHAR: MECHANISMS AND APPLICATIONS IN WASTEWATER TREATMENT 223
5.1. Sorptive Removal of Phenolic Endocrine Disruptors by Functionalized Biochar: Competitive Interaction Mechanism, Removal Efficacy and Application in Wastewater 224
5.1.1. Introduction 224
5.1.2. Experimental 225
5.1.3. Results and Discussion 230
5.1.4. Concluding Remarks 251

5.2. Sorption of Hydrophobic Organic Contaminants on Functionalized Biochar: Protagonist Role of π-π Electron-Donor-Acceptor Interactions and Hydrogen Bonds 252

5.2.1. Introduction 252

5.2.2. Materials and Methods 254

5.2.3. Results and Discussion 257

5.2.4. Concluding Remarks 276

CHAPTER SIX: CONCLUSIONS AND RECOMMENDATIONS 278

6.1. Conclusions 278

6.2. Contributions to the Field.....279

6.3. Recommendations for Further Research 279

REFERENCES 281

NOMENCLATURES

EDCs = Endocrine disrupting chemicals

SMT = Sulfamethazine

SZT = Sulfatiazole

SMX = Sulfamethoxazole

Al^{3+} = Aluminium ion

E1 =Estrone

E2 = 17β-estradiol

E3 = Estriol

E1 = Estrone

EE2 = 17α-ethynylestradiol

*4t*BP = 4-*tert*-butyl phenol

BPA = Bisphenol A

HNO_3 = Nitric acid

H_2SO_4 = Sulfuric acid

fBC = Functionalized biochar

CNT = Carbon nanotubes

MWCNTs = Multiwalled carbon nanotubes

SWCNTs = Single walledcarbon nanotubes

PCPs = Personal care products

AGRs = Antibiotic resistant genes

ECs = Emerging contaminants

Kow = Octanol–water partition coefficient

BC = Biochar

AC = Activated carbon

SEM = Scanning electron microscope

EDS = Energy dispervise spectroscopy

XRD = Powder X-ray diffraction

BET = Brunauer-Emmett-Teller

FTIR = Fourier transform infrared spectroscopy

XPS = X-ray photoelectron spectroscopy

PO_4^{3-} = Phosphate

Cl^- = Chloride ion

NO_3^- = Nitrate ion

SO_4^{2-} = Sulphate ion

CEC = Cationic exchange capacity

H/C = Hydrogen/carbon ratio

HNO_3 = Nitric acid

NaOH = Sodium hydroxide

$NaBH_4$ = Sodium borohydrate

M_{dry} = Dried mas

M_{vm} = Weight of volatime matter

M_{fc} = Fraction of fixed carbon

M_{ash} = Weight of ash

Na_2CO_3= Sodium carbonate

CH_3OH =Methanol

C_2H_5OH= Ethanol

$NaHCO_3$ = Sodium bicharbonate

KCl = Potassium chloride

NaCl = Sodium chloride

HA = Humic acid

R^- = Alkyel group

$AlCl_3$ = Aluminium chloride

CH_3-CO-CH_3 = Acetone

C=C = Carbon-carbon double bonds

K_2HPO_4 = Potassium biphosphote

$MgSO_4$ = Magnesium sulphate

PHEN = Phenanthrene

PABA = para-amino benzoic acid

DNB = *1,3*-Dinitro benzene

EDA = Electron donor-acceptor

EDD = Electron-donor-donor

CAP/CP = Chloramphenicol

TAP = Thiamphenicol

FF = Florfenicol

EM = Erythromycin

RTM = Roxithromycin

SD = Sulfadiazine

SM = Sulfamerazine

SP = Sulfapyridine

TC = Tetracycline

CTC = Chlortetracycline

OTC = Oxytetracycline

DXC = Doxycyclinehyclate

NFC = Norfloxacin

CIP = Ciprofloxacin

OFC = Ofloxacin

CARB = Carbodox

LNCM = Lincomycin

TRMP = Trimethoprim

WWTPs = Wastewater treatment plants

DWTPs = Drinking water treatment plants

STPs = Municipal sewage treatment plants

pK_a = Acid dissociation constant

MBR = Membrane bioreactor

AOPs = Advanced oxidation processes

UV = Ultraviolet

TiO_2 = Titanium dioxide

COD = Chemical oxygen deman

PPCPs = Pharmaceutical personal care products

-OH= Hydroxyl group

-COOH = Carboxylic group

$-NH_2$ = Amino group

-CH = Alkyl group

-CO = Ketonic group

-COOR = Ester group

ZnO = Zinc oxide

UF = Ultrafiltration

O/C = Oxygen/ carbon ratio

N/C = Nitrogen/carbon ration

CAHB = Charge assisted hydrogen bonds

E^0 = Redox potential

ZVI = Zerovalent iron

nZVI/ Fe^0 = Nonosized zero valent iron

1MbBBC600 = Bamboo derived functionalized biochar (fBC-1)

TGA= Thermogravimetric analysis

K_d = Distribution coefficient

BJH= Barrett-Joyner-Halenda

DI= Deionised water

PFO = Pseudo first order

PSO= Pseudo second order

IDM = Intraparticle diffusion

Q_{max} = Maximum sorption capacity

K_L= Langmuir fitting constant

$Q_{max(total)}$ = Summerized Langmur maximum sorption capacity

$K_{F(total)}$ = Summerized freundilich constant

$C_6H_5^-$ = Aryl group

ΔG = Free energy change

K_{aw} = Water dissociation constant

TDS = Total dissolved solid

I_G/I_D = Raman spectroscopy D and G band ratio

k = Rate constant

NO= Nitroso

HOAM = Hydroxlamino

m/z = Mass to charge ratio

DO = Dissolved oxygen

RP = Reverse phase

C18 = 18 C-12

Vis = Visible

$LC\text{-}MS_{(Qtof)}$ = Triple quad liquid chromatography-mass spectroscopy

ESI = Electrospray ionisation

PTFE = Poly tetraflouro ethylene

MP-AES = Microwave plasma-atomic emission spectroscopy

IC = Ion chromatography

EAA = Electon acceptor-acceptor

ΔpH = pH change

LOD = Limit of detection

CMs = Carbonaceous materials

HOCs = Hydrophobic organic contaminants

^{1}H NMR = Proton nuclear magnatic resonance spectroscopy

δ = Chemical shifts in NMR

PMM = Polanyi-Mane Model

Cs = Solubility of compound

S_v = Sorbed volumn

ρ_{HOC} = Density of HOC compounds

K_{HD} = Hexadecane partition coefficient

2,4-D = 2,4-Dichlorophenoxyacetic acid

MCPA = 2-methyl-4-chlorophenoxyacetic acid

LIST OF FIGURES

Figure 1.1: The price of different adsorbents [57]. 41

Figure 2.1: Sources of Antibiotics [24].....50

Figure 2.2: Chemical structures of EDCs and resonance form of phenolic group in EDCs.. 54

Figure 2.3: Routes of potential exposure of sex steroids from livestock [96]. 55

Figure 2.4: Routes of potential exposure to sex steroids from livestock [100]. 56

Figure 2.5: Figure demonstrates that all hormone-sensitive physiological systems are vulnerable to EDCs [1]. 59

Figure 2.6: ECs removal achieved by activated sludge process with the corresponding reference after the compound name. a = antidepressant, b = contrast agent, c = gastroesophageal, d = vasodilator, e = antineoplastic, f = diuretic. The concentrations are in mg L^{-1} for empty columns.....71

Figure 2.7: Constructed wetlands for wastewater treatment. a CW with free-floating plants (FFP). bCW with free water surface and emergent macrophytes (FWS). c CW with horizontal subsurface flow (HSSF, HF). d CW with vertical subsurface flow (VSSF, VF) [113].....75

Figure 2.8: Comparative average removal efficiency of ECs with standard deviation (error bar) for wastewater treatment (activated sludge, biologically activated carbon, microalgae, MBR and constructed wetlands) and sludge treatment (aerobic and anaerobic).....78

Figure 2.9: ECs removal efficiencies achieved by ozonation process with the corresponding reference after the compound name. Concentrations are in mg L^{-1} for empty columns and in g L^{-1} for dark columns. 83

Figure 2.10: ECs removal efficiencies achieved by ozonation in the presence of H_2O_2 (a) and UV in the presence of H_2O_2 (b), with the corresponding reference after the compound name. Concentrations are in mg L^{-1} for empty columns and g L^{-1} for dark columns. 1 = corrosion inhibitor, 2 = pain reliever, 3 = contrast agent, 4 = anti-inflammatory. 84

Figure 2.11: ECs removal efficiencies achieved by Fenton process (Figure 2.10a) and by UV photolysis (Fig. 2.10b). Concentrations are in mg L^{-1} for empty columns and in g L^{-1} for clofibric acid. 1 = corrosion inhibitors, 2 = anti-diabetics, 3 = contrast agents, 4 = anti-inflammatory, 5 = pain reliever, 6 = anticonvulsant, 7 = lipid regulators. 86

Figure 2.12: ECs removal efficiencies achieved by photo-Fenton (a) and UV photocatalysis (UV/TiO_2) (b), with the corresponding reference after the compound name. Concentrations are in mg L^{-1} for empty columns and in g L^{-1} for chloramphenicol. 1 = pesticide, 2 = corrosion inhibitor, 3 = contrast agent, 4 = antidepressant, 5 = anti-diabetic, 6 = gastroesophageal, 7 = lipid regulator, 8 = diuretic, 9 = beta blocker, 10 = pain reliever, 11 = NSAID, 12 = stimulant [225].....92

Figure 2.13: Comparative average removal efficiency of ECs with standard deviation (error bar) by different chemical treatment technologies.....94

Figure 3.1: Fixed bed pyrolyser (reactor) for pyrolysis of biomass. 110

Figure 4.1.1: Molecular structures of sulfonamides antibiotics and their equilibrium species. 119

Figure 4.1.2: DSC-TGA graph for biomass raw material (bamboo). 122

Figure 4.1.3: The chemical speciation of (a) sulfamethoxazole modified from Fukahori et al. [308]; (b) sulfathiazole took from Pei et al. [309], and (c) sulfamethazine modified from Teixidó et al. [59].....126

Figure 4.1.4: (a) Effect of pH on the distribution coefficient (Kd) with standard deviation (error bars) for removal of sulfonamide antibiotics; (b) single and competitive sorption kinetics data

with PSO and IDM kinetics model fittings (initial concentration of sulfonamide antibiotics being 10 mg L^{-1} for single solute, and 3.33 mg L^{-1} for each competitive solute at room temperature using 100 mg L^{-1} functionalized biochar dosages).....127

Figure 4.1.5: Pseudo first order (PFO) kinetic model for the kinetics of sulfonamide sorption on functionalized biochar, in single and competitive mode (model fitted to origin pro version 9.1 software). 128

Figure 4.1.6: STZ adsorption isotherm plots and model fits from single solute (initial concentration 0.5–50 mg L^{-1}), and from mixtures (initial individual concentrations were 0.33–16.67 mg L^{-1}) at pH 3.5 and different temperatures. 132

Figure 4.1.7: SMX adsorption isotherm and model fits (Langmuir and Freundlich) at different temperatures using initial concentrations of 0.5-50 mg L^{-1} at pH 3.25 for single solutes, and at 1-50 mg L^{-1} in mixture mode at pH 3.5. 133

Figure 4.1.8: SMT adsorption isotherm and model fits (Langmuir and Freundlich) at different temperatures using initial concentrations of 0.5-50 mg L^{-1} at pH 4.5 for single solutes, and at 1-50 mg L^{-1} in mixture mode at pH 3.5. 134

Figure 4.1.9: Change of K_d values (with SD as error bars) against equilibrium concentrations for (a) competitive solutes with total initial solution concentrations (Co) at 1–50 mg L^{-1} and each solute concentration was 0.33–16.67 mg L^{-1} (i.e. Co/3), and for (b) single solute (C_o = 0.5–50 mg L^{-1}). 136

Figure 4.1.10: Proposed sorption mechanism for single and competitive antibiotics (R1 for SMT, R2 for STZ, R3 for SMX) on functionalized biochar with possible resonance effects for π-π interactions. 137

Figure 4.1.11: Change of pH for blank samples (without antibiotics) at different adsorbent dosages leading to proton release in solution. 140

Figure 4.1.12: FTIR spectra for raw bamboo biomass, biochar (BBC380), and functionalized biochar (1MbBBC600) for the sorption of single and competitive solutes (before and after adsorption). 142

Figure 4.1.13: Raman spectra with band ratio (I_D/I_G) for biochar (BBC380), and functionalized biochar (1MbBBC600 i.e. fBC-1) before and after sorption of single and competitive solutes. 144

Figure 4.2.1: Effect of pH on K_d (with standard deviation) during the removal of sulfonamides and chloramphenicol antibiotics using fBC (80 mg L^{-1}) with initial individual antibiotic concentration of 1.0 mg L^{-1} at 25 °C (a). Competitive sorption kinetics data with PSO and PFO model fitting using 1.0 mg L^{-1} initial antibiotics concentration and 80 mg L^{-1} of fBC at pH 4.0–4.25 (b). 156

Figure 4.2.2: Zeta potential values of fBC and pH shift during pH effect study. 157

Figure 4.2.3: Sorption isotherm plots and model fitting for mixtures of antibiotics (initial concentration of each antibiotic was 0.250–20.0 mg L^{-1}) at pH 4.0–4.25 using fBC dosage of 80 mg L^{-1}. 160

Figure 4.2.4: FTIR (a) and Raman spectra (b) with band ratio (I_D/I_G) of fBC before and after sorption experiments for competitive solutes in mixture mode. 162

Figure 4.2.5: Possible resonance structures of antibiotics and different functional groups in fBC and their electron donor and acceptor sites. 163

Figure 4.2.6: Proposed sorption mechanisms for the removal of antibiotics in competitive mode using fBC. 163

Figure 4.2.7: Sorption of antibiotics (%) in mixture mode with 1.0 mg L^{-1} initial concentration of each antibiotic from lake water (a) and synthetic wastewater (b) with different dosages of fBC at pH 4.0–4.25 and 25 °C. 167

Figure 4.3.1: Nitrogen sorption isotherm for fBC-1 and fBC-2 (a). Barret-Joyner-Halenda (BJH) surface/volume mesopore analysis (adsorption/desorption) with cumulative pore size distribution of fBC-1 and fBC-2 (b). 175

Figure 4.3.2: (a) FTIR spectra of biochar and fBC, (b) Raman spectra of fBCs (with band intensity ratio, I_G/I_D) before and after chloramphenicol sorption. 176

Figure 4.3.3: Effect of pH on the equilibrium K_d of chloramphenicol on biochar, fBC-1 and fBC-2 at 25 °C, using initial chloramphenicol concentration of 15.5 μM L^{-1}, 50–60 mg L^{-1} fBCs or 100 mg L^{-1} biochar. Error bars indicate the standard deviation. 177

Figure 4.3.4: Effects of (a) humic acid concentration, (b) salt concentration, and (c) soil concentration on the equilibrium K_d of chloramphenicol at 25 °C, using 50–60 mg L^{-1} fBC-2 at pH 4.0–4.5. 179

Figure 4.3.5: (a) Sorption isotherm plots and model fitting with initial chloramphenicol concentrations of 0.774–154.7 μM L^{-1} at pH 4.25, 25 °C using 50–60 mg L^{-1} fBC or 100 mg L^{-1} biochar over 40 h. (b) Change of K_d values (with SD as error bars) against equilibrium concentrations from isotherm studies. 182

Figure 4.3.6: Proposed sorption mechanism for the removal of chloramphenicol from different water using fBC. 184

Figure 4.3.7: Effects of competitors phenanthrene and PABA on the adsorption of chloramphenicol at pH 1.82–1.85 (a), pH 4.20–4.56 (b), and pH 9.15–9.60 (c) in deionized water. Phenanthrene and PABA concentrations at 1.0 mg L^{-1}, chloramphenicol concentration at ~ 3.10 μM L^{-1}, fBC-2 dosage at 40–50 mg L^{-1}. Error bars represent the standard deviation. 186

Figure 4.3.8: Sorption of PABA and phenanthrene in the presence or absence of chloramphenicol [65] in deionized water at different pH values. Solution compositions: phenanthrene and PABA concentrations at 1.0 mg L^{-1}, CP concentration at ~ 3.10 μM L^{-1}, fBC-2 dosage at 40–50 mg L^{-1}. Error bars represent the standard deviation. 188

Figure 4.3.9: (a) Sorption of chloramphenicol (initial concentration 3.10 μM L^{-1}) from deionized water, lake water and synthetic wastewater at different dosages of fBC-2 against residual concentrations at pH 4.0–4.5, 25 °C (contact time was 18 h). (b) Reusability of fBC-2 (on percentage basis) for the removal of chloramphenicol under the same condition from different water samples. 191

Figure 4.3.10: Percentage of regeneration of chloramphenicol. 193

Figure 4.4.1: SEM cross-sectional images of fBC, nZVI-fBC and nFe_3O_4-fBC composite (after application of nZVI-fBC), respectively (a–c) using scanning electron microscope (SEM) with energy dispersive spectrometer (EDS) and XRD pattern of nZVI (d). 202

Figure 4.4.2: SEM image of nZVI. 202

Figure 4.4.3: EDS plot of nZVI. 203

Figure 4.4.4: XPS analysis of nZVI-fBC composite before sorption experiments. Spectra were obtained by plotting counts against binding energy for C1s (a), O1s (b), Fe2p (c) and overall survey (d) in a wide scan. 204

Figure 4.4.5: FTIR spectroscopy of nZVI-fBC composite before and after the sorption of chloramphenicol. 205

Figure 4.4.6: XRD pattern of fBC, nZVI-fBC and nFe_3O_4-fBC (a). Raman spectra of nZVI and nZVI-fBC composite (with band ratio, I_G/I_D) for the removal of chloramphenicol before and after experiments (b). 206

Figure 4.4.7: XPS analysis of nZVI-fBC (after 1st cycle). Spectra were obtained by plotting counts against binding energy for C1s (a), O1s (b), Fe2p (c) and overall survey (d) in a wide scan. 207

Figure 4.4.8: Percentage removal (±, standard deviation) of chloramphenicol with time using nZVI (a) and nZVI-fBC composite (b). The initial concentration of chloramphenicol was 3.10 μM L^{-1}, pH 4.0–4.5, 25 °C from different water matrices with different dosages of nZVI and nZVI-fBC composite.....208

Figure 4.4.9: Sorption of chloramphenicol by fBC and Fe_3O_4-fBC composite with the Freundlich and Langmuir model fit. 212

Figure 4.4.10: Proposed reduction and dechlorination mechanisms for the removal of chloramphenicol from water and wastewater. 213

Figure 4.4.11: Reduced products of chloramphenicol as identified by LC-MS/QTOF from deionized water, synthetic wastewater and lake water using nZVI only (sample collected after 8 h). 214

Figure 4.4.12: Chloramphenicol transformation by-products identified by their retention times (2.1 min, 2.7 min) in LC and mass spectra by LC-MS/QTOF from deionized water (a) and lake water (b) using nZVI only (sample collected after 8 h). LC-MS/QTOF method run for 13 min and data plotted up to 5 min.....215

Figure 4.4.13: Chloramphenicol transformation products highlighted by their retention times after 10 min (a), 30 min (b), 150 min (c), and 12 h (d) using nZVI-fBC in synthetic wastewater during the 1st cycle application. LC-MS/QTOF method run for 13 min and data plotted up to 5 min. 215

Figure 4.4.14: The 2nd cycle application of nZVI-fBC (nZVI-fBC transformed to nFe_3O_4-fBC) for the removal of chloramphenicol from synthetic wastewater. Small fraction of reduced product indicates that sorption was dominating in the 2nd and subsequent cycles. 216

Figure 4.4.15: Chloramphenicol sorption mechanisms at pH 4.0-4.5. 219

Figure 4.4.16: Percentage of sorption and reduction (cumulative basis, after excluding the amount of recoverable chloramphenicol) using nZVI-fBC composite (in the 1st cycle) followed

by sorption only onto nFe_3O_4-fBC composite (a). Reusability of nFe_3O_4-fBC composite for the repetitive applications (up to 7th cycle) for the removal of chloramphenicol (3.10 μM L^{-1} initial concentration) at pH 4.0–4.5, 25 °C from different water (b). 220

Figure 4.4.17: Sorption of methylene blue by nFe3O4-fBC with the Langmuir and Freundlich model fit. 221

Figure 4.4.18: Use of a magnet bar to demonstrate easy separation of nFe_3O_4-fBC composite after experiments. 222

Figure 5.1.1: SEM image of fBC-2 before (a) and after (b) sorption of EDCs. 230

Figure 5.1.2: Nitrogen adsorption–desorption isotherm for fBC-2: Barret-Joyner-Halenda (BJH) surface/volume mesopore analysis (a), and cumulative pore size distribution (b). 233

Figure 5.1.3: Raman spectra for fBC-2 before and after sorption experiments. Raman shifts measurement was carried out using Renishaw inVia Raman spectrometer equipped with a 17 mW Renishaw Helium-Neon Laser 633 nm and CCD array detector at 50% laser intensity. 234

Figure 5.1.4: XPS analysis of fBC-2. Spectra were obtained by plotting counts against binding energy in a wide scan for C1s (a), O1s (b), P 2p(c) and overall survey (d).....235

Figure 5.1.5: Effect of pH on solid phase concentration (μg g^{-1}) during EDCs sorption in competitive mode using fBC-2 at a dosage of 80 mg L^{-1} at 25 °C (a). Zeta potential values of fBC-2 using 0.01 M KCl solution at different pH with fBC-2 dosage of 400 mg L^{-1} together with initial and equilibrium pH values (b). 236

Figure 5.1.6: Kinetic model fit for EDCs adsorption on fBC-2 at 25 °C. (a) Weber-Morris plots, (b) external mass transfer plots, and (c) Boyd plots.....237

Figure 5.1.7: Solid phase concentration vs. aqueous concentration at equilibrium for the sorption of EDCs using 100 mg L^{-1} of fBC-2 at 25 °C.....240

Figure 5.1.8: The Langmuir isotherm model fits for sorption of EDCs onto fBC-2. 241

Figure 5.1.9: Logarithm plot of distribution coefficient (K_d) vs aqueous equilibrium concentration for the sorption of EDCs using 100 mg L^{-1} of fBC-2 at 25 ºC.....242

Figure 5.1.10: Resonance structures of EDCs and different functional groups in fBC-2. ...245

Figure 5.1.11: Sorption of EDCs in mixture mode with initial concentration of each EDC at ~500 μg L^{-1} from MBR sewage effluent at different dosages of fBC-2 at pH 3.0–3.25, 25 °C. 249

Figure 5.2.1: (a) Adsorption isotherms of estrone (E1), 17β-estradiol (E2), estriol (E3), 17α-ethynylestradiol (EE2) and bisphenol A (BPA) on fBC-2 at pH 3.0-3.5. Solid lines are the polynomial fitting curves using PMM. (b) Effect of pH on solid phase concentration (μg kg^{-1}) during HOC sorption (initial concentration of each HOC was ~500 μg L^{-1}) by fBC-2 with dosage of 40-60 mg L^{-1}, 25 ºC. 259

Figure 5.2.2: PMM Sorption Isotherm Fitting for HOCs. Isotherm Parameters were Normalized by the Primary Solute Solubility with b= 1, and S_e of Single-Solute Isotherms. 259

Figure 5.2.3: Individual sorption of different concentrations of (a) phenanthrene (PHEN) and (b) 1,3-dinitrobenzene (DNB) on fBC-2 at different pH, 25 ^{0}C using fBC-2 dosage of 18-25 mg L^{-1} and 40-60 mg L^{-1}, respectively for PHEN and DNB. 262

Figure 5.1.4: Removal percentage NON-2 during sorption by fBC-2 (30-35 mg L^{-1}) at different pH, highlighting the role of π-H-bonding and H-bonding with fBC-2. 263

Figure 5.2.5: (a) Comparison of K_d/K_{HW} between phenanthrene (PHEN) and HOCs such as estrone (E1), 17β-estradiol (E2), estriol (E3), 17α-ethynylestradiol (EE2) and bisphenol A (BPA). K_d/K_{HW} was calculated at C_e = 0.002 C_s. The K_d/K_{HW} values of solutes were directly labelled on their respective bars due to the off-scale values. The differences among them are

consistent with the explanation that π-π bonds played a major role after eliminating hydrophobic effects. The π-π bonds formed among HOCs and fBC-2 were a donor/acceptor system, and much stronger than those between PHEN and fBC-2. **(**b**)** Relationship between log K_{HW} *vs* log K_d as calculated at $C_e = 0.002\ C_s$. 264

Figure 5.1.6: Sorption performance of (a) estrone (E1) and (b) bisphenol A (BPA) in the absence and presence of competitor such as π-electron-donor phenanthrene (PHEN) and π-electron-acceptor 1,3-dinitrobenzene (DNB). Their interactions indicated the role of co-solutes and the role of π-π electron-donor-donor or donor-acceptor multi-system on the sorption performance of HOCs by fBC-2. Error bar representing the standard deviation. Sorption performance of 17*β*-estradiol (E2), estrio (E3) and 17*α*-ethynylestradiol (EE2) in the absence and presence of π-electron-donor-acceptor system is represented in Figure 5.2.7. Each HOC initial concentration was ~1000 μg L^{-1} and fBC-2 dosage was maintained 40-60 mg L^{-1}. ...266

Figure 5.2.7: Sorption performance of (a) 17*β*-estradiol (E2), (b) estriol (E3), and (b) 17*α*-ethynylestradiol (EE2) in the absence and presence of competitors such as π-electron-donor phenanthrene (PHEN) and π-electron-acceptor *1,3*-dinitrobenzene (DNB). Their interactions indicated the role of co-solutes and the role of π-π electron-donor-donor or donor-acceptor multi-system on the sorption performance of HOCs by fBC-2. Error bar representing the standard deviation. The initial concentration of HOC was ~1000 μg L^{-1} and fBC-2 dosage was maintained 40-60 mg L^{-1}.....267

Figure 5.2.9: Sorption performance of (a) estrone (E1) and (b) bisphenol A (BPA) in the absence and presence of competitors such as π-electron-donor phenanthrene (PHEN) and π-electron-acceptor *p*-amino benzoic acid (PABA). Their interactions indicated the role of co-solutes and the role of π-π electron-donor-donor or donor-acceptor multi-system on the sorption performance of HOCs by fBC-2. Error bar representing the standard deviation. The initial concentration of HOC was ~1000 μg L^{-1} and fBC-2 dosage was maintained 40-60 mg L^{-1}. 269

Figure 5.2.10: Sorption performance of (a) 17*β*-estradiol (E2), (b), estriol (E3), and (b) 17*α*-ethynylestradiol (EE2) in the absence and presence of competitors such as π-electron-donor phenanthrene (PHEN) and π-electron-acceptor *p*-amino benzoic acid (PABA). Their interactions indicated the role of co-solutes and the role of π-π electron-donor-donor or donor-

acceptor multi-system on the sorption performance of HOCs by fBC-2. Error bar representing the standard deviation. The initial concentration of HOC was ~1000 μg L^{-1} and fBC-2 dosage was maintained 40-60 mg L^{-1}. 270

Figure 5.2.11: UV-Vis spectra difference in the acceptor-donor mixture showing the charge-transfer absorption band of π-π complexes. (a) Donor-phenanthrene (PHEN), acceptor 1,3-dinitrobenzene (DNB) and their mixing interaction, (b) Donor-PHEN, acceptor-DNB and HOC-estrone (E1) interactions, (c) Donor-PHEN, acceptor-DNB and HOC-estriol (E3) interactions, and (d) Donor- PHEN, acceptor-DNB and HOC-BPA interactions clearly indicating the difference of absorption band of π-π complexes.....271

Figure 5.2.12: ^{1}H NMR observed frequency shift for different protons in specific carbon bonded protons in the respective structure of structure of E1, BPA, DNB, and PHEN (Figures a-c). ΔHz of each proton in each component in their mixture specified within first bracket. Data obtained from a series of combine mixing solution of solutes and their increased shielding by extra-nuclear electrons (i.e. increasing magnetic field at fixed frequency) from a fixed concentration of solute in methanol-d4 solvent. Observed frequency shift (ΔHz) for each solute in solution was measured by multiplying the chemical shift (δ) of each solute and spectrophotometer frequency for different proton positions (marked as green color) as shown in figure (d). Structural proton positions were labelled based on ^{1}H NMR peaks accessible at http://sdbs.db.aist.go.jp/sdbs/cgi-bin/cre_result.cgi?STSI=151281072529897. (d) Illustration of offset geometry of HOCs in which proton number lies in the structure.....273

Figure 5.2.13: Sorption of PABA at different concentrations and different pH using fBC-2 dosage of 40-60 mg L^{-1}……..276

LIST OF TABLES

Table 2.1: Physicochemical properties of major types of antibiotics investigated by different studies. 51

Table 2.2: Physicochemical properties of the target EDCs. 57

Table 2.3: Advantages and challenges of different technologies in the removal of ECs. 62

Table 2.4: ECs removal efficiency by nitrification and denitrification treatment technologies. 65

Table 2.5. ECs removal efficiency by biological activated carbon [131]. 66

Table 2.6: ECs removal efficiency from WWTPs by different biological treatment technologies. 67

Table 2.7: ECs removal efficiency by aerobic, anaerobic and facultative processes. 72

Table 2.8: ECs removal efficiency by biosorption and MBR based systems. 73

Table 2.9: ECs removal efficiency by different constructed wetland processes. 76

Table 2.10: ECs removal efficiency by gamma radiation (conventional) and AOPs based treatment technologies. 87

Table 2.11: The removal efficiency of EDCs, pesticides and beta blockers achieved by hybrid systems. 98

Table 2.12: Pharmaceuticals removal efficiency by hybrid systems. 99

Table 3.1: Yield of biochar prepared from different biomass.....112

Table 4.1.1: Physicochemical properties of the antibiotics investigated in this study.....119

Table 4.1.2: The basic properties, zeta potential and EDS data of biomass and biochar samples. 122

Table 4.1.3: Summary of BET and BJH physical parameters for biochar and functionalized biochar.....123

Table 4.1.4: Summary of the kinetic model parameters for sulfonamide antibiotic adsorption on functionalized biochar.....129

Table 4.1.5: Summary of the Freundlich isotherm parameters for sulfonamide antibiotic adsorption on functionalized biochar.....129

Table 4.1.6: Summary of the Langmuir isotherm parameters for sulfonamide antibiotic adsorption on functionalized biochar.....130

Table 4.1.7: pH shift for different species of SMT, SMX and STZ antibiotics on functionalized biochar.....139

Table 4.1.8: ΔGo values calculated from water dissociation constant (K_{aw}) at different temperatures.....145

Table 4.1.9: Summary of Raman spectroscopy peak assignment in char [51, 317] and observed in this study before and after adsorption.....149

Table 4.2.1: Physicochemical properties of the antibiotics investigated in this study.....153

Table 4.2.2: Summary of the kinetic model parameters for antibiotics sorption on fBC at 25 ± 0.5 °C. 158

Table 4.2.3: Summary of the Freundlich and Langmuir isotherm parameters for competitive antibiotic sorption on fBC at 25 ± 0.5 °C. 159

Table 4.3.1: Physicochemical properties of chloramphenicol. 169

Table 4.3.2: EDS analysis data of biochar and fBC.....172

Table 4.3.3: Physicochemical properties of lake water and synthetic wastewater. 173

Table 4.3.4: The Freundlich and Langmuir isotherm parameters for the sorption of chloramphenicol by biochar and functionalized biochar. 181

Table 4.3.5: Zeta potential values of fBC-1 and fBC-2. 183

Table 4.4.1: Zeta potential values (mV) of Fe_3O_4-fBC composite and nZVI.....199

Table 4.4.2: Chemical composition of synthetic wastewater.....200

Table 4.4.4: EDS of fBC, nZVI and nZVI-fBC. 201

Table 4.4.5: Reduction kinetic parameters of chloramphenicol in different water types using nZVI. 209

Table 4.4.6: The Freundlich and Langmuir isotherm parameters for the sorption of chloramphenicol using fBC and Fe_3O_4-fBC. 212

Table 5.1.1: Physicochemical characteristics of synthetic wastewater and MBR sewage effluent. 227

Table 5.1.2: Limit of detection (LOD) of EDCs by HPLC equipped with UV and fluorescence detectors. 228

Table 5.1.3: Summary of BET and BJH physical parameters for fBC-2.....231

Table 5.1.4: Kinetic parameters calculated from the PSO and Waber-Morris kinetic models for the sorption of EDCs on fBC-2 at 25 ^{0}C. 238

Table 5.1.5: Summary of the Langmuir isotherm parameters for EDCs sorption on fBC-2 at 25±0.5 ^{0}C. 242

Table 5.1.6: Calculated ΔG^{0} (kJ mole^{-1}) values for EDCs at 25 ^{0}C with initial concentrations of each EDC at 250-3000 µg L^{-1}. K_d values were taken as L kg^{-1}. 243

Table 5.1.7: ΔG^{o} values calculated from water dissociation constant (K_{aw}) at 25 ^{0}C. 247

Table 5.1.8: EDC removal from synthetic wastewater with different dosages of fBC-2 at 46 h, 50 h and 64 h. (LOD = limit of detection) 250

Table 5.2.1: Physicochemical Properties of Selected HOCs. 253

Table 5.2.2: XPS Spectra Summery for fBC-2 [25, 397]. 255

Table 5.2.3: Summary of the Freundlich Isotherm Parameters for Each HOC Adsorption on fBC-2 at 25 ± 0.5 °C. 258

Table 5.2.4: Summary of the PMM Isotherm Parameters for Each HOC Adsorption on fBC-2 at 25 ± 0.5 °C (d=1). 258

Table 5.2.5: Hexadecane-Water Partition Coefficient and Sorption Coefficient Relationship. 264

LIST OF PUBLICATIONS

Peer-Reviewed Publications

(1). Mohammad Boshir Ahmed,** John L Zhou, Huu Hao Ngo, Wenshan Guo, Md Abu Hasan Johir, Kireesan Sornalingam, M. Sahedur Rahman. "Chloramphenicol interaction with functionalized biochar in water: sorptive mechanism, molecular imprinting effect and repeatable application". ***Sci. Total Environ. 609 (2017): 885-895.

(2). Mohammad Boshir Ahmed,** John L Zhou, Huu Hao Ngo, Wenshan Guo, Md Abu Hasan Johir, Kireesan Sornalingam, Dalel Belhaj, Monem Kallel. "Nano-Fe^0 immobilized onto functionalized biochar gaining excellent stability during sorption and reduction of chloramphenicol via transforming to reusable magnetic composite". ***Chem. Eng. J. 322 (2017): 571-581.

(3). Mohammad Boshir Ahmed, Md Abu Hasan Johir, John L Zhou, Huu Hao Ngo, Wenshan Guo, Kireesan Sornalingam. "Photolytic and photocatalytic degradation of organic UV filters in contaminated water". ***Curr. Opin. Green Sustain. Chem.*** 6 (2017): 85-92. (**Special issue on catalysis**).

(4). Mohammad Boshir Ahmed**, John L Zhou, Huu Hao Ngo, Wenshan Guo, Md Abu Hasan Johir, Dalel Belhaj. "Competitive sorption affinity of sulfonamides and chloramphenicol antibiotics toward functionalized biochar for water and wastewater treatment". ***Bioresour. Technol. 238 (2017): 306-312.

*** (5). Mohammad Boshir Ahmed**, John L. Zhou, Huu Hao Ngo, Wenshan Guo, Md Abu Hasan Johir, Kireesan Sornalingam "Single and competitive sorption properties and mechanism of functionalized biochar for removing sulfonamide antibiotics from water". ***Chem. Eng. J.*** 311 (2017), 348-358.

(6). Mohammad Boshir Ahmed**, John L. Zhou, Huu Hao Ngo, and Wenshan Guo. "Adsorptive removal of antibiotics from water and wastewater: progress and challenges". ***Sci. Total Environ. 532 (2015): 112-126. (**Hot Paper** & ***Highly cited paper according to web of science***)

(7). Mohammad Boshir Ahmed**, John L. Zhou, Huu Hao Ngo, and Wenshan Guo "Insight into biochar properties and its cost analysis". ***Biomass Bioenerg. 84 (2016): 76-86.

(8). Mohammad Boshir Ahmed**, John L. Zhou, Huu Hao Ngo, Wenshan Guo and Mengfang Chen "Progress in the preparation and application of modified biochar for improved contaminant removal from water and wastewater. ***Bioresour. Technol. *214 (2016)*, 836-851.

***** (**9**). **Mohammad Boshir Ahmed**, John L. Zhou, Huu Hao Ngo, Wenshan Guo, Nikolaos S Thomaidis, Jiang Xu "Progress in the biological and chemical treatment technologies for emerging contaminant removal from wastewater: a critical review". ***J. Hazard. Mater.*** 323 (2017), 274-298 (***on special issue, most downloaded paper in J. Hazard. Mater.***). (**Hot Paper** & ***Highly cited paper according to web of science***).

(10). Mohammad Boshir Ahmed**, Huu Hao Ngo, Md Abu Hasan Johir, Kireesan Sornalingam. "Sorptive removal of phenolic endocrine disruptors by functionalized biochar: competitive interaction mechanism, removal efficacy and application in wastewater". ***Chem. Eng. J. (2017), 335, 801-811.

(11). Kireesan Sornalingam, Andrew McDonagh, John L Zhou, Md A Johir, **Mohammad Boshir Ahmed**. "Photocatalysis of estrone in water and wastewater: Comparison between Au-TiO_2 nanocomposite and TiO_2, and degradation by-products". ***Sci. Total Environ.*** 610 (2018): 521-530.

(12). Dalel Belhaj, Donyez Frikha, Khaled Athmouni, Bouthaina Jerbi, **Mohammad Boshir Ahmed**, Zouhaier Bouallagui, Monem Kallel, Sami Maalej, John Zhou, Habib Ayadi. "Box-Behnken design for extraction optimization of crude polysaccharides from Tunisian Phormidium versicolor cyanobacteria (NCC 466): partial characterization, in vitro antioxidant and antimicrobial activities." ***Int. J. Biological Macromol.*** (2017).

(13). Narottam Saha, M. Safiur Rahman, **Mohammad Boshir Ahmed**, John L. Zhou, Huu Hao Ngo, and Wenshan Guo "Industrial metal pollution in water and probabilistic assessment of human health risk." ***J. Environ. Manage.*** 185 (2017): 70-78.

(14). Bentuo Xu, **Mohammad Boshir Ahmed**, John L. Zhou, Ali Altaee, Minghong Wu, Gang Xu. "Photocatalytic removal of perfluoroalkyl substances from water and wastewater: Mechanism, kinetics and controlling factors." ***Chemosphere***, 189 (2017), 717-729.

(15). Mohammad Boshir Ahmed, A.T. M. Kamrul Hasan, Md. Mohiuddin, Mohammad Asadullah, Md. Sahedur Rahman, A. Khaleque. "Effects of heating rate and heating up time to central of biomass particles for bio-oil production." ***Bangladesh J. Sci. Indust. Res***. *51*(2017), 13-22.

(16). Marwa Mohsen, **Mohammad Boshir Ahmed**, John L. Zhou. "Particulate Matter Concentrations and Heavy Metal Contamination Levels in the Railway Transport System of Sydney, Australia". ***Transport. Res. Part D: Transport. Environ. 62, 112-124.*** 62(2018), 112-124.

(17). Bentuo Xu, **Mohammad Boshir Ahmed**, John L. Zhou, Ali Altaee, Minghong Wu, Gang Xu. "Graphitic carbon nitride (g-C_3N_4) based nanocomposites for the photocatalysis of

organic contaminants under visible irradiation: progress, limitations and future directions". ***Sci. Total Environ.*** *633 (2018), 546-559.*

(18). Dalel Belha, Khaled Athmouni, **Mohammad Boshir Ahmed**, Nissaf Aoiadni, Abdelfattah El Feki, John L. Zhou, Habib Ayadi. "Polysaccharides from Phormidium versicolor (NCC466) protecting HepG2 human hepatocellular carcinoma cells and rat liver tissues from cadmium toxicity: evidence from in vitro and in vivo tests". ***Int. J. Biological Macromol.*** 113 (2018), 813-920.

List of Submitted Journal Articles:

(19). Mohammad Boshir Ahmed**, John L Zhou, Huu Hao Ngo, Md. Abu Hasan Johir, Liying Sun, Mohammad Asadullah, Dalel Belhaj. "Sorption of Hydrophobic Organic Contaminants on Functionalized Biochar: Protagonist Role of π-π Electron-Donor-Acceptor Interactions and Hydrogen bonds". ***J. Hazard. Mater. (2018).

(20). Tanjina Nur, Paripurnanda Loganathan, **Mohammad Boshir Ahmed**, Mohammad Johir, Jaya Kandasamy, Saravanamuthu Vigneswaran*. Struvite production using membrane-bioreactor wastewater effluent and seawater. ***Desalination*** *(2018), Short Communication.*

(22). Bouthaina Jerbi, Dalel Belhaj, Sikandar I Mulla, Khaled Athmouni, **Mohammad Boshir Ahmed**, John L Zhou, Habib Ayadi, Monem Kallel. Uptake, accumulation, biochemical responses and health risk of heavy metals in soil-tomato system through urban sewage sludge amendment: A case study in Sfax, Tunisia. **Environ. Sci. Pollut. Res.** ***(2018).***

[Publications made during the PhD candidature including articles not entirely related to this Thesis. *Articles related to the Thesis.]

Contribution to Scientific Forums:

***(1). Mohammad Boshir Ahmed,** John L. Zhou, Huu Hao Ngo, and Wenshan Guo "Removal of sulfamethazine and sulfathiazole from water using modified bamboo biochar". 22nd -25th of August, 2016. The Synergy of Science and Industry: Biochar's Connection to Ecology, Soil, Food and Energy. Oregon State University, Portland, Oregon, USA.

(2). Dalel Belhaj, Bouthaina Jerbi, Khaled Athmouni, **Mohammad Boshir Ahmed**, Sikandar Mulla, John Zhou, Habib Ayadi. Ecotoxicological effect s of 17 α-ethinylestradiol (EE2) and its removal by monoculture of phytoplankton species and their consortium. May 2018. 3rd

International Conference on Integrated Environmental Management for Sustainable Development (ICIEM-2018), Sousse, Tunisia. http://www.iciem-conference.com

***(3). Mohammad Boshir Ahmed,** John L Zhou, Huu Hao Ngo, Wenshan Guo, Md Abu Hasan Johir, Kireesan Sornalingam, Dalel Belhaj, Monem Kallel. "Nano-Fe^0 immobilized onto functionalized biochar gaining excellent stability during sorption and reduction of chloramphenicol via transforming to reusable magnetic composite". July 26-27, 2018. 6^{th} Edition of International Conference on "Water Pollution and Sewage Management"- Be a part of Solution, Not the Pollution!!, Rome, Italy.

***(4)**. **Mohammad Boshir Ahmed,** John L Zhou, Huu Hao Ngo. "Interactions of emerging contaminants-antibiotics with functionalized biochar". August 20-23, 2018. Biochar 2018 - "The Carbon link in Watershed Ecosystem Services", Wilmington, Delaware USA.

[*Presentation made during the PhD candidature including proceedings and oral presentations.*]

[*Presentation related to the Thesis]

AWARDS

1. Finalist for "**NSW Young Water Professional of the Year Award**", the **Australian Water Association**, NSW, and Australia.
2. "**Top 35 of the Antibiotics Travel Awards 2017"** shortlisted by "**Antibiotics**" journal authority from worldwide applications.
3. **2017 HDR** Students "**Publication Award and Certificate"** from Faculty of Engineering and Information Technology, University of Technology Sydney (UTS), Sydney, Australia for publishing in high quality Journals.
4. **2016 HDR** Students "**Publication Award and Certificate"** from Faculty of Engineering and Information Technology, University of Technology Sydney (UTS), Sydney, Australia for publishing in high quality Journals.
5. **2015 HDR** Students "**Publication Award and Certificate"** from Faculty of Engineering and Information Technology, University of Technology Sydney (UTS), Sydney, Australia for publishing in high quality Journals.
6. **International Research Scholarship** and **Faculty of Engineering & Information Technology Scholarship** from University of Technology Sydney (UTS), Sydney, Australia.
7. **FEIT Travel funds** for the year of 2016 and 2018 from UTS.
8. **Vice Chancellor Travel fund** in 2018 from UTS.
9. **One-Off-Scholarship** from UTS in 2018.

ABSTRACT

In the last few decades, water pollution by different organic and inorganic species has become one of the most critical issues in many regions of the world. The consumption of the contaminated water is of major human health concern. The presence of antibiotics and EDCs in the aquatic environment causes critical problems to human health and aquatic organisms. The efficacy for removing antibiotics and EDCs in traditional wastewater treatment plants is not satisfactory by considering technology, cost and overall performance. On the other hand, adsorptive materials are cost effective and highly suitable for removal of antibiotics and EDCs. In this study, different adsorptive materials such as biorchar, functionlaized biochar and a biochar composite sorbent were prepared by the utilization of woody biomasses (bamboo and eucalyptus) and scrap iron material. Biochar was prepared at 380-400 ^{0}C via pyrolysis process and then modified using *o*H_3PO_4 to produce functionalized biochar (fBC) at 600 ^{0}C. The functionalized biochars were named as fBC-1(prepared from bamboo) and fBC-2 (prepared from eucalyptus globules). Finally, fBC-2 was used to prepare a biochar composite with zero-valent-iron (synthesized from scrap iron). These materials were used to remove antiobiotics and EDCs in single and competitive mode.

Single and competitive sorption properties and mechanism of functionalized biochar for removing sulfonamide antibiotics from water:

Single and competitive sorption of ionisable sulphonamides sulfamethazine, sulfamethoxazole and sulfathiazole on functionalized biochar was highly pH dependent. The equilibrium data were well represented by both Langmuir and Freundlich models for single solutes, and by the Langmuir model for competitive solutes. Sorption capacity and distribution coefficient values decreased as sulfathiazole > sulfamethoxazole > sulfamethazine. The sorption capacity of each antibiotic in competitive mode is about three times lower than in single solute sorption. The kinetics data were best described by the pseudo second-order model for single solutes, and by PSO and intra-particle diffusion models for competitive solutes. Adsorption mechanism was governed by pore filling through diffusion process. The findings from pH shift, FTIR spectra and Raman band shift showed that sorption of neutral sulfonamide species occurred mainly due to strong H-bonds followed by π^+-π electron-donor-acceptor (EDA), and by Lewis acid-

base interaction. Moreover, EDA was the main mechanism for the sorption of positive sulfonamides species. The sorption of negative species was mainly regulated by proton exchange with water forming negative charge assisted H-bond (CAHB), followed by the neutralization of –OH groups by H^+ released from functionalized biochar surface; in addition, π-π electron-acceptor-acceptor (EAA) interaction played an important role.

Competitive sorption affinity of sulfonamides and chloramphenicol antibiotics toward functionalized biochar for water and wastewater treatment:

Competitive sorption of sulfamethazine (SMT), sulfamethoxazole (SMX), sulfathiazole (STZ) and chloramphenicol toward functionalized biochar (fBC) was highly pH dependent with maximum sorption at pH ∼4.0–4.25. The Langmuir and Freundlich models well represented equilibrium data in the order STZ > SMX > CP > SMT. Kinetics data were slightly better fitted by the pseudo-second-order model than pseudo first-order and intra-particle-diffusion models. Maximum sorptive interactions occurred at pH 4.0–4.25 through H-bonds formations for neutral sulfonamides species and negative charge assisted H-bond (CAHB) formation for CP, in addition to π-π electron-donor-acceptor (EDA) interactions. EDA was the main mechanism for the sorption of positive sulfonamides species and CP at pH < 2.0. Sorption of negative sulfonamides species and CP at pH > 7.0 was regulated by H-bond formation and proton exchange with water by forming CAHB, respectively. The results suggested fBC to be highly efficient in removing antibiotics mixture.

Chloramphenicol interaction with functionalized biochar in water: sorptive mechanism, molecular imprinting effect and repeatable application:

Biochar and functionalized biochar (fBC-1 and fBC-2) were prepared and applied to remove antibiotic chloramphenicol from deionized water, lake water and synthetic wastewater. Results showed that chloramphenicol removal on biochar was pH dependent and maximum sorption occurred at pH 4.0–4.5. The sorption data of chloramphenicol fitted better with the Langmuir isotherm model than the Freundlich isotherm model with the maximum Langmuir sorption capacity of 233 $\mu M\ g^{-1}$ using fBC-2. Chloramphenicol sorption on fBC-2 followed the trend: deionized water > lake water > synthetic wastewater. The presence of humic acid decreased the sorption distribution

coefficient (K_d) while the presence of low ionic strength and soil in solution increased K_d value significantly. The mechanism of sorption on fBC mainly involved electron-donor-acceptor (EDA) interactions at pH < 2.0; formation of charge-assisted hydrogen bond (CAHB) and hydrogen bonds in addition to EDA in the pH 4.0–4.5; and CAHB and EDA interactions at pH > 7.0. Additionally, solvent and thermal regeneration of fBC-2 for repeatable applications showed excellent sorption of chloramphenicol under the same condition, due to the creation of a molecular imprinting effect in fBC-2. Consequently, fBC-2 can be applied with excellent reusability properties to remove chloramphenicol and other similar organic contaminants.

Nano-Fe0 immobilized onto functionalized biochar gaining excellent stability during sorption and reduction of chloramphenicol via transforming to reusable magnetic composite:

The widely used nano-sized zero-valent iron (nZVI or nFe^0) particles and their composite material lose reductive nature during application, and the stability of transformed composite material for repeatable application is not addressed to date. To shed light on this, nZVI was synthesized from scrap material and immobilized on functionalized biochar (fBC) to prepare nZVI-fBC composite. Comparative study between nZVI and nZVI-fBC composite on the removal of chlorinated antibiotic chloramphenicol from different water types was conducted. The results suggested that nZVI was solely responsible for reduction of chloramphenicol. Whereas nZVI-fBC could be applied once, within a few hours, for the reduction of chloramphenicol (29–32.5%) and subsequently sorption (67.5–70.5%) by transforming to a fully magnetic composite (nFe_3O_4-fBC) gaining stability with synergistic sorption performance. In both cases, two reduction by-products were identified namely 2-chloro-N-[1,3-dihydroxy-1-(4-aminophenyl)propan-2-yl]acetamide (*m*/*z* 257) and dechlorinated N-[1,3-dihydroxy-1-(4-aminophenyl)propan-2-yl]acetamide (*m*/*z* 223). The complete removal of 3.1 μM L^{-1} of chloramphenicol in different water was faster by nZVI-fBC (∼12–15 h) than by stable nFe_3O_4-fBC composite (∼18 h). Both nZVI-fBC and nFe_3O_4-fBC composites removed chloramphenicol in the order: deionized water > lake water > synthetic wastewater. nFe_3O_4-fBC showed excellent reusability after regeneration, with the regenerated nFe_3O_4-fBC composite (after 6 cycles of application) showing significant performance for methylene blue

removal (~287 mg g^{-1}). Therefore, the transformed nFe_3O_4-fBC composite is a promising and reusable sorbent for the efficient removal of organic contaminants.

Sorptive removal of phenolic endocrine disruptors by functionalized biochar: Competitive interaction mechanism, removal efficacy and application in wastewater:

Sorptive removal of six phenolic endocrine disrupting chemicals (EDCs) estrone (E1), 17β-estradiol (E2), estriol (E3), 17α-ethynylestradiol (EE2), bisphenol A (BPA) and 4-*tert*-butylphenol (4*t*BP) by functionalized biochar (fBC-2) through competitive interactions was investigated. EDC sorption was pH dependent with the maximum sorption at pH 3.0–3.5 due to hydrogen bonds and π-π interactions as the principal sorptive mechanism. Sorption isotherm of the EDCs was fitted to the Langmuir model. Sorption capacities and distribution coefficient values followed the order E1 > E2 ≥ EE2 > BPA > 4*t*BP > E3. The findings suggested that EDC sorption occurred mainly through pseudo-second order and external mass transfer diffusion processes, by forming H-bonds along with π-π electron-donor–acceptor (EDA) interactions at different pH. The complete removal of ~500 μg L^{-1} of each EDC from different water decreased in the order: deionised water > membrane bioreactor (MBR) sewage effluent > synthetic wastewater. The presence of sodium lauryl sulphonate and acacia gum in synthetic wastewater significantly suppressed sorption affinity of EDCs by 38–50%, hence requiring more fBC to maintain removal efficacy.

Sorption of Hydrophobic Organic Contaminants on Functionalized Biochar: Protagonist Role of π-π Electron-Donor-Acceptor Interactions and Hydrogen Bonds:

Sorption of five potent endocrine disruptors as representative hydrophobic organic contaminants (HOCs) namely estrone (E1), 17*β*-estradiol (E2), estriol (E3), 17*α*-ethynylestradiol (EE2) and bisphenol A (BPA) on functionalized biochar (fBC-2) was systematically examined, with a particular focus on the importance of π-electron-donor (phenanthrene: PHEN) and π-electron-acceptors (1,3-dinitrobenzene: DNB, *p*-amino benzoic acid: PABA) on sorption. Experimental results suggested that hydrogen-bond formations and π-π-electron-donor-acceptor (EDA) interactions were the dominant sorption mechanisms. The sorption of HOCs followed the order of E1 > E2 > EE2 > E3 > BPA based on the Freundlich and Polanyi-Mane-models. The comparison of adsorption coefficient (K_d) normalized against

hexadecane-water partition coefficient (K_{HW}) between HOCs and PHEN indicated strong π-π-EDA interactions. π-π interactions among DNB, PHEN and HOCs in methanol-d_4 were verified by the observed upfield frequency shifts using proton nuclear magnetic resonance (^{1}H NMR) which identified the specific direction of π-π interactions. UV-vis spectra showed charge-transfer bands for π-donors (PHEN and HOCs) with the model π-acceptor (DNB) also demonstrating the role of π-π EDA interactions. The role of π-electron-donor and π-electron-acceptor domains in fBC was identified at different solution pH. Therefore, π-π EDA interaction together with hydrogen-bond formation were the key mechanism responsible for sorptive removal of HOCs.

UNIVERSITY OF TECHNOLOGY SYDNEY

Faculty of Engineering and Information Technology

CHAPTER: ONE

INTRODUCTION

CHAPTER ONE: INTRODUCTION

1.1. Background

Due to the rapid population growth, water pollution, and increasing demand for clean water, advanced wastewater treatment is becoming an international focus for the rational use of scarce water resources and as a means of safeguarding aquatic environments from the harm caused by wastewater disposal. Reclamation and reuse of treated wastewater have become an important topics in the sustainable management of water because high-quality water resources are becoming increasingly limited. In recent decades, the wastewater treatment industry has identified the discharge of emerging organic contaminants such as endocrine disrupting chemicals (EDCs) and pharmaceuticals and personal care products (PPCPs) into waterways. Most of the wastewater treatment plants are primarily designed to remove nutrients and easily degradable carbon compounds. It has been shown that they have limited capacities to remove pharmaceuticals, making them major sources of these micropollutants in rivers and streams. Certain pharmaceuticals such as antibiotics, EDCs, pesticides and PCPs, are of particular concern since emission may foster the development of resistant pathogens discharged into the aquatic environments. To mitigate this problem with the micro-pollutants, many technologies have already been considered as full or pilot plant basis via conventional wastewater treatment and advanced treatment technologies. However, each process has some internal or technological problem even with the new issue of the intermediate compound formation. Also, the development of the proper technology for wastewater treatment is very important to minimise the future global water need that is likely to be one of the most significant challenges of the twenty-first century. Thus, adsorption is a process still widely used for the remediation of diverse types of pollutants. My research will mainly focus on the removal of emerging contaminants such as antibiotics and EDCs using low-cost adsorbents such as biochar, functionalized biochar and their composite.

1.1.1. Adverse Effects of Antibiotic Residues

Antibiotics are the potent medicines that have been used for several decades in both human and animals, for therapeutic treatment of infections related diseases, and for protecting their health [2]. Among the various pharmaceuticals, antibiotic usage has been rapidly increasing all over the world; thus they have received widespread attention [3]. Of particular concern are antibiotic

residues in the environment which can induce antibiotic resistant genes (ARGs) from extended exposure at relatively low concentrations [4]. The past and ongoing usage of antibiotics produces significant residues which are directly or indirectly introduced into the aquatic and terrestrial environments [5], and residues of human and veterinary antibiotics have been detected in many different matrices [6-11]. Antibiotics have different half-lives in the environment, some are highly persistent [12], and therefore their contamination levels in the environment have been increasing. Several studies [13-15] showed significant impacts that exposure to antibiotics (μg L^{-1} – mg L^{-1}) might cause on aquatic organisms in their survival, growth and body weight. Thus pharmaceutical chemicals, especially antibiotics, are gaining the recognition of emerging environmental contaminants as being classified as recalcitrant bio-accumulative compounds [16]. Hence antibiotics are regarded as toxic and hazardous chemicals [15, 17, 18]. Even low concentrations of antibiotics in water can pose severe problems to the ecosystem such as their potential risks of environmental toxicity and promotion of microbial resistance [19-22]. The appearance of the compounds in water results in several side effects such as aplastic anaemia. Aplastic anaemia is a condition that occurs when the human body stops producing enough new blood cells, causing fatigue and a higher risk of infections and uncontrolled bleeding. Different negative effects of chloramphenicol were discovered, e.g., fatal bone marrow depression and aplastic anaemia as reported by Liu et al. [23]. Additionally, antibiotics are responsible for the production of resistant microorganisms, resulting in severe problems of public health such as difficulties in treating pathologies and imbalance of microbial ecosystems [24].

1.1.2. Adverse Effects of EDCs

Phenolic structure based compounds such as the natural estrogens 17β-estradiol (E2), estriol (E3) and estrone (E1), synthetic estrogen 17α-ethynylestradiol (EE2), and industrial compounds such as octyl phenol, nonylphenol, 4-*tert*-butyl phenol (*4t*BP) and bisphenol A (BPA), are the most potent EDCs [25]. EDCs are a large and relatively new group of unregulated compounds [26] and can potentially cause deleterious effects in aquatic and human life at environmentally relevant concentrations (ng L^{-1} to μg L^{-1}) which are becoming a growing concern [27, 28]. ECs concentration may range from a few ng L^{-1} to a few hundred μg L^{-1} [29]. Such concentrations in the aquatic environment may cause ecological risk such as interference with endocrine system of high organisms, sexual differentiation, neurological and immune

systems disturbance, microbiological resistance, and accumulation in soil, plants and animals [30], as these EDCs are not completely removed by conventional wastewater treatment processes [31-33]. They can affect water quality and potentially affect drinking water supplies, ecosystem and human health [32, 34, 35]. Their environmental bioaccumulation exacerbates the abnormal hormonal control causing reproductive impairments, decreased fecundity, increased incidence of breast and testosterone cancers, and persistent antibiotic resistance [36]. EDCs are exogenous substances or mixtures that alter the functions of the endocrine systems and consequently cause adverse health effect in an intact organism, or its progeny or populations [37]. The effects associated with EDCs are breakage of eggs of birds, fishes and turtles, problems in reproductive systems, change in the immunologic system of marine mammals, reduction of sperm of human organ, increase in the incidence of breast, testicle and prostate cancers, and endometriosis [35]. Consequently, the potential long-term effects of EDCs in water are still uncertain and need further investigation.

1.1.3. Removal Technologies of Antibiotics and EDCs

Of the various physical, chemical and biological methods for removing antibiotics and EDCs, adsorption and reduction methods are promising because they are economical and effective, result in less sludge production and therefore, experience minimal disposal problems. These methods are also able to handle shock loadings and operate over a wide range of temperatures and pH. Furthermore, these methods seem to be the most suitable for the following scenarios: small water supplies contaminated by these contaminants because of its simplicity and effectiveness; selective removal in the presence of other ions when adsorbents with selectivity for the contaminant are used; and easy regeneration of adsorbents for multiple reuse and consequently reducing operational costs . Before discharging wastewater into the environment, it is highly important for antibiotic residues to be removed, but it usually involves high cost. Case studies of providing cost-effective solutions for antibiotic removal are urgently needed [38, 39]. Although processes such as advanced oxidation can convert antibiotic molecules into simple compounds or even mineralize them entirely these processes are costly and difficult to maintain for the total removal of compounds including antibiotics at industrial scale. Thus, physicochemical treatment technologies are proving to be a highly suitable treatment option for organic contaminants [24, 40]. The adsorption process is very efficient [40], simple to design and operate; and it is relatively inexpensive and unaffected by the potential toxicity as

for biologically based processes [41]. Adsorption processes are widely used to remove organic contaminants from contaminated stream onto adsorbent surfaces, although its application to antibiotic removal has been reported for around 30 compounds so far. The efficiency of adsorption processes is profoundly affected by the type of adsorbent, adsorbate properties, and the composition of the waste stream [42].

EDCs are poorly removed in sewage treatment plants [26, 28, 43, 44] and are a primary source of their discharge and occurrence in surface water, groundwater, seawater and sediment [26, 45]. EDCs are relatively hydrophobic organic compounds according to their octanol-water partition coefficient (K_{ow}) values and have only one pK_a value. Many separation processes such as coagulation, flocculation and precipitation have been used for the removal of EDCs from different water [28, 44]. Conventional biological processes such as activated sludge, constructed wetlands, bio-filtration have shown limited removal of EDCs [28, 44], while advanced treatment processes such as granular activated carbon, photolysis, photocatalysis, ferrate [26] free radical oxidation, Fenton oxidation, sonolysis, membrane separation, chlorination and ozonation have shown more satisfying results [28, 34, 44, 46]. Some hybrid systems such as membrane bioreactor (MBR) followed by ultrafiltration/nanofiltration/reverse osmosis, flocculation followed by activated sludge and ultrafiltration can also remove EDCs efficiently from water and wastewater [44, 47]. However, a significant problem of hybrid systems is the high capital investment and operation cost. Physical separation processes such as activated carbon adsorption, membrane filtration and ion exchange usually show superior removal efficiencies of the EDC [29, 48]. Adsorption of EDCs on carbonaceous materials has been studied using activated carbon [49-51] black carbon, single- or multi-walled carbon nanotubes (SWCNT, MWCNT) [52, 53] and biochar [26, 54, 55]. Biochar is a low-cost sorbent for the efficient removal of many hydrophilic and hydrophobic organic contaminants [56, 57]. Sorption of EDCs has also been studied using alumina, silica and hydrophobic medium [58].

1.1.4. Removal of Antibiotics and EDCs by Biochar, Functionalized Biochar and Their Composite

Several adsorbents such as ion exchange resins, carbonaceous materials (such as carbon nanotubes or CNTs, graphene, activated carbon, biochar), naturally occurring, agricultural wastes, zeolites, metal oxides and hydroxides, layered double hydroxides, industrial wastes,

biosorbents and other synthetic organic and inorganic compounds have been used by previous researchers to remove antibiotics and EDCs from water [59]. In this study, I used sorption techniques for the removal of antibiotics and EDCs by preparing biochar, functional biochar and its composites. Biochar is a low-cost sorbent. A comparison is shown among activated carbon, carbon nanotubes, biochar and resin (**Figure 1.1)** about the cost of different sorbents. However, most studies have not comprehensively covered the chemical mechanisms and solution factors such as pH. Neither have they investigated the presence of other anions that may influence the adsorption processes and modelling of adsorption.

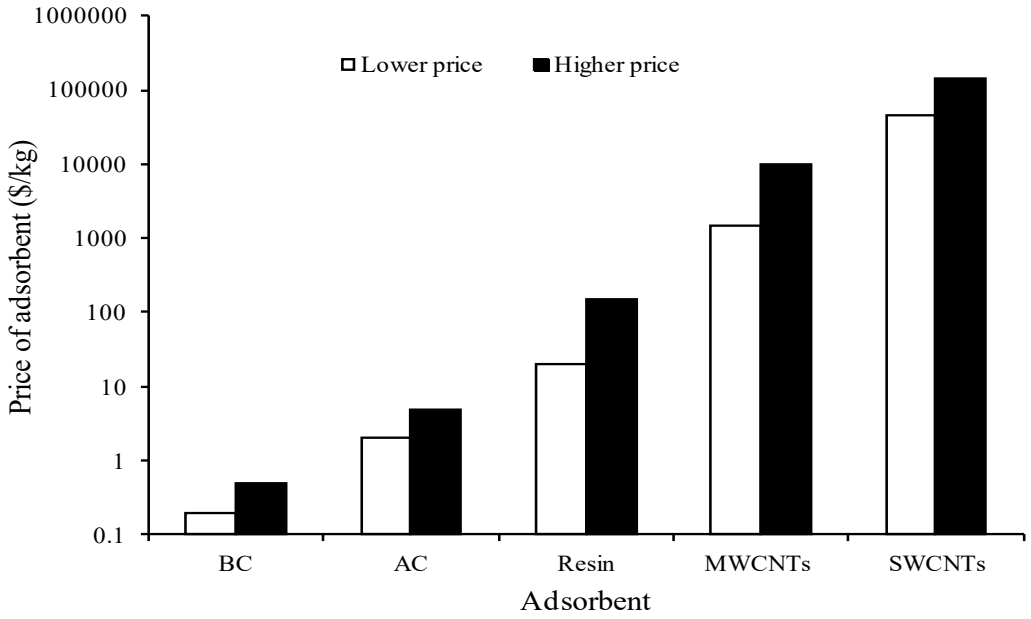

Figure 1.1: The price of different adsorbents [57].

1.2. Research Hypothesis

In this study, I have used woody materials to produce adsorbent for removing pollutants from water and wastewater. Applicability of the adsorbent to wastewater treatment depends on the adsorption capacity, regeneration ability and treatment design. The principal hypothesis for this research is that antibiotics and endocrine disruptors can be effectively removed from water and wastewater using biochar, functionalized biochar and its composites. The following hypothesis is that biochar is an efficient, affordable and sustainable adsorbent. Most of the studies for removal of organic contaminants are based on single component removal mode. In this study,

I focus on both single and competitive sorption of antibiotics and EDCs. Competitive sorption of organic compounds is of great importance, as these kinds of study have rarely been conducted. Therefore, identifying the proper removal mechanism and development of models for competitive sorption are of great importance. With the regeneration of adsorbent and the applicability of biochar and functionalized biochar in water and synthesized wastewater treatment will be economically achievable. These contaminants in wastewater sources must be removed or reduced to avoid environmental and health hazards that can be a by-product of the adsorption process. However, there may be competition for adsorption between anions, cations and other contaminants which needs to be investigated.

1.3. Objectives

The overall aim of this research is to explore, in detail, the mechanisms and applications of antibiotics and EDCs removal by biochar adsorbents in water and wastewater. To achieve this overall aim, this study has set out specific targets as follows:

- Reviewing current studies in the literature on water pollution by antibiotics and EDCs, together with technologies for removing them from the aqueous solution;
- Exploring novel low-cost materials for EDCs and antibiotics removal from water, based on findings in the literature review and conducting experimental studies;
- Determining optimal conditions such as temperature, and modification technique development for adsorbents preparation;
- Characterizing the developed materials in the pre and post adsorption states;
- Conducting parametric studies to determine the factors influencing adsorption processes such as pH, effects of salt, soil, water matrix, desorption, and temperature;
- Eliciting adsorption isotherm and kinetic models of single and competitive solutes of contaminants on the material;
- Evaluating the regeneration of the adsorbents after adsorption of antibiotics from the aqueous solution;
- Investigation of the competitive adsorption of antibiotics and EDCs when they are present at different concentration ratios in synthetic wastewater, Lake water and MBR effluent.
- Modelling of equilibrium adsorption data by using Langmuir, Freundlich and Polanyi-Mani models.

- ❖ Model batch adsorption kinetic data using pseudo-first-order, pseudo- second-order, intraparticle diffusion and boundary layer kinetic models.
- ❖ Design of the reactor for production of adsorbents.
- ❖ Develop a suitable method to regenerate the adsorbents for reuse so that the adsorbent becomes cost-effective.
- ❖ Most importantly, determining adsorption mechanisms of EDCs and antibiotics onto the adsorbent based on literature review, experimental, theoretical and instrumental findings.

1.4. Research Significance

This study especially focused on the use of functionalized biochar (fBC) which is an excellent adsorbent for removing pollutants such as antibiotics and EDCs from water and wastewater. It is the first time that fBC was applied to remove a mixture of antibiotics and EDCs together with the single solute system. In general, the applicability of the adsorbent to wastewater treatment depends on the adsorption capacity, regeneration ability and treatment design. Therefore, considering those factors, fBC is a potentially excellent sorbent for removing antibiotics and EDCs. I have mainly focused on the elucidation of detail understanding of the mechanisms of removal antibiotics and EDCs from different waters such as DI water, synthetic wastewater, lake water and membrane bioreactor (MBR) effluent.

1.5. Thesis Outline

This thesis consists of six chapters as follows:

Chapter 1 named “introduction” presents a context for this study, and identifies the research problem and methods of antibiotics and EDCs removal, together with the research hypothesis, research objectives and their significance. The main tasks to achieve the objectives and scope of this research are also emphasized in details. Chapter 1 is the introductory chapter of the thesis, and explains the background and significance of the PhD research.

Chapter 2 named as “literature review” and offers a detailed review of the relevant scientific literature. Then, the water pollution caused by antibiotics and EDCs (definition, sources, adverse effects and regulations) are discussed. Subsequently, the chapter introduces

technologies for removing antibiotics and EDCs from water and wastewater. Chapter 2 concludes with key findings from the literature review and determines the proper research direction.

Chapter 3 named as “materials and methodologies” and provides the information about materials and methodologies that have been used in this study.

Chapter 4 titled with “antibiotics removal from water and wastewater: mechanisms and applications” refers to four subheadings and each subheading described the removal mechanisms of different antibiotics and application of functionalized biochar and composite materials for different wastewater treatment.

Chapter 5 explores “endrocrine disruptors removal by functional biochar: mechanisms and applications in wastewater treatment” using functionalized biochar as a sorbent. This chapter has two main subheadings. This chapter discussed single and competitive sorption of EDCs with detailed assessment of sorption mechanisms.

Chapter 6 summarizes significant findings of this work for antibiotics and EDCs removal from water and wastewater together with recommendations for future study.

UNIVERSITY OF TECHNOLOGY SYDNEY

Faculty of Engineering and Information Technology

CHAPTER: TWO

LITERATURE REVIEW

CHAPTER TWO: LITERATURE REVIEW

2.1. Introduction

Due to water pollution, climate change and population growth, clean water scarcity is becoming a significant problem for many countries around the world. According to a projection by the International Water Management Institute, a very significant portion of the world is expected to suffer from both physical (1000 m^3 per person/annum renewable water supply) and economic water scarcity by 2025 [60]. Reclamation and reuse of treated wastewaters have become essential themes in the sustainable management of water because many countries are now experiencing severe water shortages. As the global supplies of clean water diminish and demand water rises, advanced wastewater treatment is becoming an international focus for the rational use of scarce water resources and as a means of safeguarding aquatic environments from the harm caused by wastewater disposal.

Australia is at the crossroads regarding its ability to cope with increasing water scarcity in that it has to choose between the more expensive capital and environmental options of more storages and desalination, or minimise these via better water reuse strategies and increased clean water productivity. There are different types of organic and inorganic contaminants responsible for water pollution. Among organic contaminants, antibiotics and EDCs are emerging organic contaminants in water and wastewater, which have to be removed by appropriate water treatment process to produce clean water. This chapter reviews the literature on biochar and modified biochar background for contaminants removal; antibiotics and EDCs in water and wastewater together with their definitions, characteristics, sources, occurrence and their relevant regulations; and their comparative removal technologies. Subsequently, the techniques for removing the pollutants from aqueous solution, focusing on adsorption and reduction methods using low-cost adsorbents are also mentioned and discussed. Finally, chapter 2 summarizes major literature findings and research gaps, which guide the thesis research.

2.2. Antibiotics and EDCs in the Aquatic Environment

2.2.1. Definition, Characteristics, Source, Occurrence and Pollution of Antibiotics in the Aquatic Environment

A. Definition

Antibiotics are defined as a group of compounds that eradicate microorganisms or inhibit their growth [2]. Antibiotics are unique among medicines in that they act selectively on bacteria, among them the pathogens while leaving human cells and tissues unaffected [61]. Nevertheless, the term "antibiotic" can be more broadly defined to incliude antibacterial, antiviral, antifungal and antitumor substances. Most of these chemicals are natural from the microbial origin, however possibly semi-synthetic or totally synthetic [2, 24]. The chemicals are widely used in large quantities to treat bacterial diseases in both humans and animals for therapeutic treatment of infections related diseases, and for protecting their health [62].

B. Characteristics of Antibiotics

Antibiotics can be classified by either their chemical structure or mechanism of action **(Table 2.1**). There are over 250 different antibiotic entities registered for use in human and veterinary medicine [63]. Among the various pharmaceuticals, antibiotic usage has been rapidly increased all over the world. Thus it has received widespread attention [3]. Antibiotics have different half-lives in the environment, some are highly persistent [12], and therefore their contamination levels in the environment have been increasing. The physicochemical properties of antibiotics will affect their distribution in the environment as reported by Kemper (2008) [64].

Some common antibiotics are chosen for the present study including sulfamethoxazole (SMX), sulfamethazine (SMT), sulfathiazole (STZ) and chloramphenicol [65]. SMX, SMT and STZ are a compound belonging to the sulphonamide group, and chloramphenicol is belonged to chloramphenicol class of antibiotic. Concerning the different classes of antibiotics, sulfonamide antibiotics such as sulfamethazine (SMT), sulfamethoxazole (SMX) and sulfathiazole (STZ) are commonly used in human therapy as well as veterinary medicine because they are endowed with broad activity spectrum against Gram bacteria to prevent and control infectious diseases [57, 66]. However, a significant fraction of sulfonamides remains unmetabolised through the digestive system and is released continually to soil and water due to their high water solubility [44, 67]. They can potentially damage aquatic organisms and

impact on human health through the food chain [68]. Therefore, the adverse impact of such compounds has received extensive attention.

On the other hand, chloramphenicol class of antibiotics have been commonly employed in veterinary clinics since the 1950s and effective against Gram-positive and Gram-negative cocci and bacilli. Chloramphenicol, however, has genotoxic effects and causes severe side effects such as aplastic anaemia, leukopenia, agranulocytosis and anaemia [69]. Although chloramphenicol has been banned since the 1990s in many countries for use in food-producing animals, it is still widely used due to its low cost and easy availability [62, 69]. The occurrence and fate of chlorinated pollutants in the environment are recognized as a significant problem due to the adverse effects on human health through the formation of emerging antibiotic-resistant bacteria and antibiotic-resistant genes [70, 71]. The characteristics of SMT, SMX, STZ and CP such are shown in **Table 2.1**.

C. Sources and Occurrence of Antibiotics in the Environment

Antibiotics are widely used both in veterinary and human medicine with annual consumption was 100000-200000 tons [72]. Some of the antibiotics, e.g. chloramphenicol being banned from application to food-producing animals in developed countries, these chemicals are still used in many developing nations due to their low cost, effectiveness, availability and limited or no regulatory guidelines in place [2, 62]. Human and veterinary antibiotics have been detected in different matrices, as observed by Homem and Santos [24]. Recent studies have shown that several antibiotics are detected in surface and groundwater [73]. Most antibiotics enter the environment, notably in the aquatic matrix, through discharge or disposal from medical, municipal, and agricultural sources [73, 74]. **Figure 2.1** illustrates the pathway of antibiotics going into the natural environment through a diversity of sources. The chemicals can contaminate soil, surface and groundwater via runoff or leaching by using manure of livestock, aquaculture, poultry, pets as fertilizer for agriculture production [24]. In the same way, disposal and excretion of households, industry, hospitals and services introduce human antibiotics into the environment [24]. According to Ahmed et al. (2017) [44], most of wastewater treatment plants (WWTPs) and drinking water treatment plants (DWTPs) are not prepared to eradicate high polar micropollutants such as antibiotics. Thus, antibiotics can enter the surface water, groundwater and drinking water [44].

First reports regarding the appearance of antibiotics in water were seen around 40 years ago [75]. According to Homen et al., [24], the presence of antibiotics in environmental matrices

has been investigated. Antibiotics have been detected in several environmental matrices including surface water, groundwater, seawater, drinking water, wastewater treatment plants effluent, hospital wastewater and biosolids [73, 76]. Typically, the concentrations of antibiotics are in the higher mg L^{-1} range in hospital effluents and lower mg L^{-1} range in municipal wastewater and ng L^{-1} in surface, sea and groundwater [24, 73]. According to Adams et al., [75], concentrations of pharmaceuticals in surface water, groundwater and partially treated water are usually less than 0.1 µg L^{-1} and concentrations in treated water are generally below 0.05 µg L^{-1}. For instance, concentrations of chloramphenicol in municipal sewage, the Nanming River and the sediment of Nanming River of Guiyang City, China were reported at 47.4 µg L^{-1}; 19.0 µg L^{-1} and 1138 µg L^{-1}, respectively [23, 65]. The chemical was also revealed in sewage treatment plant effluents and river water at concentrations up to 0.56 and 0.06 µg L^{-1}, respectively [23].

Furthermore, sediments from rivers that are influenced by agricultural activities have higher antibiotics levels than sediments from other areas [77]. Due to the use of manure or sludge as fertilizers, the appearance of antibiotics in soil is also more prevalent. Thus, the findings of these compounds in vegetables and cereals were also reported by Homan et al., [24]. Current literature shows detection of TCs at up to 0.15 µg L^{-1} in groundwater and surface water, 86–199 µg kg^{-1} in the soil, 4.0 mg kg^{-1} in liquid manure, and 3µg L^{-1} in farm lagoons [19]. The antibiotics are very stable in the environment due to their high polarity and non-volatile nature [78].

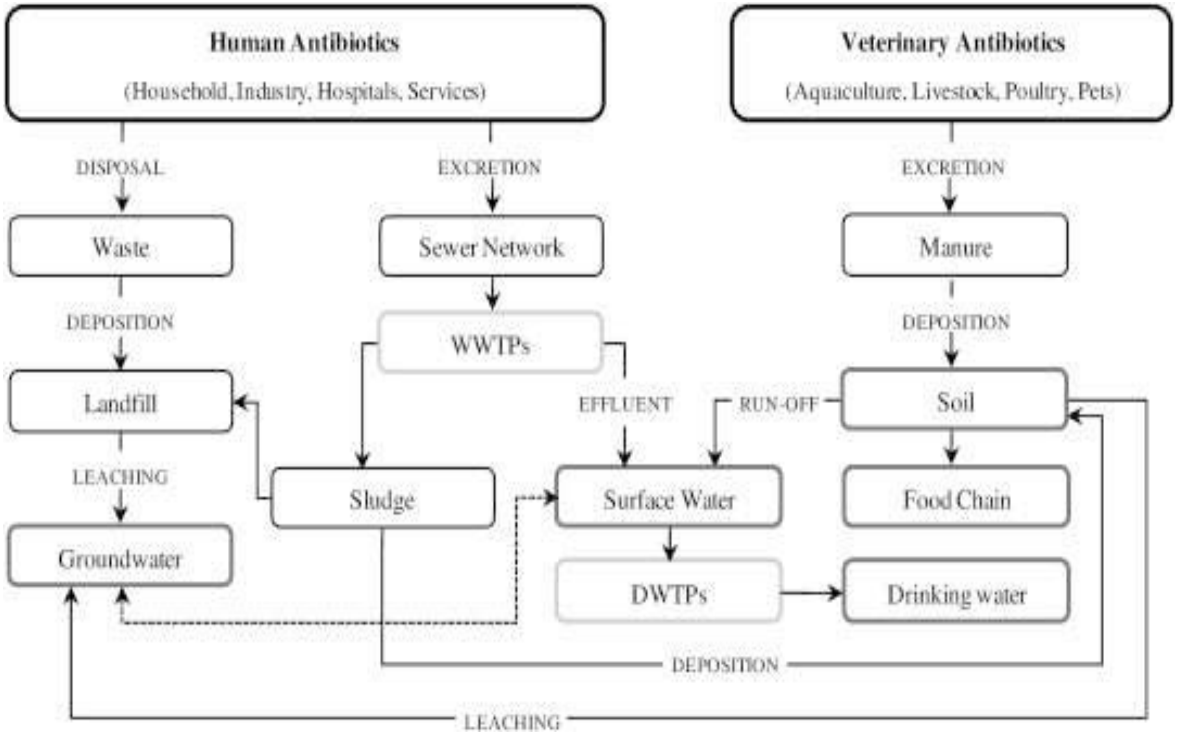

Figure 2.1: Sources of Antibiotics [24].

Table 2.1: Physicochemical properties of major types of antibiotics investigated by different studies.

Class	Compound	Acronym	CAS Number	logk_{ow}[a]	pK_a[a]	Molecular mass	Molecular formula	Reference
Chloramp-henicols	Chloramphenicol	CAP	56-75-7	1.14	n/a[b]	323.13	$C_{12}H_{12}Cl_2N_2O_5$	[79]
	Thiamphenicol	TAP	15318-45-3	-0.27	n/a	356.22	$C_{12}H_{15}Cl_2NO_5S$	
	Florfenicol	FF	76639-94-6	0.37	n/a	358.21	$C_{12}H_{14}Cl_2FNO_4$	
Macrolides	Erythromycin	ETM	59319-72-1	3.06	8.9	731.95	$C_{38}H_{69}NO_{12}$	[79]
	Roxithromycin	RTM	80214-83-1	2.75	9.17	837.05	$C_{41}H_{76}N_2O_{15}$	
Sulfon-amides	Sulfadiazine	SD	68-35-9	-0.34	2.0/6.48	250.28	$C_{10}H_{10}N_4O_2S$	[79, 80]
	Sulfamerazine	SM	127-79-7	0.44	2.06/6.90	264.30	$C_{11}H_{12}N_4O_2S$	
	Sulfamethazine	SMT	57-68-1	0.14	2.65/7.65	278.34	$C_{12}H_{14}N_4O_2S$	
	Sulfamethoxazole	SMX	723-46-6	0.89	1.6/5.7	253.28	$C_{10}H_{11}N_3O_3S$	
	Sulfathiazole	ST	72-14-0	0.05	2.2/7.24	255.32	$C_9H_9N_3O_2S$	
	Sulfapyridine	SP	144-83-2	0.35	2.9/8.54	249.29	$C_{11}H_{11}N_3O_2S$	
Tetracyclines	Tetracycline	TC	60-54-8	-1.37	3.3	444.43	$C_{22}H_{24}N_2O_8.HCl$	[79, 80]
	Chlortetracycline	CTC	64-72-2	n/a	3.3/7.55	515.34	$C_{22}H_{23}ClN_2O_8.HCl$	
	Oxytetracycline	OTC	2058-46-0	-0.9	9.5	496.90	$C_{22}H_{24}N_2O_8.HCl$	
	Doxycyclinehyclate	DXC	24390-14-5	2.37	3.02/7.97	544.98	$C_{22}H_{24}N_2O_9.HCl$	
Flouro-quinolones	Norfloxacin	NFC	70458-96-7	-0.46	3.11/6.10	319.33	$C_{16}H_{18}FN_3O_3$	[80]
	Enrofloxacin	EFC	93106-60-6	0.70	3.85/6.19	359.4	$C_{19}H_{22}FN_3O_3$	
	Ciprofloxacin	CIP	85721-33-1	0.28	6.09	331.34	$C_{17}H_{18}FN_3O_3$	
	Ofloxacin	OFC	82419-36-1	-0.02	n/a	331.34	$C_{18}H_{20}FN_3O_3$	
Imidazoles	Metronidazole, Fenbendazole, Oxfendazole			-0.02-3.9	2.4	171.5-315.3		[81]
β-Lactams	Penicillins, Ampicillin, Meropenem, Cephalosporins, Ceftiofur, Penicillin G, Cefotianm			0.9-2.9	2.7	334.4-470.3		[81]
Others	Carbadox	CARB	6804-07-5	n/a	n/a	262.2	$C_{11}H_{10}N_4O_4$	[80]
	Lincomycin	LNCM	859-18-7	n/a	7.80	443.0	$C_{18}H_{34}N_2O_6S.HCl$	
	Trimethoprim	TRMP	738-70-5	n/a	3.24/6.76	290.3	$C_{14}H_{18}N_4O_3$	

D. Effects of the Antibiotics Pollution on Water

Even low concentrations of pharmaceuticals in water can pose severe problems to the ecosystems due to their potential toxicity and promotion of microbial resistance [19-21, 72]. The appearance of the compounds in water results in several side effects such as aplastic anaemia. Aplastic anaemia is a condition that occurs when the human body stops producing enough new blood cells, causing fatigue and a higher risk of infections and uncontrolled bleeding. While being banned from application to food-producing animals in developed countries, these chemicals are still used in many developing nations due to their low cost, effectiveness and availability [62]. Conventional wastewater treatment methods can not effectively remove antibiotics. Thus, they can accumulate causing a severe problem for the aquatic organism and the ecosystem [62, 82]. Different adverse effects of CP were discovered, e.g., fatal bone marrow depression and aplastic anaemia as reported by Liu et al. [23]. Additionally, Antibiotics are responsible for the production of resistant microorganisms, resulting in serious problems of public health such as difficulties in treating pathologies and imbalance of microbial ecosystems [24].

Among the various pharmaceuticals, antibiotic usage has been rapidly increased all over the world. Thus it has received widespread attention [3]. Of particular concern are antibiotic residues in the environment which can induce antibiotic resistant genes (ARGs) from extended exposure at relatively low concentrations [4]. The past and ongoing usage of antibiotics produce significant residues which are directly or indirectly introduced into the aquatic and terrestrial environments [5], and residues of human and veterinary antibiotics have been detected in many different matrices [6-11, 83].

Antibiotics have different half-lives in the environment, some are highly persistent [12], and therefore their contamination levels in the environment have been increasing. Several studies [13-15] showed significant impacts that exposure to antibiotics ($\mu g L^{-1}$ – $mg\ L^{-1}$) might cause on aquatic organisms on their survival, growth and body weight. The release of antibiotics into the natural water bodies mainly comes from the effluents of municipal sewage treatment plants (STPs) and pharmaceutical manufacturing plants. As reviewed by Michael et al. [84] and Rizzo et al. [85], urban wastewater treatment plants are likely to be hotspots for the release of antibiotics and ARGs in the natural environment. Thus pharmaceutical chemicals, especially antibiotics, are gaining the recognition of emerging environmental contaminants as being classified as recalcitrant bio-accumulative compounds [16]. Hence antibiotics are regarded as toxic and hazardous chemicals [15, 17].

Before discharging wastewater into the environment, it is essential for antibiotic residues to be removed, but it usually involves high cost. Case studies of providing cost-effective solutions for antibiotic removal are urgently needed [38, 39]. Although processes such as advanced oxidation can convert antibiotic molecules into simple compounds or even mineralize them entirely these processes are costly [86] and difficult to maintain for the total removal of compounds including antibiotics at industrial scale.

2.2.2. Definition, Characteristics, Source, Occurrences and Pollution of EDCs in the Aquatic Environment

A. Definition

According to the U.S. Environmental Protection Agency, an endocrine-disrupting compound has been defined as 'an agent that interferes with the synthesis, secretion, transport, binding, or elimination of natural hormones in the body that are responsible for the maintenance of homeostasis, reproduction, development and/or behaviour' [87, 88]. Therefore, EDCs are exogenous substances or mixtures that alter the functions of the endocrine systems and consequently cause adverse health effect in an intact organism, or its progeny or populations [89, 90]. Estrogenic compounds are those who can mimic (or block) the effect of endogenous estrogen, and therefore, represent one class of endocrine disruptors. There are three primary classes of endocrine disrupting chemicals, namely: estrogenic (or anti-estrogenic), androgenic (or anti-androgenic), and thyroidal [91].

B. Characteristics of EDCs

EDCs can be either natural chemical that are found in human and animal food or synthetic chemicals used as industrial solvents or lubricants and their byproducts (e.g. polychlorinated biphenyls, polybrominated biphenyls, dioxins). Other synthetic EDCs include plastics, e.g. bisphenol A, plasticizers, pesticides (e.g. dichlorodiphenyltrichloroethane), fungicides (e.g. vinclozolin) and some pharmaceutical agents (e.g. diethylstilbestrol). However, from different observations, endocrine disruptors can also be categorized into three groups such as (i) pesticides, (II) chemicals in products; and (iii) food contact materials [88, 92]. Considering the structural features of EDC, it is complicated to establish a relationship with them. This is because of the distinct mechanism of action of EDC in the human and animal body. Sometimes

EDCs metabolites are more hazardous than the parent compound itself. Although, some structural features are indicative of endocrine disruption, therefore, not possible to determine whether a compound is an EDC based on its structure [88].

EDCs have been detected in natural environments [16, 93, 94]. EDCs are relatively hydrophobic organic compounds according to their octanol-water partition coefficient (K_{ow}) values and have only one pK_a value. The chemical structures and physicochemical properties of the selected EDCs are shown in **Figure 2.2** and **Table 2.2**, respectively. Phenolic structure based compounds such as the natural estrogens 17β-estradiol (E2), estriol (E3) and estrone (E1), synthetic estrogen 17α-ethynylestradiol (EE2), and industrial compounds such as octyl phenol, nonylphenol, 4-*tert*-butyl phenol (*4t*BP) and bisphenol A (BPA), are the most potent EDCs [25]**.**

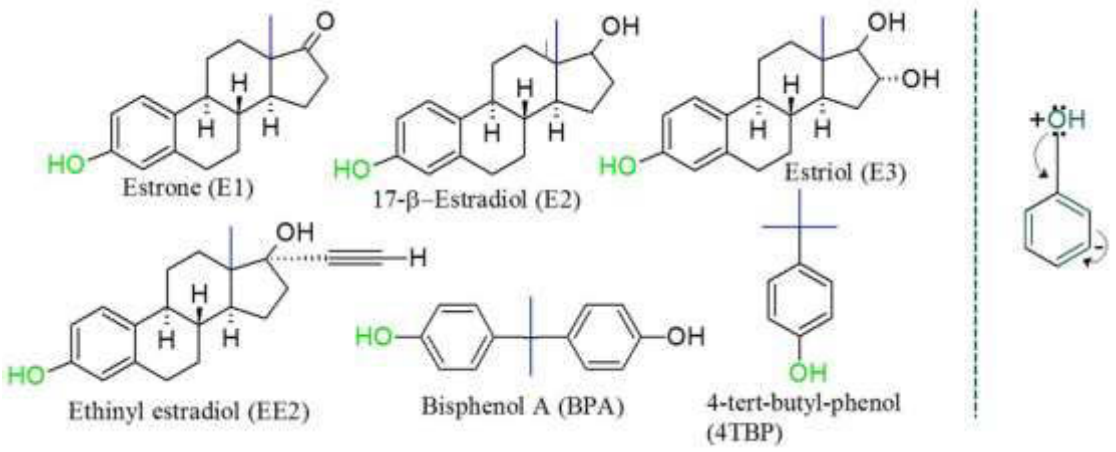

Figure 2.2: Chemical structures of EDCs and resonance form of phenolic group in EDCs.

C. Sources and Occurrence of EDCs in the Aquatic Environment

The sources of EDC exposure are usually diverse and widely distributed throughout the aquatic environment. However, the situation is neither constant nor can be predicted easily since there is a significant usage difference of these substances among the countries. The whole scenario becomes more complicated as some of these EDCs have been banned in some countries while others countries still using especially synthetic EDCs [88]. Human exposure to EDC occurs with environmental contamination of the food chain, especially freshwater fish and meat, contact with contaminated household dust, and occupational exposure [95]. Some chemicals were banned or otherwise removed from production years ago but persist in the environment.

For example, a family of industrial polychlorinated biphenyl compounds generally act as oestrogen mimics and are still found in significant quantities in the environment, although their manufacture in the USA was banned in 1977 [95]. EDCs are high production volume chemicals found in a myriad of household products. Bisphenol A (BPA), for example, is present in polycarbonate plastics, including beverage and food storage containers, epoxy resins that line the interior of metal cans, and in ink used for thermal paper receipts. Synthetic oestrogens from anticonceptional pills, such as ethinylestradiol, are commonly found in surface water, as a result of their widespread use. Thus, exposure to EDCs is ubiquitous and unavoidable, and there is growing concern that living in an EDC contaminated world may be contributing to adverse health trends, such as early puberty and infertility, because of growing evidence that some EDCs can produce varied effects. **Figures 2.3 and 2.4** show the routes of potential exposure of sex steroids from livestock and different exposure routes of EDCs, respectively.

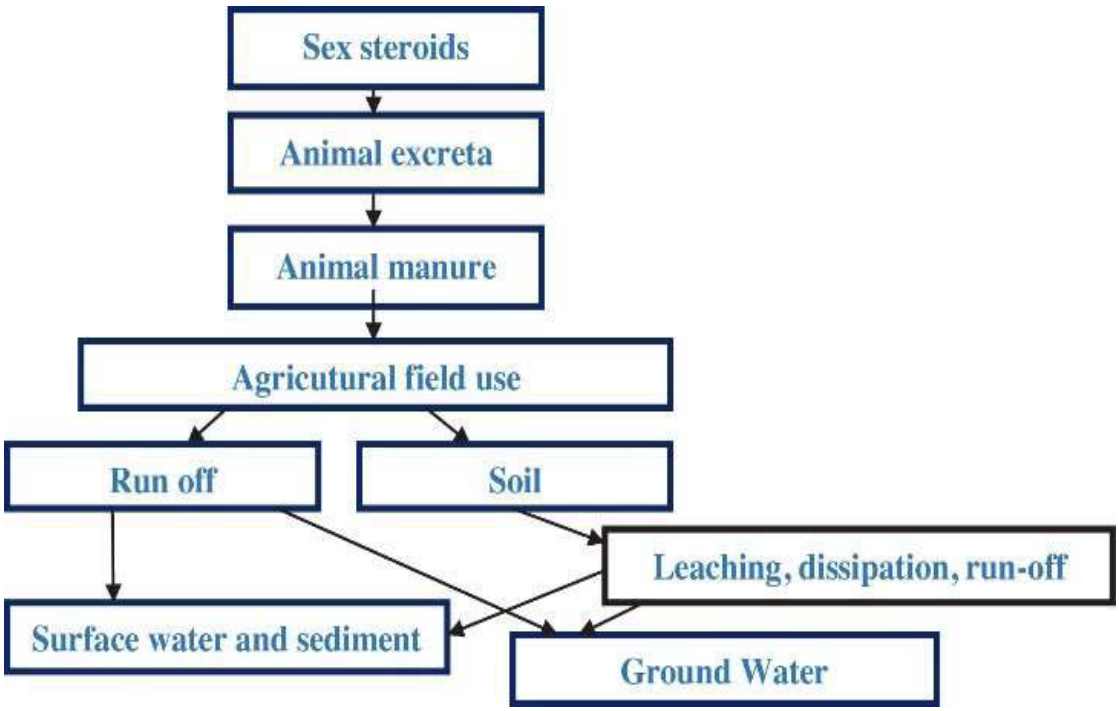

Figure 2.3: Routes of potential exposure of sex steroids from livestock [96].

On the other hand, EDCs as emerging contaminants are ubiquitously present in municipal wastewater effluents. EDCs are the ingredients mostly detected in municipal sewage, daily household products, pharmaceutical production plants, wastewater, hospitals, landfills, and natural aquatic environment [44, 97, 98]. ECs concentration may range from a few ng L^{-1}

to a few hundred μg L^{-1} [98, 99]. Such concentrations in the aquatic environment may cause ecological risk and accumulate in soil, plants and animals as these ECs are not completely removed by conventional wastewater treatment processes [44].

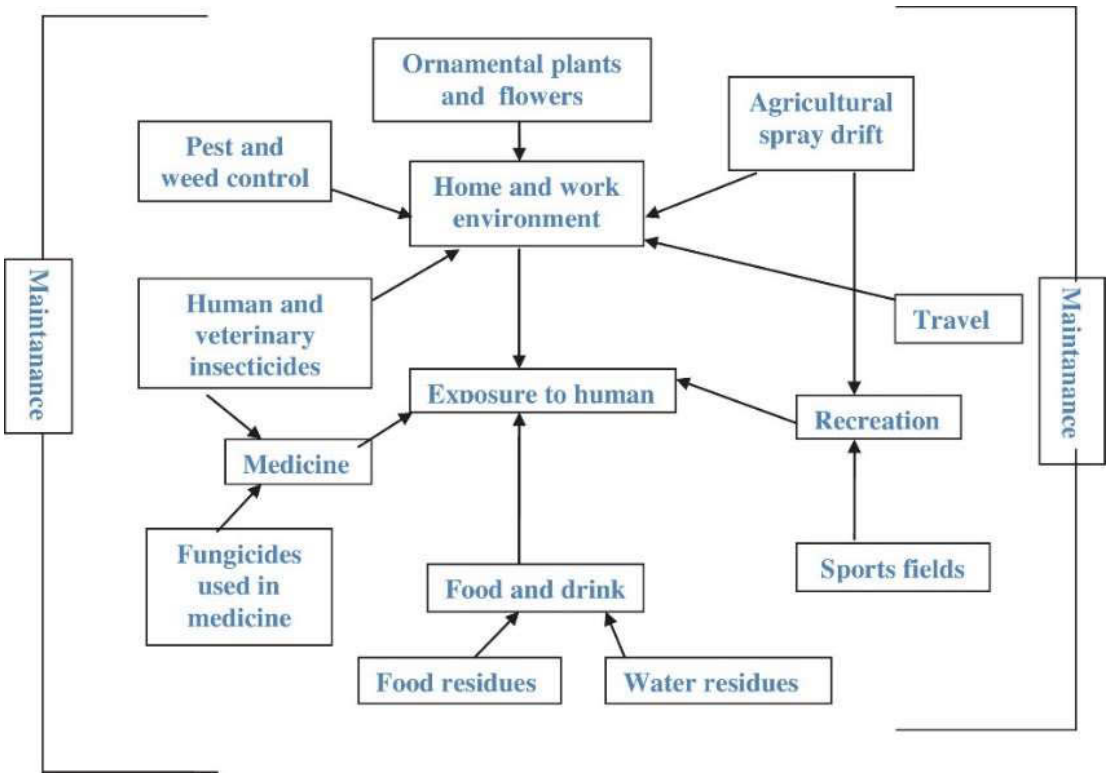

Figure 2.4: Routes of potential exposure to sex steroids from livestock [100].

Table 2.2: Physicochemical properties of the target EDCs.

Compound	Molar mass ($g\ mol^{-1}$)	Molar volume (cm^{-3})	Size of molar volume (nm)	Molar density ($g\ cm^{-3}$)	Volume of molecule (cm^{-3})	*log* K_{ow}	*log* K_{oc}	pK_a	Water solubility ($mg\ L^{-1}$)	Reference
E1	270.37	232.1 ± 3.0	0.321	1.164 ± 0.06	3.85×10^{-22}	3.13-3.43	3.1-3.5	10.34±0.05	30	[27]
E2	272.38	232.6 ± 3.0	0.322	1.170 ± 0.06	3.86×10^{-22}	2.81	3.5	10.46±0.03	13	[27]
E3	288.38	229.6 ± 3.0	0.328	1.255 ± 0.06	3.81×10^{-22}	2.81	3.5	10.38±0.02	13	[27]
EE2	296.40	244.4 ± 3.0	0.331	1.21 ± 0.01	4.06×10^{-22}	3.67-4.20	3.8	10.40	4.7-19	[27]
BPA	228.29	199.5 ± 3.0	0.304	1.143 ± 0.06	3.31×10^{-22}	3.32		9.6-10.02	120	[43]
4*t*BP	150.22	154.5 ± 3.0	0.264	0.971 ± 0.06	2.57×10^{-22}	3.31	3.39	10.16	610	Pubchem

- $\log_{Kow}$ of BPA and *4t*BP was taken from PubChem. Molar mass, molar volume and molar density were calculated using ChemSketch software.
- Apparent size of molar volume (nm) was calculated using equation $apparent\ size = \frac{0.1\times MW^{0.3321}}{2}$.

D. Effects of EDC Pollution on Environment and Aquatic Organisms

EDC is a major research topic, which has been very active over last 15 years, although the effects of EDCs in wildlife have been studied mainly since the 1940s [88]. Endocrine disruption system is a system consisting of many interacting tissues that talk to each other and the rest of the body using signals mediated by molecules called hormones. The hormone is responsible for controlling some processes in the body that start from our early development processes such as cell differentiation for development and bone formation to our adulthood control-ling tissue and organ functions. The human endocrine system is shown in **Figure 2.5**. The endocrine hormone system acts via hormones, which travel through the blood to produce effects on distant cells and tissues via integrated complex interacting signalling pathways usually involving hormone receptors. There are about 50 different hormone and hormone-related molecules (cytokines and neurotransmitter) in humans that integrate and control normal body functions across and between tissues and organs over the lifespan [88, 101].

However, EDCs can cause adverse effects due to exogenous endocrine disruption in the reproductive, sexual differentiation, neurological and immune systems even at low concentrations (ng L^{-1} to μg L^{-1}), and have attracted increasing attention [27, 43]. Exposure in people is typically a result of contamination of the food chain, inhalation of contaminated house dust or occupational exposure. They produce their effects by mimicking, antagonising or altering endogenous steroid levels (androgens or oestradiol, E2) via changing rates of their synthesis or metabolism and⁄or expression or action at receptor targets [95]. The effects associated with EDCs are breakage of eggs of birds, fishes and turtles, problems in reproductive systems, change in immunologic system of marine mammals, reduction of sperm of human organ, including reduced female fecundity, longer time to conception, higher miscarriage rates and decreased sperm motility increase in the incidence of breast, testicle and prostate cancers, and endometriosis [34, 95]. Adverse effects of EDC exposure on reproductive physiology have also been seen in numerous animal models, mainly when exposure occurs early in development. In mammal and other vertebrates, EDC exposure during development alters both male and female gonad development, reduction in sperm counts, abnormal sperm, and changes in sexual behaviour, such as demasculinisation and feminisation of male offspring [95].

Other EDCs effects include:

i. Neurodevelopmental processes because many accumulate in fatty tissues of exposed individuals, are readily transferred across the placenta prenatally, and are expressed in breast milk.

ii. Emotional reactivity and stress responses

iii. Several studies have investigated the effects of EDCs on sexually dimorphic brain circuits

iv. Effect nervous system due to hormonal balance.

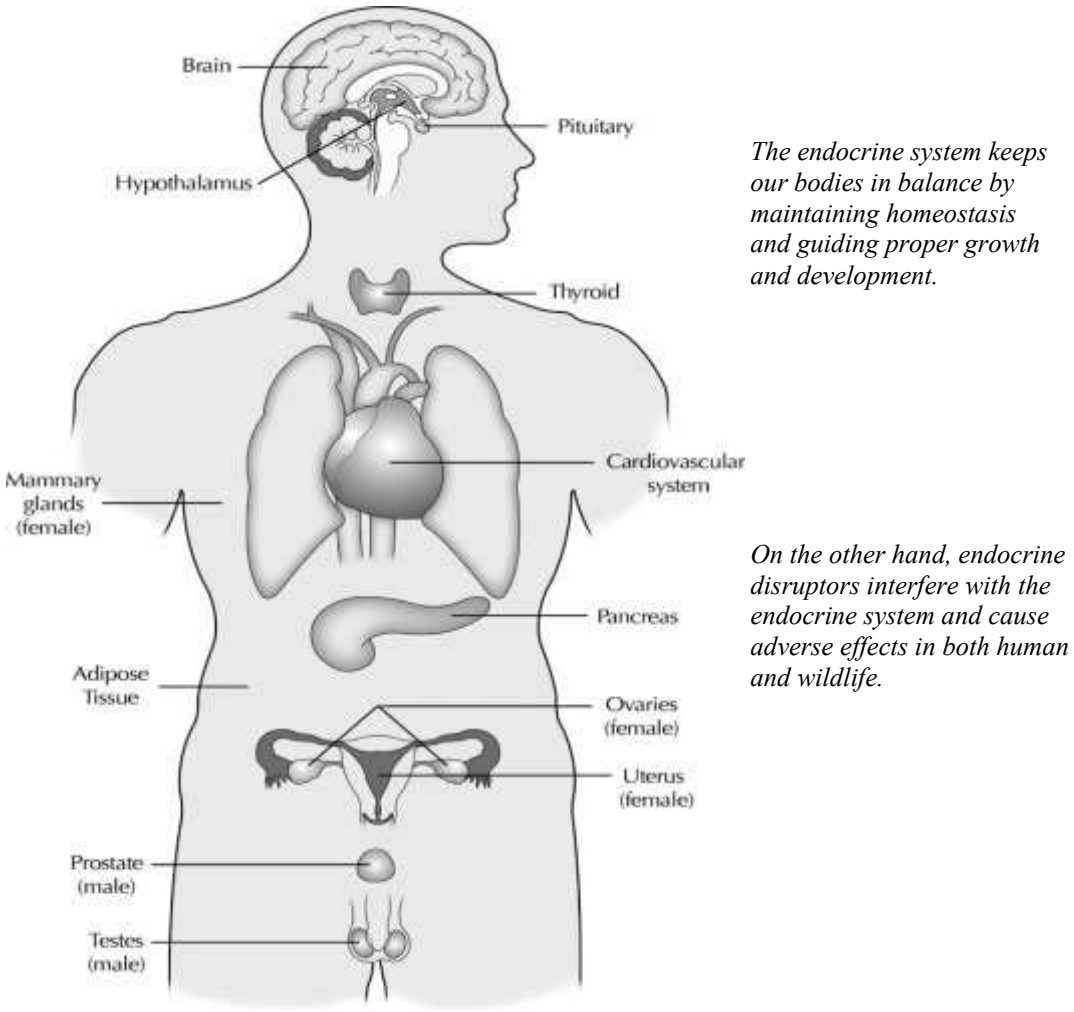

Figure 2.5: Figure demonstrates that all hormone-sensitive physiological systems are vulnerable to EDCs [1].

2.2.3. Relevant Regulations for Antibiotics and EDCs Residues

Emerging contaminant such as pharmaceuticals and specifically antibiotics are generally controlled by stringent regulatory processes and necessarily rigorous preclinical and clinical studies to evaluate their efficacy and safety before commercialization 0.25, 0.01, 0.05 and 0.80 mg L^{-1}, respectively [75, 102]. Therefore, antibiotics are generally better characterized than other environmental pollutants. Several legal limits have set up by the European Union (1990)

for antibiotics in food such as 4-1500 μg kg^{-1} for milk and 25-6000 μg kg^{-1} for other food products, especially from animal origin. However, there is no legislation applied to environmental matrices [24]. At present, different government and non-government organizations including the European Union, the North American Environmental Protection Agency, the World Health Organization, or the International Program of Chemical Safety are considering these problems and setting up directives and legal frameworks to protect and improve the quality of freshwater resources to remove emerging contaminants such as EDCs and antibiotics [34]. The US Environmental Protection Agency established the Endocrine Disruptor Screening Program to identify screening methods and toxicity testing strategies that can be used to determine whether chemicals are endocrine disruptors, but this process is incomplete [103]. The Organization for Economic Co-operation and Development (OECD) is also currently developing methods to identify EDCs. However, there currently is no consensus within the scientific community for a strategy to definitively determine whether a chemical is an endocrine disruptor, and definitions of the term vary. Some naturally occurring and humanmade chemicals are widely considered endocrine disruptors, including certain pharmaceuticals, pesticides, industrial chemicals, combustion by-products, phytoestrogens, and hormones excreted by animals and humans. There are many other chemicals for which there is limited, incomplete evidence of potential endocrine activity or for which the evidence of endocrine activity is controversial. An even higher number of chemicals have not yet been tested for potential endocrine activity using any of the available methods. Additionally, therefore, any list of chemicals defined as EDCs is not exhaustive [90].

2.3. Antibiotics and EDCs Removal Technologies

A variety of different physical, chemical and biological technologies have already been used to remove or degrade the residues of emerging contaminants over the last few decades [29, 104]. Biological treatment technologies are by far the most widely used for emerging contaminants removal, including activated sludge (AS), constructed wetland (CW) [105], membrane bioreactor (MBR), aerobic bioreactor, anaerobic bioreactor, microalgae bioreactor, fungal bioreactor, trickling filter, rotating biological reactor, nitrification, enzyme treatment and biosorption. It has been reported that some non-biodegradable organic micropollutants cannot be sufficiently removed using biological treatment processes. Chemical treatment technologies are also widely used for the degradation of these micropollutants, including

conventional oxidation methods such as Fenton, ozonation, photolysis and advanced oxidation processes (AOPs) such as ferrate, photo-Fenton, photocatalysis, solar driven processes, ultrasound process, and electro-Fenton process. Moreover, some hybrid systems have recently been applied to enhance the removal of a wide range of ECs. The advantages and challenges of different processes for the removal of ECs are outlined in **Table 2.3**. The majority of polar and semi-polar pesticides and pharmaceuticals will remain partitioned in the aqueous phase due to their relatively high water solubility. Hence their removal by physical processes such as sedimentation and flocculation is not effective [106], and has been reported to be less than 10% [107]. On the other hand, a variety of methods to remove antibiotics and other pharmaceuticals from aquatic matrix such as advanced oxidation processes, combined chemical/biological treatment, aerobic digestion integrated with activated carbon, ion exchange, coagulation, flocculation, sedimentation, ultraviolet irradiation, have been attempted [20, 24, 62, 73]. However, it was reported that these conventional methods were moderately ineffective in removing antibiotics from aquatic media [20]. Adsorption using cost-effective adsorbents is considered an effective process that removes antibiotics from aqueous solution [20].

2.3.1. Biological Treatment Technologies

Biological treatment technologies have been widely applied for the removal of ECs predominantly by the mechanism of biodegradation. Biodegradation is the process by which large molecular weight ECs are degraded by microorganisms such as bacteria, algae and fungi into small molecules [108], and even biomineralised to simple inorganic molecules such as water and carbon dioxide. In conventional biodegradation process, microorganisms use organic compounds as primary substrates for their cell growth and induce enzymes for their assimilation [99]. Some ECs are toxic and resistant to microbial growth hence inhibiting biodegradation, in which case a growth substrate is needed to maintain microbial growth for biodegradation, a process known as cometabolism [99]. Biodegradation methods have traditionally been used in wastewater treatment systems for the removal of ECs. They can be divided into aerobic and anaerobic processes. Aerobic applications include activated sludge, membrane bioreactor, and sequence batch reactor. Anaerobic methods include anaerobic sludge reactors and anaerobic film reactors. The wastewater characteristics play a vital role in the selection of biological treatment [97, 109]. The wastewater treatment processes can be broadly classified as conventional processes and non-conventional processes, which are described in subsequent sections.

Table 2.3: Advantages and challenges of different technologies in the removal of ECs.

Treatment process	Advantages	Challenges	Reference
Conventional	A wide range of ECs removal from wastewater	The relatively high cost of operation and maintenance	[32, 35, 110,
Biological activated carbon	Removal of residual disinfection/oxidation products Not generating toxic active products	Regeneration and disposal issues of high sludge Processing of sludge can increase total cost by 50-60%	111]
Microalgae reactor	Resource recovery of algal biomass used as fertilizer High-quality effluent & no acute toxicity risk associated with ECs	Removal efficiencies affected by cold season EDCs cannot degrade properly	[112]
Activated sludge	Lower capital and operational costs than AOPs Environmental friendly than chlorination	Low efficiencies for pharmaceuticals and beta blockers A large amount of sludge containing ECs Unsuitable where COD levels are greater than 4000 mg L^{-1}	[32, 97, 109, 113]
Non-conventional	Low energy consumption and low operational & maintenance costs	Clogging, solids entrapment and sediments formation	[114]
Constructed wetland	High performance on the removal of estrogens, PCPs, pesticides and pathogens	Biofilm growth, chemical precipitation and seasonal dependent Needs large area of lands and long retention time	
MBR	Effective for the removal of biorecalcitrant and ECs Small footprint	High energy consumption and fouling, control of heat and mass transfer High aeration cost and roughness of membrane Pharmaceutical pollutants have low efficiencies	[32, 97, 115]
Chemical process	Reduced turbidity arising from suspended inorganic and organic particles	Ineffective micropollutants removal	[32, 114]
Coagulation	Increased sedimentation rate through suspended solid particles formation	A large amount of sludge Introduction of coagulant slats in the aqueous phase	
Ozonation	Strong affinity to ECs in the presence of H_2O_2 Selective oxidant favouring disinfection and sterilization properties	High energy consumption, the formation of oxidative by-products Interference of radical scavengers	[32, 110]
AOPs	Major ancillary effects on removal of ECs such as EDCs, pharmaceuticals, PCPs and pesticides Short degradation rate	Energy consumption issues, operational & maintenance cost Formation of toxic disinfection by-products Interference of radical scavengers	[32, 110]
Fenton and Photo-Fenton	Degradation and mineralization of ECs Sunlight can be used by avoiding UV light	The decrease of $OH^{\bullet}$ forming chloro and sulfate–Fe(III) complexes or due to scavenging of $OH^{\bullet}$ forming $Cl_2^{\bullet}$ and $SO_4^{\bullet-}$ in the presence of chloride and sulphate ions	[97, 116]
Photocatalysis (TiO_2)	Degrading persistent organic compounds High reaction rates upon using a catalyst Low price and chemical stability of TiO_2 catalyst and easier recovery	Difficult to treat a large volume of wastewater The cost associated with artificial UV lamps and electricity Separation and reuse of photocatalytic particles from slurry suspension	[98]
Physical process	Can remove pathogens	Not fully effective in removing some ECs as pore sizes vary from 100-1000 times larger than the micropollutants The high cost of operation	[97]
Micro- or ultra-filtration	Applicable for heavy metal removal		
Nanofiltration	Useful for treating saline water and WWTP influents Can remove dyestuff and pesticides	High energy demand, membrane fouling and disposal issue Limited application in pharmaceutical removal	[32, 91]
Reverse osmosis	Useful for treating saline water and WWTP influents Can remove PCPs, EDCs and pharmaceuticals	High energy demand, membrane fouling and disposal issue Corrosive nature of finished water & lower pharmaceutical removal	[32, 91, 97]

A. Conventional Treatment Processes

Removal or degradation capacity of ECs depends on the chemical and biological persistence of ECs, their physicochemical properties, the technology used, and operation conditions. For the polar substances, e.g. most pharmaceuticals and their corresponding metabolites, the most important removal process is through the biological transformation or mineralization by microorganisms. The removal rates strongly depend upon the treatment technology, the operation conditions, and target contaminants [117]. The identification of degradation products in environmental samples is a challenging task because not only they are present in very low concentrations but also they are mixed with complex matrices that may interfere with detection [117, 118]. The conventional wastewater treatment plants frequently used techniques such as biological processes, filtration and coagulation/flocculation/sedimentation [24, 73]. The biological process degraded organic compounds in activated sludge tanks and treating large effluent flow rates. However, this technique cannot be applied for treatment of highly toxic pollutants due to their being toxic to microorganisms [24]. The filtration removes the solid particles by passing the wastewater via a filtration media such as sand, coal, diatomaceous earth, granular activated carbon. The disadvantage of filtration is it cannot degrade pollutants, but accumulate it in the solid phase, creating a new waste [119]. Coagulation, flocculation and sedimentation utilizes chemicals to increase the solids sedimentation, pollutants precipitation and colloids formation and is easy to settle down. Nevertheless, the methods achieve low efficiency for removing Antibiotics and need the following treatment to remove the pollutants from water [24].

(i) Biological Trickling Filter

A biological trickling filter is a three-phase system with fixed biofilm carriers. Wastewater enters the bioreactor through a distribution zone, trickles down over the biofilm surface, and air moves upward or downward in the third phase [120]. Bio-trickling filters have been used in wastewater treatment plants for decades in the removal of biochemical oxygen demand [121], chemical oxygen demand (COD), pathogen decontamination, odour and air pollution control, but their application to ECs removal has not become broad practice [122-124]. Trickling filters or biobeds were used either alone or in combination with other treatment processes such as activated sludge. Some bio-processes such as activated sludge, aerated lagoon and trickling filters have reported very different removal efficiencies from almost complete removal to no removal of some pharmaceuticals from different wastewater sources [125]. Kasprzyk-Hordern

et al. [3] monitored 55 pharmaceuticals, PCPs, EDCs and illicit drugs during wastewater treatment by trickling filter and activated sludge processes from South Wales, UK over a period of five months. They concluded that the activated sludge treatment was a much more efficient process than trickling filter beds for the removal of organic micropollutants. Overall, out of 55 pharmaceuticals and PCPs studied only a few were characterised by low removal efficiency (< 50%) during activated sludge treatment. In comparison, the WWTP utilising trickling filter beds resulted in, on average, less than 70% removal of all 55 PPCPs studied with half of them not being removed, while the WWTP utilising activated sludge treatment gave a much higher removal efficiency of over 85% [3, 126]. Hence there is a need to develop or modify the present bio-trickling process to attain higher and steadier removal efficiency for a wide range of ECs.

(ii) Biological Nitrification and Denitrification

Nitrification is the biological oxidation of ammonium to nitrite and nitrate, and denitrification is the biological process which is used to degrade organic compound by the oxidation of nitrate/ nitrite to nitrogen gas [127]. Denitrification process is carried out at anoxic (i.e. absence of oxygen but the presence of nitrate) conditions [128, 129]. Differences in results from recent studies may originate from the variation in operating conditions (hydraulic retention time, sludge retention time, mixed liquor pH and temperature). These kinds of conditions are mostly applied together with MBR for the wastewater treatment. For example, Phan et al. [128] studied ECs removal from wastewater using nitrifying and denitrifying condition in MBR. The sludge retention time was 25 days, and nitrification was carried out by autotrophic bacteria under aerobic conditions and denitrification process carried out under anoxic conditions. The treatment duration was adequate to support the proliferation of both heterotrophic and slow-growing nitrifying microorganisms that sustain high organics removal.

Removal of EDCs such as estrone (E1), 17α-ethinylestradiol (EE2), 17β-estradiol (E3), bisphenol A, 4-*tert*-butylphenol and 4-*tert*–octylphenol and PCPs (such as benzophenone, galaxolide, oxybenze, salicylic acid and tonalide) by denitrification has been found to be 82-100% at μg L^{-1} level influent concentration. The fate of some EDCs and pharmaceuticals by denitrification process was also studied, but the result was not satisfactory [130]. On the other hand, nitrification process was found suitable to remove some ECs such as E1, E2 and EE2, galaxolide, tonalide, ibuprofen, naproxen, erythromycin and roxithromycin. In comparison, applied to same compound removal, denitrification process seems to be more suitable than

nitrification process (denitrification > nitrification) for the removal of ECs (**Table 2.4**). A challenge in the denitrification and nitrification process is the relatively low removal efficiencies for a wide range of ECs, but this process can be integrated with MBR and other processes to improve its removal efficiencies.

Table 2.4: ECs removal efficiency by nitrification and denitrification treatment technologies.

EC category	ECs	Biological treatment technology				Reference
		Nitrification (aerobic reactor)		De-nitrification (anoxic reactor)		
		Influent conc. (μg L^{-1})	Removal (%)	Influent conc. (μg L^{-1})	Removal (%)	
EDCs	EE2	5.5±2.6	87±11	5; 5.8±1.9	93; 20±13	[128, 130]
	E3			5	97	[128]
	E1	6.6±1.4	99	5; 6.4±0.8	100; 72±2	[128, 130]
	17β-estradiol 17-acetate			5	100	[128]
	E2	6.6±1.4	99	5; 6.4±0.8	100; 72±2	[128, 130]
	Bisphenol A			5	86	[128]
	4-*tert*-butylphenol			5	81	[128]
	4-*tert*-octylphenol			5	82	[128]
Antibiotics	Erythromycin	17.7±2.2	89±2	23.9±0.1	20±10	[130]
	Roxythromycin	17.4±5.9	91	18.8±1.2	15±7	[130]
	Sulfamethaxazole	21.1±1.6	22±5			[130]

(iii) Biological Activated Carbon

The accumulation or artificial immobilization of microorganisms under proper temperature and nutrition condition on the surface of activated carbon produces the biological activated carbon. In that case, activated carbon (mostly granular form) acts as a carrier which can exert the adsorption and biodegradation roles simultaneously [131-133]. The mechanism involves the interaction of granular activated carbon particles, microorganisms, contaminants and the dissolved oxygen in solution [134]. In most of the cases, biological activated carbon process is used after ozonation for the removal of contaminants, and biological activated carbon can be part of a tertiary treatment process for reclamation purpose as it can efficiently remove both nitrogen and organic carbon [133]. Such comparative removal efficiencies by filtration, ozonation followed by biological activated carbon are listed in **Table 2.5**, where it can be observed that biological activated carbon process can be more effective in the removal of ECs (ng L^{-1} level) especially pesticides (such as atrazine and triclosan), beta-blocker (atendol) and pharmaceuticals (analgesics, antibiotics, lipid regulator and anti-depressant) when ozonation

process has been carried out first. Biological activated carbon process showed lower efficiency in the removal of some EDCs such as E3, bisphenol A, and octylphenol but did remove 99% of E1 [131]. Thus biological activated carbon process can be very attractive if this process is combined with some oxidation process such as ozonation. Therefore for the removal of ECs, it can be concluded that biological activated carbon process followed the order of pesticides > beta blockers > pharmaceuticals > EDCs > PCPs. As biological activated carbon process was found to be less effective in the removal of EDCs and PCPs including some pharmaceuticals, thus this process should mostly be applied in the hybrid system.

Table 2.5. ECs removal efficiency by biological activated carbon [131].

ECs category	ECs		Treatment technology		
		Influent ($\mu g\ L^{-1}$)	Filtration Removal (%)	Ozonation/H_2O_2 Removal (%)	BAC Removal (%)
EDCs	E1	69	66±18	98±2	99±0.7
	E3	3	71	83	83
	Bisphenol A	43	72	78	78
	Octylphenol	50	42	42	42
Pesticides	Atrazine	3	5±5	69±8	92±2
	Triclosan	203±70	3±5	99±0.5	99±0.2
Beta blockers	Atendol	1267	46 ±11	99±0.7	99±0
PCPs	Atorvastatin	58	6±7	99±0.2	99±0.2
	Benzophenone	233	16±11	56±14	57±16
Analgesics	Carbamazepine	180	-4±3	99	99
	Diclofenac	165	-9	99	99
	Ibuprofen	13	49	83	92
	Naprox	72	-10±12	99±0.2	99±0.1
	Primidone	183			
Anti-depressants	Fluoxetine	44±5	-5±12	99±0.2	99±0.1
Lipid regulators	Gemifibrozil	890	55±11	99	99
Antibiotics	Sulfamethoxazole	443±172	-3±14	98±0.2	99
	Trimethoprim	620	30±5	99	99
Stimulants	Caffeine	43	-89±116	74±19	74±19

(iv) Microalgae/Fungi Based Treatment

Biologically based wastewater treatment by microorganisms (bacteria, algae and fungi) can simulate the ability of natural ecosystems to attenuate pollution from water in a cost-effective and sustainable way. Microorganism based treatment systems have been proved to effectively remove some ECs with the mechanism of degradation and phytoremediation [92, 135]. Microorganisms produce some enzymes which are responsible for the biodegradation of the ECs. For example, some fungi produce extracellular enzymes with low substrate specificity

and are very suitable for the degradation of some ECs even at low water solubility [121]. On the other hand, microalgae (phytoplankton) based wastewater treatment technologies such as high rate algal ponds have high attention due to the resource recovery of algal biomass, use of fertilizer, protein-rich feed or biofuel and high-quality effluent. High rate algal pond is shallow raceway reactors in which microalgae and bacteria grow in symbiosis. Such system is responsible for the degradation of organic matter by heterotrophic bacteria, which consume oxygen by micro-algal photosynthesis. Such system does not require aeration [136]. Some of the ECs such as pharmaceutical antibiotics (azithromycin, erythromycin, sulfathazole, sulfapyridine and sulfamethazine) can be removed up to 100% by fungal reactors. EDCs such as E1, E2 and EE2 can be removed by more than 95% at a concentration level of 1 μg L^{-1} in algae-based polishing pond treatment based system (**Table 2.6**). Microalgae-based treatment system can well remove many types of ECs including EDCs at a concentration level of 9 to 24 μg L^{-1}. Thus microorganism based treatment processes require depth study on the culture and growth of the microorganisms for the efficient removal of ECs. Moreover, to improve its pesticides removal efficiencies, this process can be integrated with biological activated carbon process.

Table 2.6: ECs removal efficiency from WWTPs by different biological treatment technologies.

Categories of ECs	ECs	Biological treatment technology						Reference
		a. Polishing pond (algae)		b. Fungal reactor		c. Micro-algae		
		Influent (μg L^{-1})	Removal (%)	Influent (μg L^{-1})	Removal (%)	Influent (μg L^{-1})	Removal (%)	
EDCs	EE2	1.0	95					[108, 137]
	E2	1.0	95					[108, 137]
	E1	1.0	95					[108, 137]
	Bisphenol A					00-24	85	[112]
	Octylphenol					00-24	93	[112]
Antibiotics	Azithromycin			0.04-84.71	100			[138, 139]
	Ciprofloxacin			0.04-84.71	35			[138, 139]
	Erythromycin			0.04-84.71	100			[138, 139]
	Sulfathiazole	200	36	0.01-0.21	86			[108, 139]
	Sulfapyridine	200	45	0.01-0.21	100			[108]
	Sulfamethazine	200	15	0.01-0.21	91			[108]
	Sulfamethoxazole	200	20					[108]
	Tetracycline	200	89					[108]
	Oxytetracycline	200	93					[108]

(v) Activated Sludge Process

Activated sludge is a process where biomass produced in wastewater by the growth of microorganisms in aeration tanks takes place in the presence of dissolved oxygen [140]. Among all conventional wastewater treatment processes, the activated sludge process is the most widely used and applied in so many ECs removal around the world, and as the proportion of removal by primary setting, chemical precipitation, aerating volatilization and sludge absorption is small, the majority of ECs in wastewater is removed by biodegradation [141, 142]. This process utilizes bacteria and protozoa for treating sewage and industrial wastewaters by the utilization of air and a biological floc. These kinds of microorganisms can break down the organic matter into carbon dioxide, water and other inorganic compounds. It has lower capital cost than advance oxidation processes and generally more environmentally friendly than chlorination process [32, 113]. **Figure 2.6** shows the removal of 102 targets ECs including 23 EDCs, 3 pesticides, 4 beta blockers, 11 PCPs, 10 surfactants, and pharmaceuticals by activated sludge processes [32, 47, 140, 142-148]. Ten types of surfactants have been successfully removed (95-98%) by the activated sludge processes at a concentration of several mg L^{-1}. Higher removal efficiencies of surfactants by activated sludge may be due to their sorption susceptibility toward microorganisms and also degradation nature of the contaminants (**Figure 2.6b**) [140]. Activated sludge process is also very effective in the removal of EDCs in the range of 75-100% (**Figure 2.6a**). Some of the EDCs such as androstenedione, androsterone, EE2, coumestrol, E3, E1, 2 hydroxy estrone (2-OH E1), alpha hydroxyl estrone (α-OH E1), progesterone, testosterone, bisphenol A and octylphenol have highest estrogenic removal up to 100% at 15-700 ng L^{-1} concentration level. This is due to their structure, relative binding, biotransformation and affinity. Thus microorganisms can easily accumulate and degrade such compounds into simpler substances [141, 149]. An environmental condition such as dissolved oxygen is a vital factor for the removal of EDCs and their removal efficiency is higher in aerobic conditions than in anaerobic conditions [150]. Activated sludge is also suitable for the removal of many PCPs at 78-90% although cashmeran, celestolide and 2,4-D are less well degraded (around 60%) due to both sorption and biodegradation [140]. The removal of polar herbicides (atrazine, diuron, and triclosan) and beta blockers (metrolol, atenolol, metoprolol) was found to be poor during activated sludge treatment (**Figure 2.6a**), which was due to adsorption onto suspended solids rather than biodegradation [140]. Activated sludge process based treatment plant with lower retention time has a limited capacity to remove highly polar pharmaceuticals since most of such compounds cannot be metabolized by microorganisms as

a source of carbon and may even inhibit the activity of the microorganisms [140, 151]. But some pharmaceuticals such as stimulant drugs (caffeine, nicotine and paraxanthine) and some metabolites (carbamazepine 10-OH, carbamazepine 2-OH, carbamazepine 3-OH, and carbamazepine–DiOH) were found to be well removed (95-99.9%) from wastewater due to their sorption onto the suspended solids (**Figure 2.6b**). Pharmaceuticals such analgesic ECs can be removed up to 65 to 100%. The removal of pharmaceutical ECs by activated sludge system followed the general order of stimulant drugs > metabolites > analgesics > antibiotics > anti-inflammatory > lipid regulator > NSAIDs > other pharmaceuticals (fluoxetine, iopromide, omeprazole, ranitidine and tamoxifen). Overall trend for ECs removal by activated sludge process can be written as surfactants > EDCs > PCPs > pesticides > pharmaceuticals > beta blockers. Finally, current knowledge about the degradation mechanism in activated sludge is not complete and activated sludge can generate some human and natural metabolites that can be more toxic than the parental compounds [140] which should be carefully addressed. The activated sludge process can also be integrated with ozonation or MBR to improve the removal efficiencies of ECs.

(vi) Aerobic, Anaerobic and Facultative Microbiological Treatment

During wastewater treatment, many ECs are sorbed (if not degraded) to some extent on suspended solids, and as a result, they are found in sludge through sedimentation occurring in primary and secondary clarifiers [152]. Aerobic, anaerobic and facultative bioreactor based biological treatment process is used for the stabilization of excess sludge derived from activated sludge [153-155]. The main mechanism involves bacteria present in the activated sludge consuming ECs and converting them into carbon dioxide. Digestion (anaerobic) is one of the most widely used processes for sludge stabilization where treated sludge is often discharged on the soil or reused for agricultural purposes, and the fate of ECs is mainly governed by ECs molecular structure such as the presence of electron accepting or donating functional groups [156]. If the sludge including ECs is directly used in agricultural, then it may be a threat to the environment and human health [157, 158]. The sludge retention time and temperature may influence degradation of ECs. Some other factors such as microbial population, target compounds bioavailability and co-metabolic phenomena can affect the biodegradation of some ECs [159]. Degradation by aerobic, anaerobic and facultative digesters, ponds, lagoons or bioreactor of different categories of ECs is represented in **Table 2.7** [160, 161], which shows that anaerobic process for ECs degradation has been mostly studied in EDCs removal from

activated sludge. The removal efficiencies ranged from 60 to 100% with high concentrations of ECs [162]. Some of the EDCs such as E2, EE2, bisphenol A and nonylphenol have been found to have high removal efficiencies by aerobic biodegradation process. Pharmaceutical-based ECs have well been removed (65-100%) by the treatment in aerobic lagoons due to an increase of hydraulic retention time [140, 160].

To summarise, conventional treatment systems such as activated sludge, biologically activated carbon and microalgae systems can successfully be applied to some extent for a specific class of ECs removal. More effective and specific treatment is required to reduce the environmental and potential impact of the effluents. Thus these processes can be coupled with other chemical and physical treatment processes such as ozonation, ultrasound, ultrafiltration, and photo–Fenton processes. Also, there is a need to increase our knowledge about the fate of ECs during wastewater treatment for the implementation of better removal technologies. Future work on WWTP will show to what extent ECs can be removed from wastewater and to what extent the implementation of improved technology is feasible, taking into account other micro-pollutants as well as the broad variety of complex matrices.

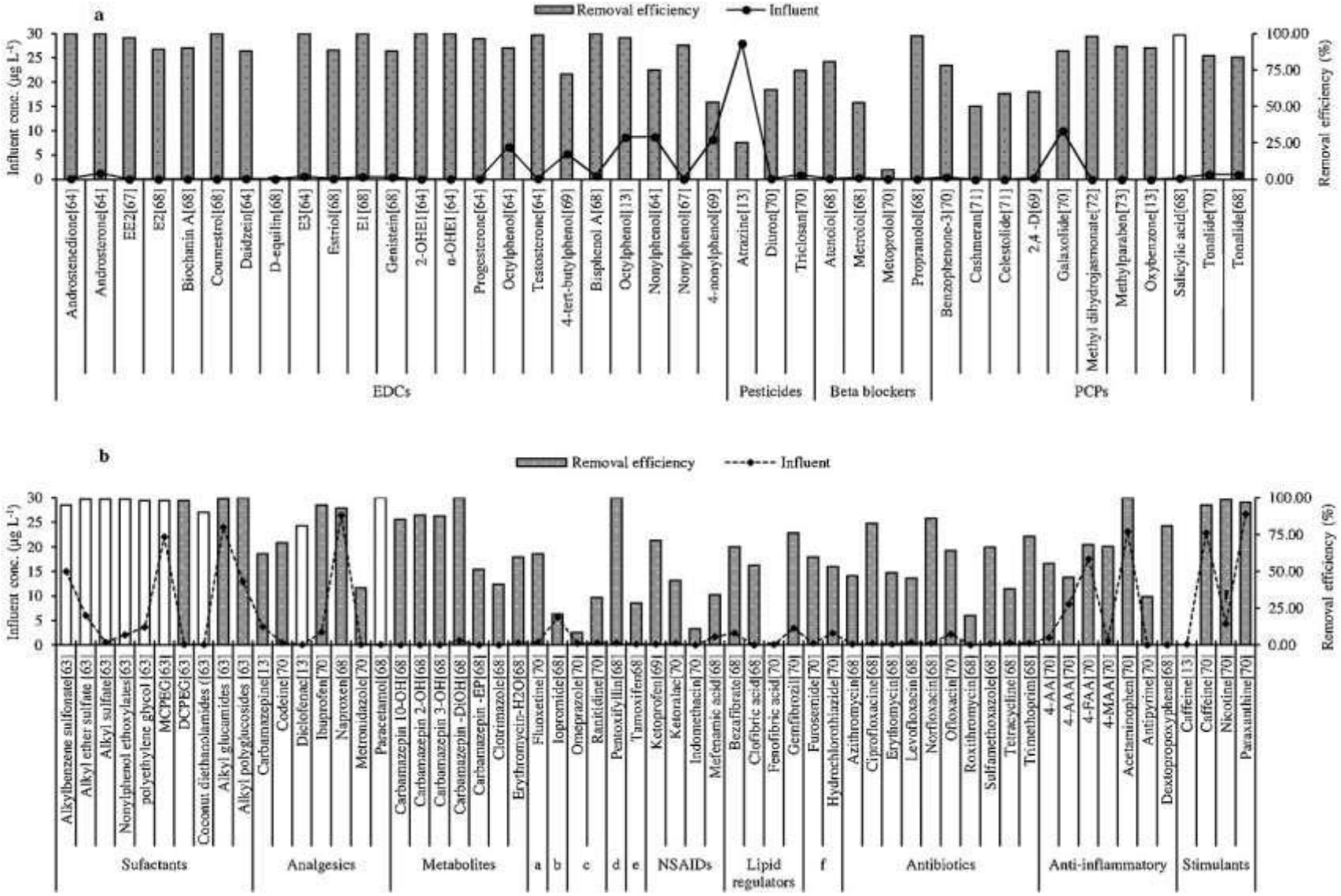

Figure 2.6: ECs removal achieved by activated sludge process with the corresponding reference after the compound name. a = antidepressant, b = contrast agent, c = gastroesophageal, d = vasodilator, e = antineoplastic, f = diuretic. The concentrations are in mg L^{-1} for empty columns.

Table 2.7: ECs removal efficiency by aerobic, anaerobic and facultative processes.

ECs category	ECs	Source	Biological treatment technology				Reference
			a. Influent conc. (μg L^{-1})	Aerobic Removal (%)	b. Influent conc. (μg L^{-1})	Anaerobic Removal (%)	
EDCs	EE2	a. & b. WWTP	0.185	100	X. 04-400 0.185	X. 85 100	[141]
	E2	a. & b. WWTP	0.003-0.226	90-100	X. 04-400 M.0.003-0.226 1000	X. 85 M. 90-100 95	[141, 157]
	E1				X. 04-400	X. 85.00	[157]
	Estrone sulphate conjugate				X. 04-400	X. 36.00	[157]
	Bisphenol A	a. & b. WWTP a. AS/ river water	0.00-0.018	38-99	M. 0.00-0.018 0.05-10.00 100000	M. 38-99 08-22 100	[141]
	Nonylphenol	a. & b. WWTP b. AS	0.381-5.320 350000-388000	85-99 98-99	X. 04-400 M.0.381-0.320 5000	X. 100 M. 85-99 85.5	[141, 154, 157]
	Nonylphenol monoethoxylate				X. 04-400	X. 88	[157]
	Nonylphenol polyethoxylate				X. 04-400	X. 66	[157]
	Nonylphenol diethoxylate				X. 04-400	X. 88	[157]
Antibiotics	Sulfapyridine		Z. 0.03-25.57	Z. 74	X. 04-400	X. 99	[108, 157, 160]
	Sulfamethazine	a. Pharmaceutical and hospital WW	02-05	64-94			[159]
	Sulfamethoxazole	a. Pharmaceutical and hospital WW	Z. 0.03-25.57	Z. 78 64-93	X. 04-400	X. 23	[108, 157, 159, 160]
	Trimethoprim	a. Pharmaceutical and hospital WW	01-05 1	64-96			[159, 163]

B. Non-conventional treatment processes

(i) Biosorption

Biosorption is a biologically based treatment process functioning with a different mechanism than biodegrading process. In biosorption, microorganisms are immobilized onto an adsorbent, and thus sorption and bio-oxidation occur [164]. After that pollutants can passively concentrate and bind onto certain biomass cellular structure. Nguyen et al. [165] compared the role between biosorption and biodegradation in ECs removal from wastewater, by using live cultured and harvested white–rot fungus (*T. versicolour*) and that inactivated by sodium azide. Biosorption based removal of some ECs has been shown in **Table 2.8**. Removal of ECs such as 17β-estradiol-17α–acetate, pentachlorophenol, 4-*tert*-octylphenol and triclosan was achieved by more than 80% as their octanol-water partitioning coefficient (K_{ow}) is high. Banihashemi has also studied biosorption of ECs such as EE2, bisphenol A and benzophenoneand Droste [166] who indicated that the soluble concentration decreased rapidly for selected microconstituents

(triclosan > EE2 > bisphenol A) and the soluble and solid phase concentrations continued to decrease slowly during the length of the experiment which indicates the possible biodegradation of these compound in both phases. The removal of estrogens can occur by a combination of biosorption and biodegradation interactions due to their high K_{ow} values and low biodegradable nature with low Henry's Law constant [167].

Table 2.8: ECs removal efficiency by biosorption and MBR based systems.

Categories of ECs	ECs	Biosorption				MBR		Reference
		Live (fungus)		Inactivated (fungus)				
		Influent (μg L^{-1})	Removal (%)	Influent (μg L^{-1})	Removal (%)	Effluent (μg L^{-1})	Removal (%)	
EDCs	Androstenedione					1.775	99	[168]
	Androsterone					1.775	98	[168]
	E1	50	72	50	31.5	5	96.53	[168, 169]
	E2	50	60.5	50	29.5	5	99.50	[165, 169]
	EE2	50	62	1. 50; 2. 10	1. 38; 2. 76	5	92.85	[165, 169]
	E3	50	4.5	50	13	5	97.56	[165, 169]
	17 β –Estradiol-17-acetate	50	79	50	84	5	99.10	[165, 169]
	Bisphenol A	50	65	1. 50; 2. 10	1. 24; 2. 59	5	94.22	[165, 166]
	4-ter butylphenol	50	33	50	10.5	5	92.76	[165, 169]
	nonylphenol					1.58	98.7	[168]
	Octylphenol					1.725	70.2	[168]
	4 –ter octylphenol		90		82.5	5	96.50	[165, 169]
	4-n-nonylphenol					5	97.18	[169]
	Testosterone					1.85	99	[168]
	Dihydrotesterone					0.82	100	[170]
Antibiotics	Azithromycin					0.142	74.00	[33]
	Clarithromycin					2.722	87.00	[33]
	Erythromycin					0.08	79.00	[33]
	Ofoxacin					2.9	90.00	[33]
	Sulfamethoxazole					0.268; 1.625	69.00; 95.2	[33] [168]
	Trimethoprim					1.55	36.8	[168]

(ii) Membrane Bioreactor

Recently, MBR is widely viewed as being a state-of-the-art technology for municipal and industrial wastewater treatment due to its high effluent quality achieved concerning many ECs [171-174]. MBR can effectively remove a wide range of ECs including compounds that are resistant to activated sludge process and constructed wetland [32, 107, 175]. This can be done due to sludge retention on the membrane surface which can promote microbial degradation and physical retention of all molecules larger than the molecular weight of the membrane. Removal of ECs in MBR system can be affected by sludge age, concentration, and the existence of anoxic and anaerobic compartments, the composition of wastewater, operating temperature, pH and conductivity [32]. Ozonation process is most widely used together with MBR process.

Adsorption and biodegradation were found to be responsible for the removal of ECs by MBR treatment. Adsorption mechanism will be dominating when the log K_{ow} is more significant than 3.2. Highly hydrophobic compounds (log K_{ow} > 3.2) did not accumulate in the membrane, and some compounds with a moderate hydrophobicity accumulate significantly in the solid phase. The results provide a framework to predict the removal and fate of some ECs by MBR treatment [176]. **Table 2.8** shows the removal efficiency of some ECs by MBR system. MBR is better for the removal of 15 target EDCs and their removal efficiencies varied from 92 to 99% at high concentrations (1-5 μg L^{-1}). In comparison to conventional activated sludge process, MBR can remove the higher amount of EDCs from wastewater [165, 166, 168-170, 177]. Some of the pharmaceutical can be well removed while other pharmaceuticals were found to be poorly degraded in MBR [33, 166, 169, 170, 177]. For example, antibiotics (azithromycin, clarithromycin, erythromycin, ofloxacin and sulfamethoxazole), analgesics (carbamazepine, citalopram, ibuprofen, lorazepan, metronidazole, primidone and trazodone), anti-inflammatory drug (acetaminophen) and stimulant (caffeine) were found to be removed by MBR at 75-95%. The removal of other pharmaceuticals (**Table 2.8**) was not satisfactory, although the removal rate of some of them was higher than biosorption process and algal-based polishing ponds treatment process. In general, the removal of some slowly degradable pharmaceuticals such as antibiotics and analgesics in MBRs is better due to the relatively long sludge ages, which leads to the development of distinct microbial communities in MBRs compared to activated sludge plants. However, from the literature results, it could not be concluded that pharmaceutical removal in MBR reactors is better as many other factors have been indicated that may affect biodegradation rates, which are not directly related to the reactor configuration [106]. Other factors such as membrane fouling, clogging, operational failures are still costly compared to constructed wetland and other established technologies [115, 140]. Moreover, scale–up from pilot MBR to industry-scale WWTPs should also be investigated to assess if the processes and ECs elimination in the pilot plants are still valid in large scale operations.

(iii) Constructed Wetland

A constructed wetland (CW) is a biologically based wastewater treatment engineered system that is designed and constructed to reproduce the processes occurring in natural wetland within a more controlled environment. Constructed wetland based wastewater treatment is achieved through an integrated combination of biological (biodegradation), physical (sorption) and

chemical (oxidation) interactions among plants, substrate and soil [114]. Soil acts as the primary supporting material for plant growth and microbial films. Moreover, the soil matrix has a decisive influence on the hydraulic processes. Both chemical soil composition and physical parameters such as grain-size distributions, interstitial pore spaces, effective grain sizes, degrees of irregularity and the coefficient of permeability are all important factors influencing the biotreatment system [178]. A constructed wetland is classified as subsurface/surface flow (SFCW), horizontal flow (HFCW) and vertical flow (VFCW) systems according to their wastewater flow regime (**Figure 2.7**) [113] [179]. Moreover, a constructed wetland can be combined to form hybrid systems to take advantage of the characteristics of each different system [108]. ECs removal efficiencies by differently constructed wetland are shown in **Table 2.9**. EDCs such as E1, E2, EE2, steroid estrogens, bisphenol A, and phthalates can be successfully removed by 75-100% [114, 180].

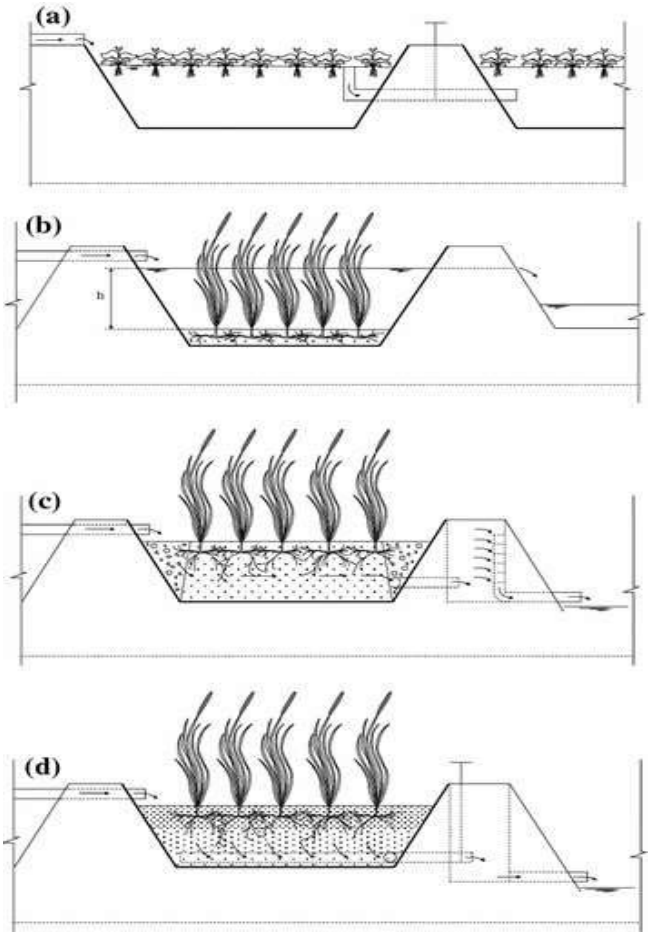

Figure 2.7: Constructed wetland for wastewater treatment. a CW with free-floating plants (FFP). b CW with free water surface and emergent macrophytes (FWS). c CW with horizontal subsurface flow (HSSF, HF). d CW with vertical subsurface flow (VSSF, VF) [113].

Table 2.9: ECs removal efficiency by different CW processes.

Categories of ECs	ECs	Source	CWs treatment technologies								Reference
			c.	CWs	d.	HFCW	e.	VFCW	f.	SFCW	
			Influent (µg L^{-1})	Removal (%)	Influent (µg L^{-1})	Removal (%)	Influent (µg L^{-1})	Removal (%)	Influent (µg L^{-1})	Removal (%)	
EDCs	EE2	a.WWTP	0. 59- 6.56	75.3-94			X. 0.39-1.00	X. 75			[114, 180]
	E2	a.WWTP	1.35- 9..05	84-99			X.0.39- 1.00	X. 84			[114, 180]
	E1	a.WWTP	0..39-10.5	67.8-95.8			X.0.39-1.00	X. 68			[114, 180]
	Steroid estrogens	a.WWTP	0.164-0.259	100							[114]
	Bisphenol A	a.WWTP. c. Urban WW	0.05-0.3	80-100	Z. 0.1-56 M. 1.8	Z. 99 M. 89	M. 4.06	M. 47.78	1.35	100	[114][111-113]
	Diethylphthalate	a.WWTP	0.151-3.788	80-100							[114]
	Di-n-butylphatalate	a.WWTP	0.043-6.134	100							[114]
Antibiotics	Amoxicillin				Y. 0.06-46	Y. 21-45			Y. 0.06-46	Y. 27-42	[181]
	Ampicillin								Y. 0.06-46	Y. 32.00	[181]
	Clarithormycin				Y. 0.06-46	Y. 31-39			Y. 0.06-46	Y. 11-32	[181]
	Doxycycline				Y. 0.06-46	Y. 71-75			Y. 0.06-46	Y. 62-65	[181]
	Erythomycin				Y. 0.06-46	Y. 64					[181]
	Monensin								Z. 100-1000	Z. 21-37	[182]
	Sulfamethoxazole				Y. 0.06-46	Y. 80-87			Y. 0.06-46	Y. 59-71	[181, 183]
									Z. 0.01-0.90	Z. 15-80	
	Sulfadimethoxine				Y. 0.06-46	Y. 99			Y. 0.06-46	Y. 67-99	[181]
	Trimethoprim				Y. 0.06-46	Y. 92-99			Y. 0.06-46	Y. 65-88	[181]

Here, X. Microcosm Y. Mesocosm, Z. Pilot and M. Full plant, HFCW = Horizontal flow constructed wetlands, VFCW = Vertical flow constructed wetlands, and SFCW = Surface flow constructed wetlands.

Surface flow CW has been found effective for the removal of pesticides, beta blocker such as mecoprop, MCPA, terbuthylazine and triclosan from 80% to 100%. The constructed wetland also showed an excellent removal capacity for pharmaceutical ECs. Full-scale surface flow constructed wetland has pronounced effect in the removal of analgesics from wastewater [184]. On the other hand, HFCW was found to be better than SFCW for the removal of antibiotics from wastewater. Overall removal efficiencies based on the effluent quality by constructed wetland can be written as EDCs (constructed wetland) > pharmaceuticals (HFCW > SFCW > VFCW). Constructed wetland technology can be successfully applied for small communities for the remediation of a wide range of ECs but it will not difficult to use it in large cities due to lack of space to perform such wastewater treatment processes [185]. Moreover, the future applications of constructed wetland can be due to high costs of other technologies such as MBR, ultrafiltration and oxidation processes, or the removal efficiency was not satisfactory for a wide range of ECs.

(vi) Comparison of Different Treatment Technologies

Biological treatment processes can be applied to remove a wide range of ECs from wastewater. The comparison of different biological based conventional and non-conventional treatment processes is carried out regarding their average removal efficiencies, and this relationship is represented in **Figure 2.8.** EDCs based ECs can well be removed by MBR and activated sludge processes. The general trend for the average removal of EDCs can be written as MBR > activated sludge > aerobic > Constructed wetland > microalgae > biological activated carbon > anaerobic process. However, a wide range of EDCs can be removed by activated sludge. Pesticides can be well removed by biological activated carbon-based treatment technologies. The average removal efficiencies of pesticides by different biological processes decreased as biological activated carbon > microalgae > constructed wetland > MBR > activated sludge. Beta-blocker ECs can be comparatively better removed by MBR process, and the order of different biological processes can be organised as MBR > aerobic > activated sludge (**Figure 2.8**). The application of other biological processes in the removal of beta-blockers was not studied sufficiently. Average removal efficiencies of different PCPs based ECs were found to be better removed by MBR processes. Based on the average removal efficiencies by biological treatment processes, PCPs followed the trend of MBR > microalgae > constructed wetland > activated sludge > biological activated carbon > anaerobic process. Surfactant-based ECs can be well removed by activated sludge. Surfactants removal by other biological processes has not been studied extensively. On the removal of pharmaceutical-based analgesic ECs,

biological activated carbon and aerobic processes were found to be better processes. Activated sludge process was found to be less effective in the removal of pharmaceutical-based analgesics. Average removal efficiencies of analgesic ECs by different biological processes can be written as aerobic > biological activated carbon > microalgae > constructed wetland > MBR > anaerobic > activated sludge. Some of the pharmaceutical lipid regulators and anti-inflammatories were found to be removed by activated sludge only. The average removal efficiency of antibiotics was found better removed by biological activated carbon process. The general trend of different antibiotics removal followed the order of biological activated carbon > aerobic > MBR > anaerobic > constructed wetland > activated sludge. Finally, some of the miscellaneous pharmaceuticals can be better removed by microalgae process, as represented in **Figure 2.8**.

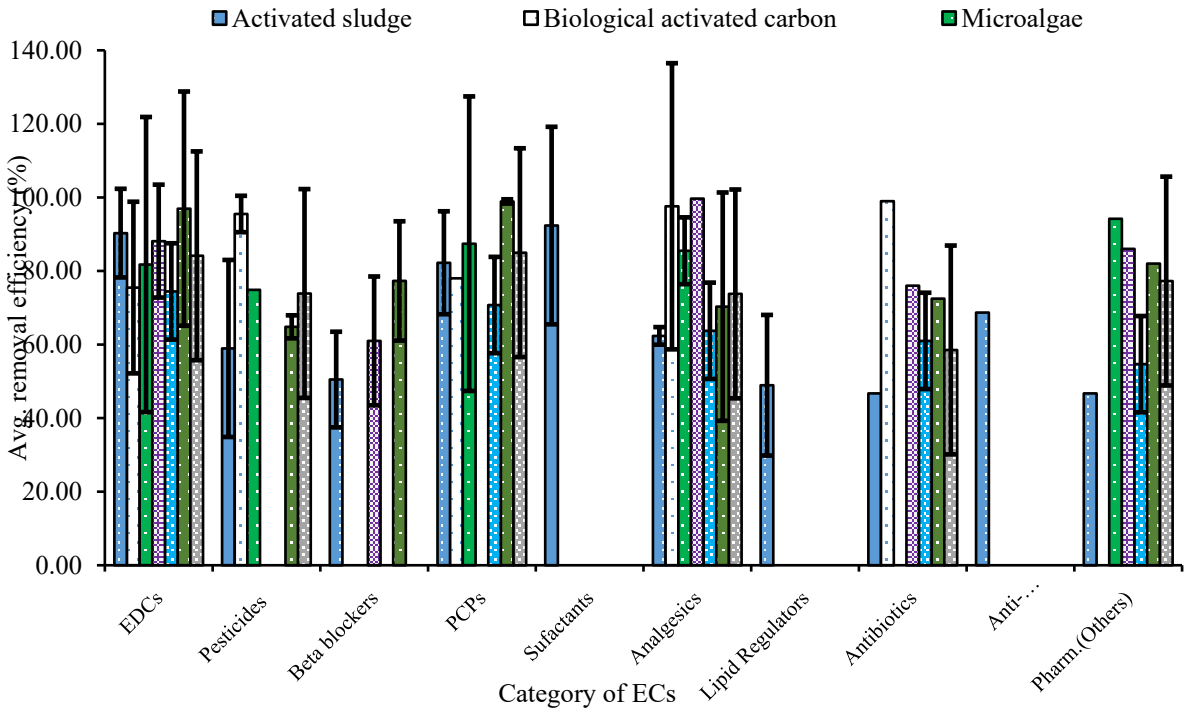

Figure 2.8: Comparative average removal efficiency of ECs with standard deviation (error bar) for wastewater treatment (activated sludge, biologically activated carbon, microalgae, MBR and constructed wetlands) and sludge treatment (aerobic and anaerobic).

2.3.2. Chemical Treatment Technologies

Biological-based wastewater treatment systems can be useful in removing much class of antibiotics depending on the type of the wastewater treatment process. For example, polar pharmaceuticals and beta blockers showed variable removal efficiencies in different biological

processes. Therefore, alternative treatment technologies can be considered with the intention of finding suitable polishing techniques to remove ECs further. These technologies are broadly defined as aqueous phase oxidation methods based on the intermediary of highly reactive chemical species [186]. Oxidation reactions have primarily been used to supplement rather than replace conventional systems and to enhance the treatment of ECs [187]. A chemical agent such as chlorine, UV radiation, hydrogen peroxide, ozone, as well as the combination of these oxidants including transition metals and metal oxides based catalysts in the so-called advanced oxidation processes (AOPs) are required for chemical oxidation of ECs from wastewater. Also, an energy source such as ultraviolet-visible radiation, electric current, solar, gamma-radiation and ultrasound are also used [188]. Oxidations of ECs are based on the production of free radicals, in particular, the hydroxyl radical and facilitate the conversion of pollutants to less harmful and more biodegradable compounds [188, 189]. The ultimate aim of chemical oxidation is the mineralisation of pollutants, with conversion to carbon dioxide, water, nitrogen and other minerals. Rate constants for most reactions involving hydroxyl radicals in aqueous solution are usually in the order of 106-109 M^{-1} s^{-1} [116]. Chemical oxidation processes may change a compound's polarity and the number of functional groups which affect the functionality of the pharmaceutical in the body.

A. Conventional Oxidation Processes

(i) Chlorination of Antibiotics and EDCs

Chlorine gas or hypochlorite has often been used for disinfecting the drinking water in the post-treatment stage because of its low cost and high efficiency [190]. Recently, chlorinated species such as chlorine, chlorine dioxide, and hypochlorous acid were also utilized for treating wastewater containing pharmaceuticals. Due to its oxidizing power, chlorine oxidizes them to readily biodegradable and less toxic compounds [191]. Most of the chemical oxidation processes have demonstrated high effectiveness in the degradation of ECs present in wastewater system which is oxidized to readily biodegradable and less toxic compounds. Sometimes less reactive species such as chlorine (gaseous chlorine and hypochlorite) and bromine have also been used in wastewater treatments. The effect of chlorine on the removal of some ECs has been carried out by Noutsopoulos et al. [192] using 1000 ng L^{-1} of each ECs pollutant after exposing initial chlorine dose of 11 mg L^{-1} for 60 min. The maximum removal efficiencies were 95% and 100% respectively for naproxen and diclofenac. The removal of

EE2 by chlorination was found to be up to 100% within 10 min [193]. The removal efficiencies of other ECs such as nonylphenol, nonylphenol mono-ethoxylate, nonylphenol diethoxylate, bisphenol A, triclosan, ibuprofen, and ketoprofen ranged from 34% to 83%. Removal of some ECs may be enhanced using increased chlorine dose or extended contact time as well as chlorination is affected by pH [194]. Moreover, on the removal of some ECs such as amitriptyline hydrochloride, methyl salicylate and 2–phenoxyethanol revealed that the reaction rate of chlorination process efficiency was three orders of magnitude lower than that of ozonation process [195]. Also, chlorine and chlorine dioxide are potent oxidants which may produce some sub-products during wastewater treatment, and the degree of mineralization achieved is not acceptable [35].

(ii) Oxidation of Antibiotics

One of the alternative treatment methods for removing antibiotics from aqueous solution is oxidation and advanced oxidation processes. The methods use oxidation reagent or oxidants to oxidize the pollutants to less toxic compounds. Oxidants were used such as chlorine and molecular ozone. Advanced oxidation processes are oxidative methods based on the generation of intermediate radicals, the hydroxyl radicals ($OH^{\cdot}$), which are extremely reactive and less selective than chlorine or molecular ozone. The advanced oxidation processes are very useful to treat many organic pollutants [196].

(iii) Ozonation of Emerging Contaminants Inclduing EDCs

Ozone is a potent oxidant that reacts selectively with double bonds and aromatic rings of ECs with a high electron density [197]. Due to its selective reaction with nucleophilic molecules, molecular ozone can oxidize organic compounds which have carbon-carbon double bonds, aromatic bonds or nitrogen, phosphorous, oxygen or sulphur atoms [189]. Ozonation is also an AOP which involves the direct reaction of ECs with ozone molecule through the action of secondary oxidants such as hydroxyl radical produced from ozone in aqueous solution [35, 198]. This increases the oxidation capacity. Ozonation has been implemented as the principal treatment method or to enhance the biodegradability and efficiency of subsequent treatment. Ozone production is an energy-intensive process, therefore making it costly to implement. An ozone treatment system may increase the energy demand over a conventional wastewater treatment plant by 40-50%. The use of ozone as a means of breaking down pharmaceuticals in

wastewater has been the subject of numerous studies over the last 10 years [97]. Ozonation has shown a broad range of effective removal of ECs, and in general, this process can remove all types of ECs by 90% to 100% (**Figure 2.9**). From **Figure 2.9a,** it can be seen that ozonation process has pronounced effect in the degradation of EDCs such as E1, E3, E2, EE2, bisphenol A and nonylphenol at a high concentration level (up to 50 μg L^{-1}) with a removal efficiencies of 100% except E1 (90%). This may be due to the high K_{ow} and high susceptibility of EDCs toward degradation by ozonation [34, 198]. A degradation of 95-100% of pesticides including alachlor, atrazine, chlorfenyvinphos, diuron and isobroturum rapidly occurred even at higher concentration level (up to 18 mg L^{-1}). However, 2,4-D and diazinon have shown less tendency toward ozonation oxidation process [199]. Many pharmaceuticals were found to be effectively removed by ozonation except perindopril, phenytoin, sertraline, and ketoprofen (**Figure 2.9b**) [34, 200, 201].

Figure 2.10a shows the removal efficiencies of antibiotics and other ECs by ozonation in the presence of hydrogen peroxide. Pesticides, pharmaceuticals and beta blockers can be very successfully removed up to 97-100% by the ozonation process in the presence of H_2O_2 at environmental relevant concentration [34, 198]. The problem with ozonation is the high energy consumption, the formation of some oxidative byproducts and interference of radical scavenger [110] [32]. Thus, these are the matters which need to be considered for future ozonation research.

(iii) Fenton Process

Fenton is an oxidation process that involves reactions of hydrogen peroxide in the presence of iron to produce hydroxyl radicals [202] [203]. Since iron is abundant and non-toxic, Fenton reactions are a viable option for wastewater treatment. Its oxidation enhances oxidation power of H2O2 to $OH^{\cdot}$, and the chain reactions of Fenton chemistry can be represented as:

$$Fe^{2+} + H_2O_2 \rightarrow Fe^{3+}\ OH^{\cdot} + OH^{-} \qquad (2.1)$$

$$Fe^{3+} + H_2O_2 \rightarrow Fe^{2+} + HO_2^{\cdot} + H^{+} \qquad (2.2)$$

Ferrous ion can be regenerated from Fe(III) through above reaction [204]. However, reaction 2.2 is much slower than reaction 1. As a result, Fe(III) accumulates in the solution and then precipitates as $Fe(OH)_3$ sludge [204]. Thus the removal of Fe from solution can decrease the process efficiency. Moreover, it requires a large number of reagents that increases the operational costs. Another drawback of traditional Fenton process is the consumption of formed $OH^{\cdot}$ by hydrogen peroxide and ferrous ions according to following reactions.

$$OH^{\cdot} + Fe^{2+} \rightarrow Fe^{3+} + OH^{-} \quad (2.3)$$

$$OH^{\cdot} + H_2O_2 \rightarrow H_2O + HO_2^{\cdot} \quad (2.4)$$

At high reagent concentrations, these reactions can strongly hinder the efficiency of the process since $HO_2^{\cdot}$ formed is a weak oxidant compared to $OH^{\cdot}$. For the remediation of ECs in wastewater the iron concentrations used, normally added as ferrous sulphate, are commonly in the range of 10–50 mg L^{-1}. As hydrogen peroxide is consumed in the reaction, the added amount of this reagent is strongly dependent on the amount of organic matter and on the intensity of treatment that is required. **Figure 2.11** shows the removal of some ECs using only Fenton process. By applying only Fenton process, the removal of ECs was not satisfactory compared to other oxidation processes such as photo-Fenton and ozonation (**Figure 2.11a**). Thus it requires adding some other compound such as hydrogen peroxide or using a catalyst, solar or any other light source to promote the ECs removal from wastewater.

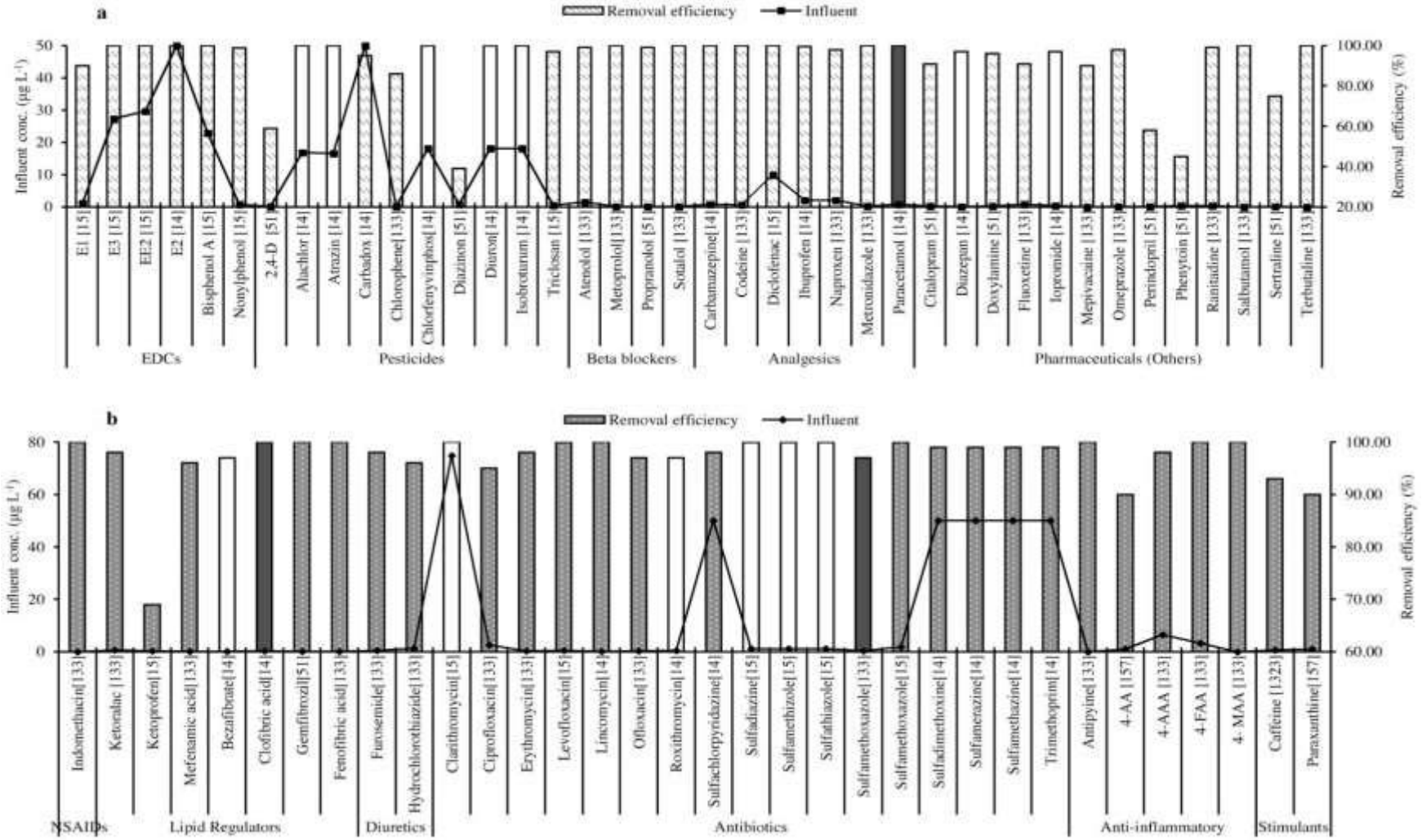

Figure 2.9: ECs removal efficiencies achieved by ozonation process with the corresponding reference after the compound name. Concentrations are in mg L^{-1} for empty columns and in g L^{-1} for dark columns.

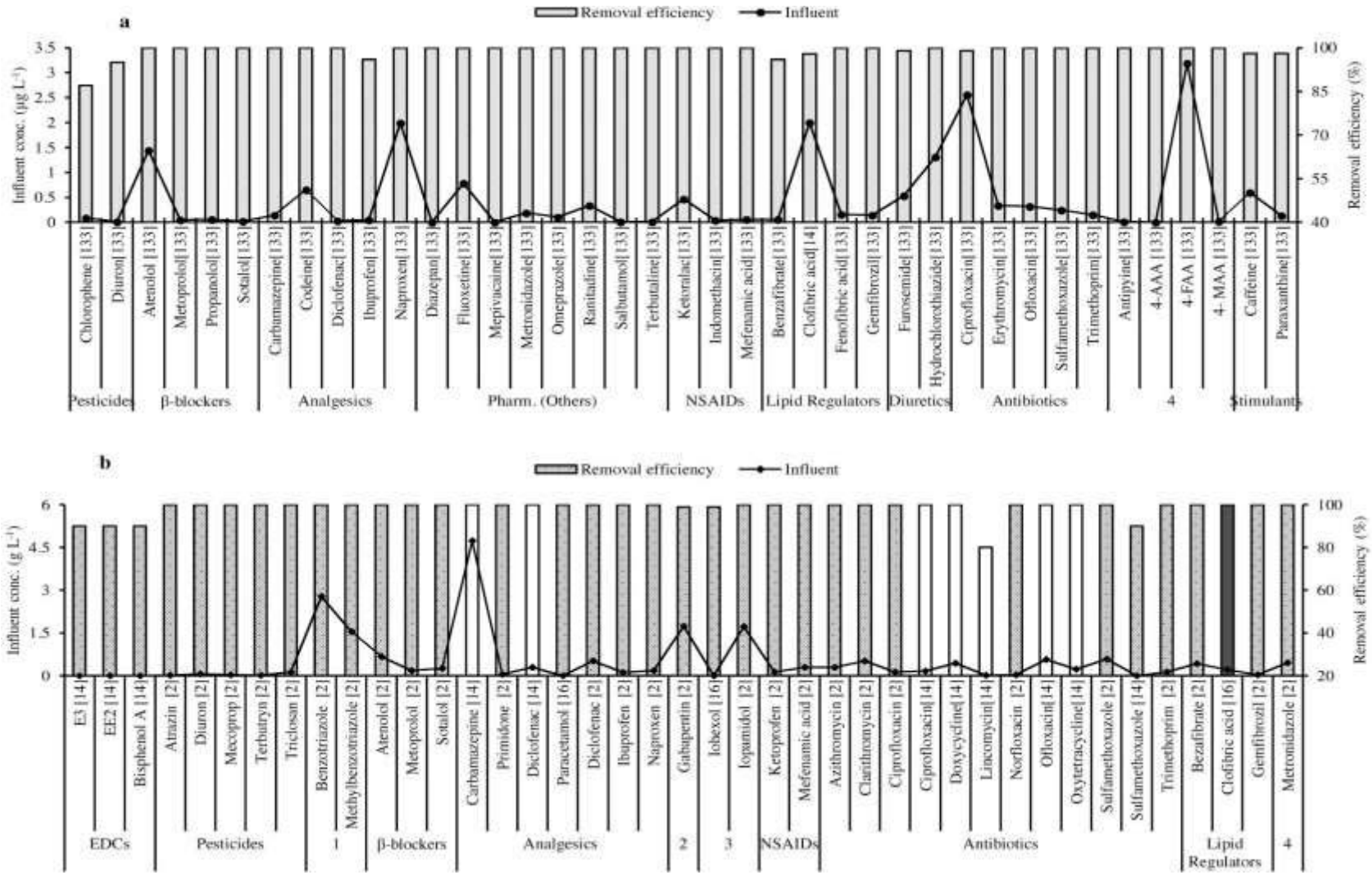

Figure 2.10: ECs removal efficiencies achieved by ozonation in the presence of H_2O_2 (a) and UV in the presence of H_2O_2 (b), with the corresponding reference after the compound name. Concentrations are in mg $L^{-1}$for empty columns and g L^{-1} for dark columns. 1 = corrosion inhibitor, 2 = pain reliever, 3 = contrast agent, 4 = anti-inflammatory.

(iv) Photolysis

Photolysis is a process in which molecules of ECs undergo decomposition as a result of the absorption of light or radiations [77, 205, 206]. Though different sources of light are utilised, disinfection of water using UV remains as a commonly used technique. There are two types of photolysis, namely direct photolysis where the direct absorption of photons lead to degradation of pollutants and indirect photolysis which occurs in the presence of photosensitisers such as using of hydrogen peroxide or other photosensitisers [207]. **Figure 2.11** and **Figure 2.10** show the UV photolytic removal of some ECs in the absence (**Figure 2.11b**) and presence of hydrogen peroxide (**Figure 2.10**), respectively. **Figure 2.11b** shows that photolytic process has high efficiency in the removal of EDCs (conc. level 5-10 μg L^{-1}) and pesticides from 80% to 100% [141, 169]. Some pharmaceuticals such as diclofenac, iopamidol, ketoprofen, mefanamic acid, oxytetracycline and tetracycline can be completely removed. On the other hand, UV photolysis process was found to be less effective in the removal of beta blockers. In general, UV photolysis process followed the order of ECs removal as beta blockers < other pharmaceuticals < analgesics pharmaceuticals < antibiotics < pesticides < EDCs.

Also, UV photolysis in the presence of hydrogen peroxide has much more pronounced effect in the removal of ECs as represented in **Figure 2.10b**. Regarding removal efficiencies, UV photolysis in the presence of hydrogen peroxide has been found better than only UV photolysis. UV photolysis/H_2O_2 process can remove most of ECs successfully for up to 100% except some ECs such as lincomycin and diclofenac removal (around 80%), when ECs concentrations were mg L^{-1}. Thus it can be stated that UV photolysis is less capable than UV photolysis/H_2O_2 for the removal of all ECs except EDCs where they followed the order of UV photolysis > UV photolysis/H_2O_2.

Moreover, gamma radiations have also successfully been applied in the removal of ECs from wastewater. Data for the removal of some pharmaceutical ECs are represented in **Table 2.10**, which show that gamma radiation based oxidation process can successfully remove 100% of chloramphenicol at a concentration level of mg L^{-1} [208]. Other ECs showed removal efficiencies in a range of 80-95% except for sulfamethoxazole (53%). The maintenance and production cost of gamma radiation can be a burden to obtain a cost-effective removal of ECs. Therefore this kind of process is still at early stage and requires more research.

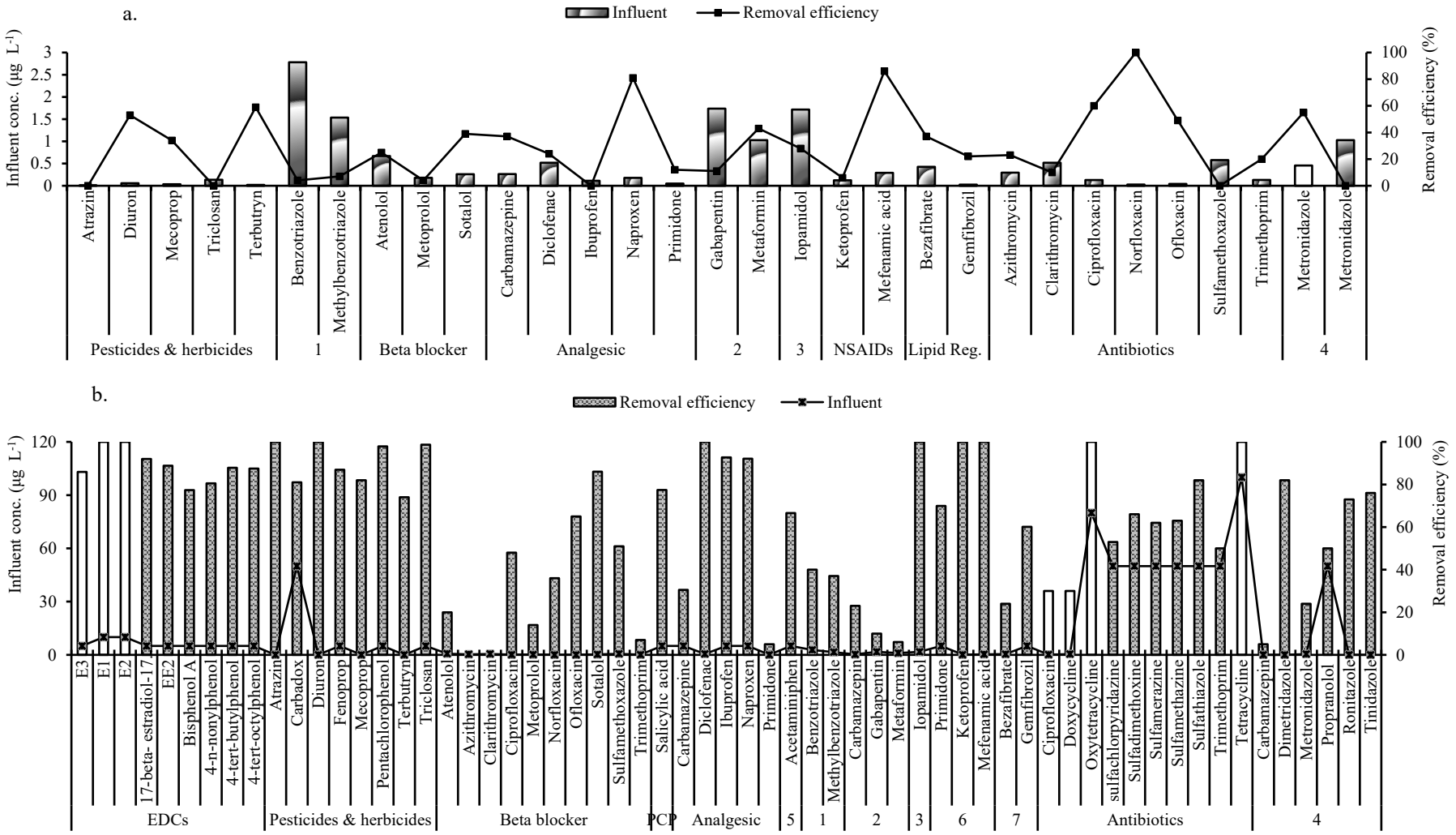

Figure 2.11: ECs removal efficiencies achieved by Fenton process (Figure 2.10a) and by UV photolysis (Figure 2.10b). Concentrations are in mg L^{-1} for empty columns and in g L^{-1} for clofibric acid. 1 = corrosion inhibitors, 2 = anti-diabetics, 3 = contrast agents, 4 = anti-inflammatory, 5 = pain reliever, 6 = anticonvulsant, 7 = lipid regulators.

Table 2.10: ECs removal efficiency by gamma radiation (conventional) and AOPs based treatment technologies.

Categories of ECs	ECs	Source of ECs	Influent conc. (μg L^{-1})	Chemical treatment technology	Removal (%)	Reference
Antibiotics	Amoxicillin	Water		Gamma radiation	95.00	[208]
	Cefaclor	Water	30000		100	[209]
	Chloramphenicol	Water	323132		100	[210]
	Penicillin G	Water			92.00	[208]
	Penicillin V	Water			81.00	
	Sulfamethoxazole	Water			53.00	[211]
	Cefalexin	Hospital WW	200000	Electro-Fenton	100	[212]
	Sulfamethazine	Hospital WW	55666			[213]
	Sulfamethoxazole	Hospital WW	52700		100	[163]
	Tetracycline	Hospital WW	25000		86.00	
EDCs	Progesterone	MWTPs	5	Solar Photo-Fenton	90.00	[178]
Antibiotics	Flumequine	MWTPs	5		90.00	[178]
	Ofloxacin	MWTPs	5		90.00	[178]
	Sulfamethoxazole	MWTPs	5		95.00	[178]
	Amoxicillin	Water	104000	Photocatalysis/H_2O_2	100	[214]
	Ampicillin	Water	105000		100	
	Cloxacillin	Water	10300		100	
	Ofoxacin	MWTPs	1	Solar photocatalysis	85.00	
	Trimethoprim	MWTPs	1		85.00	
	Sulfamethoxazole	Hospital WW	52700		100	[163, 215]

B. Advanced Oxidation Processes (AOPs)

(i) Ferrate

Ferrate(VI) is an excellent oxidizing agent which has a powerful disinfection action. It can generate a $Fe(OH)_3$ type gel which precipitates and removes other ions. Over the last decade, the high oxidation state of ferrate from FeO_4^{2-} was of interest due to its environmental, industrial and biological importance. Ferrate can be used for the removal of ECs such as arsenic, estrogens, pharmaceuticals and PCPs [216]. The main mechanism involved in water treatment is oxidation/disinfection by Fe^{6+} and coagulation/flocculation by Fe^{3+}. Several ECs such as E1, E2, EE2, bisphenol A, 4-*tert*-octylphenol and sulfamethoxazole have been

degraded from 6400 to 7700 M^{-1} s^{-1} at pH 7 [217]. Ferrate can oxidize some organic micropollutants by up to 90% at ng L^{-1} level pollutant concentrations. Ferrate has been observed to be superior in disinfecting coliforms in WWTPs and sewage sludge. However, the main problems with ferrate process are high preparation costs and poor stability of ferrate ions. Moreover, ferrate process has limited application in some ECs removals. However, this process had no adverse effects, and thus ferrate processes for ECs removal should be further explored with good potential [218].

(ii) Electro-Fenton Process

The electro-fenton process has recently been developed to overcome the drawbacks of the traditional Fenton process and to increase the efficiency of pollutant removal [204]. In this process, H_2O_2 is electrochemically generated in situ in a controlled way [219]:

$$O_2 + 2H^+ + 2e^- \rightarrow H_2O_2 \qquad (2.5)$$

Another electrochemical process is also used named photoelectron–Fenton process. In this process, conditions remain the same as electro–Fenton process but simultaneously irradiated with UVA light. Thus it accelerates the degradation rate of contaminants in the reaction phase and increases the regeneration rate of Fe^{2+}. Moreover, $OH^{\cdot}$ can also be produced from the following reactions [204]:

$$[Fe(OH)]^{2+} + hv \rightarrow Fe^{2+} + OH^{\cdot} \qquad (2.6)$$

$$Fe(OOCR)^{2+} + hv \rightarrow Fe^{2+} + CO_2 + R^{\cdot} \qquad (2.7)$$

Electro-Fenton processes appear to be environmentally friendly and efficient, since in situ generation of the Fenton's allows thereby avoiding (i) the cost of reagents and risks related to their transport and storage, the formation of sludge, and (iii) parasite reactions due to maintenance of small reagent concentrations in the medium [163]. Electrochemical Fenton processes can be enhanced by the additional application of UV radiation or ultrasound. Solar radiation can also be used (solar photoelectro-Fenton process). However, the problem is that additional energy is required for photo-or sound assistance, and their installation and operational costs are involved in comparison to classical EAOPs except for solar photoelectron-Fenton process [217]. These kinds of AOPs based treatment can oxidize ECs at higher concentration (mg L^{-1} or g L^{-1}) than relevant to the environmental levels. Some antibiotics such as cephalexin, sulfamethazine, sulfamethoxazole, tetracycline and acetaminophen were found to show enhanced removal capacity by the electro-Fenton process

[163, 212]. The solar photoelectron-Fenton process has also been applied for the removal of beta-blocker such as atendol, metoprolol tartrate, propranolol hydrochloride, with 88-93% efficiency [220]. Thus electro-Fenton process seems to be better than solar photoelectro-Fenton process. The most important advantage of these processes is that they can degrade pharmaceuticals of higher concentrations very effectively than by some conventional processes. The problem with such kinds of AOPs based treatment is that the maintenance and operation cost is high. Conventional treatment processes such as activated sludge, constructed wetlands, microorganism based algal treatment and biosorption based treatment are cost-effective but cannot degrade when influent contaminants concentration is high.

(iii) Photo-Fenton Process

Photo-Fenton reactions are widely used AOPs for the removal of ECs in wastewater. These processes involve the use of UV lights to produce radicals by reactions of hydrogen peroxide in the presence of iron. Photo-Fenton reactions are also possible in sunlight avoiding the use of UV light. Photo-Fenton studies are usually developed in acidic or near neutral conditions which are optimum for aquatic solutions not containing organic matter. In acidic solutions, Fe^{3+} forms the hydroxyl complexes such as $Fe(OH)^{2+}$ and $Fe(OH)_2^{4+}$, which absorb light in the UV/visible region, undergoing photoreduction to generate $OH^{\cdot}$ and Fe^{2+} (reaction 7). Thus the whole mechanism is enhanced as more $OH^{\cdot}$ are being produced, and Fe^{2+} can be recycled at a higher rate for the reaction with H_2O_2. In the case that the pH increases to near neutral, the ferric ions precipitate to form amorphous ferric oxyhydroxides, in the absence of other ion complex substances. Thus the Fe^{2+} can react with the hydrogen peroxide to give $OH^{\cdot}$, and the oxidized ligand can be involved in new reactions to the micropollutants degradation [94]. Hence, the effluent has to be acidified to reach this value and then neutralization is required before discharge. However, important efforts are being devoted to developing photo-Fenton processes under milder conditions. Oxidation of different ECs by the photo-Fenton process is represented in **Figure 2.12a**. In general, many types of pharmaceuticals ECs have been found to show higher removal efficiencies (95-100%) by photo–Fenton process except penicillin G [31, 36, 94, 202]. Six anti-inflammatory ECs (such as antipyrine, 4AA, 4AAA, 4FAA, 4MAA and metronidazole) have been successfully degraded by this process with higher removal efficiencies than by other processes. However, photo-Fenton was found to be less effective in the removal of EDCs with relatively high K_{ow} values. Four pesticides including atrazine,

diuron, mecoprop and terbutryn were found to be better oxidized by photo-Fenton process except for triclosan and abamectin (**Figure 2.12a**).

Alternatively, the solar photo-Fenton process was also applied in the removal of ECs by up to 90% at a contaminant concentration of 5 μg L^{-1} (**Table 2.10**) [178]. Thus it can be concluded that UV based photo–Fenton process can remove the higher amount of pharmaceutical and beta blocker ECs than solar photo–Fenton based process: UV photo-Fenton > solar photo-Fenton.

(iv) Photocatalysis

Photocatalysis is the transformation of chemicals by a catalyst that is activated in the presence of light that provides adequate energy [27, 105]. Most photocatalysts are semiconductor metal oxides which characteristically possess a narrow band gap. Photocatalysis is used to overcome the disadvantages of photolysis, especially the slow rate of degradation. The catalyst takes part in the reaction, increases the rate of reaction but remains unchanged by the end [221]. Titania is the most widely investigated of the heterogeneous photocatalysts due to its cost-effectiveness, inert nature and photostability [214]. Also, ZnO has been reported to catalyse the photo-oxidation of pharmaceuticals such as carbamazepine and antibiotic tetracycline. In fact, fast removal of tetracycline was measured with ZnO under optimized conditions (basic pH), although the major drawback of this material is that it suffers from corrosion at low pH values. Removal efficiencies of ECs by photocatalysis are presented in **Figure 2.12.** EDCs such as E1, E2, EE2, E3, bisphenol A and progesterone can be highly be degraded by up to 100%, and the removal efficiencies are higher than photo-Fenton based AOPs (**Figure 2.12b**). The high degradation rate of pharmaceuticals such as analgesics can be easily achieved using photocatalysis process. The removal of ECs by a photocatalytic process generally followed the order of EDCs > analgesics pharmaceuticals > pesticides > other pharmaceutical. For the removal of pesticides such as aldrin, diazinon, malathion and some antibiotics such as amoxicillin, ampicillin and cloxacillin, an alternative process such as photocatalysis in the presence of hydrogen peroxide can also be applied with excellent removal efficiencies (99-100%) [222, 223].

(v) Solar Photocatalysis

The solar photocatalytic process is an emerging and promising technology both as an alternative treatment to conventional wastewater treatment methods and enhancement of

biodegradability of highly toxic and recalcitrant pollutants [224]. A promising alternative to semiconductor-based solar photocatalysis of some pharmaceutical ECs can also be applied. Data shows that up to 85% can remove many ECs by solar photocatalysis process [193, 214].

(vi) Semiconductor Photocatalysis

Semiconductor photocatalysis is the technique which uses artificial or sunlight to activate a semiconductor (commonly TiO_2 due to its high stability, good performance and low cost) for degrading pollutants. The removal mechanism of this technology includes both hydroxyl radicals and other radical species derived from oxygen [24]. The removal efficiency of Antibiotics by semiconductor photocatalysis depends on catalyst concentration, wavelength, radiation intensity, pH and water matrix. The technique can use solar energy and achieves high efficiency. Thus it is energy saving. In contrast, it is difficult to apply widely as it depends on the penetration of light through aqueous solution [24]. It can be time-consuming and costly.

(vii) Electrochemical Processes

The electrochemical process has also been used to remove toxic organic compounds. In this technique, pollutants are oxidized in anodes (graphite, TiO_2, Ti-based alloys, Ru or Ir oxides, boron-doped diamond) in the presence of an electrolyte. Direct anodic oxidation can destroy antibiotics or indirectly in the liquid bulk with the mediation of electroactive species [226]. Advantages of this technique are effective, versatile, cost-effective, easy and clean technology [226]. The technology can also treat wastewater containing high concentrations of both antibiotics and COD [24]. However, the applicability of this technology is limited to small flow rates, and the high operating cost is also a disadvantage. The process performance depends on the nature and structure of the electrode material, experimental conditions (pH, temperature) and electrolyte composition [227].

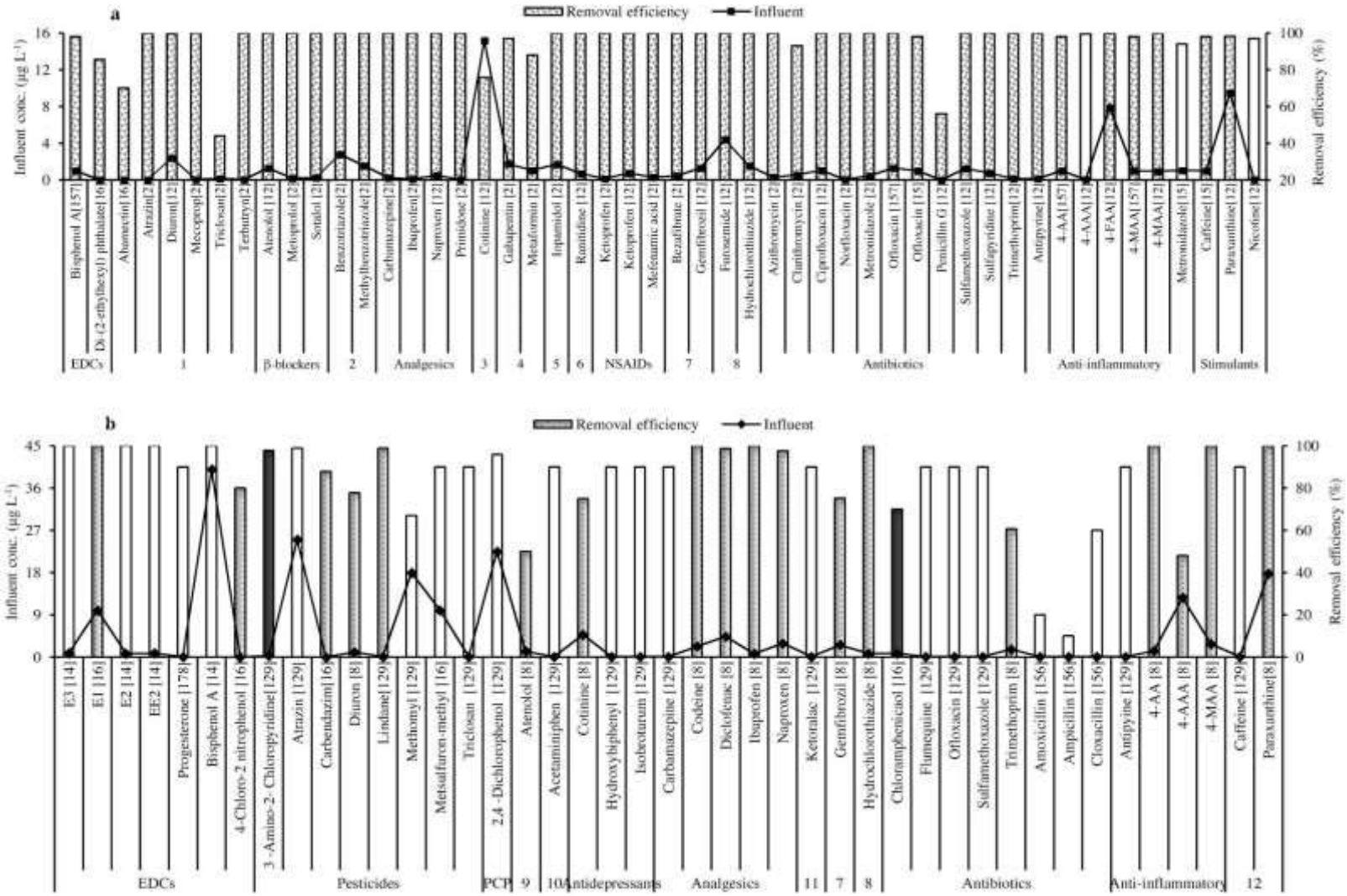

Figure 2.12: ECs removal efficiencies achieved by photo-Fenton (a) and UV photocatalysis (UV/TiO_2) (b), with the corresponding reference after the compound name. Concentrations are in mg L^{-1} for empty columns and in g L^{-1} for chloramphenicol. 1 = pesticide, 2 = corrosion inhibitor, 3 = contrast agent, 4 = antidepressant, 5 = anti-diabetic, 6 = gastroesophageal, 7 = lipid regulator, 8 = diuretic, 9 = beta blocker, 10 = pain reliever, 11 = NSAID, 12 = stimulant [225].

(viii) Miscellaneous Processes

Besides AOPs based processes some other technologies have also been applied for the removal of ECs from WWTPs, which include anodic oxidation [215, 228], ultrasound irradiation (sometimes called sonochemical irradiation) and titanium-based ultrasound irradiation. EDCs such as E1, E2, E3 and equilin were found to be removed by up to 80-90% from aqueous solution by ultrasound processes at a concentration of 10 μg L^{-1} [229, 230]. Naddeo et al [231] investigated sonochemical degradation of 23 ECs (such as acetaminophen, atenolol, atrazine, carbamazepine, diclofenac, progesterone, metoprolol, dilantin, DEET, pentoxifylline, oxybenzone, caffeine, iopromide, erythromycin, fluoxetine, trimethoprim, propranolol, sulfamethoxazole, ibuprofen, naproxen, bisphenol-A, gemfibrozil, and triclosan) from wastewater treatment plant (at 1.00 μg L^{-1}concentration level). It was found that a strong degradation for all ECs at an average value of 70% due to the breakdown of the conjugated double bonds. However, triclosan was found faster degradation rate (95%) and erythromycin was found lowest degradation rate (50%). The all the ECs degradation followed the pseudo-first order kinetic model. A significant reduction of the discharge of ECs into the environment could be expected with catalysis, ultrasound irradiation and solar energy. Recent investigations increasingly focus on those systems; however, commercial applications are still scarce.

(viii) Comparison of Different Chemical Processes

Comparative removal of ECs by different chemical based oxidation processes is shown in **Figure 2.13**, where the average removal of different categories of ECs by Fenton and UV photolysis processes was found less effective than other chemical oxidation processes. It is also clearly seen that ozonation, ozonation in the presence of hydrogen peroxide and photo-Fenton processes showed greater efficiency in the removal of a wide range of ECs. Other processes were found to have a mixed effect in the removal of ECs. The average removal efficiencies of EDCs followed the order: ozonation ≥ UV photocatalysis > photo-Fenton > UV photolysis/H_2O_2 > solar photo-Fenton > UV photolysis. On the removal of pesticides, UV photolysis/H_2O_2 and electro-Fenton processes showed almost similar high average removal efficiencies. The order of the removal of pesticides can be written as electro-Fenton ≈ UV photolysis/H_2O_2 > ozonation/H_2O_2 > photo-Fenton > Fenton ≈ ozonation > UV photolysis > solar photo-Fenton. On the other hand, the average removal efficiencies of beta blockers can be written as ozonation/ H_2O_2 ≈ UV photolysis/ H_2O_2 ≈ photo-Fenton > electro-Fenton> ozonation > UV photocatalysis > UV photolysis > Fenton process. The average removal efficiencies of

analgesic pharmaceuticals by different chemical oxidation methods can be written as UV photolysis/H_2O_2 ≈ ozonation/H_2O_2 = photo-Fenton > ozonation > photocatalysis ≈ solar photo–Fenton > UV photolysis > Fenton process. For antibiotics, their average removal efficiencies can be ranked as ozonation/H_2O_2 > UV photolysis/H_2O_2 > ozonation > Photo-Fenton ≈ electro-Fenton > solar photo-Fenton > UV photocatalysis > UV photolysis. This kind of relationships for pharmaceutical lipid regulators, anti-inflammatory and miscellaneous pharmaceuticals can be developed (**Figure 2.13**). Thus it can be concluded that chemical-based oxidation processes possess excellent oxidation characteristics in the removal of a wide range of ECs. However, the main problem with chemical-based treatment technologies is that comparatively high costs associated with the maintenance and operation, power consumption, handling of the large volume of influents as well as these kinds of processes also produced different by-products in the aqueous phase. The by-products can further create problems in the overall processes and can also further increase the cost of the processes.

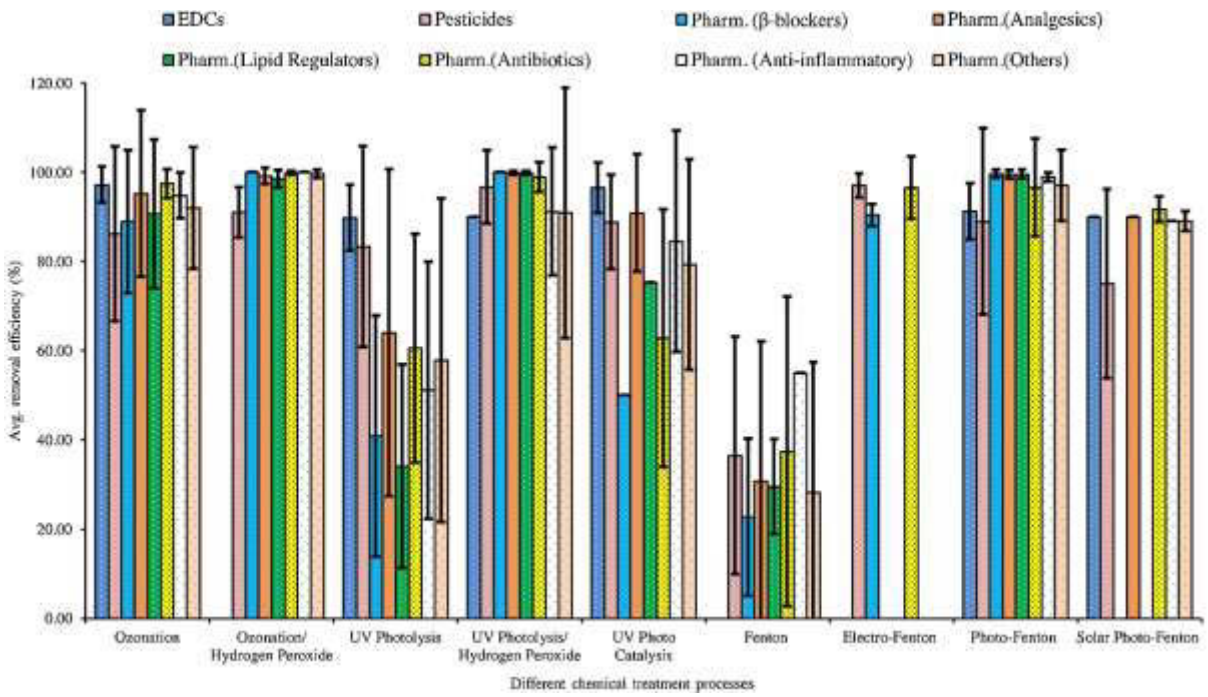

Figure 2.13: Comparative average removal efficiency of ECs with standard deviation (error bar) by different chemical treatment technologies.

2.3.3. Physical Treatment Technologies

(i) Membrane Processes

The application of membrane technology for removing antibiotics from aqueous solution has been increased. The process is unable to degrade the toxicants but transfers them into a

concentrated form. There are several kinds of the membrane to abate Antibiotics such as reverse osmosis, nanofiltration, ultrafiltration and ion exchange.

(ii) Reverse Osmosis, Nano- and Ultrafiltration

Reverse osmosis is a kind of membrane techniques [232]. This process is often used to immobilize large molecules and ions of pollutants. The flow occurs against the concentration gradient in reverse osmosis. This technique can efficiently remove dissolved salts but not effectively abate organic compounds. Moreover, reverse osmosis is simple and has high energy efficiency. Nevertheless, the membranes are very quickly fouled or damaged. In comparison with other techniques, reverse osmosis is a slow process for removing Antibiotics from wastewater [24]. Other membrane processes are nanofiltration and ultrafiltration [232]. The technologies are cross-flow filtrations and usually charged (carboxylic groups, sulfonic groups). Hence, ion repulsion is the primary factor in this treatment, and it can remove smaller molecules such as antibiotics. Furthermore, these membrane processes are sensitive to temperature.

(iii) Ion Exchange

The water treatment by ion exchange is the use of ion exchange resin (anion or cation exchangers) to exchange with cations or anions in a liquid medium [233]. The most used materials for ion exchange resin is polymeric (styrenic and acrylic) due to their stability and great selectivity [234]. Ion exchange is also a reversible process which allows an extended using time of the resin. On the other hand, the technique requires backwashing and regeneration regularly, and fouling is also a problem [235].

(iv) Combined Processes

Combination of different technologies in one water treatment system is necessary to maximize the cleaning performance. However, the combination of techniques at different stages for water treatment needs a careful study to avoid negative influences. For instance, most microorganisms in an iodegradation tank are sensitive to the toxic pollutants or chemicals from previous treatment stages. Thus, advanced oxidize processes or adsorption has been used as a pre-treatment step to oxidize the pollutants, making them less toxic and biodegradable before treating with microorganisms [236].

(vi) Adsorption Process

The adsorptive removal of organic pollutants from water has been widely applied. The most common adsorbents are solid materials. Sorption has studied remediation of antibiotic contaminated water on various sorbents such as natural sorbents, clays, a chitosan derivative, activated carbon, and more [82]. There are two different kinds of adsorption regarding the nature of forces involved including chemical and physical adsorption. In physical adsorption, van der Waals interactions are main forces which are moderately weak. On the other hand, chemical adsorption relates to the electron transfer and chemical bonds formed between antibiotics and the solid surface. The interactions in chemical adsorption are strong and limited to the monolayer coverage [237]. The advantage of adsorption is removing Antibiotics instead of producing potentially more dangerous metabolites [238]. Conversely, the technology did not destroy the antibiotics but concentrated them on adsorbents' surface. The conventional and most used adsorbent is activated carbons. However, their high cost means full application of this adsorbent is difficult. Thus, adsorption using cost-effective adsorbents is considered an effective process that removes antibiotics from aqueous solution [20]. Physical treatment processes have been found very useful and economical in removing antibiotics among which sorption has emerged as a cost-effective method for pollutant removal; unaffected by the potential toxicity as for biological processes; and easy to design and operate [44, 239, 240]. Also, sorption is a vital process because it may dramatically affect the fate and impacts of contaminants in the environment through different mechanisms [45]. The efficiency of sorption process is profoundly affected by the properties of sorbate, sorbent, and operating conditions [241]. The degree of sorption mainly depends on the physicochemical properties of the micropollutants, type of solid matrices, surface area, porosity, pore diameter, and environmental conditions [240, 242, 243].

The sorption of antibiotics onto carbonaceous materials such as biochar [55, 240, 244, 245], activated carbon [29], carbon nanotubes[57], graphene, clay minerals [57], and hollow polymer nanorods [239] has been widely studied and proved very useful [57]. The sorption of antibiotics using biochar was found particularly efficient [56, 57]. Biochar has a high hydrophobicity and aromaticity and is an excellent sorbent for hydrophobic organic contaminants, e.g. aromatics [246, 247].

Many separation processes such as coagulation, flocculation and precipitation have been used for the removal of EDCs from different water [28, 44]. Conventional biological processes such as activated sludge, constructed wetlands, bio-filtration have shown limited removal of EDCs [28, 44], while advanced treatment processes such as granular activated carbon,

photolysis, photocatalysis, ferrate [26] free radical oxidation, Fenton oxidation, sonolysis, membrane separation, chlorination and ozonation have shown more satisfying results [28, 34, 44, 46]. Some hybrid systems such as membrane bioreactor (MBR) followed by ultrafiltration/nanofiltration/reverse osmosis, flocculation followed by activated sludge and ultrafiltration can also remove EDCs efficiently from water and wastewater [44, 47]. However, a significant problem of hybrid systems is the high capital investment and operation cost. Physical separation processes such as activated carbon adsorption, membrane filtration and ion exchange usually show superior removal efficiencies of the EDC [29, 48]. Adsorption of EDCs on carbonaceous materials has been studied using activated carbon [49-51] black carbon, single- or multi-walled carbon nanotubes (SWCNT, MWCNT) [52, 53] and biochar [26, 54, 55]. Biochar is a low-cost sorbent for the efficient removal of many hydrophilic and hydrophobic organic contaminants [56, 57]. Sorption of EDCs has also been studied using alumina, silica and hydrophobic medium [58].

2.3.4. Hybrid Technologies

The conventional wastewater treatment processes are not adequate for the removal of many ECs effectively. A variety of hybrid treatment technologies are reported in the literature, and during the last few years, significant improvements have been achieved in their application in wastewater treatment, to prevent the release of ECs into the aquatic media via effluent discharge. Most of the hybrid systems consist of biological-based treatment system followed by some physical or chemical treatment systems. Chemical oxidation based treatment such as ozonation is the most widely used process to combine with a biological process. Some examples of these combinations include ozonation followed by biological activated carbon**,** MBR-reverse osmosis/ultrafiltration/microfiltration/ozonation, filtration and activated sludge followed by ultrafiltration. Microfiltration and ultrafiltration are increasingly being considered as alternatives to granular media filtration [248].

The remediation of 31 targets ECs such as EDCs, pesticides and beta blockers by hybrid systems is represented in **Table 2.11**. Some EDCs such as E1, E2, EE2, E3, 17β-estradiol 17-acetate, bisphenol A, 4-n-nonylphenol and 4-*tert*-butyl phenol can be better removed up to 99% by the combined use of MBR and some physical treatment technologies such as reverse osmosis, ultrafiltration or nanofiltration at concentrations up to 5 μg L^{-1}. Combination of flocculation activated sludge and ultrafiltration can also be employed, but removal efficiencies of EDCs were low in some cases. This kind of combination can be more cost-effective than MBR based hybrid systems. In term of removal of high influent concentrations of EDCs, MBR

based hybrid system can be better employed. The general trend for EDCs removal can be written as hybrid MBR with reverse osmosis or nanofiltration or ultrafiltration > flocculation–activated sludge–ultrafiltration > constructed wetland.

Table 2.11: The removal efficiency of EDCs, pesticides and beta blockers achieved by hybrid systems.

ECs category	ECs	Treatment process	ECs source	Influent (μg L^{-1})	Removal (%)	Reference
EDCs	E1	MBR + UF	Synthetic WW	5	99.4	[169]
		MBR + RO	Synthetic WW	5	99.6	[169]
		Flocculants + AS + UF	WW	0.025	96.0	[146]
		MBR + NF	Synthetic WW	5	99.3	[169]
	E2	MBR + UF	Synthetic WW	5	99.5	[169]
		MBR + RO	Synthetic WW	5	99.4	[169]
		Flocculants + AS + UF	WW	0.014	96.5	[146]
		MBR + NF	Synthetic WW	5	99.6	[169]
	EE2	MBR + UF	Synthetic WW	5	95.5	[169]
		MBR+ NF	Synthetic WW	5	94.0	[169]
		MBR + RO	Synthetic WW	5	93.61	[169]
		Flocculants + AS + UF	WW	0.041	95.0	[146]
	E3	MBR + NF	Synthetic WW	5	97.7	[169]
		MBR + RO	Synthetic WW	5	96.1	[169]
		MBR + UF	Synthetic WW	5	98.3	[169]
	17β-estradiol-17-acetate	MBR + UF	Synthetic WW	5	99.0	[169]
		MBR+ NF	Synthetic WW	5	99.3	[169]
		MBR + RO	Synthetic WW	5	100	[169]
	Bisphenol A	Flocculants +AS+ UF	WW	0.857	95.0	[146]
		MBR + UF	Synthetic WW	5	98.6	[169]
		MBR+ NF	Synthetic WW	5	89.3	[169]
		MBR + RO	Synthetic WW	5	90.5	[169]
		VFCWs+HFCWs+FWCWs	Urban WW	4.06	99.0	[249]
	4-n-nonylphenol	MBR + UF	Synthetic WW	5	96.9	[169]
		MBR+ NF	Synthetic WW	5	96.6	[169]
		MBR + RO	Synthetic WW	5	100	[169]
		Flocculants +AS+ UF	WW	14.635	97.0	[146]
	4-*tert*-butylphenol	MBR + UF	Synthetic WW	5	95.5	[169]
		MBR + UF	Synthetic WW	5	98.2	[169]
		MBR+ NF	Synthetic WW	5	91.0	[169]
		MBR+ NF	Synthetic WW	5	95.7	[169]
		MBR + RO	Synthetic WW	5	83.5	[169]
		MBR + RO	Synthetic WW	5	93.8	[169]
		Flocculants +AS+ UF	WW	4.385	98.0	[146]

AS = activated sludge, RO = reverse osmosis, MF = micro-filtration, UF = ultra-filtration, NF = nano-filtration, BAC = biological activated carbon.

The removal of antibiotics and other pharmaceuticals is represented in **Table 2.12**, which shows that MBR–reverse osmosis can successfully remove more than 99% of azithromycin, clarithromycin, erythromycin, ofloxacin, sulfamethoxazole, diazepam, lorazepam, famotidine, ranitidine and clopidogrel. Ozonation followed by biological activated carbon hybrid system can be well applied in the removal of a wide range of ECs such as erythromycin, lincomycin, roxithromycin, trimethoprim, caffeine, citalopram, doxylamine, phenytoin, risperidone, sertraline, hydrochlorothiazole and perindopril. However, this hybrid system was found less effective in the removal of chloramphenicol, sulfamethaxazole, tylosin, dapsone and perindopril. Combine application of ultrafiltration, activated carbon and ultrasound was found highly effective in the removal of antibiotic amoxicillin even at 10 ppm level [250]. Ozonation followed by ultrafiltration hybrid system can be used up to 100% removal of some pharmaceuticals such as clarithromycin, clindamycin, sulfamethazine, 4-aminoantipyrine, enalapril and norbenzoylecgonine but this process was found lower effective in the removal of licomycin, ofloxacin, venlafaxine and irbesartan (**Table 2.12**). Thus on the removal of pharmaceutical antibiotics and different pharmaceuticals hybrid systems followed the order of MBR–reverse osmosis ≥ ozonation-biological activated carbon > ozonation-ultrafiltration.

Table 2.12: Pharmaceuticals removal efficiency by hybrid systems.

ECs	Technology	Influent conc. (μg L^{-1})	Removal (%)	Reference
Amoxicillin	Ultrafiltration+ Activated carbon+ Ultrasound	10000	99.9	[250]
Azithromycin	MBR + RO	0.142	99.5	[33]
Chloramphenicol	Ozonation + BAC		33.3	[108, 132]
Clarithromycin	MBR + RO	2.722	99.5	[33]
	Ozonation + Ultrasound	0.35	94.3	[251]
Clindamycin	Ozonation + Ultrasound	0.01	100	[251]
Erythromycin	Ozonation + BAC	0.167	98.4	[108, 132]
	MBR + RO	0.08	99.5	[33]
Lincomycin	Ozonation + BAC	0.003	80.6	[108, 132]
	Ozonation + Ultrasound	0.21	66.7	[251]
Ofloxacin	MBR + RO	2.9	99.5	[33]
	Ozonation + Ultrasound	0.35	42.9	[251]
Roxithromycin	Ozonation + BAC	0.081	97	[108, 132]
Sulfamethaxazole	MBR + RO	0.268	99.5	[33]
	Ozonation + BAC	0.023	77.4	[108, 132]
Sulfamethazine	Ozonation + Ultrasound	0.21	100	[251]
Sulfathiazole	Ozonation + BAC	0.001	58.3	[108, 130]
Trimethoprim	Ozonation + BAC	0.027	99.3	[108, 130]

In summary, MBR based reverse osmosis/nanofiltration/ultrafiltration has been found highly efficient in the removal of a wide range of ECs such as EDCs, antibiotics and other pharmaceuticals. Other issues such as process cost, membrane fouling and energy demand need to be considered in designing such hybrid systems. Ozonation followed by biological activated carbon was found to better result in the removal of pesticides & herbicides, beta blockers, pharmaceuticals pain reliever, lipid regulators, analgesics, antibiotics and different pharmaceuticals. However, this process still suffers from lower efficiencies of some ECs. Ozonation followed by ultrasound hybrid system is a recent development, and this process can be very potent in the removal of some ECs, but this process can be experienced with some difficulties such as high costs, and lower efficiencies in the removal of some ECs. Regarding cost, activated sludge based hybrid systems (activated sludge-ultrafiltration, activated sludge-gamma radiation) can also be a good alternative but need to consider the high retention time and sludge processing costs. The constructed wetland based hybrid system was found less effective in the removal of many ECs. Data on the removal of PCPs and surfactants by hybrid systems are scarce. In future, some AOPs based treatment processes such as photolysis in the presence of hydrogen peroxide and photo–Fenton processes can be carefully merged with the conventional processes.

2.4. Biochar and Functionalized Biochar

Biochar is a stable solid, carbon dominant product which is obtained by thermal (mostly pyrolysis) or hydrothermal processes when biomass materials are heated at an elevated temperature in a reactor with little or no oxygen [57, 252, 253]. Activated or modified BC is obtained when BC is further activated or modified either chemically or physically to improve their diameters of the pores, create some new porosity leading to the high surface area and to enhance sorptive properties for inorganic and organic contaminants [254]. Raw BC may have poor ability to selectively adsorb contaminants when their concentration is high [255, 256]. Moreover, BC application is restricted due to their limited functionalities. Modified BCs with enriched surface functional groups had enhanced sorption capacity for a particular contaminant or mixture of contaminants than that of primary BC [257, 258]. For example, hydrous manganese oxide modification of peeled pine wood BC exhibited five folds higher Pb^{2+} sorption capacity than the parent BC [259]. Thus modification of BC surface area is gaining more attention to improve BC performance. Consequently, various modification or activation methods including surface oxidation and functionalization have been applied to improve their performance in environmental remediation [260]. These modifications can increase the number

of surface sorption sites, improve stability, introduce more positive charges and modified surface functional groups on the modified surface of BC [261].

The specific properties of BC and modified BC which include low cost, specific surface area, pore volume, pore size, enriched surface functional groups and minerals enabled BC and modified BC to be used as an effective sorbents to remove many organic and inorganic contaminants from aqueous solutions [262]. BC also has the potential to help mitigate climate change via carbon sequestration, denitrification, sludge conditioning and dewatering, increased soil fertility and agricultural productivity [263, 264]. When applied in soils, BC can introduce additional benefits including better plant growth, reduced fertilizer requirements, reduced soil acidity, increased soil cationic exchange capacity (CEC) and improved respiration [265].

Modified BC is prepared so that they can sorb target heavy metals or organic contaminants through additional/improved functionality. Nano-composite sorbents with nano-sized metal oxy-hydrates are attached to carbonaceous surfaces within the BC matrix. Elements such as oxygen, hydrogen, sulfur, nitrogen together with carbon are generally present in the BC's core structure in the form of different functional groups and other chemical structures. The atomic ratios such as H/C (aliphatic), O/C and N/C (polar index) are related to the specific properties of the BC. In the core structure of BC, the functional groups such as hydroxyl as phenol, carboxyl, a carbonyl group, lactones, quinones, amines, amides and others are responsible for accumulating contaminants from water or wastewater. Those functional groups on the carbon surface are mainly produced as a result of thermal or hydrothermal processes such as pyrolysis, activation and others before and after treatment of raw biomass or BC. Due to those modifications newly modified BC or activated BC is produced which is responsible for improving the performance of BC for the removal of specific contaminants from water or wastewater. This has generated more interest in using BC and modified BC in many multidisciplinary research areas including water and wastewater treatment [56, 57].

Further improvements in enhancing the chemical and physical properties of BC-based sorbents are possible because most of the BC were directly produced from precursors without any modifications. Different methods such as physical modification, chemical modification, impregnation and heat treatment have been reported in the literature [266, 267] to modify the surface of carbonaceous materials. This research sheds light on the chemical mechanism underlying treatment methods that enable the BC surface to remove specific contaminants.

The focus has increasingly shifted to the production, characteristics, applications and opportunities for BC and modified BC to treat wastewater. Removing cations, anions, organic contaminants including dyes through the sorptive process can well be done by modified biochars. Modified BC is low-cost sorbent (compared to AC, graphene and carbon nanotubes)

and have similar removal capacity for contaminants [268]. Thus I have chosen biochar and its modification for the removal of ECs mostly antibiotics.

2.5. Adsorption of Antibiotics and EDCs Using Biochar and fBC

Thus, physicochemical treatment technologies are proving to be a highly suitable treatment option for organic contaminants [24]. The adsorption process is very efficient, simple to design and operate; and it is relatively inexpensive and unaffected by the potential toxicity as for biologically based processes [41]. Adsorption processes are widely used to remove organic contaminants from contaminated stream onto adsorbent surfaces [24], although its application to antibiotic removal has been reported for around 30 compounds so far. The efficiency of adsorption processes is highly affected by the type of adsorbent, adsorbate properties, and the compositions of the waste stream [42].

Biochar has received increasing recognition as an essential soil component, in carbon sequestration and water remediation [245, 246, 269-272]. Owing to its high hydrophobicity and aromaticity, biochar is an excellent sorbent for hydrophobic organic contaminants, e.g. aromatics [56, 246]. Biochar properties including surface functionality can be further improved through different modification technologies [55]. Studies on the adsorption of ionic organic compounds to biochar and functionalized biochar are limited compared to non-ionic hydrophobic organic contaminants [59, 273, 274]. Nonetheless, from the few studies that have used engineered carbon nanomaterials and biochars as adsorbents [273-275], it can be expected that biochar can significantly affect or even dominate the sorption of ionic organic contaminants such as sulfonamides in the environment. For example, it was observed that, under environmentally relevant conditions, distribution coefficient *(K_d)* values of two sulfonamides (SMX and sulfapyridine) to multi-walled carbon nanotubes and crop residue-derived biochar could be in the order of 10^4 L kg^{-1}. These are several orders of magnitude higher than the reported K_d values to soils and clay minerals [274, 275]. Adsorption of sulfonamides to biochar is expected to be heavily influenced by solution conditions and antibiotic speciation, e.g. neutral, cationic or anionic forms under different pH conditions (Figure 1). Different species can interact with biochar through different mechanisms [59, 273]such as π-π EDA interaction, nucleophilic addition, electrostatic attraction, pore filling, partitioning into un-carbonized fraction and formation of CAHB with surface oxygen groups. This is particularly the case under alkaline conditions with multiple surface groups of sulphonamides and with certain type of biomass materials and biochar preparatory conditions [57, 59, 257, 276].

2.6. Sorption and Reduction of Chloramphenicol Antibiotics Using ZVI and Its Composites

It has been demonstrated that ZVI (redox potential, $E^o = -0.44$ V) and several other zero-valent metals can serve as efficient reducing agents for the remediation of chlorinated organic compounds, nitro-aromatic compounds, heavy metals, nitrate, dyes and phenolic compounds from groundwater and wastewater [65, 277-283]. To date, most of the studies have focused on using ZVI to remove chlorinated hydrocarbons from water [62, 281, 284, 285] due to dechlorinative reduction nature of ZVI. However, ZVI can be easily oxidized in the presence of oxygen. Powder state unstable [286]. These phenomena leading to ZVI applications in fixed bed column or other dynamic flow systems result in the high-pressure drop and restriction of nZVI for field-scale applications [286]. Attempts have been proposed to enhance the nZVI transport in natural subsurface environments with the common objective of stabilizing the colloidal suspensions. nZVI has already been coated/impregnated with polymeric materials (such as polystyrene sulfonate, polyacrylic acid, and carboxymethylcellulose), combined with resin, biochar [287], activated carbon [288, 289], multi-walled carbon nanotube [290], clay mineral supported (e.g. kaolinite, and bentonite) [291-296], and modified with hydrophilic carbon, and embedded in a silica matrix to obtain a stable nZVI suspension [297]. It was reported that nZVI particles modified by covalently binding with carboxymethylcellulose exhibited high transport potential in packed beds of glass, beads, sand and soil [297]. All these researchers reported that nZVI-composites materials were applied once for contaminant removal. Also, the fate of these nZVI-composites for a further stage of application is not clear. Theoretically and practically, nZVI particles in composite materials lose their reductive nature during application when in contact with the contaminants and eventually produce different species either in solution or in the composite. The questions that arise are: what is the transformed ZVI-composite material? Is it stable and usable for further and repetitive applications? What are its unique characteristics regarding chemical structure and interfacial properties? Thus to shed light on nZVI and its composite, I have synthesized nZVI from scrap materials and immobilized on functionalized biochar (fBC), which were tested for the removal of a chlorinated antibiotic chloramphenicol over repetitive cycles. Chloramphenicol as an antibiotic can cause genotoxic and other side effects such as aplastic agranulocytosis, anaemia, and leukopenia [299]. Low removal efficiencies of chloramphenicol from wastewater have been reported using biological treatment technologies as it does not degrade in the metabolic system and thus, has frequently been detected in surface water, groundwater, and even in drinking water [16, 44]. The removal of chloramphenicol from wastewater has been reported

using different physicochemical methods [284, 300, 301], among which ZVI has been widely applied [62, 284, 285]. Moreover, different studies reported different reduction products [62, 284, 285, 299], and so far no study has been conducted using ZVI and ZVI-carbonaceous composite for removing chloramphenicol except deionized water. Hence, the application of ZVI and its composite for removing chloramphenicol from different water and the identification of byproducts are of great importance. Also, such kind of composite may possess simultaneous sorption and reduction which has not been reported. Thus the calculation of the amount of sorption and reduction is necessary to differentiate the role of each in such composite materials.

2.7. Conclusions and Research Gaps

Recently, the removal of EDCs and antibiotics from aqueous solution has gained extensiveinterest from academic researchers and wastewater treatment practitioners. From the literature review, some principal findings are summarized as below:

- Antibiotics are unique medicines in that they act selectively on bacteria, among them the pathogens while leaving human cells and tissues unaffected. The mainstream of these substances is natural from the microbial origin, however possibly semi-synthetic or synthetic. Antibiotics are widely used in large amounts for treating bacterial diseases in both humans and animals. The compounds can pollute soil, surface and groundwater via runoff or leaching from the manure of livestock, aquaculture, poultry and pets as fertilizer for agriculture production. Antibiotics in water can pose serious problems to the ecosystem and have several side effects, e.g. aplastic anaemia. Numerous methods to eliminate antibiotics from the aquatic environment, e.g. advanced oxidation processes, combined chemical/biological treatment, aerobic digestion integrated with activated carbon, ion exchange, coagulation, flocculation, sedimentation, ultraviolet irradiation, have been researched. Among these techniques, the most efficient, economical and environmentally friendly method for the removal of antibiotics from water is adsorption using cost-effective adsorbents. Many typical low-cost adsorbents obtained from natural minerals, agricultural waste/by-products and industrial waste/by-products have been applied for removing antibiotics from aqueous solution.
- EDCs are exogenous substances or mixtures that alter the functions of the endocrine systems and consequently cause adverse health effect in an intact organism, or its progeny or populations. Estrogenic compounds are those who can mimic (or block) the effect of endogenous estrogen, and therefore, represent one class of endocrine

disruptors. EDCs can cause adverse effects due to exogenous endocrine disruption in the reproductive, sexual differentiation, neurological and immune systems even at low concentrations (ng L^{-1} to μg L^{-1}). Exposure in people is typically a result of contamination of the food chain, inhalation of contaminated house dust or occupational exposure. They produce their effects by mimicking, antagonising or altering endogenous steroid levels (androgens or oestradiol, E2) via changing rates of their synthesis or metabolism and / or expression or action at receptor targets. The effects associated with EDCs are breakage of eggs of birds, fishes and turtles, problems in reproductive systems, change in immunologic system of marine mammals, reduction of sperm of human organ, including reduced female fecundity, longer time to conception, higher miscarriage rates and decreased sperm motility increase in the incidence of breast, testicle and prostate cancers, and endometriosis. Adverse effects of EDC exposure on reproductive physiology have also been seen in numerous animal models, mainly when exposure occurs early in development. In mammal and other vertebrates, EDC exposure during development alters both male and female gonad development, reduction in sperm counts, abnormal sperm, and changes in sexual behaviour, such as demasculinisation and feminisation of male offspring. Many advance treatment processes have been applied for removing of EDCs. However, the removal success still not satisfactory.

- In physical treatment processes, adsorption process was found to be a prominent method for removing antibiotics and EDCs. Therefore, as a low-cost adsorbent, mainly, functionalized biochar is a good candidate due to its adsorption capacity and large quantity. Functionalized biochar prepared from bamboo and eucalyptus wood is a low-cost sorbent and is potential for removing antibiotics and EDCs. It is documented that varieties of magnetic materials have been used for removing antibiotics from aquatic matrices, e.g. scrap iron, iron nanoparticles, magnetite, magnetic montmorillonite, iron oxides, microscale zero-valent iron, nanoscale zero-valent iron. Thus, immobilization of ZVI onto functionalized biochar will be also able to increase for removing organic contaminants.
- To date, adsorption mechanism has been theoretically explained in most of the literature and the proposed sorptive removal mechanisms of antibiotics and EDCs included hydrogen bond formations, π-π electron-donor acceptor interactions, electrostatic and non-electrostatic interactions, complexation through different mechanisms and redox interactions.

Research Gaps:

Even though much work has been conducted for removing EDCs and antibiotics from water using different adsorbents and reductants, some important research gaps still exist as follows:

- There is a lack of studies on using biochar and functional biochar adsorbents for treating water containing antibiotics and EDCs. Subsequently, more research is needed to understand more and confirm whether the application of biochar and functional biochar in removing antibiotics and EDCs from water is warranted and advantageous.
- Removal of a mixture of contaminants using a novel modification process of adsorbents in water treatment is very interesting. However, the amount of research in this field has been limited. Further studies need to be conducted to choose optimal conditions for the use of this technique to produce the best adsorbent.
- Current studies have only confirmed adsorption mechanisms of antibiotics, EDCs based on the theoretical aspects, and therefore there is little research focusing on the driving forces for the pollutants removal by adsorbents. Thus, there is a real need for research to provide detail understanding of the uptake pathways of EDCs and antibiotics adsorption.
- Most of the studies on using adsorbents for the abatement of EDCs and antibiotics from aqueous solution are in a single compound based. It is a common phenomenon that if a mixture of compounds present in a solution then the adsorbents should have some tendency to remove all of contaminants based on their sorption affinity and their removal mechanism may vary based on contaminant types. However, none of the previous studies has focused on this issue.
- The removal mechanisms with experimental proof have not been established, and this kind of approaches can be a good option for future study.
- Study gap on the reduction and adsorption of chloramphenicol anitibiotics using functionalized biochar-ZVI composite materials.

UNIVERSITY OF TECHNOLOGY SYDNEY

Faculty of Engineering and Information Technology

CHAPTER: THREE

MATERIALS AND METHODS

CHAPTER THREE: MATERIALS AND METHODS

3.1. Materials

3.1.1. Experimental Materials

Antibiotics such as sulfamethoxazole, sulfamethazine, sulfathiazole and chloramphenicol were purchased from Sigma Aldrich. EDCs estrone (E1), 17β-estradiol (E2), estriol (E3), 17α-ethynylestradiol (EE2), bisphenol A (BPA) and 4-*tert*-butylphenol (4*t*BP) were purchased from Sigma Aldrich. Organic solvents such as methanol, methanol-*d4*, ethanol, acetonitrile, hexadecane, acetone, 2-nonanone (NON-2), and formic acid of HPLC grade were purchased from Sigma-Aldrich, Australia. Peptone, beef extract, humic acid, tannic acid, sodium lignin sulphonates, Na-laryl sulphate, acacia gum powder, arabic acid, ammonium sulphate, KCl, NaCl, HCl, NaOH, H_2SO_4, $AlCl_3$, $CaCl_2$, K_2HPO_4, NH_4HCO_3, and $MgSO_4.3H_2O$ were of analytical-grade. Phenanthrene (98%), 1,3-dinitrobenzene (DNB), and *para* amino benzoic acid (PABA, > 99%) were also purchased from Sigma-Aldrich. A Zorbax Bonus RP C_{18} column (5.0 μm, 2.1 ×1.50 mm) was purchased from Agilent Technologies.

3.1.2. Woody Biomass Collection and Processing

Woody materials were chosen for the preparation of biochar, functional biochar and composite material. Eucalyptus wood (*Eucalyptus globulus*) was supplied by New Forest Asset Management Pty. Ltd., Portland, Victoria, Australia. Eucalyptus wood is abundantly grown in green triangle region of South and Western Australia. At first the raw material was cut into 1.0-4.0 mm small particle. After washing with DI water and drying, samples were stored for further utilization.

Untreated bamboo wood (Bamboo asper poles) sample was donated by Baron Bay Bamboo. Biomass material was initially cut into 3.0-5.0 cm long pieces, and it was then dried. Then biomass materials were further cut into 1.0-4.0 mm sizes small particle using UTS engineering workshop facilities. After washing with DI water and drying, samples were stored for further utilization.

3.1.3. Scrap Iron Materials

Scrap iron waste (a mixture of iron material and plastics) was collected from UTS engineering workshop for the extraction of iron and for the preparation of nano-zero valent iron (nZVI/Fe^0). Firstly, scrap material was washed several times with tap water and dried at 105 ^{0}C in a furnace overnight. This sample was stored for further use.

3.1.4. Stock Solutions of Antibiotics and EDCs

Each antibiotic and EDC stock solution was prepared in methanol with an initial concentration of 1 g L^{-1} and stored at 4 ºC for further use. The stock solution was then diluted to the desired concentrations and sorption experiments conducted. In case of a mixture of antibiotics and EDCs, each stock solution was directly added to the aqueous solution (co-solute was added up to 1% to avoid co-solute effect in mixed condition) and mixed thoroughly to make desired concentration and rest of the contaminants added one by one. Concentrations were checked by calibrating the result.

3.1.5. Furnace and Reactor for Biochar & Functionalized Biochar Preparation

A fixed bed reactor has used for the pyrolysis of the biomass particles (**Figure 3.1**). The reactor was heated inside an electrical furnace (model: L51 SP, GS Geprüfte Sicherheit, BG-PRÜFZERT, W- Germany) by under oxygen hungry conditions by providing nitrogen environment. As shown in the figure, pyrolysis reactor with biomass feeding placed inside the furnace and turned on the switch at the desired temperature. After that, nitrogen gas passes through the inlet into the reactor according to the following set up. During pyrolysis, a mixture of gasses products produced and they passed through the outlet of the reactor system to vent directly. After a desired period, the reactor took out and biochar and functionalized biochar collected.

3.1.6. Synthetic Wastewater, MBR Sewage Effluent and Lake Water

Lake water (pH 7.2, temperature 19.9 ºC, total dissolved solids 116 mg L^{-1}, total organic carbon 75.56 mg L^{-1}, and total carbon 76.72 mg L^{-1}) was collected from the Victoria Park, NSW, Australia, and was filtered through 1.2 μm filter paper before being stored at 4 ºC. Synthetic wastewater was prepared based on a recent study [33]. MBR sewage effluent was collected from Central Park water treatment plant, Sydney, Australia. After collecting, MBR effluent was filtered through 1.2 μm syringe filter and measured physicochemical properties such as pH, turbidity, UV_{254}, total organic carbon (TOC), chemical oxygen demand, conductivity, alkalinity, dissolved oxygen, inorganic ions, and metal ions were measured. MBR effluent was stored in the fridge and subsequently used for another experimental purpose. Deionized water, lake surface water, MBR effluent and synthetic wastewater were spiked with antibiotics and EDCs before contact with materials to assess the extent of sorption in different water types.

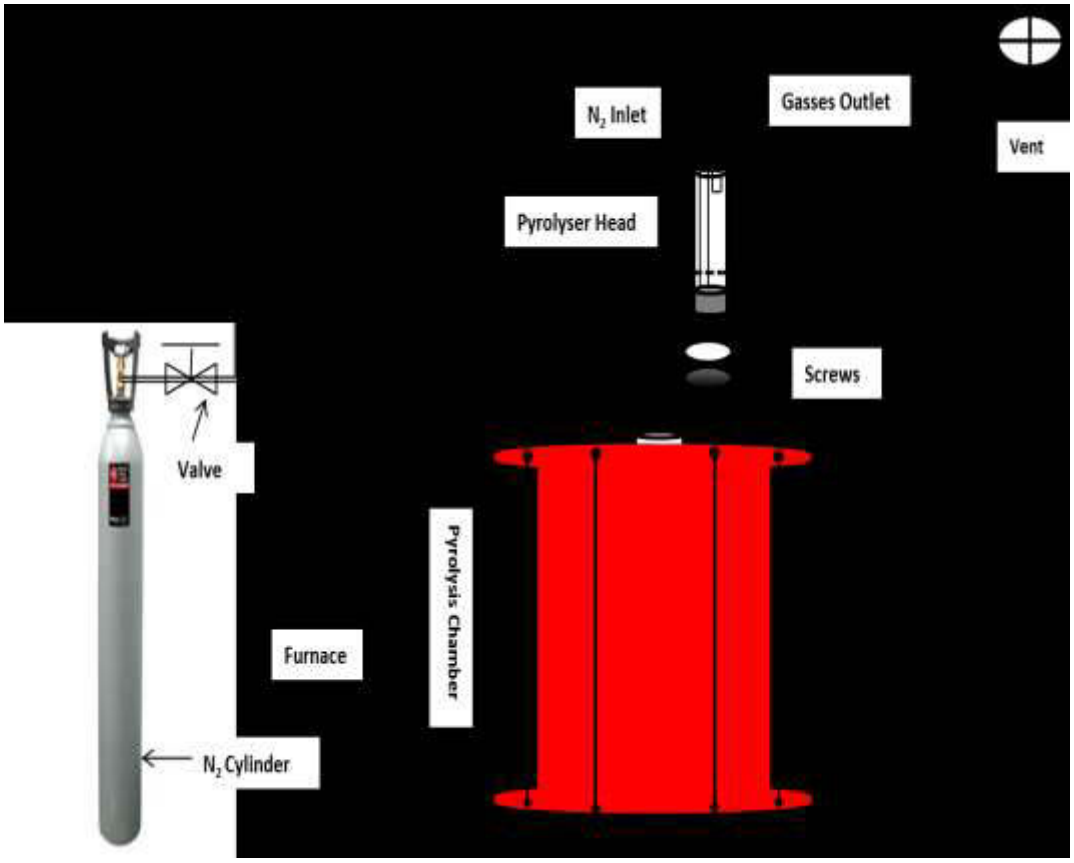

Figure 3.1: Fixed bed pyrolyser (reactor) for pyrolysis of biomass.

3.2. Methods

3.2.1. *Preparation and Functionalization of Adsorbents, Synthesis of ZVI & Preparation of Composite*

3.2.1.1. Preparation of Biochar

Bamboo and *Eucalyptus Globulus* woods (30.0 g – 48.0 g) were selected for the production of biochar. Biomass particle sizes were in the range of 600 µm- 2.0 mm (or, 3.00 cm long and 8.00 mm wide). A fixed bed reactor has been used for the pyrolysis of the biomass particles (**Figure 3.1**). The reactor was heated inside an electrical furnace by under oxygen hungry conditions. The reactor temperature was set for 380 °C and gradually pyrolyzed at an average heating rate of 10.00-11.40 °C/min under nitrogen supply at a constant pressure of 2.5 psi. When the temperature reached at 380 °C, nitrogen pressure was raised to 10 psi and maintained for 20 minutes. The residence time at pyrolysis temperature was 2 h. After paralyzing the biochar, sample was allowed to cool down to room temperature inside the furnace. Prepared biochar was rinsed with tap water and DI for several times to minimize the impurities and ash contents. Then

pH was adjusted around 7.0 and drying at 80 °C. All biochar samples were then examined for their physical and chemical characteristics without further treatment. The prepared biochar named as BBC380 and EGBC380.

3.2.1.2. Functionalization of Biochar

Modification of bamboo biochar was carried out by soaking 15.3 g of BBC380 into 50% of 30 ml orthophosphoric acid ($o$$H_3PO_4$). The mixture was last for 3 hours with continuous stirring in an orbital shaker at 50 °C. The mixture was ten transfers into a reactor and finally heated at 600 °C for two hours with a continuous flow of nitrogen at 2.5 psi. The modified was finally then washed and dried at 120 °C for overnight. The modified biochar named as **m1bBBC600, i.e. fBC-1**.

Modification of *Eucalyptus globulus* biochar has been carried out by soaking 8.0 g of BBC380 into 50% of 30.0 mL ortho phosphoric acid ($o$$H_3PO_4$). The mixture was last for 3 hours with continuous stirring in an orbital shaker at 50 °C. The mixture was ten transfers into a reactor and finally heated at 600 °C for two hours with a continuous flow of nitrogen at a 2.5 psi. The modified was finally then washed and dried at 120 °C for overnight. The modified biochar named as **fBC-2**.

3.2.1.3. Synthesis of ZVI and Preparation of ZVI-Biochar Composite

Scrap iron waste (a mixture of iron material and plastics) collected from UTS engineering workshop was washed several times with tap water. The scrap iron material (30 g) was mixed with 120 mL of 10% HNO_3 for 10 min to remove impurities. The residual iron material was transferred to 600 mL of 15% H_2SO_4 (v/v) and stirred for 3 h at 60 ^{0}C. The residues were separated by settling. This ferrous sulphate solution (green colour) was obtained by filtration and stored as a stock solution for further use. The stock solution iron concentration was measured and found iron concentration being 21.9 g L^{-1}.

The stock solution (15 mL) was diluted 10 times with deionized water and pH was adjusted to ~5.0 using 2 M NaOH solution. Thus, ferrous sulphate was transformed to reddish brown ferric sulphate and stirred for few minutes. Then, 15 mL of 1.6 M $NaBH_4$ was added drop-wise into the solution and mixed vigorously for 30 min, and nZVI was produced (**Eq. 3.1**). The nZVI solution was centrifuged at 2000 rpm for 7 min and washed with ethanol. Finally, nZVI was dried in a vacuum oven for 8 h and stored in an airtight container until further use [302].

$$4Fe^{3+} + 3BH_4^- + 9H_2O \rightarrow 4Fe^0 + 3H_2BO_3^- + 6H_2 + 12H^+ \qquad (3.1)$$

To produce a nZVI-fBC composite, 5 mL of the stock solution was diluted ten times, and pH was adjusted to 5.0 using 2 M NaOH and mixed thoroughly for 5 min. Then 1.0 g of fBC was added to the solution and mixed for 2 h, and 5 mL of ethanol was added. Next, 5 mL of 1.6 M $NaBH_4$ was added drop-wise into the solution and mixed vigorously for another 2 h. Thus, nZVI was immobilized onto fBC surface. Finally, the product was filtered, washed, dried and stored to obtain a nZVI-fBC composite.

3.2.2. Characterization Methods

Proximate analysis, including yield, moisture content, mobile matter, ash and residual matter contents (fixed carbon) of bamboo and eucalyptus wood were determined. Detail description about proximate analysis can be found in **chapter 4 (section 4.1.2.3)**. The yield of biochars has been represented in **Table 3.1.** From the table 3.1, we can see that yield tend to be decreases as the pyrolysis temperature goes up. In comparison, maximum yield was found for the bamboo biochar at 380 °C, and minimum yield was found for eucalyptus L. at pyrolysis temperature 600 °C. This was due to the release of more volatile fraction from the raw materials. In general, the release of volatile matter increased as the temperature goes up.

Table 3.1: Yield of biochar prepared from different biomass.

Raw material	Types of BC	Temp.	W_1	W_2	Final Wt. (g)	Yield (%) $_{\text{dry basis}}$
Bamboo	BBC380	380	47.5	44.84	19.5	43.5
	BBC600	600	20	18.88	6.7	35.50
Eucalyptus G.	EGBC380	380	31.0	28.36	9.85	34.73

W_1= Initial wt.(g),$_{\text{wet basis}}$ & W_2 = Initial wt.(g),$_{\text{dry Basis}}$

Different instrumental characterization techniques were employed for the characterization of biochar, functionalized biochar and composite materials. Fourier transform infrared spectroscopy (FTIR), Scanning electron microscope (SEM) with energy dispersive spectroscopy (EDS), thermogravimetric analysis (TGA) with differential scanning calorimetry (DSC), Brunauer-Emmett-Teller BET, X-ray diffraction (XRD), X-ray photoelectron spectroscopy (XPS), Zeta potential and sizer, and Raman spectroscopy were used to obtain the surface morphology, elemental composition, mineral species, surface area, surface charge, and functional groups. Details on those instruments are given below:

A. SEM-EDS

Surface morphology and elementary composition of the material samples were analysed by Zeiss Evo SEM (Carl Zeiss Microscopy, USA) with attached EDS at 15kV-30kV. For different particles, images were collected at different magnifications.

B. XRD

Powder X-ray diffraction (XRD) was used to identify the surface homogeneity or heterogeneity of biochar, fBC, ZVI, and composite. The sample was pulverized to powdered form and smeared on a metal holder at room temperature. XRD analysis of the samples was carried out using a Bruker D8 Discover diffractometer (Bruker, Germany) using Cu Kα radiation, in the scattering angle 2θ range 20°–80° at a rate of 5° per min.

C. XPS

XPS is a surface sensitive technique which can determine the binding energy of elements in the top 10 nm of a sample. The abundance of surface functional groups of samples was obtained by using X-ray Photoelectron Spectroscopy (XPS) (Thermoscientific, UK).

D. BET

BET characterization was applied to the raw and modified adsorbents. The specific surface area and porosity distributions were calculated using Brunauer-Emmett-Teller nitrogen adsorption-desorption isotherms and the Barrett-Joyner-Halenda (BJH) method, respectively, by utilizing a Micromeritics 3-FlexTM surface characterization analyzer at 77 K.

E. Zeta Potential

To analyze the surface relating zeta potential of the adsorbents, Malvern Zeta potential and Sizer was utilized. Adsorbents with Milli-Q water were adjusted at different solution pH values and then shaken at 150 rpm for 24 hours. Subsequently, zeta potential values of the samples were measured by Nano-ZS Zetasizer (Malvern, Model: ZEN3600). Zeta potential values of materials were measured with 0.1 M KCl background solution (for constant ionic strength).

F. TGA-DSC

Thermo-gravimetric analysis and differential scanning calorimetry (TGA-DSC) tests were done using SDT Q600 instrument. TGA-DSC analysis was carried out at 0-800 ^{0}C.

G. ^{1}H NMR

Proton nuclear magnetic resonance (^{1}H NMR) spectra were recorded at a specific concentration of solutes at room temperature using an Agilent 500 MHz NMR instrument. Samples were prepared in methanol-d_4 and measured after 24-30 hours. The chemical shifts (δ) were recorded by internally referenced to methanol-*d4* solvent and observed proton frequency shift was calculated based on NMR instrument frequency and chemical shift.

H. Raman Spectroscopy

Raman shifts measurement was carried out using Renishaw in via Raman spectrometer (Gloucestershire, UK) equipped with a Leica DMLB microscope (Wetzlar, Germany), 17 mW at 633 nm Renishaw helium-neon laser source and CCD array detector using 50% laser intensity.

I. Furnace

An electrical furnace (model: L51 SP, GS Geprüfte Sicherheit, BG-PRÜFZERT, W- Germany) was used to prepare biochar and fBC.

J. FTIR

Fourier transform infrared spectroscopy (FTIR) (Miracle-10: Shimadzu) was used to determine surface functional groups. The spectra were obtained at 4 cm^{-1} resolution by measuring the absorbance from 400 to 4000 cm^{-1} using a combined 40 scans.

Experimental findings of those instruments for different materials can be found on chapter 4 and 5 in details in characterization subsections.

3.2.3. Batch Adsorption Experiments for Removing Antibiotics and EDCs

Antibiotics such as SMX, SMT, CP, and SMZ and EDCs such as E1, E2, E3, EE2, BPA and 4*t*BP stock solutions (1.0 g L^{-1}) were prepared methanol solution and were used to obtain the starting solute concentrations in batch sorption studies. The amount of methanol added in the final solution was less than 1.0% of the total volume; hence, it was insignificant for the co-solvent effect. Different concentration of each solute was used to get the data for isotherm and kinetics studies. Effect of pH was also studied, and effect of different ions was also performed. Details on batch adsorption methods of antibiotics and EDCs can be found the **chapters 4 and 5**.

3.2.4. The Analytical Method of the Antibiotic and EDCs Concentrations

The initial and final concentrations of adsorbates were measured by high-performance liquid chromatography (**Jasco HPLC Instrument**) equipped with an auto-sampler; Liquid chromatography-mass spectrometry (LC-MS); Microwave Plasma-Atomic Emission Spectroscopy (MP-AES), total organic carbon (TOC) analyser and UV-Vis spectroscopy. Details instrumental description of each instrument is described below, and the detail analytical methods can be found in chapter 4 and 5 in materials and methods subsections.

A. UV-Vis Spectroscopy

Ultraviolet-visible **spectroscopy** or **spectrophotometry** (**UV-Vis** or **UV/Vis**) refers to absorption spectroscopy or reflectance spectroscopy in the ultraviolet-visible spectral region. This means it uses light in the visible and adjacent ranges. The absorption or reflectance in the visible range directly affects the perceived colour of the chemicals involved. In this region of the electromagnetic spectrum, atoms and molecules undergo electronic transitions. Absorption spectroscopy is complementary to fluorescence spectroscopy, in that fluorescence deals with transitions from the excited state to the ground state, while absorption measures transitions from the ground state to the excited state. To measure concentrations of organic compounds a UV–visible spectroscopy (Shimadzu) was employed.

B. LC-MS (QTOF)

Liquid chromatography-mass spectrometry (LC-MS) is now a routine technique with the development of electrospray ionisation (ESI) providing a robust and straightforward interface. It can be applied to a wide range of biological molecules and the use of tandem MS and stable isotope internal standards allows highly sensitive and accurate assays to be developed although some method optimisation is required to minimise ion suppression effects. Fast scanning speeds allow a high degree of multiplexing and many compounds can be measured in a single analytical run. Chloramphenicol and its reduced products were identified by LC-MS/QTOF in positive mode, on an Agilent Poroshell 120 EC-C_{18} column (2.7 μm, 4.6 mm × 50 mm). The elution began with 95% pure water and 5% methanol, ending with 1% pure water and 99% methanol within 9 min at a flow rate of 0.35 mL min−1. Following elution, the mobile phase was changed to 95% water and 5% methanol. The total run time was 13 min.

C. HPLC

High-performance liquid chromatography or high-pressure liquid chromatography (HPLC) is a chromatographic method that is used to separate a mixture of compounds in Anal. Chem. and biochemistry to identify, quantify or purify the individual components of the mixture. Reversed-phase HPLC/UHPLC chromatography is a commonly used separation mode. It provides dynamic retention of compounds possessing hydrophobic and organic functionality. A combination of hydrophobic and van der Waals type interactions between all the target compound and both the stationary and mobile phases enables the retention of these compounds by reversed phase. The initial and supernatant concentrations were measured using HPLC (Jasco) with aliquots from each reactor being taken and filtered through a 0.2 μm PTFE filter followed by 50 μL of sample injection. HPLC equipped with an auto-sampler, a UV detector at 285 nm, and a Zorbax Bonus RP C_{18} column (5.0 μm, 2.1 × 1.50 mm, Agilent Technologies) was used for separation.

D. MP-AES

Microwave Plasma-Atomic Emission Spectroscopy (MP-AES) represents an entirely new elemental analysis technique that has been designed to improve analytical performance and productivity while decreasing operating costs by eliminating the flammable and expensive gas requirements used in typical elemental analysis techniques. The Nitrogen based plasma operates from a compressed air supply and Nitrogen generator, resulting in a significant reduction in operating costs and reduced infrastructure costs. Also, the state-of-the-art design of the Agilent 4100 MP-AES reduces the number of costly consumables such as hollow cathode lamps used in Atomic Absorption techniques. Iron concentration was determined using microwave plasma atomic emission spectroscopy (4100-MP-AES, Agilent Technologies).

E. TOC Analyser

Total organic carbon (TOC) is the amount of carbon found in an organic compound and is often used as a non-specific indicator of water quality or cleanliness of pharmaceutical manufacturing equipment. TOC may also refer to the amount of organic carbon in soil, or in a geological formation, particularly the source rock for a petroleum play; 2% is a rough minimum. Dissolved organic carbon concentration measurement of MBR effluent, lake wastewater and synthetic wastewater before and after sorption experiments were carried out using a Multi N/C 2000 analyser (Analytik Jena AG) after filtering the water samples through 1.2 μm glass fibre filters.

UNIVERSITY OF TECHNOLOGY SYDNEY

Faculty of Engineering and Information Technology

CHAPTER: FOUR

ANTIBIOTICS REMOVAL FROM WATER AND WASTWATER: MECHANISMS AND APPLICATIONS

CHAPTER FOUR: ANTIBIOTICS REMOVAL FROM WATER AND WASTEWATER: MECHANISMS AND APPLICATIONS

4.1. Single and Competitive Sorption Properties and Mechanism of Functionalized Biochar for Removing Sulfonamide Antibiotics from Water

4.1.1. Introduction

Antibiotics can selectively act on bacteria and pathogens without affecting human cells and tissues [57, 67, 303]. Concerning the different classes of antibiotics, sulfonamide antibiotics such as sulfamethazine (SMT), sulfamethoxazole (SMX) and sulfathiazole (STZ) are commonly used in human therapy as well as veterinary medicine because they are endowed with broad activity spectrum against Gram bacteria to prevent and control infectious diseases [66, 304]. However, a large fraction of sulfonamides remains un-metabolised through the digestive system and is released continually to soil and water due to their high water solubility [44, 67]. They can potentially damage aquatic organisms and impact on human health through the food chain [68]. Therefore, the adverse impact of such compounds has received extensive attention.

Biochar has received increasing recognition as an important soil component, in carbon sequestrations and water remediation [245, 246, 269-272]. Owing to its high hydrophobicity and aromaticity, biochar is an excellent sorbent for hydrophobic organic contaminants e.g. aromatics [56, 246]. Biochar properties including surface functionality can be further improved through different modification technologies [55]. Studies on the adsorption of ionic organic compounds to biochar and functionalized biochar are limited compared to non-ionic hydrophobic organic contaminants [59, 273, 274]. Nonetheless, from the few studies that have used engineered carbon nanomaterials and biochars as adsorbents [273-275], it can be expected that biochar can significantly affect or even dominate the sorption of ionic organic contaminants such as sulfonamides in the environment. For example, it was observed that, under environmentally relevant conditions, distribution coefficient (K_d) values of two sulfonamides (SMX and sulfapyridine) to multi-walled carbon nanotubes and crop residue-derived biochar can be in the order of 10^4 L kg^{-1}. These are several orders of magnitude higher than the reported K_d values to soils and clay minerals [274, 275]. Adsorption of sulfonamides to biochar is expected to be heavily influenced by solution conditions and antibiotic speciation e.g. neutral, cationic or anionic forms under different pH conditions (**Figure 4.1.1**). Different species can interact with biochar through different mechanisms [59, 273] such as π-π EDA interaction, nucleophilic addition, electrostatic attraction, pore filling, partitioning into un-carbonized

fraction and formation of CAHB with surface oxygen groups. This is particularly the case under alkaline conditions with multiple surface groups of sulphonamides, and with certain type of biomass materials and biochar preparatory conditions [57, 59, 257, 276].

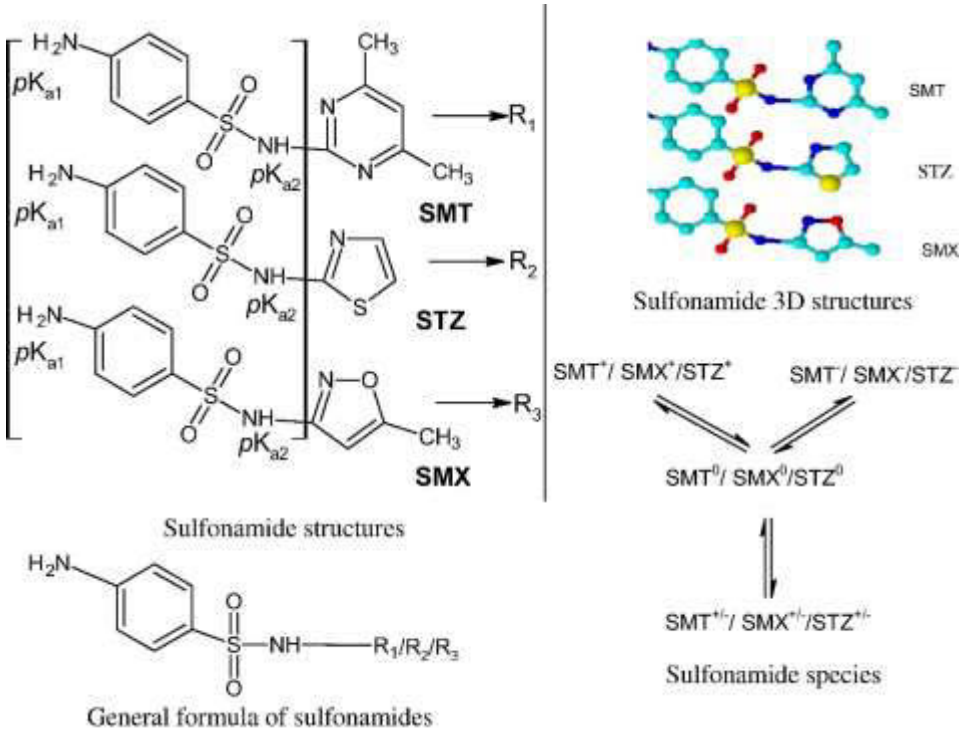

Figure 4.1.1: Molecular structures of sulfonamides antibiotics and their equilibrium species.

Table 4.1.1: Physicochemical properties of the antibiotics investigated in this study.

Group	Compound	Molecular mass	log K_{ow}[a]	$pK_{a1/a2}$[b]	Solubility[a] (mg L^{-1})
Sulfonamides	SMX	253.3	0.89	1.97/6.16	610
	STZ	255.3	0.05	2.04/6.93	373
	SMT	278.3	0.14	2.04/6.99	1500

[a]Values obtained from U.S. National Library of Medicine: http://toxnet.nlm.nih.gov; [b]Values obtained from ChemAxon: http://www.chemicalize.org

To date, the majority of adsorption studies of different antibiotic residues have been conducted using single solutes, and studies are scarce on the competitive nature and mechanisms of antibiotic mixtures using different adsorbents. These include, for example, natural clay, activated carbon, ion exchange resins, graphene, carbon nano-tubes and biochar. This study therefore aims to bridge this gap in our knowledge so that the mechanism of single and competitive nature of three widely used sulfonamides antibiotics (sulfamethazine,

sulfamethoxazole and sulfathiazole) using functionalized biochar is better understood. Their physicochemical properties are shown in **Table 4.1.1**. Laboratory experiments were conducted to elucidate and compare the single and comparative interactions of sulfonamides onto functionalized biochar. Experimental data were fitted to different isotherm models, and the adsorption affinities were compared. The governing adsorption mechanisms were analysed. The effects of pH and temperature on the adsorption were examined to verify the proposed sorption mechanisms and adsorption properties. The research findings will contribute to improved understanding of the adsorption behaviour and mechanism of antibiotics mixture.

4.1.2. Experimental Section

4.1.2.1. Chemicals and Reagents

The antibiotic standards (purity > 99%) of SMT, SMX and STZ, HPLC-grade organic solvents such as methanol, acetonitrile and acetone, and analytical-grade aluminium chloride, potassium chloride and formic acid were purchased from Sigma-Aldrich, Australia.

4.1.2.2. Preparation of Biochar and Functionalized Biochar

Biomass was selected for the preparation of biochar as reported in Ahmed et al. [56]. Briefly, 50 g of bamboo biomass material was cut into 0.6–2 mm size particles and placed into a fixed bed reactor. Biomass material was gradually pyrolyzed at 380 ºC in a reactor inside the furnace at an average heating rate of 10–11.4 °C min^{-1} under continuous nitrogen supply at 2.5 psi for 2 h. When the temperature reached at 380 °C, nitrogen pressure was increased to 10 psi and maintained for 20 min. The reactor was cooled at room temperature and biochar was grinded and finally washed and dried. The prepared biochar coded as BBC380.

Functionalization of BBC380 was carried out by soaking 15.3 g of BBC380 in 30 mL of 50% *ortho*-phosphoric acid (H_3PO_4) for 3 h at 50 °C. H_3PO_4 was selected based on previous studies [55, 305]. The mixture was then heated at 600 °C for 2 h with the same heating rate as used before under continuous nitrogen supply at 2.5 psi, cooled at room temperature, and washed with distilled water 4 times while adjusting pH to 7, followed by drying overnight at 120 °C, to obtain the functionalized biochar (1MbBBC600 i.e. fBC-1). Average fBC-1 particles size ranged from 75 to 1000 μm.

4.1.2.3. Characterizations of Biomass, and Functionalized Biochar

The physicochemical characteristics of raw biomass, biochar and functionalized biochar were extensively examined using Fourier transform infrared spectroscopy (FTIR), BET, Raman spectroscopy, thermogravimetric analysis (TGA) and others (**Tables 4.1.2 and 4.1.3, Figure 4.1.2).** The yield, moisture content, mobile matter, ash and residual matter contents (fixed carbon) were determined. Briefly, the yield was measured by the difference between initial weight and after pyrolysis of the biomass on dry basis. Moisture content was determined after drying in oven at 105 ºC for 12 h and cooling in a desiccator. Mobile or volatile matter was calculated by placing 1 g of dry biomass in covered crucible in a furnace at 450º C for 30 min. The weight difference was measured as percentage volatile matter. Ash content was determined by taking 5.0 g of dry sample in a crucible and placed in a furnace and heated at 550 ºC for 8 h. Then cooled in a desiccator and final weight was measured as percentage of ash content. The weight of the original sample, subtracted by its moisture content, ash content and volatile matter content corresponds to the stable carbon fraction of that sample and hence, this fraction is termed 'fixed carbon or fixed-C fraction'.

$$\%M_{fc} = (M_{dry} - M_{vm} - M_{ash})/ (M_{dry} - M_{ash}) \times 100 \quad (4.1.1)$$

where $\%M_{fc}$ is the fraction of fixed carbon (wt%), M_{vm} is the weight of volatile matter in the sample (kg), M_{dry} is the oven dry weight of the sample (kg) and M_{ash} is the weight of the ash residue of the sample (kg).

The produced samples were examined by using energy dispersive spectrometer (EDS) to determine the elemental composition of biochar and functionalized biochar (Zeiss Evo-SEM). EDS was measured on different parts of the biochars and average results are reported in **Table 4.1.2**. Structural analysis was conducted using FTIR (Miracle-10 from Shimadzu). The spectra were obtained at 4 cm^{-1} resolution by measuring the absorbance from 400 to 4000 cm^{-1} using a combined 40 scans. Raman shifts measurement was carried out using Renishaw in via Raman spectrometer (Gloucestershire, UK) equipped with a 17 mW Renishaw Helium-Neon Laser 633 nm and CCD array detector. Thermo-gravimetric analysis and differential scanning calorimetry (TGA-DSC) tests were done using SDT Q600. The specific surface area and porosity distributions were calculated using Brunauer-Emmett-Teller [127] nitrogen adsorption-desorption isotherms and the Barrett-Joyner-Halenda (BJH) method, respectively, by utilizing a Micromeritics 3-FlexTM surface characterization analyzer at 77 K. Zeta potential values were measured using 50 mg of functionalized biochar in 100 mL of 1-mM KCl solution at different pH. Samples were pre-equilibrated for 48 h. Zeta potential values were determined using a Nano-ZS Zeta-seizer (Malvern, Model: ZEN3600). Zeta potential was

measured three times at each pH (50 scans each time) and the average and standard deviation was calculated.

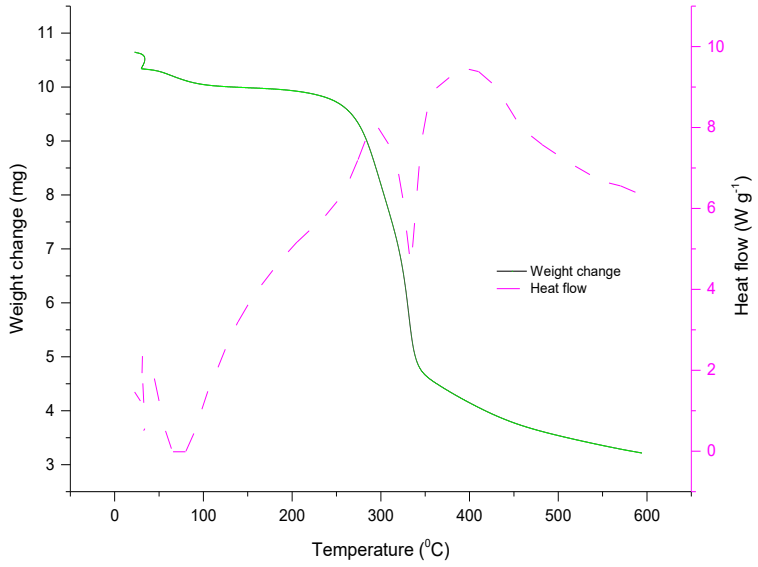

Figure 4.1.2: DSC-TGA graph for biomass raw material (bamboo).

Table 4.1.2: The basic properties, zeta potential and EDS data of biomass and biochar samples.

Sample	**Composition data**				
	$Yield_{dry\ basis}$ (%)	Moisture content (%)	Ash (%)	Volatile mater (%)	Fixed carbon (%)
Biomass		5.61	12.93	63.83	26.67
BBC380	43.50				
1MbBBC600					
Initial pH	1.62	3.00	4.35	6.13	10.00
Final pH	1.15	2.74	3.39	4.09	8.28
Zeta potential (mV)	5.34±0.32	-3.25±0.24	-12.76±1.23	-19.6±1.15	-45.9±4.67

Sample	**EDS analysis**			
	C %	O%	P%	Molar O/C
BBC380	81.18±2.9	18.83±0.9	-	0.232
1MbBBC600	51.96±2.5	39.52±1.2	9.16±1.0	0.761

Table 4.1.3: Summary of BET and BJH physical parameters for biochar and functionalized biochar.

Surface Area	**BBC380**	**1MbBBC600 i.e fBC-1**
Single point surface area at P/Po = 0.30	0.44 $m^2 g^{-1}$	0.82 $m^2 g^{-1}$
BET Surface Area	0.50 $m^2 g^{-1}$	1.12 $m^2 g^{-1}$
Langmuir Surface Area	0.11 $m^2 g^{-1}$	7.23 $m^2 g^{-1}$
t-Plot Micropore Area	0.47 $m^2 g^{-1}$	
t-Plot External Surface Area	0.027 $m^2 g^{-1}$	1.71 $m^2 g^{-1}$
BJH Adsorption cumulative surface area of pores between 17 Å and 3000 Å diameter	0.19 $m^2 g^{-1}$	1.11 $m^2 g^{-1}$
BJH Desorption cumulative surface area of pores between 17 Å and 3000 Å diameter	0.031 $m^2 g^{-1}$	1.64 $m^2 g^{-1}$
D-H Adsorption cumulative surface area of pores between 17 Å and 3000 Å diameter	0.21 $m^2 g^{-1}$	1.33 $m^2 g^{-1}$
D-H Desorption cumulative surface area of pores between 17 Å and 3000 Å diameter	0.0215 $m^2 g^{-1}$	1.53 $m^2 g^{-1}$
Pore Volume		
t-Plot micropore volume	0.00023 $cm^3 g^{-1}$	0.00043 $cm^3 g^{-1}$
BJH Adsorption cumulative volume of pores between 17 Å and 3000 Å diameter	0.00053 $cm^3 g^{-1}$	0.0023 $cm^3 g^{-1}$
BJH Desorption cumulative volume of pores between 17 Å and 3000 Å diameter	0.00048 $cm^3 g^{-1}$	0.0025 $cm^3 g^{-1}$
Pore Size		
BJH Adsorption average pore diameter (4V/A)	113.5 Å	83.8 Å
BJH Desorption average pore diameter (4V/A)	613.8 Å	59.8 Å
D-H Adsorption average pore diameter (4V/A)	153.7 Å	77.8 Å
D-H Desorption average pore diameter (4V/A)	892.3 Å	62.3 Å

4.1.2.4. Sorption Experiments Using Functionalized Biochar

Stock solutions of SMX, SMT and STZ were prepared with DI water in 1% methanol (insignificant co-solvent effect) without adjusting the pH. The studies on pH effect were conducted at different pH values starting from 1.5 to 10 for 24 h at room temperature to determine sorption equilibrium time. The solution pH was adjusted using 0.1 M HCl and 0.1 M NaOH solution before adding functionalized biochar. Batch single and competitive experiments were carried out at different temperatures (21 ± 0.5, 25 ± 0.5 and 30 ± 0.5 °C) by mixing and shaking 100 mg L^{-1} of functionalized biochar in 100 mL solution on an orbital shaker at 120 rpm for 40 h at a pH of 3.25, 4.50, 3.50 and 3.50, respectively, for SMX, SMT, STZ and mixtures of three antibiotics. The control experiments without adsorbents were also executed. The kinetics studies for single and competitive antibiotics were done using the same pH and adsorbent dosage as carried out in isotherm studies for 24 h. After equilibrium, final solution pH was measured and the supernatant concentration was measured with HPLC with aliquots from each reactor being taken and filtered through a 0.20 μm PTFE filter.

4.1.2.5. Analytical Method

The concentrations of antibiotics were measured by HPLC (Jasco) equipped with an auto-sampler and UV detector at 285 nm, by 20 µL injection. A reverse phase Zorbax Bonus RP C_{18} column (5.0 µm, 2.1 × 1.50 mm, Agilent Technologies) was used for the separation. Mobile phase A was composed of acetonitrile and formic acid (99.9:0.1) while mobile phase B was composed of Milli-Q water and formic acid (99.9: 0.1). The elution used 40% of A and 60% of B at a flow rate of 0.4 mL min^{-1}, which was changed to 0.2 mL min^{-1} at 0.1 min. The method was run over 8 min.

4.1.2.6. Distribution Coefficient, Kinetics and Isotherm Equations

The adsorption data obtained in the experiments were fitted to two different isotherm models namely Langmuir and Freundlich isotherm models and three kinetic equations. The apparent sorption distribution coefficient (K_d, L kg^{-1}) is defined by the ratio of adsorbate concentration on sorbent (Q_e, mg kg^{-1}) to the adsorbate concentration in solution (C_e, mg L^{-1}):

$$K_d = \frac{Q_e}{C_e} = \left(\frac{C_0 - C_e}{C_e}\right)\frac{V}{M} \quad (4.1.2)$$

where Q_e is the solid-phase concentration (mg g^{-1}), and C_o is the initial concentration (mg L^{-1}). The kinetic equations such as pseudo first order (PFO), pseudo second order model [306] and intra-particle diffusion model [17] can be represented as follows:

$$\text{PFO: } Q_t = Q_e(1 - e^{-K_1 t}) \quad (4.1.3)$$

$$\text{PSO: } Q_t = \frac{K_2 Q_e^2 t}{1 + K_2 Q_e t} \quad (4.1.4)$$

$$\text{IDM: } Q_t = K_i t^{\frac{1}{2}} + C \quad (4.1.5)$$

Parameters were estimated by nonlinear regression weighted by the dependent variable. Where, K_i is the apparent diffusion rate constant (mg g^{-1} $min^{-1/2}$), K_1 (min^{-1}) and K_2 (g mg^{-1} min^{-1}) are PFO and PSO kinetic rate constant, respectively, and C is a constant (mg g^{-1}) that provides the thickness of the boundary layer.

Langmuir and Freundlich isotherm models can been represented in following.

$$\text{Freundlich model: } Q_e = K_F {C_e}^{1/n} \quad (4.1.6)$$

$$\text{Langmuir model: } Q_e = \frac{Q_{max} K_L C_e}{1 + K_L C_e} \quad (4.1.7)$$

where Q_{max} is the maximum adsorption capacity (mg g^{-1}), n is a dimensionless number related to surface heterogeneity, K_F is the Freundlich affinity coefficient (mg^{1-n} L^n g^{-1}) and K_L is the Langmuir fitting parameter (L mg^{-1}).

4.1.3. Results and Discussion

4.1.3.1. Influences of pH on Distribution Coefficient

Sulfonamides sorption on carbonaceous materials revealed pronounced pH dependence. The effect of pH on the sorption coefficients is shown in **Figure 4.1.4a**. Sulfonamides sorption was greatly governed by the electrostatic interactions between antibiotics and functionalized biochar surface. The distribution coefficient (K_d) values (**Eq. (1))** for the sorption of sulfonamides reached their first maxima at pH 3.50 for STZ, at pH 3.25 for SMX and at pH 4.5 for SMT. A further increase of pH up to 5 (for SMX and STZ) and up to 7 (for SMT) resulted in a decrease in K_d values. Maximum sorption was due to the adsorption of neutral species of sulfonamides. Selected sulfonamides behaved as positive species at solution pH < 2.5 for SMT and STZ and pH < 1.6 for SMX (**Figure 4.1.3**). Biochar surface also became positive because the surface zeta-potential was also positive below pH 2.5. Hence less adsorption is expected due to electrostatic repulsion of positively charged biochar surface and sulfonamide antibiotics. The adsorption of antibiotics at pH < 2.5 may be dominated by the interaction between the protonated aniline ring of sulfonamide antibiotics and the π-electron rich functionalized biochar surface [59, 273]. The second sharp increase in K_d values for each single solute was observed from pH 5 to 6, 5 to 6.3, and 7 to 8, for SMX, STZ and SMT respectively; which coincided with the intersections of neutral and negative species of the three compounds. This was followed by a decreasing pattern up to pH 10. These trends may be due to the shifting of pH to neutral species region of sulfonamides as a result of proton release from functionalized biochar surface. The pH test showed that final solution pH became significantly lower and shift toward neutral region if the initial solution pH was maintained at above 7. A further increase of pH up to 10, the sorption of SMX^-, STZ^- and SMT^- species declined due to negative surface zeta-potential value and the negative surface electrostatic repulsion. However, the negatively charged biochar surface was still able to sorb to negative species from solutions through the formation of CAHB [59, 307].

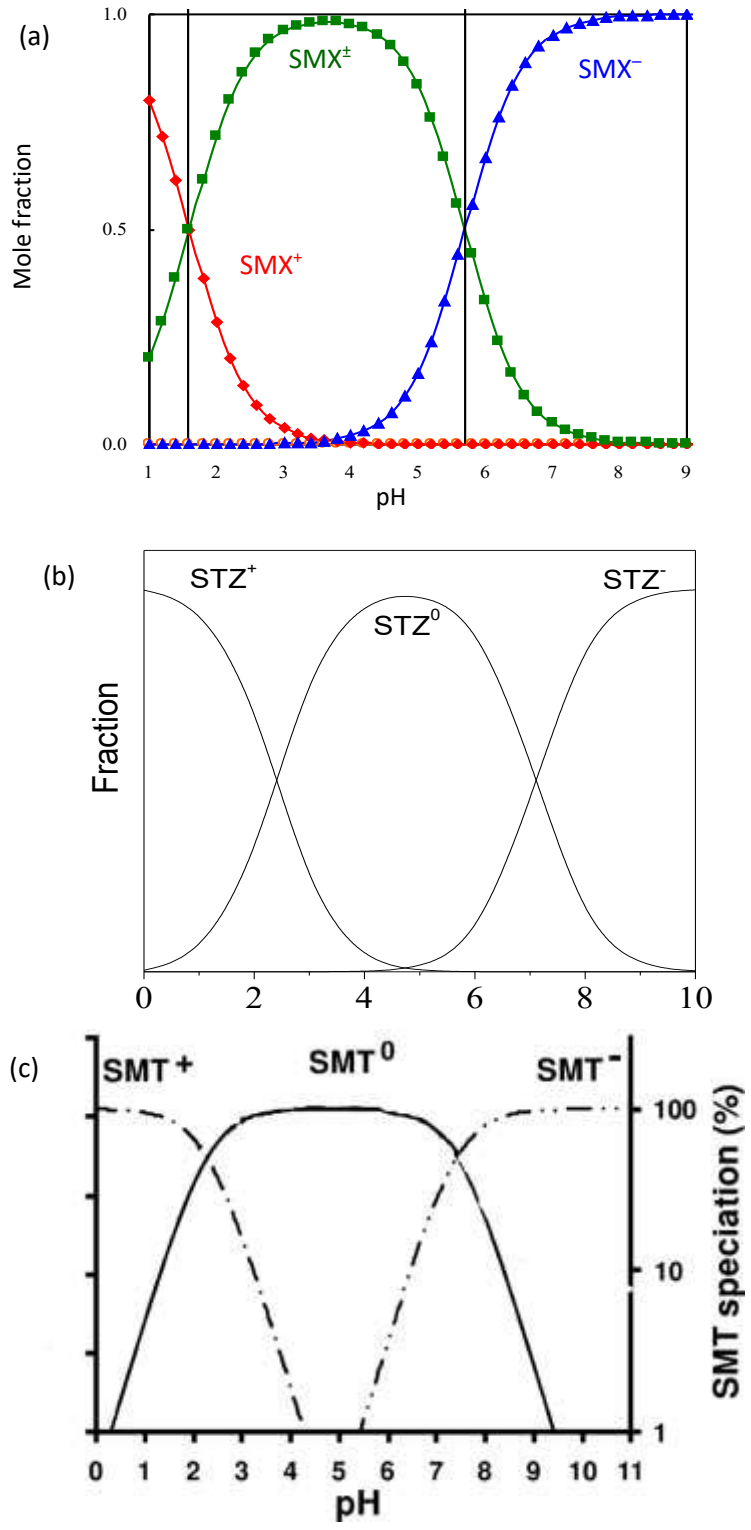

Figure 4.1.3: The chemical speciation of (a) sulfamethoxazole modified from Fukahori et al. [308]; (b) sulfathiazole took from Pei et al. [309], and (c) sulfamethazine modified from Teixidó et al. [59].

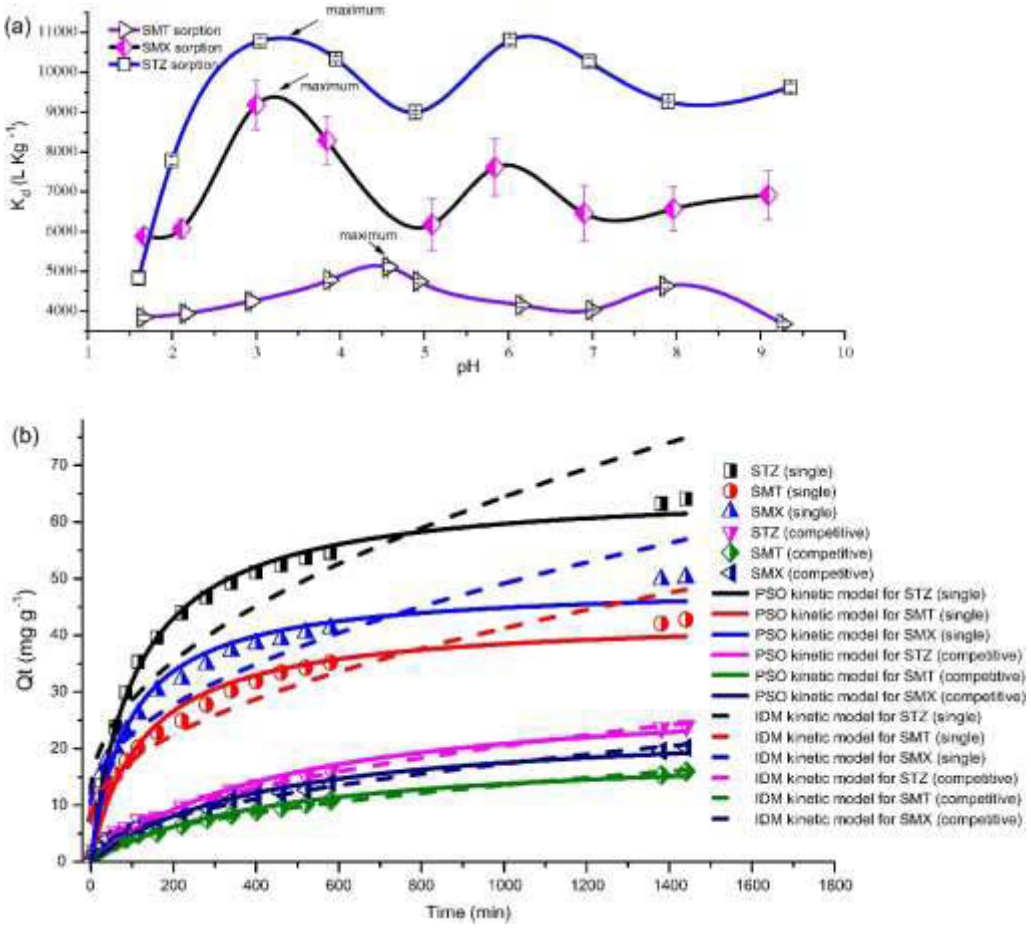

Figure 4.1.4: (a) Effect of pH on the distribution coefficient (K_d) with standard deviation (error bars) for removal of sulfonamide antibiotics; (b) single and competitive sorption kinetics data with PSO and IDM kinetics model fittings (initial concentration of sulfonamide antibiotics being 10 mg L^{-1} for single solute, and 3.33 mg L^{-1} for each competitive solute at room temperature using 100 mg L^{-1} functionalized biochar dosages).

4.1.*3.2. Sorption Kinetics for Single and Competitive Solutes*

The kinetics of sulfonamide antibiotics sorption by functionalized biochar at different times were fitted to pseudo-first-order (PFO), pseudo-second-order [306] and intra-particle diffusion model [17] as presented in **Eqs. (2)–(4)**. Based on the correlation coefficient (R^2) and $Q_{e,cal}$ values, the kinetics of sorption for all single solutes closely followed the PSO chemisorption kinetic model rather than PFO and IDM [310] (**Figures 4.1.4b and 4.1.5**). Moreover, IDM may not be the best model to describe the rate controlling mechanism of single solutes as r^2 value was significantly lower than PSO plot (**Table 4.1.4**). The values of PSO rate constant K_2 and IDM rate constant K_i decreased as SMX > SMT > STZ and STZ > SMX > SMX, respectively, for single solutes.

IDM showed higher r^2 values than the PSO model (**Table 4.1.4**), suggesting the competitive sorption kinetics of sulfonamide antibiotics on functionalized biochar were

controlled by a diffusion-dominated mechanism, which is consistent with a previous study [271], and can be explained by the PSO. Other processes such as the boundary layer diffusion or external mass transfer may also regulate the sorption process. $Q_{e,cal}$ values were higher for PSO than those of PFO. The K_i values followed the order STZ > SMX > SMT for competitive solutes. Maximum sorption capacities for PSO followed the trend of STZ > SMX > SMT.

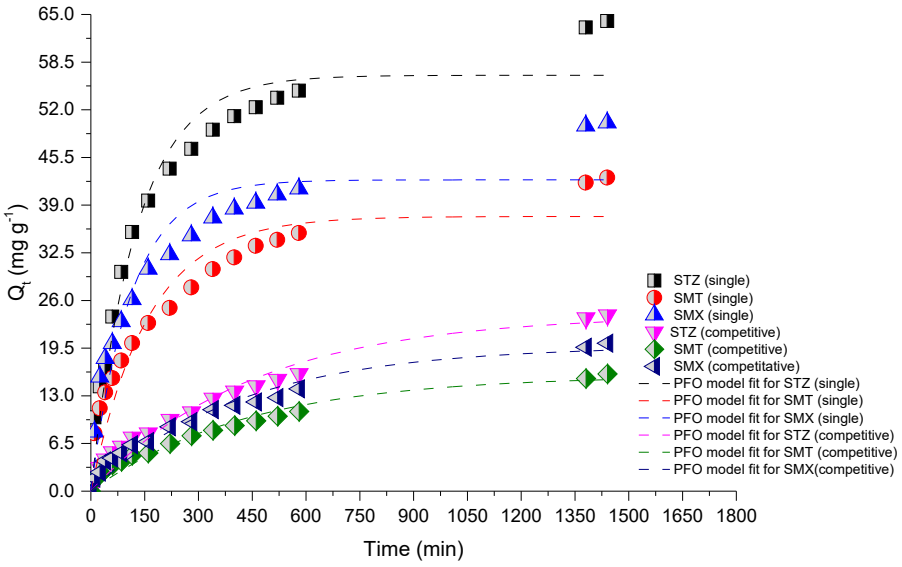

Figure 4.1.5: Pseudo first order (PFO) kinetic model for the kinetics of sulfonamide sorption on functionalized biochar, in single and competitive mode (model fitted to origin pro version 9.1 software).

Table 4.1.4: Summary of the kinetic model parameters for sulfonamide antibiotic adsorption on functionalized biochar.

Adsorbent (1MbBBC600)										
Antibiotic		PFO at 21±0.5 °C			PSO at 21±0.5 °C			Intra-particle Diffusion Model		
		$Q_{e\ cal}$ (mg g^{-1})	K_1 (min^{-1})	r^2	$Q_{e\ cal}$ (mg g^{-1})	K_2 (g mg^{-1} min^{-1})	r^2	C (mg g^{-1})	K_i (mg g^{-1} $min^{-0.5}$)	r^2
STZ	Single solute	56.71±1.70	0.00783	0.960	66.08±1.17	0.0001412	0.992	12.01±3.2	1.66±0.18	0.857
SMT		37.46±1.84	0.00627	0.907	43.30±1.18	0.0001840	0.963	7.25±1.49	1.08±0.08	0.921
SMX		42.08±1.81	0.00889	0.903	48.96±2.75	0.0002241	0.966	10.37±2.05	1.23±0.02	0.889
STZ	Competitive	24.08±1.35	0.00222	0.956	30.40±1.85	0.0000718	0.973	0.26±.016	0.64±0.01	0.997
SMT	solute	15.78±0.88	0.0023	0.955	19.80±1.20	0.0001158	0.972	0.28±0.13	0.42±0.01	0.996
SMX		19.83±1.08	0.00241	0.955	24.65±1.42	0.0000996	0.973	0.41±0.21	0.54±0.011	0.994

Table 4.1.5: Summary of the Freundlich isotherm parameters for sulfonamide antibiotic adsorption on functionalized biochar.

Adsorbent (1MbBBC600)										
Antibiotics		At 21 ± 0.5 °C Temperature			At 25 ± 0.5 °C Temperature			At 30 ± 0.5 °C Temperature		
		K_F	n	r^2	K_F	n	r^2	K_F	n	r^2
STZ	Single solute	27.029±0.946	2.599±0.072	0.998	23.120±2.06	1.795±0.092	0.995	26.052±2.05	2.5291±0.159	0.989
SMT		24.814±2.77	5.937±1.253	0.915	21.331±2.26	3.519±0.408	0.969	26.912±2.380	4.453±0.558	0.974
SMX		25.665±1.96	3.171±0.237	0.984	21.855±2.73	2.7282±0.214	0.983	27.210±2.762	3.419±0.376	0.965
STZ	Competitive	12.187±0.605	2.940±0.215	0.981	10.317±1.42	2.27±0.292	0.945	8.790±1.19	2.130±0.275	0.962
SMT	solute	10.458±0.708	4.723±0.752	0.903	8.730±1.02	2.65±0.367	0.940	9.168±0.62	3.340±0.338	0.972
SMX		11.056±0.724	3.445±0.384	0.954	10.47±1.38	2.41±0.345	0.934	9.770±1.21	2.570±0.367	0.951

Table 4.1.6: Summary of the Langmuir isotherm parameters for sulfonamide antibiotic adsorption on functionalized biochar.

Adsorbent (1MbBBC600 i.e. fBC-1)										
Antibiotics		At 21 ± 0.5 °C Temperature			At 25 ± 0.5 °C Temperature			At 30 ± 0.5 °C Temperature		
		Q_{max}	K_L	r^2	Q_{max}	K_L	r^2	Q_{max}	K_L	r^2
STZ	Single solute	127.37±10.98	0.130±0.039	0.957	237.71±18.87	0.0582±.0105	0.995	124.15±6.77	0.141±0.027	0.978
SMT		42.42±2.555	2.723±1.705	0.831	65.74±6.25	0.2083±0.087	0.897	61.86±3.19	0.443±0.134	0.938
SMX		84.58±4.571	0.265±0.069	0.966	88.10±8.125	0.1974±0.077	0.929	81.63±3.125	0.289±0.052	0.978
STZ	Competitive	30.18±1.094	0.6367±0.0866	0.983	40.11±1.101	0.3151±0.064	0.996	36.03±1.40	0.271±0.032	0.995
SMT	solute	17.71±0.410	1.682±0.2194	0.979	25.11±0.424	0.5406±0.035	0.997	19.74±0.908	1.098±0.298	0.968
SMX		23.76±0.709	0.851±0.1089	0.983	34.01±0.613	0.4395±0.028	0.998	29.32±0.843	0.471±0.054	0.995

4.1.*3.3. Sorption Affinity and Temperatures Effect*

Single and competitive sorption isotherm plots for the Langmuir and Freundlich isotherm models (Eqs. **(5) and (6)**) are presented in **Figures 4.1.6-4.1.8**. The model parameters are summarized in **Tables 4.1.5 and 4.1.6**. The sorption data for single solute STZ and SMX were fitted by both the Freundlich and Langmuir isotherm models. However, the sorption data for SMT was fitted slightly better by the Freundlich model with higher r^2 values. Maximum Langmuir adsorption capacity (Q_{max}) values were 237.71, 65.74 and 88.10 mg g^{-1}, respectively, for STZ, SMT and SMX at 25 °C. Adsorption capacity was increased significantly for STZ (85%) and SMT (55%) and slightly for SMX (5%) when the temperature rose from 21 to 25 °C. A further increase in temperature from 25 to 30 °C decreased the adsorption capacity while the distribution coefficient indicated that adsorption was unfavorable through monolayer covering. This is likely due to the complex relation between chemical activation energy and exothermic reaction nature of adsorption. Specifically there is a need for temperature increase to overcome activation energy (from 21 to 25 °C), but further increase above 25 °C caused a decrease in adsorption which releases heat. Sorption affinity could be ranked as follows: STZ > SMX > SMT. Conversely, the maximum Freundlich constant K_F values with higher r^2 values were found to be 22.12, 21.33 and 21.86 mg^{1-n} L^n g^{-1} for STZ, SMT and SMX respectively, at 25 °C. These results could happen due to specific surface area, microspore volume, and introduction of additional sites onto functionalized biochar [51, 82]. The K_d values for single solute ranged between 2.56×10^3 and 8.57×10^4, 1.0×10^3 and 5.77×10^4, and 1.8×10^3 and 6.4×10^4 L kg^{-1}, for STZ, SMT and SMX respectively (**Figure 4.1.9b**). The observed K_d values, Q_{max} and K_F values for single solute of STZ, SMX and SMT were higher than reported in other studies using different adsorbents e.g. carbon nanotubes (CNTs) supported nano-composite and graphene-oxide based adsorbents and carbonaceous nano-composites [22, 51, 82, 246, 310-315]. For example, biochar prepared at 700 °C from Burcucumber plants was found to show the maximum sorption capacities of 20.56 and 37.73 mg g^{-1}, respectively for biochar (700 °C) and steam modified biochar [82]. In addition, biochars prepared from *Salvia miltiorrhiza* Bunge biomass at 600 and 800 °C showed the maximum K_F values of 0.0155 and 0.0257 mg^{1-n} L^n g^{-1}, respectively for the removal of sulfamethoxazole [246].

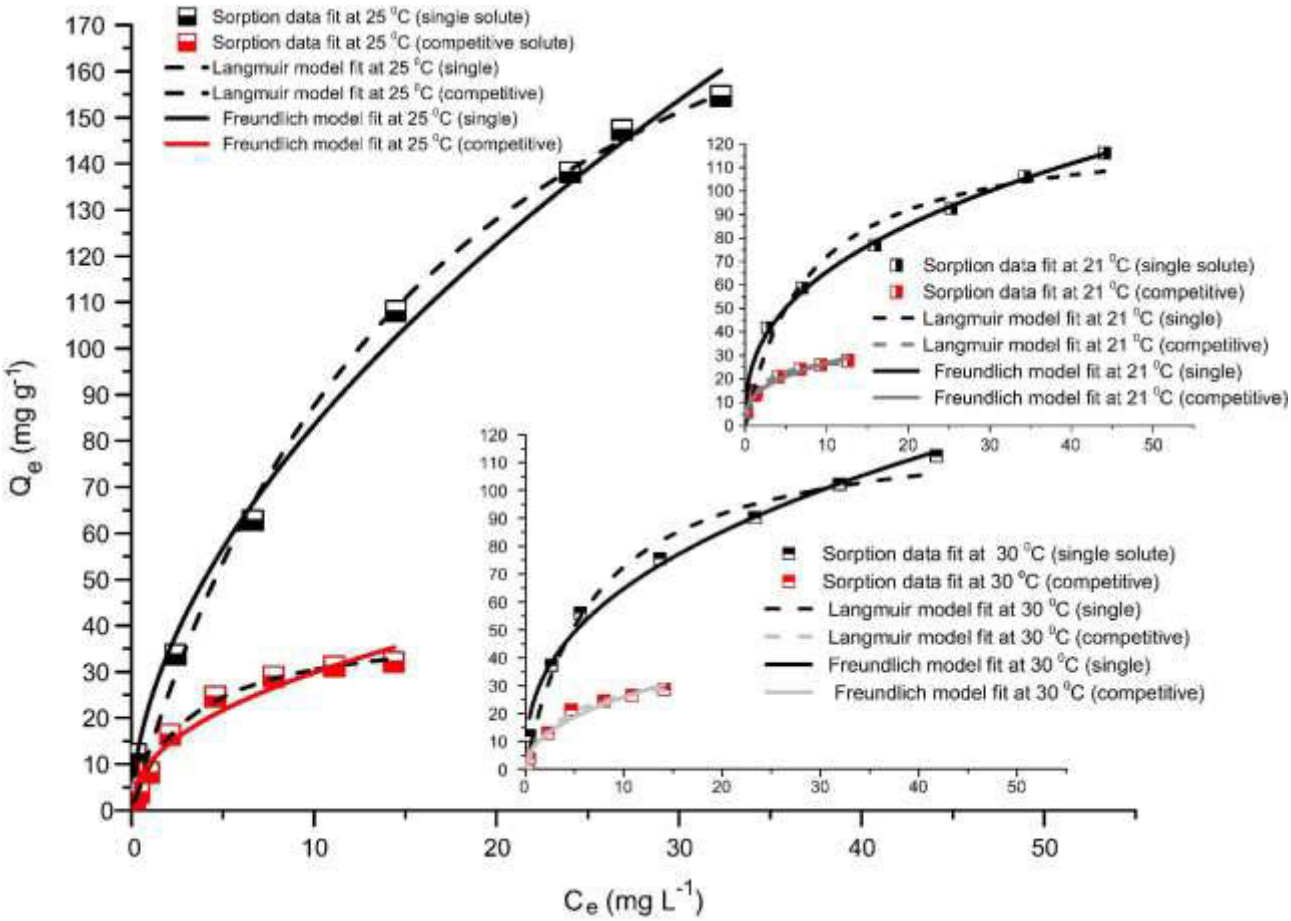

Figure 4.1.6: STZ adsorption isotherm plots and model fits from single solute (initial concentration 0.5–50 mg L^{-1}), and from mixtures (initial individual concentrations were 0.33–16.67 mg L^{-1}) at pH 3.5 and different temperatures.

Competitive removal of sulfonamide antibiotics was found to be better fitted to the Langmuir isotherm model with higher r^2 values and the maximum sorption capacities were obtained at 25 °C. The sorption affinity was the same as that for single solutes. Competitive Q_{max}values were found to be 40.11, 34.01 and 25.11 mg g^{-1}, for STZ, SMX and SMT respectively, at 25 °C. The maximum K_F values were 12.46, 10.46 and 11.06 mg^{1-n} L^n g^{-1}, respectively, for STZ, SMT and SMX at 21 °C. The K_d values for competitive solutes ranged from 2.0×10^3 and 2.5×10^4, 1.2×10^3 and 2.21×10^4, and 1.6×10^3 and 2.37×10^4 L kg^{-1}, for STZ, SMT and SMX respectively (**Figure 4.1.9a**). Further increases in temperature from 25 to 30 °C led to a decline in sorption affinity and K_d indicated that adsorption affinity was not strong enough to support homogeneous covering of the surface. Kinetics and isotherms data indicated that competitive sorption of sulfonamide solutes was better fitted by the Langmuir model.

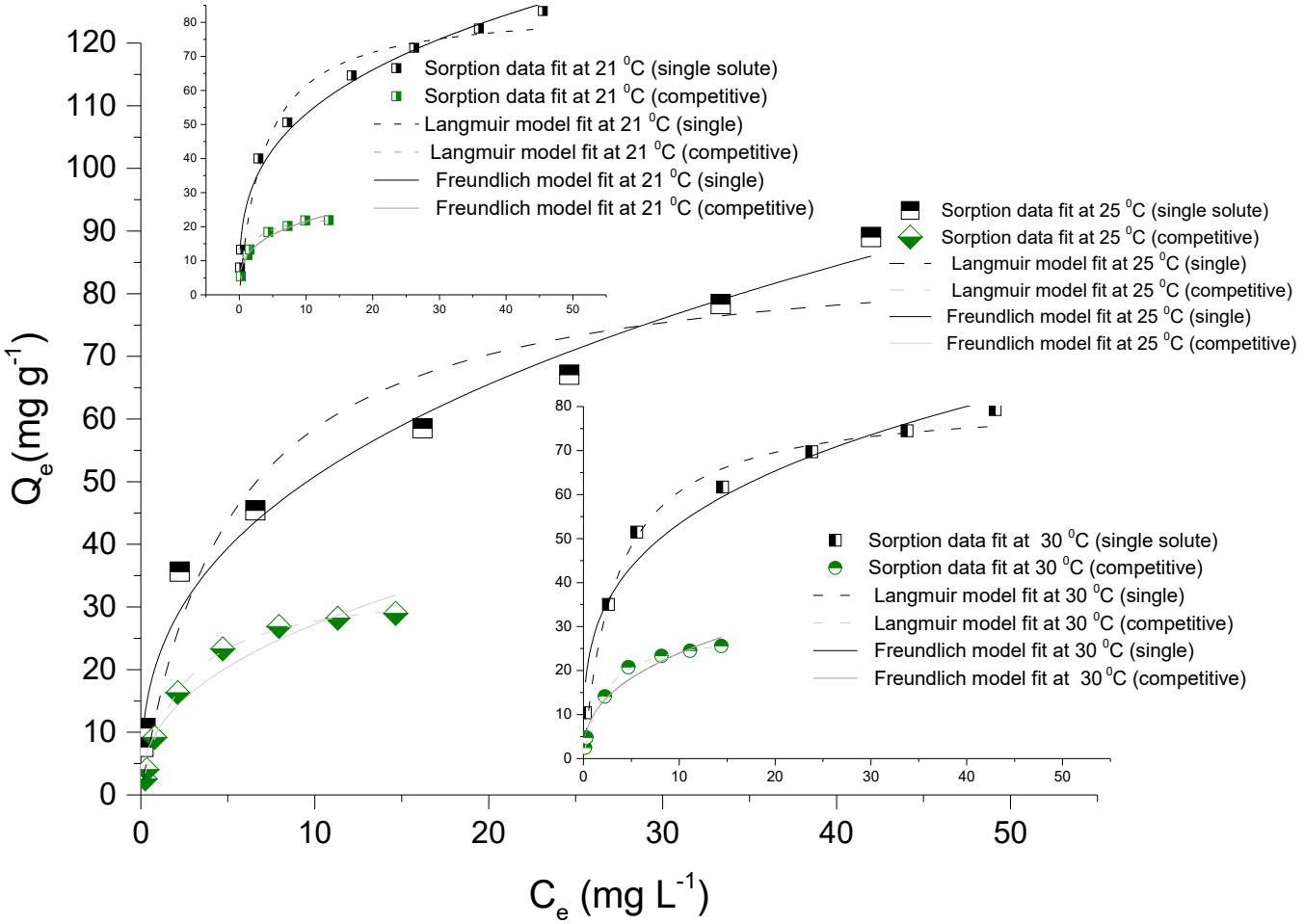

Figure 4.1.7: SMX adsorption isotherm and model fits (Langmuir and Freundlich) at different temperatures using initial concentrations of 0.5-50 mg L^{-1} at pH 3.25 for single solutes, and at 1-50 mg L^{-1} in mixture mode at pH 3.5.

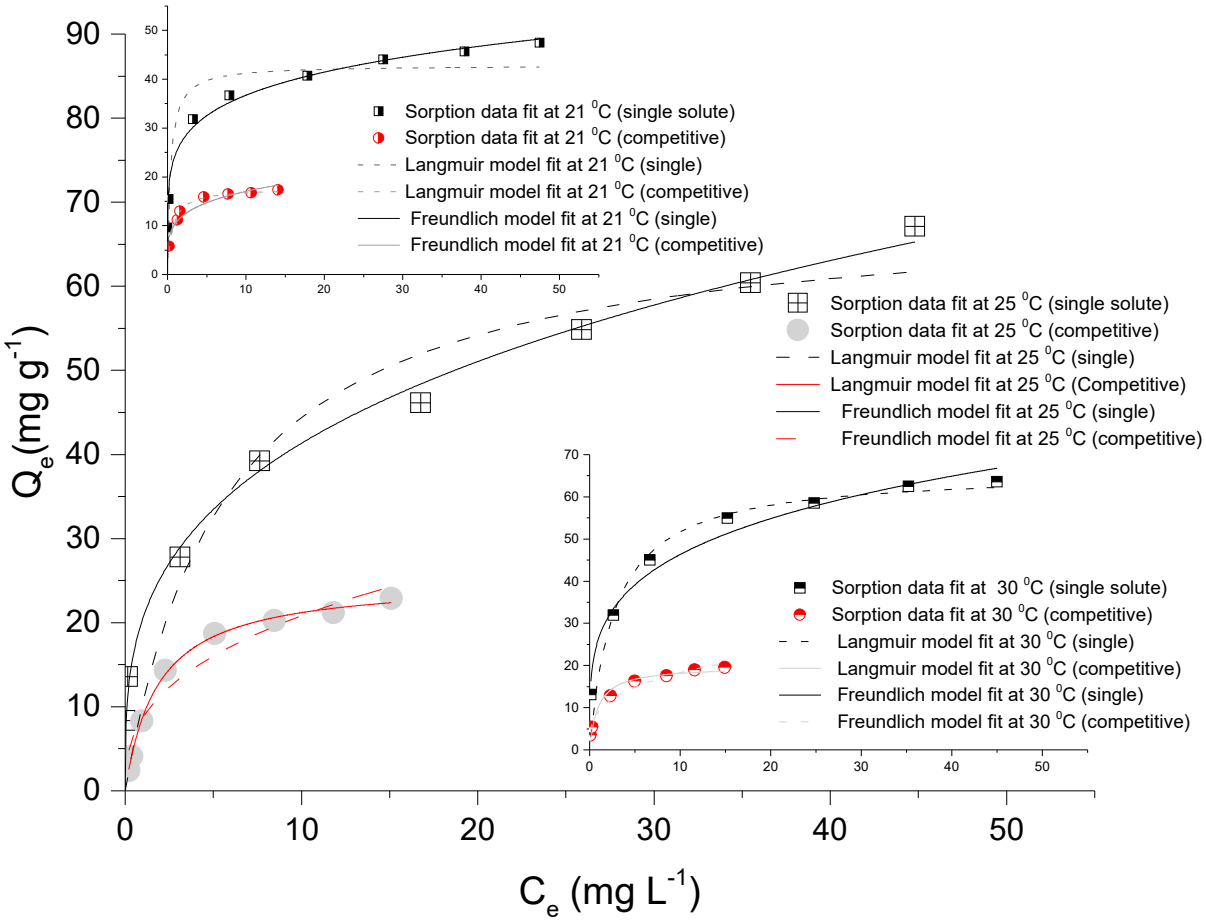

Figure 4.1.8: SMT adsorption isotherm and model fits (Langmuir and Freundlich) at different temperatures using initial concentrations of 0.5-50 mg L^{-1} at pH 4.5 for single solutes, and at 1-50 mg L^{-1} in mixture mode at pH 3.5.

Total sorption capacities of the competitive solutes were calculated (**Eqs. (4.1.9) and (4.1.11)**) by adding individual contributions to the overall sorption for both Langmuir and Freundlich models. When comparing the single solute sorption capacities, each competitive solute was found to have nearly 2-fold less adsorption capacity for overall individual sorption capacities. Overall sorption capacities of competitive solutes are almost analogous to near about the maximum sorption capacities of individual solutes sorption capacities. Hence the total sorption capacities of competitive solutes onto adsorbent surface were maintained at a similar level to single solute sorption. The results indicated that sorption on biochar was of monolayer coverage in nature.

The adsorption data obtained in the experiments can theoretically consider calculating and comparing the overall competitive sorption capacities using summarized Langmuir and Freundlich Equations.

The combined Freundlich model for 3 antibiotics:

$$Q_{total} = K_{F1}{C_{e1}}^{1/n} + K_{F2}{C_{e2}}^{1/n} + K_{F3}{C_{e3}}^{1/n} \quad (4.1.8)$$

$$K_{F(total)} = K_{F1} + K_{F2} + K_{F3} \quad (4.1.9)$$

The combined Langmuir model for 3 antibiotics:

$$Q_{total} = \frac{Q_{max1}K_{L1}C_{e1}}{1+K_{L1}C_{e1}} + \frac{Q_{max2}K_{L2}C_{e2}}{1+K_{L2}C_{e2}} + \frac{Q_{max3}K_{L3}C_{e3}}{1+K_{L3}C_{e3}} \quad (4.1.10)$$

$$Q_{max.(total)} = Q_{max1} + Q_{max2} + Q_{max3} \quad (4.1.11)$$

where K_{F1}, K_{F2}, K_{F3} are the Freundlich constant for first competitive solute, second competitive solute and third competitive solute respectively. Q_{max1}, Q_{max2} and Q_{max3} are the maximum Langmuir sorption capacity for the first, second and third competitive solute, respectively.

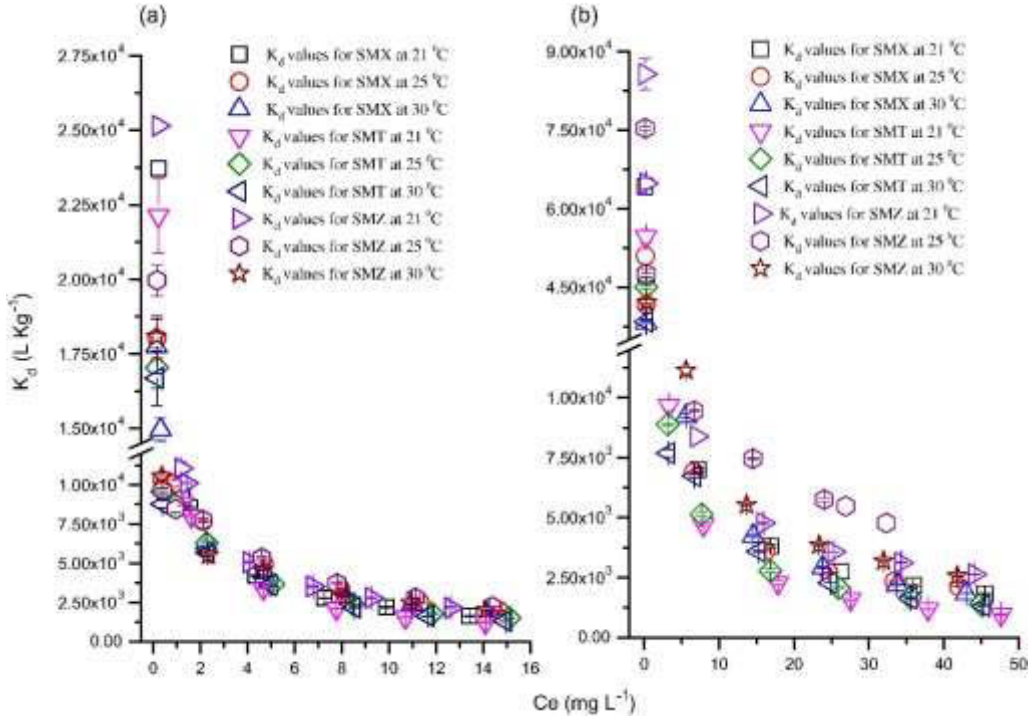

Figure 4.1.9: Change of K_d values (with SD as error bars) against equilibrium concentrations for (a) competitive solutes with total initial solution concentrations (C_o) at 1–50 mg L^{-1} and each solute concentration was 0.33–16.67 mg L^{-1}(i.e. Co/3), and for (b) single solute (C_o = 0.5–50 mg L^{-1}).

4.1.3.4. Diffusion of Sorbate Molecules

Based on our kinetics study, the competitive adsorption mechanism for STZ, SMT and SMX can partly be postulated firstly as a monolayer process involving sorbate molecules transportation and diffusion. It is a process controlled by a combination of mass transfer steps relating to external, surface microlayer, pore diffusion and adsorption on biochar surface, thus supporting IDM mechanism (**Figure 4.1.10**). Secondly, both single and competitive solutes followed the PSO kinetic model with adsorption through chemisorption with the surface functional groups being indicated. Based on the isotherm study, this can be attributed, to the adsorption of STZ and SMX following the monolayer through diffusion and chemisorption reactions with surface functional groups in biochar. Adsorption of SMT followed the Freundlich isotherm which was related to the chemisorption mechanism. In comparison to biochar, the functionalized biochar had its surface area increased by 2.3 folds while its pore diameter reduced to half. In addition, its Langmuir surface area was increased by 68 times compared to that of biochar. Moreover, BJH and Dollimore Heal (D-H) adsorption cumulative surface area of functionalized biochar was increased by 6 folds compared to biochar. However, BJH and D-H pore diameters of biochar were 113 and 154 Å which decreased to 84 and 78 Å

after functionalization (**Table 4.1.3**). Thus, higher adsorption affinities of fBC may be partly due to the increase in surface area and reduction in pore diameter, accompanied by active adsorption sites facilitating the adsorption of neutral sulfonamide molecules. This occurred through diffusion rather than sorption chemisorption. The IDM rate constant values (K_i) indicated that the diffusion of the sulfonamide molecules (both single and competitive solutes) toward biochar surface followed the trend of STZ > SMX > SMT.

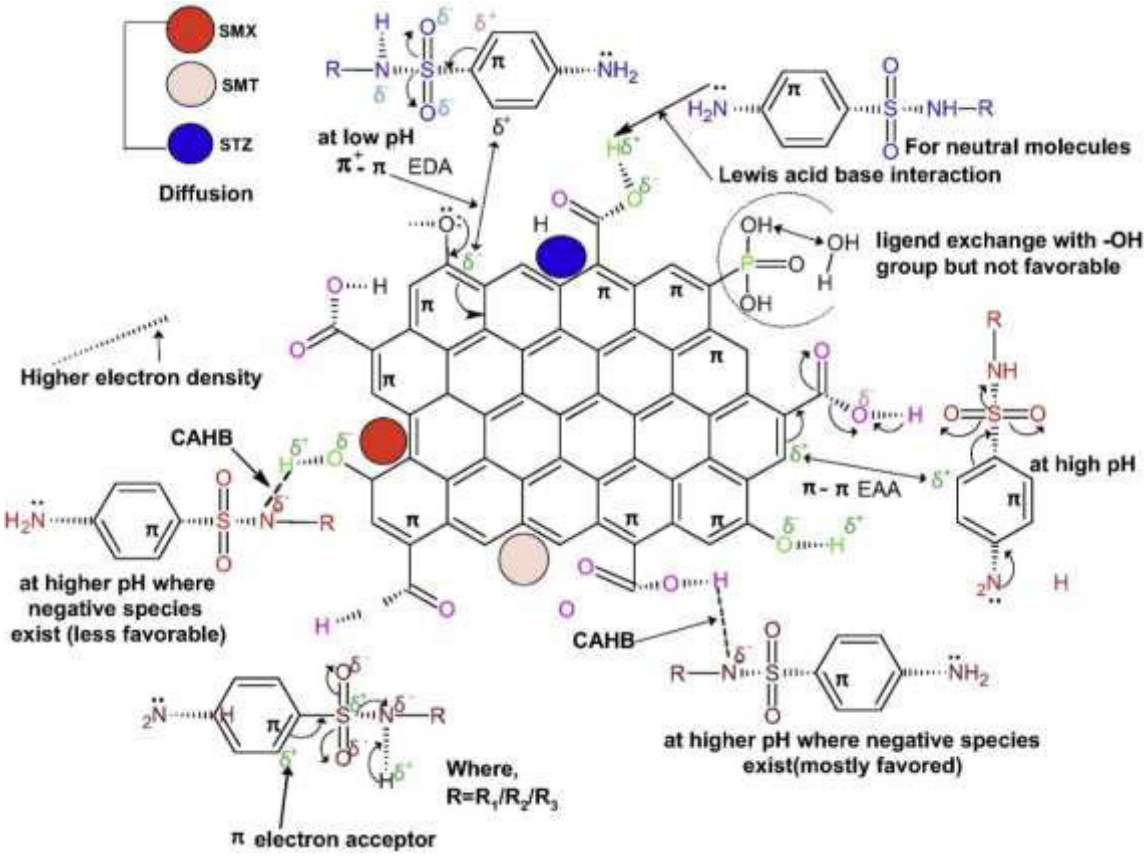

Figure 4.1.10: Proposed sorption mechanism for single and competitive antibiotics (R1 for SMT, R2 for STZ, R3 for SMX) on functionalized biochar with possible resonance effects for π-π interactions.

4.1.*3.5. Lewis Acid-Base Interaction*

Based on the structural composition of the sulfonamides, they consist of sulfonamide group (para position at benzene ring) associated with thiazole group (in sulfathiazole), 4,6-dimethylpyrimidin-2-yl group (in sulfamethazine), and 5-methyl-1,2-oxazol-3-yl group (in sulfamethoxazole) at N position of sulfonamide group and lone pair electron reach N-atom (amino group in arene ring and in heterocyclic ring). Thus, Lewis acid base electronic interaction can also contribute to the total sorption affinities of the sulfonamides due to extra

interaction of sulfonamide molecules with the lone pair electrons and protons of –COOH and –OH functional groups on the biochar surface [310]. The interaction can be written as:

RnNH-SO2-R-H2N:+H…BC=RnNH-SO2-R-H3N+…BC- (4.1.12)

where $R_n = R_1/R_2/R_3$.

Thus the adsorption of sulfonamides (both positive and negative species) would be possible with the mechanism of Lewis acid-base interaction as noted in **reaction (4.1.12)**. It is expected that the lone pair electrons in the amino group and in hetero-N participate in the resonance process with the arena unit of sulfonamides, turning it into: firstly a positive species at low pH; and secondly, a negative species at higher pH. In these cases, Lewis acid-base interaction of sulfonamide antibiotics on the biochar surface may not be effective (**Figure 4.1.10**). However, this interaction might be possible at a pH where sulfonamides remain as a neutral species and thus, loan-pair electrons of amino groups in the arene unit may donate to form a complex with the protonated enriched surface functional groups. A few experiments with the addition of co-solutes (electron-acceptor groups such as 0.01 M $AlCl_3$ and 0.025 M acetone in 10 mg L^{-1} SMT solution without adsorbent for 40 h) were conducted. It was observed that the pH change (ΔpH) was found to be 0.25–0.30 in neutral species regions. This implied that the loan-pair-electrons availability from amino group or hetero-ring system of sulfonamides to electrons-acceptor groups were not significant and may be a small contributor to the reaction mechanism governed by the Lewis acid-base interactions. Experiments using only adsorbent and co-solutes resulted in significant pH change. This could be due to the release of protons into the solutions (**Table 4.1.7, Figure 4.1.11**). Similar effects were also observed for the competition of co-solutes, the adsorbent and adsorbate; changes in final pH were due to the release of protons.

Table 4.1.7: pH shift for different species of SMT, SMX and STZ antibiotics on fBC.

Proton release test in solution (pH shift)																		
pH	SMT (single, 10 mg L^{-1})					SMX (single, 10 mg L^{-1})				STZ (single, 10 mg L^{-1})					Competitive solutes (each conc., 3.33 mg L^{-1})			
Initial pH	1.65	4. 57	6.06	8.75	9.9	1.67	3.25	5.93	10.06	1.60	3.42	4.20	8.63	9.9	1.51	3.48	5.25	9.15
Final pH	1.59	3.93	4.63	8	7.05	1.61	2.92	3.58	7.12	1.61	3.17	3.4	7.19	7.05	1.52	3.01	3.32	5.05

Effect of cosolute (electron-acceptor group)				Change of pH during sorption							
Initial pH	Final pH	fBC (mg) added in 100 mL	Electron acceptor group	SMT (mL) of 10 mg L^{-1}	Initial pH	Final pH	SMT conc. (mg L^{-1})	fBC (mg) added in 100 mL	Initial pH	Final pH	Competitive conc. (mg L^{-1})	fBC (mg) added in 100 mL
4.15	3.84	6.5	0.01M $AlCl_3.6H_2O$	90	4.38	3.75	0.5	2.1	5.6	3.9	1	1.7
7.25	8.65	7.8	0.01M $AlCl_3.6H_2O$	90	4.55	3.85	1	4.7	5.53	3.69	5	3.5
8.77	4.4	5.4	0.25M CH_3-CO-CH_3	90	4.66	4	5	6.6	5.25	3.31	10	11
3.70	3.27	5.7	0.25M CH_3-CO-CH_3	90	4.46	3.6	10	8.6	5.54	3.32	20	11.3
3.70	3.45	0	0.01M $AlCl_3.6H_2O$	100	4.55	3.41	20	11.9	5.49	3.28	30	12.2
5.15	4.75	0	0.25M CH_3-CO-CH_3	100	4.6	3.4	30	12.8	5.67	3.25	40	14.6
3.60	3	5.5	0.01M $AlCl_3.6H_2O$	0	4.2	3.25	40	16.5	5.57	3.21	50	15.5
5.33	3.81	5.8	0.25M CH_3-CO-CH_3	0	4.49	3.23	50	17.6				
3.65	3.05	5.2	0.01M $AlCl_3.6H_2O$	0								
9.63	4.65	5.7	0.25M CH_3-CO-CH_3	0								

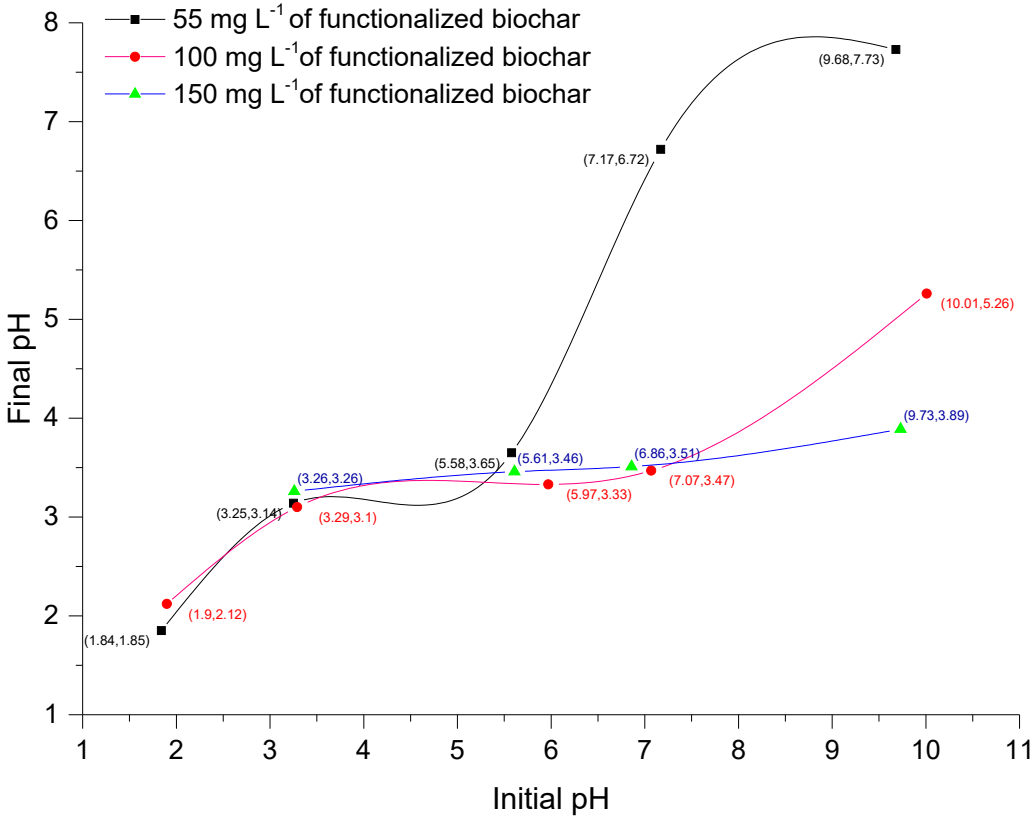

Figure 4.1.11: Change of pH for blank samples (without antibiotics) at different adsorbent dosages leading to proton release in solution.

4.1.*3.6. EDA and EAA (π-π) Interactions*

EDA interaction can be considered one of the main mechanisms for the sorption of positive species of sulfonamides on biochar surface [59, 316]. Stronger EDA interaction might be possible when the π-electron depletes aromatic ring (s) (or regions) and π-electron a rich regions (or aromatic rings) interact together [316]. More specifically, there is stronger interaction between oppositely polarized quadruples of functionalized sorbent surfaces and sorbate molecules in a parallel planar fashion. Sulfonamide molecules have a strong π-electron acceptor nature due to its amino functional groups (donates loan pair electrons to the benzene ring) and N and/or O-hetero-aromatic rings (contribution to electronic resonance). In contrast, the fBC surface was enriched with C=C, –OH, and –COOH functional groups based on our study using FTIR and Raman spectra (**Figures 4.1.12 and 4.1.13**) and other reports [51, 317]. Hence, the surface functional groups of fBC can act as a strong π-electron-donor due its: firstly, hydroxyl groups being situated in the benzene rings (especially participating in resonance as a π-electron donor); and secondly, a strong π-electron-acceptor due to its carboxyl functional groups on the benzene rings (especially, protonated carboxyl groups that taking part in electronic resonance as a π-electron acceptor). In addition, the surface of fBC at low pH likely contains few, if any, negatively charged sites because we found the zeta-potential is positive below pH 2.5. The pK_a values for carboxyl groups on aromatic ring systems are generally above 4.0 [59]. Subsequently, the surface of biochar may become positive due to protonation of unsaturated C atoms or heterocyclic N and/or S atoms.

When π-electron-acceptor is positively charged and this charge lies within or resonates with an arene unit of sulfonamides (e.g. charge in aromatic or heterocyclic aromatic amine) then a stabilized overall interaction is designed as π^+-π EDA [59, 318]. Resonance forms of positive species of sulfonamides are able to form π^+-electron (acceptor site) and sorption affinities mostly governed by the mechanism of π^+-π EDA. Teixidó et al. [59] presented clear support for π^+-π EDA interactions of SMT^+ in their study of solution pH and the effect of different cosolutes on cation exchange. Our study agrees with the literature in that the biochar surface contains –OH functional groups (**Eq. (4.1.13)**). Moreover, donor-donor and acceptor-acceptor π-electron interaction might also be possible but not as strong as π-π EDA interaction **(Eq. (4.1.14))** [319].

$H_2N\text{-}C_6H_4^{\delta+}\text{-}SO_2\text{-}NHR_n + BC^{\delta-}\text{-}OH \rightarrow H_2N\text{-}C_6H_4^{\delta+}\text{-}SO_2\text{-}NHR_n\ldots..BC^{\delta-}\text{-}HO^-$ (4.1.13)

$H_2N\text{-}C_6H_4^{\delta+}\text{-}SO_2\text{-}NHR_n + BC^{\delta+}\text{-}COOH \rightarrow H_2N\text{-}C_6H_4^{\delta+}\text{-}SO_2\text{-}NHR_n\ldots BC^{\delta+}\text{-}COOH$ (4.1.14)

where R_n = aromatic heterogeneous groups represent SMT, SMX and STZ.

It can also be hypothesized that the π-π EAA mechanism between the positive species of sulfonamides arene units and surface carboxyl groups, which may also partially contribute to the overall sorption but may not stabilize by charge repulsion. However, this also is not possible at very low pH due to pK_a values of surface carboxylic groups (> 4) [38, 39][320-322]. The results on the effect of pH change showed a very small change of pH both for single and competitive solutes **(Table 4.1.7)**. Furthermore, the release of the proton in the solution from carboxylic groups might not occur which indicates that unfavourable to behave biochar surface to act as an electron acceptor at very low pH. Thus, the π-π EAA interaction (reaction 3) can be ruled out for positive species of sulfonamides (**Figure 4.1.10**).

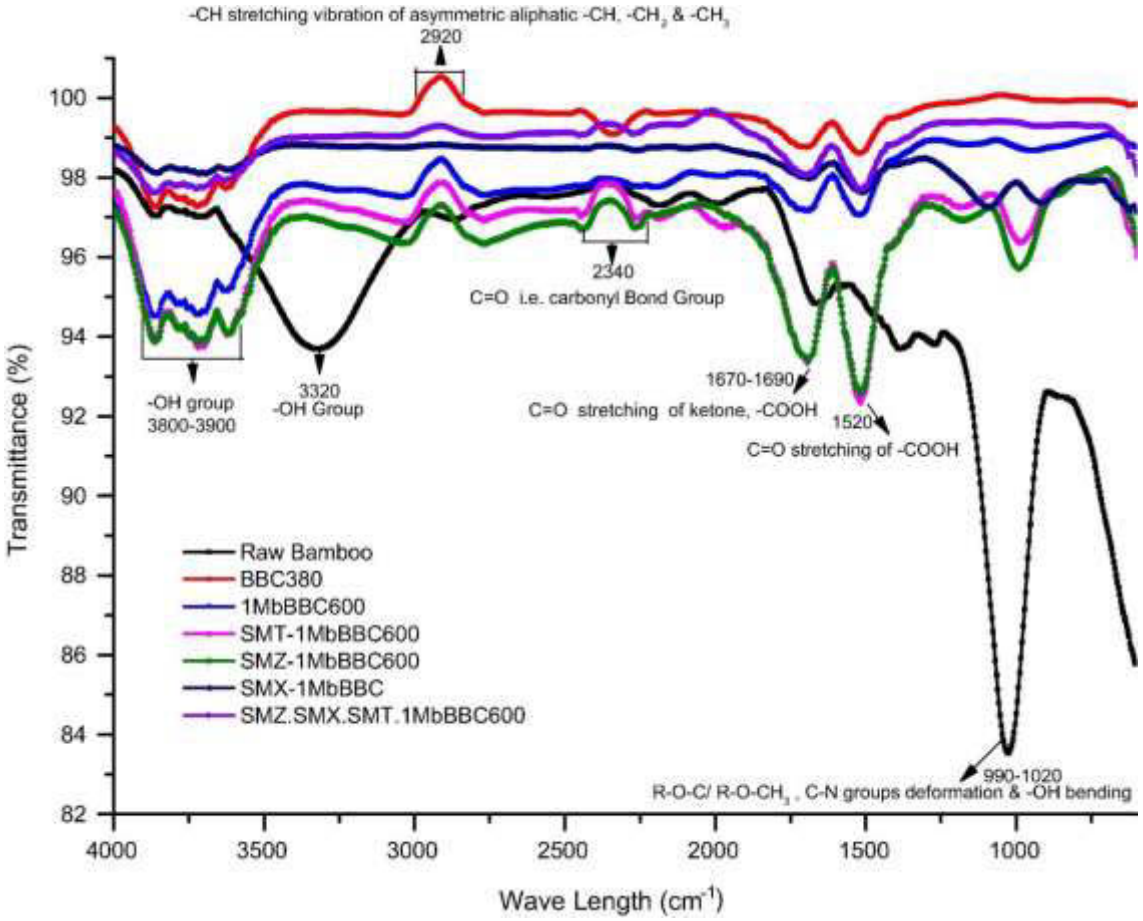

Figure 4.1.12: FTIR spectra for raw bamboo biomass, biochar (BBC380), and functionalized biochar (1MbBBC600 i.e. fBC-1) for the sorption of single and competitive solutes (before and after adsorption).

However, the maximum sorption capacities and K_d were found for the adsorption of sulfonamides neutral molecules only.

$$SMT^0/SMX^0/STZ^0 + H_2O + fBC = SMT^+/SMX^+/STZ^+ \ldots fBC + OH^- \quad (4.1.15)$$

$$SMT^0/SMX^0/STZ^0 + fBC = SMT^+/SMX^+/STZ^+ \ldots . fBC^- \quad (4.1.16)$$

$SMT^0/SMX^0/STZ^0 + fBC = SMT^{\pm/}\ STZ^{\pm} / SMX^{\pm} \ldots.\ fBC\ (-H^+)$ (4.1.17)

$SMT^0/SMX^0/STZ^0 + fBC = SMT^{\pm}/SMX^{\pm}/STZ^{\pm}\ldots..fBC + H^+$ (4.1.18)

The reaction (**Eq. (4.1.15)**) is unfavorable to exchange protons with water molecules by leaving the –OH group in the solution [313], thus solution pH should increase. We found, however, that pH shifted more to the acidic region after adsorption and this is backed up by the literature [59]. The proton transfer free energy $\Delta G^0_{H^+{}_{exch1}} = -RT\ ln(K_{a1}/K_{aw})$, where K_{aw} is the water dissociation constant for sulfonamides with values ranging from +66.14 to +70.73 kJ mol^{-1} (**Table 4.1.8**) [59]. The reaction in **Eq. (4.1.16)** shows the proton transfer from biochar surface functional groups (mostly –COOH rather than –OH) to amino N in sulfonamides molecules ($–NH^+\ldots{}^-O/^-OOC$-BC). Furthermore, proton transfer is likely not favourable by at least 15 kJ mol^{-1} at 293 k at pH 5 [59], it is augmented by the strong H-bond that forms. The reaction in **Eq. (4.1.17)** involves tautomerisation of sulfonamides to the zwitterion in the adsorbed state while the reaction in **Eq. (4.1.18)** shows the tautomerisation by forming the zwitterion and releasing protons in the solution. Thus the observed pH decreased from the initial solution pH. The stabilization of reactions **(Eqs. (4.1.17) and (4.1.18))** might be possible through the formation of a π^+-π EDA bond, which is not as strong as the positive species, of the positively charged sulfonamide ring system with the biochar surface. Overall stabilization of the cationic form of sulfonamides can be gained by releasing of a proton from surface functional groups so that a negative site can be provided. The aim here is for it to interact electrostatically with the positive charge through a strong H-bond formation. The π-π EAA interaction is less effective as biochar surface became negative above pH 2.5 and as surface carboxylate group has pK_a values of more than 4.

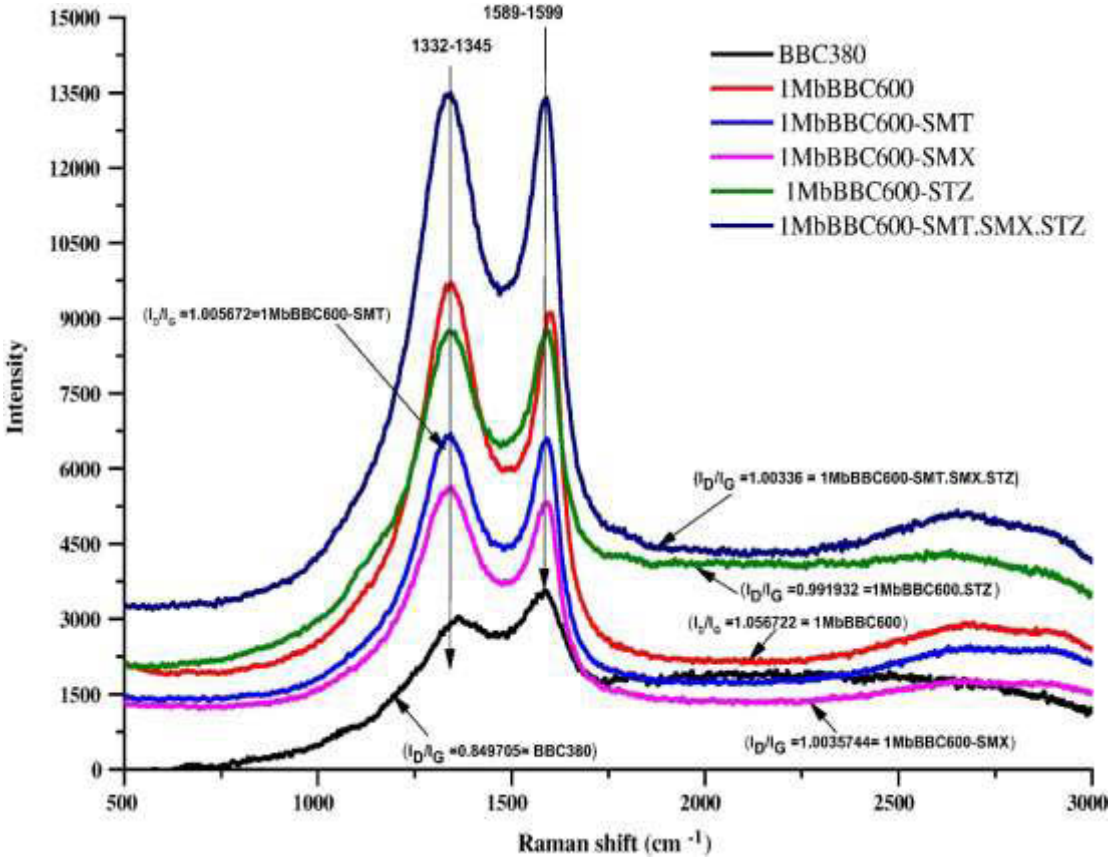

Figure 4.1.13: Raman spectra with band ratio (I_D/I_G) for biochar (BBC380), and functionalized biochar (1MbBBC600 i.e. fBC-1) before and after sorption of single and competitive solutes.

Table 4.1.8: ΔG^o values calculated from water dissociation constant (K_{aw}) at different temperatures.

Sample	Temp (°K)	pK_{a1}	pK_{a2}	$K_{a1}\times10^{-4}$	$K_{a2}\times10^{-7}$	$K_{aw}\times10^{-14}$	Ln K_{aw}	RT Ln K_{aw}	RT Ln K_{aw} (in kJ mol^{-1})	RT ln K_{a1} (in kJ mol^{-1})	RT ln K_{a2} (in kJ mol^{-1})	$\Delta G^0_{H^+_{exch}1}$ (in kJ mol^{-1})	$\Delta G^0_{H^+_{exch}2}$ (in kJ mol^{-1})
SMX	294	1.97	6.16	107.15	6.92	6.85	-32.615	-79720	-79.72	-11.09	-34.67	68.63	45.05
	298	1.97	6.16	107.15	6.92	6.85	-32.615	-80805	-80.81	-11.24	-35.14	69.57	45.66
	303	1.97	6.16	107.15	6.92	6.85	-32.615	-82161	-82.16	-11.43	-35.73	70.73	46.43
STZ	293	2.04	6.93	91.2	1.17	1.01	-32.23	-78508	-78.51	-11.44	-38.87	67.07	39.64
	298	2.04	6.93	91.2	1.17	1.01	-32.23	-79848	-79.85	-11.64	-39.54	68.21	40.31
	303	2.04	6.93	91.2	1.17	1.01	-32.23	-81188	-81.2	-11.83	-40.20	69.36	40.99
SMT	293	2.04	6.99	91.2	1.02	1.47	-31.85	-77587	-77.59	-11.44	-39.21	66.14	38.38
	298	2.04	6.99	91.2	1.02	1.47	-31.85	-78911	-78.91	-11.64	-39.88	67.27	39.04
	303	2.04	6.99	91.2	1.023	1.47	-31.85	-80235	-80.24	-11.83	-40.55	68.40	39.69

- K_{aw} values were taken from http://www.chemguide.co.uk/physical/acidbaseeqia/kw.html
- pK_{a1} and pK_{a2} were taken from **Table 4.1.1** and R =8.314 (J K^{-1} mol^{-1}) and $\Delta G^0_{H^+_{exch}1/2} = -RT\ ln(K_{a1/a2}/\ K_{aw})$

4.1.3.7. Hydrogen Bond Formation

All peak assignments from the FTIR spectra and Raman spectra indicated that functionalized biochar contains –OH, –COOH and C = C groups on the surface. In Raman spectra, two characteristic bands D and G can be assigned to carbon SP^2 hybridization **(Table 4.1.9)** [51]. The D band relates to disordered SP^2 hybridization of carbon atom containing vacancies, impurities or defects such as containing of oxygen containing functional groups. On the other hand, G band refers to the structural integrity of SP^2hybridization of carbon atoms. The intensity ratio of the D and G bands (I_D/I_G) indicates the degree of graphitization. If the ratio is <1 then high degree of graphitization; if the ratio >1 then high number of functional groups present on the surface. The I_D/I_G ratio for biochar was 0.850, which was increased to 1.06 for functionalized biochar, indicating significantly increase in the number of functional groups on the functionalized biochar surface. Similar functional groups have been found in FTIR spectroscopy [55].

At higher pH where sulfonamide negative species dominate in the solution and the biochar surface becomes negative (zeta potential = −45.9 mV), the anion exchange should be destabilized by charge repulsion. The adsorption of SMT^- was explained clearly by Teixidó et al. [59] who also noted that the adsorption was due solely or partially to adsorption of negative molecules by the release of –OH to proton exchange with water ($SMT^- + H_2O \rightarrow SMT^0 + OH^-$), followed by interaction of the resulting natural molecules with surface –COOH and –OH functional groups ($SMT^0 + BC = SMT^0 \ldots BC$). This is supported by a strongly negative CAHB. As a result pH increased as the SMT sorption increased. On the other hand, we found that the final pH reduced to several units for all single and competitive sorption of sulfonamides antibiotics. The reduction of pH in the bank solutions were significant compared to single and competitive solution of antibiotics **(Table 4.1.7 and Figure 4.1.11)**. Moreover, EDS analysis (average values) showed that the biochar particle comprised of carbon (81.17%) and oxygen (18.83%) with O/C atomic ratio of 0.23. Due to the functionalization of biochar with oH_3PO_4, the O/C ratio increased significantly to 0.76 (51.96% C, 39.52% O and 8.16% P) **(Table 4.1.2)**. This indicates the functionalized biochar had a more oxidized surface [322]. Although H_xPO_4 may be present in the core structure of functionalized biochar during preparation and surface H_xPO_4 may undergo ligand exchange reactions with hydroxide and carboxyl groups, if any, in the solution **(Eq. (4.1.19) and Figure 5)** [323]. One might assume that significance of pH may be due to the capacity of biochar to release PO_4^{3-} ions [323]. However, our experiments observed no phosphate ion release during adsorption studies

$$H_xPO_4\text{-}BC + OH^- \rightarrow BC\text{-}H_xPO_4 \leftrightarrow HO^- \quad (4.1.19)$$

Thus the release of protons in the solution may be, solely, due to the presence of carboxyl groups on functionalized biochar. The carboxylate anion is stabilized by the resonance which delocalizes electronegativity between the two oxygen atoms. As a result carboxylates are ionized over a pH range. When electron-withdrawing groups such as O or Cl, are part of the same molecule, the pK_a value tends to decrease, whereas the presence of electron-donating alkyl groups tends to increase the pK_a [323]. The standard free energy of proton exchange is given by $\Delta G^0_{H^+{}_{exch2}} = -RT\ ln(K_{a2}/K_{aw})$ and pK_{a2} values of all sulfonamides ranged from 6.16 to 6.99. Furthermore the pK_a values of surface carboxyl groups are above 4 and those surface phenolic groups' values 10 or below [320]. Thus, ΔpK_a value between surface carboxyl group and sulfonamide group is around 2.2–3 (for the surface hydroxyl group ≈ 5). As this difference narrows the bond between them becomes stronger. In the case of hydrogen dicarboxylate conjugate pairs $[RCO_2\ldots H\ldots O_2CR]^-$, where ΔpK_a is nearly zero and form a strong (−) CAHB [321]. The free energy of formation $\Delta G^o_{(-)CAHB}$ in water can be estimated from gas-phase reaction and the resulting $\Delta G^o_{(-)CAHB}$ is: firstly, about −56.2 kJ mol^{-1} for the hydrogen dicarboxylic conjugate pair; and secondly, approximately −50.2 kJ mol^{-1} for the hydrogen carboxylate-phenolate pair [321]. The free energy of proton release was calculated the from –SO_2-NH- as ranging from +38.38 to +46.43 kJ mol^{-1}, which is unfavorable for proton release in the solution (Table 1). Thus, –SO_2-NH- can initially undergo for proton exchange with water molecule and release of –OH in solution **(Eq. (4.1.20))**. The additional driving force may derive initially by the neutralization of –OH ions through the formation of negative CAHB **(Eq. (4.1.21))**. Moreover, biochar surface –COOH group releases more protons into the solution leading to the reduction of final solution pH toward the neutral species region. Thus, a secondary increase in the sorption was found while studying the effect of pH. Thus change in pH toward neutral region provided the same mechanisms as described in neutral species sorption. In addition, according to reaction (**Eq. (4.1.14))**, π-π EAA interaction now may be partially effective as biochar surface was highly negative and sulfonamide molecules also behave as negative species. When the solution pH maintained above 9, significantly reduction of pH was observed when electron-acceptor acetone cosolutes were present **(Table 4.1.7)**.

$$(\text{-}SO_2\text{-}(R_nN^- + H_2O \rightarrow (\text{-}SO_2\text{-}(R_n)NH + OH^- \quad (4.1.20)$$

$$(\text{-}SO_2\text{-}(R_n)NH + HOOC\ldots BC = (\text{-}SO_2\text{-}(R_n)N^-..H^+..^-OOC\text{-}BC)^- + H^+ \quad (4.1.21)$$

Moreover, based on Raman and FTIR spectra for sorption of sulfonamides, it can be also confirm about hydrogen bond formation mechanisms. After sorption the FTIR peaks shifted to near positions, other points remained almost same, which indicated that adsorption did enhance at those particular wave-numbers. In addition, Raman I_D/I_G values decreased after sorption of both single and competitive solutes and this further indicated that a few bonds might form with the biochar surface and the sulfonamide molecules. Finally, the I_D/I_G ratio was found to be close to 1 suggesting that surface functional groups interacted with antibiotic molecules through may be strong H-bond formation **(Figure 4.1.13)**. These bonds formation may be due to the protons linkage between biochar surface –COOH groups and antibiotics molecules.

Table 4.1.9: Summary of Raman spectroscopy peak assignment in char [51, 317] and observed in this study before and after adsorption.

Band name	Band position, cm^{-1}	Description	This study (BBC380, functionalized biochar and after adsorption)						Bond type
			BBC380	1MbBBC600	SMT.1MbBBC600	SMX.1MbBBC600	STZ.1MbBBC600	SMT.SMX.STZ.1MbBBC600	
G_L	1700	Carbonyl group C=O							sp^2
G	1590	Graphite E^2_{2g}; aromatic ring quadrant breathing; structural integrity, **alkene C=C**	1588.7	1599.25	1590.9	1591.98	1591.24	1588.71	sp^2
G_R	1540	Aromatics with 3–5 rings; amorphous carbon structures							sp^2
V_L	1465	Methylene or methyl; semi-circle breathing of aromatic rings; amorphous carbon structures							sp^2, sp^3
V_R	1380	Methyl group; semi-circle breathing of aromatic rings; amorphous carbon structures							sp^2, sp^3
D	1300	D band on highly ordered carbonaceous materials; C–C between aromatic rings and aromatics with not less than 6 rings, simply **–C=O, -OH, and –COOH groups**	1345.5	1337.31	1332.73	1344.35	1336.19	1332.42	sp^2
S_L	1230	Aryl–alkyl ether; para-aromatics							sp^2, sp^3
S	1185	$C_{aromatic}$–C_{alkyl}; aromatic (aliphatic) ethers; C–C on hydroaromatic rings; hexagonal diamond carbon sp^3; C–H on aromatic rings							sp^2, sp^3
S_R	1060	C–H on aromatic rings; benzene (ortho-di-substituted) ring							sp^2
R	960–800	C–C on alkanes and cyclic alkanes; C–H on aromatic rings							sp^2, sp^3

4.1.4. Concluding Remarks

The detailed mechanisms of sulfonamide antibiotics sorption in both single and mixture mode were studied. The maximum sorption capacity of sulfonamides decreased as STZ > SMX > SMT. The sorption of sulfonamides occurred through the formation of π^{+}-π EDA for positive species, and through proton exchange with water molecules forming (–) CAHB and by π-π EAA interaction for negative species. The maximum sorption of sulfonamides was found for neutral species due to charge pairing through strong H-bond formation and stabilization of the zwitterion via π^{+}-π EDA mechanism. The results suggest that interactions between functionalized biochar and sulfonamide antibiotics can play important roles in the removal of emerging contaminants from water. Thus, it is believed that competitive sorption of a mixture of micropollutants onto functionalized biochar surface is environmentally significant and should be further extended to wastewater application.

4.2. Competitive Sorption Affinity of Sulfonamides and Chloramphenicol Antibiotics toward Functionalized Biochar for Water and Wastewater Treatment

4.2.1. Introduction

The use of different antibiotics resulted in a reduction of the mortality and morbidity rates from epidemic and infectious diseases such as syphilis, tuberculosis, pneumonia, gonorrhea, and communicable diseases of childhood [324-326]. The occurrence of antibiotic residues in the environment is attracting attention due to their potential long-term adverse effects on human and animals [44, 57, 303, 310, 327]. In addition, antibiotics are of great concern as they are consumed in significant quantities all over the world and can particularly act on microorganisms without affecting cells and tissues [85]. Physical treatment processes have been found very effective and economic in removing antibiotics among which sorption has emerged as a cost effective method for pollutant removal; unaffected by the potential toxicity as for biological processes; and easy to design and operate [44, 239, 240]. In addition, sorption is an extremely important process because it may dramatically affect the fate and impacts of contaminants in the environment through different mechanisms [45]. The efficiency of sorption process is highly affected by the properties of sorbate, sorbent, and operating conditions [241]. The degree of sorption mainly depends on the physicochemical properties of the micropollutants, type of solid matrices, surface area, porosity, pore diameter, and environmental conditions [240, 242, 243].

The sorption of antibiotics onto carbonaceous materials such as biochar [55, 240, 244, 245], activated carbon [29], carbon nanotubes [57], graphene, clay minerals [57], and hollow polymer nanorods [239] has been widely studied and proved very effective [57]. The sorption of antibiotics using biochar was found particularly efficient [56, 57]. Biochar has a high hydrophobicity and aromaticity and is an excellent sorbent for hydrophobic organic contaminants e.g. aromatics [246, 247]. To date, the majority of adsorption studies on the removal of different antibiotic residues by carbonaceous sorbents have been conducted using single solutes, and only a few studies were reported based on the competitive nature of micropollutants [244, 328, 329]. In addition, the removal mechanisms of antibiotic mixture using different adsorbents are unclear. In reality, aquatic environment can be highly complex including mixtures of different organic and inorganic contaminants, and thus understanding the

mechanisms of competitive adsorption is of great importance. During the application of sorbent, sorbate molecules can interact with the same sites of the sorbent particles, hence faster sorption mainly occurs for the compounds which have specific affinity to be sorbed onto the specific surface of sorbent. Interactions are very simple for single solute but can be very complex for a mixture of contaminants. Therefore, we have targeted four antibiotics for their sorption onto fBC in order to check their competitive sorption affinity and to assess the sorption mechanisms as well as sorption trend in different water types.

This study aims to bridge the knowledge gap by studying the competitive sorptive capacity and mechanisms by fBC for four widely used antibiotics SMT, SMX, STZ and CP from water and wastewater. Specifically this research studied: (i) the effect of pH on competitive sorption with detailed sorption affinity mechanisms, [92] the kinetics parameters for competitive solutes, (iii) the competitive sorption isotherms parameters, and (iv) the application of fBC in removing antibiotics mixtures from lake water and synthetic wastewater under practical conditions.

4.2.2. Materials and Methods

4.2.2.1. Chemicals and Reagents

The antibiotic standards of SMT ($pK_{a1/a2}$ = 2.04/6.99, solubility = 1500 mg L^{-1}), SMX ($pK_{a1/a2}$ = 1.97/6.16, solubility = 610 mg L^{-1}), STZ ($pK_{a1/a2}$ = 2.04/6.93, solubility = 373 mg L^{-1}) and CP (pK_{a1} = 5.50, solubility = 2500 mg L^{-1}) were purchased from Sigma-Aldrich, Australia (**Table 4.2.1**). HPLC-grade organic solvents such as acetonitrile and formic acid were also purchased from Sigma-Aldrich, Australia. Ortho phosphoric acid (85%), hydrochloric acid (35%), sodium hydroxide, potassium chloride, sodium chloride were obtained from Sigma-Aldrich. *Eucalyptus* globulus wood was donated by New Forest Asset Management Pty Ltd, Portland, Victoria, Australia.

Table 4.2.1: Physicochemical properties of the antibiotics investigated in this study.

Group	Compound	Molecular mass	log K_{ow}[a]	$pK_{a1/a2}$[b]	Solubility[a] (mg L^{-1})
Sulfonamides	SMX	253.3	0.89	1.97/6.16	610
	STZ	255.3	0.05	2.04/6.93	373
	SMT	278.3	0.14	2.04/6.99	1500
Chloramphenicol[c, d]	CP	323.1	1.14	5.50	2500

[a]Values obtained from U.S. National Library of Medicine: http://toxnet.nlm.nih.gov
[b]Values obtained from ChemAxon: http://www.chemicalize.org
[c]https://www.drugbank.ca/drugs/DB00446; d. http://www.sigmaaldrich.com/content/dam/sigma-aldrich/docs/Sigma/Product_Information_Sheet/c0378pis.pdf

4.2.2.2. Preparation and Characterization of fBC

fBC was prepared according to our previous study [244]. Briefly, 25 g of eucalyptus wood biomass was pyrolyzed at 400 °C at an average heating rate of ~11.0 °C min^{-1} under constant nitrogen pressure of 2 psi for 2 h, to obtain biochar samples. Biochar functionalization was carried out by soaking 10 g of biochar in 20 mL of 50% orthophosphoric acid (oH_3PO_4) for 3 h at 50 °C. The mixture was then reheated at 600 °C for 2 h. After that, the prepared material was left to cool inside the reactor, washed and the pH adjusted to ~7.0, followed by drying overnight at 105 °C, to obtain fBC. The physicochemical characteristics of fBC were extensively examined using Fourier transform infrared spectroscopy (FTIR), Raman spectroscopy, energy dispersive spectrometry (EDS), and zeta potential instrument. The elemental composition of fBC was measured using EDS (Zeiss Evo-SEM). The identification of surface functional groups was conducted using FTIR (Miracle-10, Shimadzu), by measuring the absorbance from 400 to 4000 cm^{-1} using a combined 40 scans. Raman shifts measurement was carried out using Renishaw inVia Raman spectrometer (Gloucestershire, UK) equipped with a 17 mW Renishaw Helium-Neon Laser 633 nm and CCD array detector. Zeta potential values were measured using 500 mg L^{-1} of fBC dosage at different pH values, after pre-equilibration for 48 h, on Nano-ZS Zeta-seizer (Malvern, Model ZEN3600). Zeta potential was measured three times at each pH (50 scans each time), with the average and standard deviation being calculated.

4.2.2.3. Competitive Sorption Experiments Using fBC

The stock solutions (100 mg L^{-1}) of SMX, SMT, STZ and CP were diluted to different initial concentrations of each antibiotic. The effects of pH were studied at adjusting pH values from 1.5 to 10.9, using HCl and NaOH solutions. fBC was pre-equilibrated at the same pH for 24 h using half of the volume of a mixture of antibiotics and rest of solute was added and shaken for another 42 h. The kinetics studies were carried at a pH 4.0–4.25 (where maximum interactions occurred based on pH study) at 25 °C over 33 h using 80 mg L^{-1} of fBC. Batch competitive experiments were conducted at 25 °C using 80 mg L^{-1} of fBC with initial concentrations of 0.250–20.0 mg L^{-1} for each antibiotic in mixture mode which were shaken on an orbital shaker at 120 rpm for 42 h (apparent equilibrium time) at pH 4.0–4.25. In all cases, a constant ionic strength was maintained using 0.01 M NaCl. The control experiments without adsorbents were also executed. The application of fBC to treat lake water (TOC, 96.67 mg L^{-1}) and synthetic wastewater (TOC, 54.0 mg L^{-1}) was carried out by spiking each antibiotic (1.0 mg L^{-1}) at pH ~4.0–4.15 and 25 °C. TOC was measured by using a TOC analyzer by the filtration of the collected and prepared sample using 1.0 mm pore size syringe filter. Synthetic wastewater was composed of peptone, beef extract, humic acid, tannic acid, arabic acid, sodium lignin sulphonate, acacia gum powder, KH_2PO_4 and $MgSO_4 \cdot 3H_2O$ Control experiments in the absence fBC with different water matrices showed that there was no loss of antibiotics. At equilibrium, the solution pH was measured before the supernatant was taken and filtered through a 0.20 μm PTFE filter for antibiotic analysis using HPLC.

4.2.2.4. Antibiotics Determination and Data Fitting

The concentrations of antibiotics were measured by HPLC (Jasco) equipped with an auto-sampler and a UV detector at 285 nm, by using 70 μL injection. A reverse phase Zorbax Bonus RP C_{18} column (5.0 μm, 2.1 × 1.50 mm, Agilent Technologies) was used for the separation. Mobile phase A was composed of acetonitrile and formic acid (99.9: 0.1) while mobile phase B was composed of Milli-Q water and formic acid (99.9: 0.1).The elution started with 15% of A and 85% of B at a flow rate of 0.4 mL min^{-1}, which was changed to 0.3 mL min^{-1} at 0.1 min and maintained till 5.9 min. Then at 6.0 min the elution changed to 40% of A and 60% of B at a flow rate of 0.3 mL min^{-1} and maintained over 15 min. The competitive sorption data for all antibiotics were fitted to the Langmuir and Freundlich isotherm models and three kinetic equations. The competitive sorption distribution coefficient (K_d, L kg^{-1}) is defined by **Eq. (4.2.1)**:

$$K_d = 1000 * \frac{q_s}{C_w} = 1000 * \left(\frac{C_0 - C_w}{C_w}\right)\frac{V}{M} \quad (4.2.1)$$

where q_s is the equilibrium concentration of each antibiotic in mixture mode in sorbent (mg g^{-1}), C_w and C_o are the equilibrium and initial concentrations (mg L^{-1}) of each antibiotic in mixture mode, V is the solution volume (L), and M is the sorbent mass (g).

The kinetic equations such as the pseudo first order (PFO), pseudo second-order model [306] and intra-particle diffusion model [17] can be represented as follows:

$$\text{PFO: } q_t = q_s(1 - e^{-K_1 t}) \quad (4.2.2)$$

$$\text{PSO: } q_t = \frac{K_2 q_s^2 t}{1 + K_2 q_s t} \quad (4.2.3)$$

$$\text{IDM: } q_t = K_i t^{\frac{1}{2}} + C \quad (4.2.4)$$

Parameters were estimated by nonlinear regression analysis weighted by the dependent variable. K_i is the apparent diffusion rate constant (mg g^{-1} $min^{-1/2}$), K_1 (min^{-1}) and K_2 (g mg^{-1} min^{-1}) are PFO and PSO kinetic rate constant, respectively, and C is a constant (mg g^{-1}) that provides the thickness of the boundary layer.

The Langmuir and Freundlich isotherm models can be been represented as follows:

$$\text{Freundlich model: } q_s = K_F {C_w}^{1/n} \quad (4.2.5)$$

$$\text{Langmuir model: } q_s = \frac{q_{max} K_L C_w}{1 + K_L C_w} \quad (4.2.6)$$

where q_{max} is the maximum adsorption capacity (mg g^{-1}), n is a dimensionless number related to surface heterogeneity, K_F is the Freundlich affinity coefficient (mg^{1-n} L^n g^{-1}), and K_L is the Langmuir fitting parameter (L mg^{-1}).

4.2.3. Results and Discussion

4.2.3.1. Influence of pH on Antibiotic K_d During Competitive Interaction with fBC

The K_d values for competitive interaction of selected antibiotics on fBC were found to be pH dependence **(Figure 4.2.1a)**. All the selected sulfonamide antibiotics are ionisable while CP is nonionic. Lower K_d values were found for all positive sulfonamides species (pH 0–2.0) [59, 308, 309] and CP at pH ~1.50 (2.0×10^4 to 4.5×10^4 L kg^{-1} for SMT to STZ). The surface zeta potential value of fBC was found to be pH 2.2 **(Figure 4.2.2)**. When pH was below 2.2, zeta potential value of fBC was found to be positive. Moreover, all sulfonamides were positively charged at pH < 2.0 (due to matched pK_{a1} values). Thus, lower K_d values were highly expected due to the repulsion nature of same species and antibiotics might also get

protonated at very low pH. The adsorption of antibiotics at lower pH may be dominated by the interaction between the protonated aniline ring of antibiotics and the π-electron rich fBC surface [273].

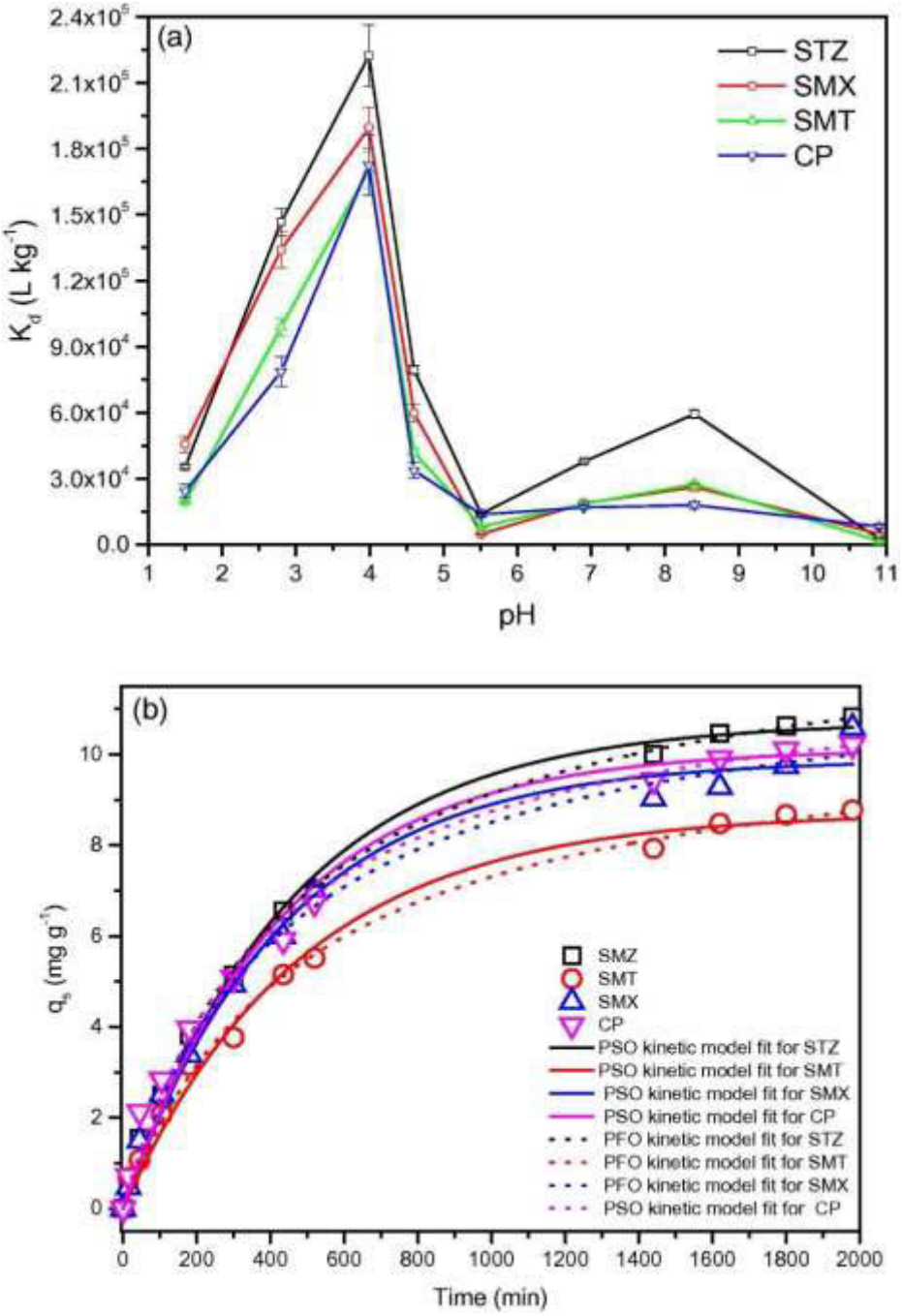

Figure 4.2.1: Effect of pH on K_d (with standard deviation) during the removal of sulfonamides and chloramphenicol antibiotics using fBC (80 mg L^{-1}) with initial individual antibiotic concentration of 1.0 mg L^{-1} at 25 °C (a). Competitive sorption kinetics data with PSO and PFO model fitting using 1.0 mg L^{-1} initial antibiotics concentration and 80 mg L^{-1} of fBC at pH 4.0–4.25 (b).

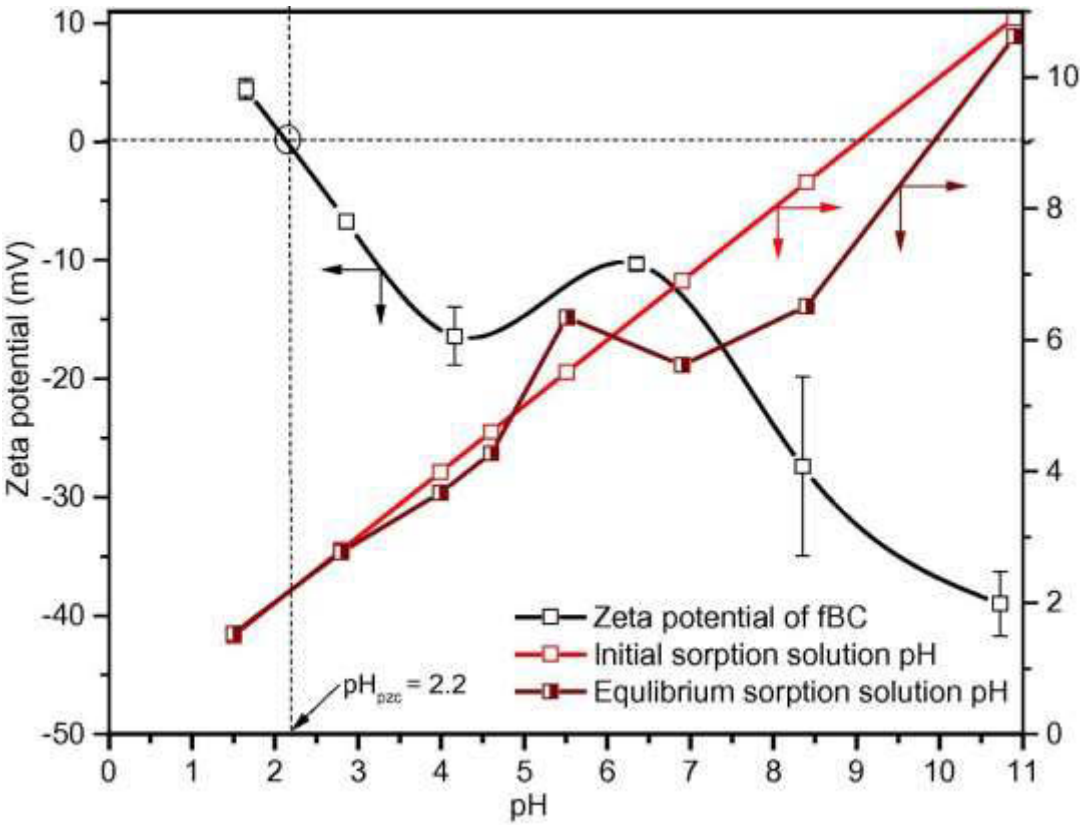

Figure 4.2.2: Zeta potential values of fBC and pH shift during pH effect study.

The maximum K_d values were observed at pH ~4.0–4.25 for STZ (2.2×10^5 L kg^{-1}), SMX (1.9×10^5 L kg^{-1}), SMT (1.7×10^5 L kg^{-1}) and CP (1.73×10^5 L kg^{-1}). The maximum K_d at this pH range was found due to the adsorption of neutral species of sulfonamides at pH ~2.0–6.0 [59, 308, 309] and nonionizable CP. The adsorption was due to the formation of strong hydrogen bonds for sulfonamides antibiotics, and due to CAHB for CP.

Further increase in pH from 4.5 to higher pH decreased the sorption. However, another small sharp increase of K_d values for all antibiotics was observed at pH ~8.5. The observed K_d values were 5.9×10^4, 2.6×10^4, 2.7×10^4, and 1.8×10^4 L kg^{-1} respectively for STZ, SMX, SMT and CP. The main reason might be due to sorption of negative species sulfonamides at pH ~6.0–11 [59, 308, 309], as well as CP, declined due to negative surface zeta potential value of fBC leading to electrostatic repulsion. However, the sorption affinity might be due to the formation of CAHB along with EDA interactions [307]. This was due to the matching of pK_{a2} values of negative species of sulfonamides and surface hydroxyl pK_a values. After that, an increase of pH up to ~11, the sorption was decreased due to highly repulsion nature of negative surface hydroxyl groups and negative species of sulfonamides. The detailed mechanisms were discussed in **Section 4.2.3.4**.

4.2.3.2. Sorption Kinetics in Competitive Mode

Kinetic experiments were carried out for 33 h with the equilibrium being reached within ~1800 min. The kinetics of mixture of antibiotics sorption by fBC was fitted to pseudo-first-order (PFO), pseudo-second-order [306] and intra-particle diffusion (IPD) models. Based on the correlation coefficient (r^2) and $q_{s,cal}$ (mg g^{-1}) values, the kinetics data for all competitive solutes were slightly better fitted to the PSO chemisorption kinetic model than PFO and IDM models but their r^2 values were comparable (**Figure 4.2.1b**). Based on the $q_{s,cal}$ values in PSO model, antibiotics followed the order of STZ (13.3 mg g^{-1}) > SMX (12.2 mg g^{-1}) > CP (12.3 mg g^{-1}) > SMT (10.9 mg g^{-1}). However, the $q_{s,cal}$ values for the PFO kinetic model followed a different order: STZ (10.73 mg g^{-1}) > CP (10.03 mg g^{-1}) > SMX (9.89 mg g^{-1}) > SMT (8.73 mg g^{-1}). IDM and PFO showed slightly lower r^2 values than the PSO model. The IPD rate constant K_i (mg g^{-1} $min^{-0.5}$) also followed the same trend as the PSO kinetic model $q_{s,cal}$ values (**Table 4.2.2**).

Table 4.2.2: Summary of the kinetic model parameters for antibiotics sorption on fBC at 25 ± 0.5 °C.

	PFO			PSO			IPD		
Antibiotic	$q_{s\,cal}$ (mg g^{-1})	K_1 (min^{-1})	r^2	$q_{s\,cal}$ (mg g^{-1})	K_2 (g mg^{-1} min^{-1})	r^2	C (mg g^{-1})	K_i (mg g^{-1} $min^{-0.5}$)	r^2
STZ	10.73±0.17	0.00221±1.10E-4	0.995	13.27±0.172	1.67E-4±8.5E-6	0.999	0.247±0.3	0.254±0.011	0.978
SMT	8.73±0.19	0.00208±1.38E-4	0.992	10.91±0.259	1.86E-4±1.7E-5	0.996	0.150±0.21	0.205±0.0078	0.984
SMX	9.89±0.23	0.00231±1.70E-4	0.992	12.15±0.333	1.93E-4±2.1E-5	0.996	0.272±0.32	0.235±0.012	0.972
CP	10.03±0.33	0.00239±2.18E-4	0.982	12.10±0.421	2.12E-4±2.9E-5	0.991	0.542±0.27	0.235±0.009	0.977

Table 4.2.3: Summary of the Freundlich and Langmuir isotherm parameters for competitive antibiotic sorption on fBC at 25 ± 0.5 °C.

	Freundlich isotherm parameters			Langmuir isotherm parameters		
Antibiotic	K_F	n	r^2	q_{max}	K_L	r^2
STZ	16.76±2.53	2.99±0.60	0.942	45.19±5.03	0.48±0.20	0.956
SMT	9.65±1.21	3.52±0.67	0.930	20.71±1.99	1.08±0.54	0.915
SMX	11.04±1.33	3.03±0.47	0.949	28.29±2.30	0.65±0.23	0.965
CP	9.81±1.28	3.52±0.70	0.925	21.35±2.27	0.97±0.52	0.906

4.2.3.3. Sorption Isotherm Models for Competitive Sorption

Compared with the Freundlich isotherm model, interactions of antibiotics with fBC in the competitive mode were better fitted to the Langmuir model with higher r^2 values for STZ and SMX. While the Freundlich isotherm model provided a better fit for SMT and CP (**Figure 4.2.3, Table 4.2.3).** The Langmuir sorption capacity (q_{max}) was found to be 45.2, 28.29, 21.35 and 20.71 mg g^{-1} for STZ, SMX, CP and SMT, respectively in competitive mode. The K_F values were 16.76, 9, 11.04, 9.81 and 9.65 mg^{1-n} L^n g^{-1}, respectively, for STZ, SMX, CP and SMT at 25 °C. These findings aligned with the results observed from pH effect and kinetics experiments. Thus, from both models, the sorption affinity can be written in the following order as STZ > SMX > CP > SMT. It is assumed that all the antibiotics in competitive mode share the same sorption sites of fBC when sorbed onto its surface. However, their sorption affinity depends on the physicochemical properties of antibiotics and fBC. The total fBC sorption capacities for all antibiotics in mixture mode were calculated by summarizing individual contributions for both Langmuir model (115.54 mg g^{-1}) and Freundlich model (47.3 mg^{1-n} L^n g^{-1}). A similar result has been reported for single and competitive sorption of three sulfonamide antibiotics [244]. Hence, fBC is capable of adsorbing a mixture of antibiotics onto its surface.

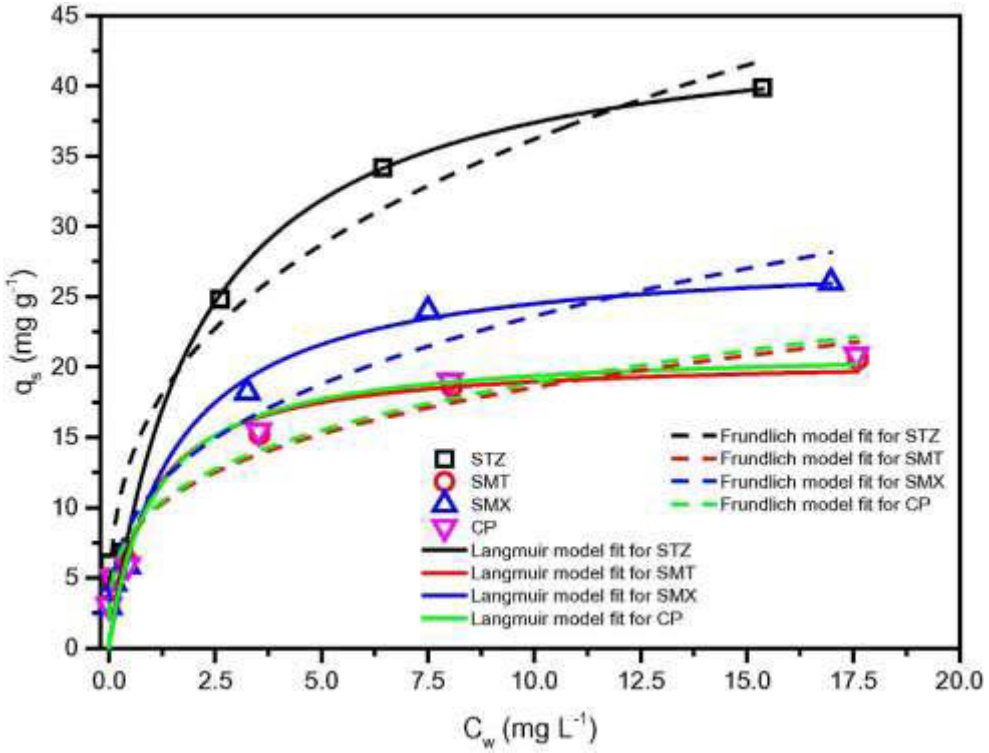

Figure 4.2.3: Sorption isotherm plots and model fitting for mixtures of antibiotics (initial concentration of each antibiotic was 0.250–20.0 mg L^{-1}) at pH 4.0–4.25 using fBC dosage of 80 mg L^{-1}.

4.2.3.4. Mechanisms of Competitive Sorption on fBC

The results from the sorption isotherms, sorption kinetics and the pH effect suggested that the fBC had very strong sorption affinity for antibiotics in competitive mode, while the affinity of the antibiotics sorption onto fBC varied from compound to compound. The sorption of SMT and CP followed the Freundlich isotherm which was related to the chemisorption mechanism. While the sorption of STZ and SMX followed the Langmuir isotherm model related the homogeneous covering of the fBC surface. The kinetic results indicated the sorption of antibiotics in competitive mode agreed well with PSO, PFO and IPD model. This result indicated that the role of surface functional groups, monolayer coverage and diffusion of sorbate molecules during competitive sorption antibiotics. Thus, high competitive sorption affinities of fBC toward antibiotics were due to a combination of effects such as surface homogeneous and heterogeneous sorption sites.

All the peaks from the FTIR spectra indicated that fBC contained phenolic -OH, C=O (carboxylic and ketonic), N=C=O (isocyanate), C≡C, and C=C groups on the surface [55, 330-332]. Moreover, EDS data showed that fBC contains mainly C (75.3%), O (10.3%) and N (11.62%), with O/C molar ratio of 0.102. FTIR spectra before and after antibiotics sorption

clearly show the sorptive nature of fBC. Spectra at ~1516 cm^{-1} (aromatic C=C), at ~2090–2218 cm^{-1} (C≡C), at ~2276 cm^{-1} (N=C=O), at ~1710 cm^{-1} (C=O, ketonic and carboxylic), at 3620–3860 cm^{-1} (phenolic, –OH groups), and at ~3020 cm^{-1} (-CH stretch) shifted to lower absorbance areas indicated that antibiotics sorption had been increased by these functional groups on fBC surface (**Figure 4.2.4a**). Raman spectra also confirmed this result. In Raman spectra, the D band indicates the degree of disordered SP^2 hybridization of carbon atom containing vacancies, impurities or defects whereas G band indicates the SP^2hybridization of carbon atoms in any carbonaceous materials (graphitic carbon). The intensity of the peaks was reduced significantly after sorption of antibiotics. The I_D/I_G ratio also decreased which also confirmed the interactions of antibiotics with the surface functional groups of fBC. The peak intensity decreased due to sorption of antibiotics by the fBC functional groups leading to blocking the functional groups available for detecting in Raman spectroscopy. This result also confirmed the role of surface disordered structure carbon atoms i.e. D bands at ~1330 cm^{-1} (in the form of oxygenated functional group) while graphitic G-bands at ~1586 cm^{-1} also decreased indicating the role of C=C i.e. π structured carbon atoms. The latter case can be explained by the electron-donar interaction nature of the arene unit in the C=C and C≡C system. Thus Raman spectra indicated the role of functional groups as well as π-π interactions due to change in the peak intensity for G and D bands. In addition, G^* band peak intensity also reduced significantly indicating the π-π interactions (**Figure 4.2.4b**). The mechanisms of antibiotic sorption can be also explained based on different pH described below.

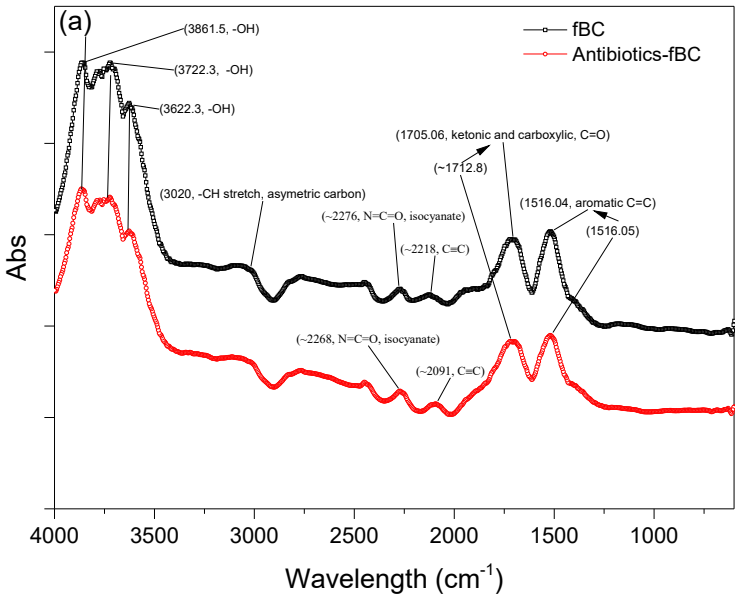

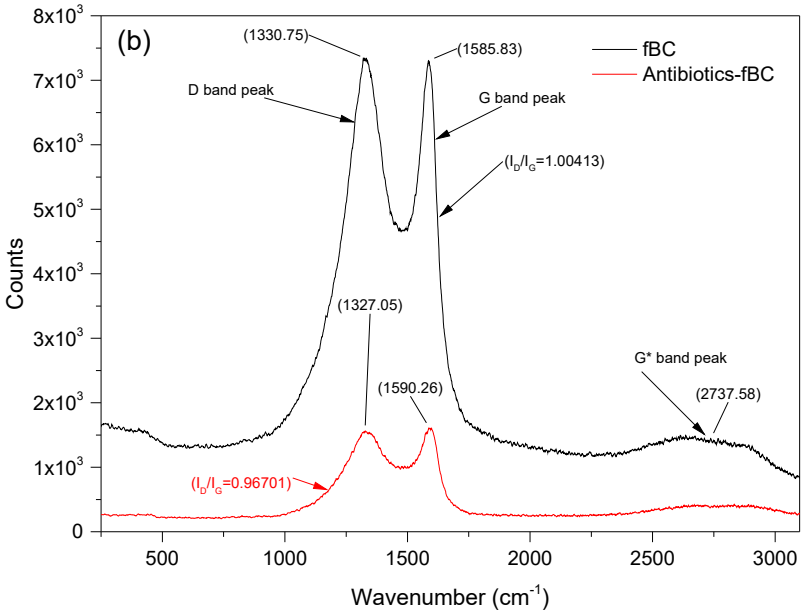

Figure 4.2.4: FTIR (a) and Raman spectra (b) with band ratio (I_D/I_G) of fBC before and after sorption experiments for competitive solutes in mixture mode.

The zeta potential value of the fBC was found to be positive at solution pH 1.5, i.e. surface of the fBC gets protonated. Hence, the weak interactions between the opposite charged quadruples might be the main reason for lower sorption of these antibiotics. However, still, there was some sorption which can mainly be explained by the EDA interactions. Stronger EDA interaction might be possible when the π-electron depletes any aromatic ring, and π-

electron rich regions interact together [244]. Antibiotics such as SMT, STZ and SMX can act as π-electron-acceptor due to their amino functional groups (donating lone pair electrons to the arene unit) and N and/or O-hetero-aromatic rings (electronic resonance). While CP can also act as the π-electron-acceptor site due to its nitro group presence on its arene unit. Moreover, fBC enriched with C═C and C≡C groups along with –OH, C═O and –COOH groups and may act as a strong π-electron-donor or acceptor sites at pH ~1.5 (**Figure 4.2.5**). The pK_a values of surface –COOH and surface –OH are ~3.0–5.0 and above 8.0, respectively, hence proton exchange is not possible for those functional groups [59]. However, the hydroxyl group in fBC can acts as a π-electron donor due to its π-electron donor capacity to the arene unit in fBC, while surface –COOH and –C═O may act as opposite effect due to its π-electron withdrawal capacity from the arene unit. Hence, at low pH, EDA interactions between –OH groups in fBC and π-electron depleted aromatic unit in antibiotics might be the main sorption mechanism (**Figure 4.2.6**). The π-π electron-acceptor-acceptor (EAA) interactions (due to BC-C═O group and BC-COOH group become electron acceptor as well as antibiotics molecules can behave as electron acceptor site) might also possible but not stronger than EDA interactions (**Figures 4.2.5 and 4.2.6**). So, at very low pH, competitive sorption of sulfonamides and CP antibiotics on to positively charged fBC were mainly due to EDA interactions, and this result is also supported by a previous study [59, 244].

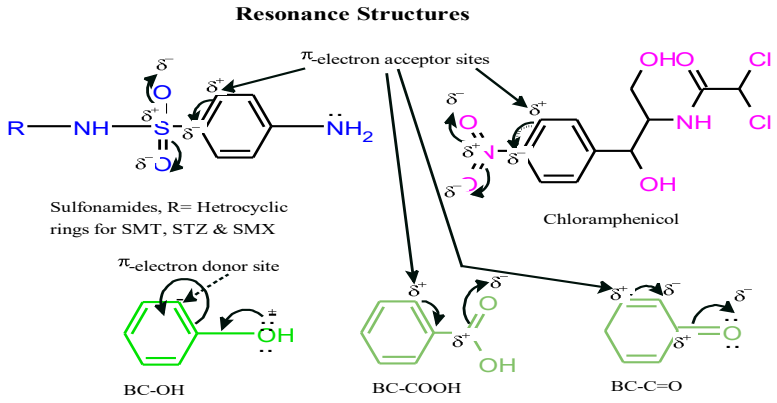

Figure 4.2.5: Possible resonance structures of antibiotics and different functional groups in fBC and their electron donor and acceptor sites.

At pH ~4.0, all sulfonamide antibiotics behaved as neutral species in the solution and CP was more stable. Maximum sorption of all selected antibiotics in competitive mode was found at this pH range. In addition to EDA, strong hydrogen bonds and CAHB formations

might be the main sorption mechanisms. As mentioned earlier, the pK_a value of surface –COOH was near ~3.0–5.0, hence, hydrogen bond formations were highly possible among fBC surface –COOH groups and with $–NH_2$ or, $–NO_2$ or hydrogen groups present in sulfonamides and CP antibiotics.

$$\text{Sulfonamides}^0/\text{CP} + H_2O + \text{fBC} = \text{Sulfonamides/CP}^+ \ldots \text{fBC} + OH^- \quad (4.2.7)$$

$$\text{Sulfonamides}^0/\text{CP} + \text{fBC} = \text{Sulfonamides/CP}^+ \ldots \text{fBC}^- \quad (4.2.8)$$

$$\text{Sulfonamides}^0 + \text{fBC} = \text{Sulfonamides}^{\pm} \ldots \text{fBC}\ (-H^+) \quad (4.2.9)$$

$$\text{Sulfonamides}^0 + \text{fBC} = \text{Sulfonamides}^{\pm} \ldots \text{fBC} + H^+ \quad (4.2.10)$$

Competitive Sorption Affinity Mechanisms

At very low pH:
(i). Repulsion interactions
(ii). BC-OH + sulfonamides/CP = EDA interactions

At pH 4.0-4.25:
(i). BC-COO^-.....H^+....^-O_2N-chloramphenicol = CAHB formations with EDA interactions
(ii). BC-COO..H + sulfonamides ($NHSO_2$-/NH/ -NH_2/CH_3) = H-bond formations

At pH above 7.0:
(i). Repulsion interactions
(ii). Sulfonamides-N^- + H_2O = sulfonamides-NH + $-OH^+$
(iii). BC-O....H + $^-$N....sulfonamides =BC-O^-.....H^+....$^-$N..sulfonamides = CAHB
(iv). BC-OH + chloramphenicol (H^+/-OH/NO_2/-NH-/-Cl) = H-bond formations

Figure 4.2.6: Proposed sorption mechanisms for the removal of antibiotics in competitive mode using fBC.

Proton exchange with water molecule should increase the solution pH by leaving –OH groups in the solution and thus final solution pH should be increased. However, pH shifted to become more acidic indicating that **Eq. (4.2.7)** was not the main mechanism (**Figure 4.2.2**), which is consistent with previous studies [59, 244]. This might be due to the formation of strong H-bond formations for neutral sulfonamides **(Eq. (4.2.8)). The Eq. (4.2.9)** involves tautomerisation of sulfonamides to the zwitterion in the adsorbed state while Eq. (10) shows the tautomerisation by forming the zwitterion and releasing protons in the solution. Thus, the observed equilibrium pH slightly decreased from the initial pH and stabilization of **Eqs. (4.2.9) and (4.2.10)** might be possible through the formation of a π-π EDA which might not be as strong as the positively charged sulfonamide ring system with the biochar surface. Overall

stabilization of the cationic form of sulfonamides can be gained through a strong H-bond formation (**Figure 4.2.2**).

On the other hand, CP has a pK_a *v*alue of ~5.50, and thus ΔpK_a for surface –COOH and CP lays ~1.0–1.5. Usually, smaller the difference stronger the hydrogen bond formations [321]. More clearly, CP can initially undergo for proton exchange with a water molecule and release of –OH in solution (Eq**. (4.2.11))** and the –OH may be neutralized by releasing proton from the surface –COOH to form negative CAHB (Eq. **(4.2.12**)). This has resulted in slight decrease in equilibrium pH **(Figure 4.2.2).** Thus at pH ~4.0–4.25, sulfonamides antibiotics molecules mainly formed strong hydrogen bonds whereas CP formed CAHB along with EDA interactions, which were the main reasons for higher sorption of those antibiotics. Moreover, ordinary hydrogen bonds formation among hydrogen in CP and –COOH in fBC might be also responsible for the high affinity. The π-π EAA interaction was less effective as biochar surface became negative above pH 2.2 and as surface carboxylate group had pK_a values more than 4.

$$CP + H_2O \rightarrow CP\ldots.H^+ + OH^- \quad (4.2.11)$$

$$CP + HOOC\ldots.BC = CP^-\ldots\ldots.H^+\ldots\ldots.^-OOC\text{-}BC + H^+ \quad (4.2.12)$$

Lewis acid-base electronic interaction might be possible at pH of ~4.0 where sulfonamides remain as a neutral species and thus, loan-pair electrons of amino groups in the arene unit may donate to form a complex with the protonated enriched surface functional groups [244].

At pH near 5.5, all the sulfonamide antibiotics remained as minimum ionized states due to intersections points, and thus minimum sorption at this pH was found. At the same time, minimum CP sorption was also found (might be just crossing the pK_a matched solution pH). Equilibrium pH moved to ~6.4 also indicating the release of –OH groups in the solution by consuming proton from the solution leading to hydrogen bond formations.

In alkaline solution, the sorption of negative sulfonamide species was found to be significantly lower than for neutral species. This was due to the repulsion of negative species sulfonamides as well as negative surface fBC. Teixidó et al. (2011)[59] noted that the adsorption of SMT^- was due to the release of –OH for proton exchange with water molecule ($SMT^- + H_2O \rightarrow SMT^o + OH^-$), followed by interactions of the resulting natural molecules with surface –COOH and –OH groups ($SMT^0 + BC = SMT^0\ldots..BC$). These kinds of bonds formation were designed as strong negative CAHB. They mentioned that pH was raised as SMT^- sorption amount increased. However, in this study it was found equilibrium pH was decreased indicating that protons were released by fBC surface. As the pK_{a2} values of all sulfonamides ranged from 6.16 to 6.99 and pK_a values of phenolic groups ranged from 7 to 10

[321], ΔpK_a value between phenolic groups and sulfonamide groups is around ~0.0–2.5. Thus, initially, sulfonamide antibiotics began with proton exchange with water molecules hence releasing –OH in solution **(Eq. (4.2.13))**, followed by neutralization of hydroxyl groups by the release of protons from fBC surface –OH groups through the formation of negative CAHB (Eq. (14)).

$$\text{Sulfonamide-N}^- + \text{H}_2\text{O} \rightarrow \text{Sulfonamide-NH} + \text{OH}^- \quad (4.2.13)$$

$$\text{Sulfonamide-NH} + \text{HO}\ldots\text{BC} = \text{Sulfonamide-N}^-\ldots\text{H}^+\ldots{}^-\text{O-BC}^- + \text{H}^+ \quad (4.2.14)$$

CP might form CAHB and weak hydrogen bonds among surface hydroxyl groups of fBC, aromatic nitro group and hydroxyl groups **(Figure 4.2.6**). EDA interactions for CP were not favorable at this pH since the hydroxyl group was deprotonated to form CAHB. In addition, EAA could be possible due to unchanged –COOH groups on fBC surface.

4.2.3.5. Treatment of Water and Synthetic Wastewater During Competitive Removal

Competitive removal of antibiotics was carried out at different dosages of fBC and pronounced differences were observed for lake and synthetic wastewater (**Figure 4.2.7**). In comparison with lake water, synthetic wastewater was found to have more influence on antibiotics removal than lake water. Final lake water TOC value was found to be 46.53 mg L^{-1}. The synthetic wastewater contained different chemicals in the form of inorganic and organic species (e.g. humic acid, sodium lignin sulfonate) that could compete with the antibiotics for fBC sorption sites and resulted in lower sorption efficiency with final TOC value of 50.5 mg L^{-1}. Regarding antibiotics themselves, in both water types, STZ sorbed even at 200 mg L^{-1} dosage of fBC while SMT required a higher dosage (~700 mg L^{-1} of fBC, synthetic wastewater) for the complete removal from the mixture solution. Overall, the trend for removing selected antibiotics in competitive mode followed the order of deionised water > lake surface water > synthetic wastewater. Therefore, fBC could be successfully applied for the treatment of a mixture of antibiotics from different water and wastewater.

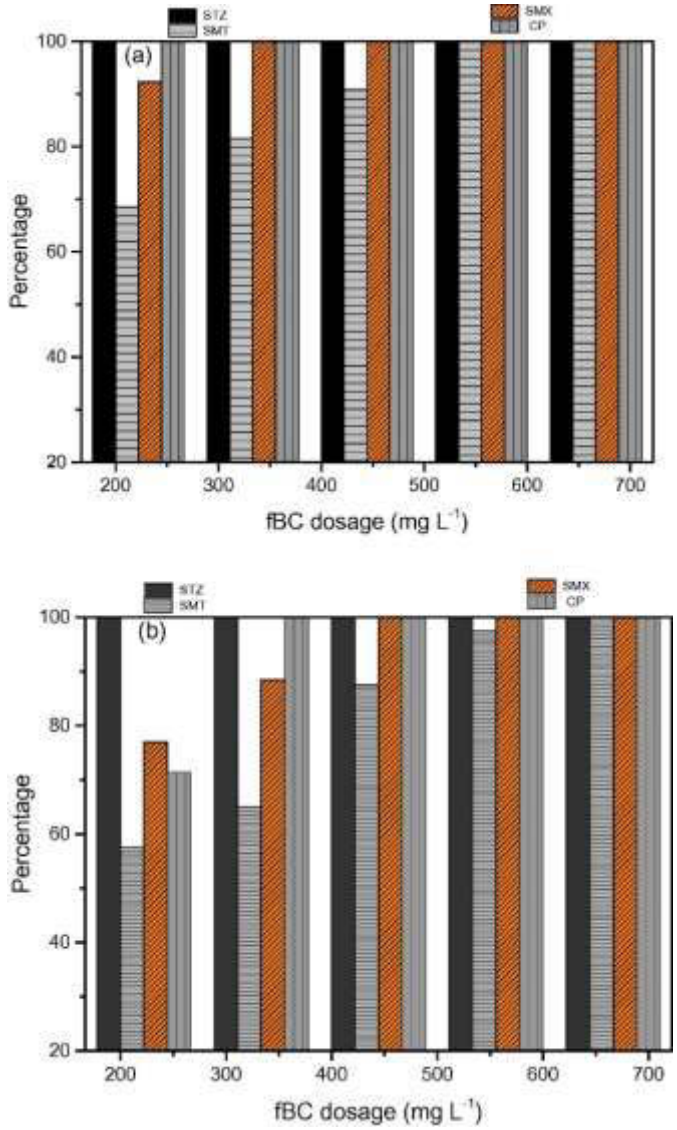

Figure 4.2.7: Sorption of antibiotics (%) in mixture mode with 1.0 mg L^{-1} initial concentration of each antibiotic from lake water (a) and synthetic wastewater (b) with different dosages of fBC at pH 4.0–4.25 and 25 °C.

4.2.4. Concluding Remarks

Competitive sorption of sulphonamides and chloramphenicol was very strong toward fBC. Competitive sorption was governed by solution pH and the maximum sorption occurred at pH 4.0–4.25. Sorption affinity decreased in the order STZ < SMX < CP < SMT. fBC was found to be highly efficient in removing these antibiotics from water and wastewater, with the sorption affinity following the order of deionized water > lake water > synthetic wastewater. The sorptive mechanisms were addressed in detail based on resonance effect of arene units. The results demonstrate that fBC is very effective in removing antibiotics mixture from water and wastewater.

4.3. Chloramphenicol Interaction with Functionalized Biochar in Water: Sorptive Mechanism, Molecular Imprinting Effect and Repeatable Applications

4.3.1. Introduction

Antibiotics are widely produced and used in large quantities to treat diseases caused by microorganisms as they can selectively act on bacteria and pathogens without affecting human cells and tissues [57, 66, 244, 298]. Considering the different classes of antibiotics, chloramphenicols antibiotics have been commonly employed in veterinary clinics since the 1950s. Chloramphenicol, however, has geno-toxic effects and causes severe side effects such as aplastic anaemia, leukopenia, agranulocytosis and anaemia [69]. Although chloramphenicol has been banned since the 1990s in many countries for use in food-producing animals, it is still widely used due to its low cost and easy availability [62, 69]. The occurrence and fate of chlorinated pollutants in the environment is recognized as an important problem due to the adverse effects on human health through the formation of emerging antibiotic-resistant bacteria and antibiotic-resistant genes [70, 71]. Low removal efficiencies of these organic contaminants have been reported through different biological treatment technologies [44]. Moreover, they are not easily degraded in the metabolite system and thus, they have been frequently detected in surface water, groundwater, and even in drinking water [16, 45]. Several chemical methods have been applied to remove chloramphenicol from water [62, 284, 300, 301]. In addition, physicochemical methods have been applied for the removal of chloramphenicol [21, 333-335]. Generally, adsorption by porous materials such as engineered activated carbon, resin, graphene oxide and carbon nanotubes is an expensive process. For this reason, biochar has received increasing interest due to its low cost [57], high hydrophobicity, aromaticity and multifunctional applications such as reduction of soil acidity, carbon sequestration and water remediation [56, 336-340]. However, biochar properties depend on biomass origin, chemical composition, physical properties, and pre and post-treatment processes [341]. Biochar properties including surface functionality can be further improved through different modification methods [55].

Adsorption of antibiotic onto biochar is expected to be heavily influenced by solution conditions and antibiotic speciation under different pH values [274, 275, 342] [59] [343]. Different species can interact with biochar through different mechanisms such as π-π electron-donor-acceptor (EDA) interaction, nucleophilic addition, electrostatic attraction, cation bridging, cation/anion exchange, pore filling, partitioning into un-carbonized fraction and

formation of the charge assisted hydrogen bond (CAHB) with surface oxygen groups [59, 298]. For example, during charcoal remove of tetracycline and chloramphenicol, Liao et al. (2013)[298] found that π-π EDA interaction, cation-π bond in conjunction with hydrogen bonding interaction were the main mechanisms while surface diffusion was less likely to be involved. However, so far no studies clearly described the sorption behavior of chloramphenicol using carbonaceous materials such as carbon nanotubes, graphene or graphene oxide, and biochar. In addition, research is lacking on the potential regeneration and repeatable application of carbonaceous sorbents. The physicochemical properties of chloramphenicol are shown in **Table 4.3.1.**

Table 4.3.1: Physicochemical properties of chloramphenicol.

Group	Compound	Molecular mass	log K_{ow}	Log p	pK^b_a	Water solubility (mg mL^{-1}) at 25°C
Chloramphenicol	Chloramphenicol	323.09	1.14	1.01	5.50	2.50

https://www.drugbank.ca/drugs/DB00446;
http://www.sigmaaldrich.com/content/dam/sigma-aldrich/docs/Sigma/Product_Information_Sheet/c0378pis.pdf

Therefore this study aimed to use biochar and fBC for removing chloramphenicol. Specifically the objectives were to (i) evaluate the interaction mechanism and performance of biochar and fBC for removing chloramphenicol; [92] study the impact of humic acid, soil and salt concentrations on the sorptive behavior of chloramphenicol; (iii) assess the sorption performance in different water matrices for removing chloramphenicol; and (iv) examine the desorption and repeatable application of fBC with special emphasis on the fingerprinting effects during regeneration from different water.

4.3.2. Materials and Methods

4.3.2.1. Chemicals

The standards of chloramphenicol (purity > 98%), potassium chloride, sodium chloride (> 99.6%), calcium chloride (> 97%), and organic solvents such as methanol, acetonitrile and formic acid of HPLC grade were purchased from Sigma-Aldrich, Australia. Peptone, beef extract, humic acid, tannic acid, sodium lignin sulphonates, Na-laryl sulphate, acacia gum

powder, arabic acid, ammonium sulphate, K_2HPO_4, NH_4HCO_3, and $MgSO_4.3H_2O$ were of analytical-grade. Phenanthrene (98%) and *para* aminobenzoic acid (PABA, > 99%) were also purchased from Sigma-Aldrich. A Zorbax Bonus RP C_{18} column (5.0 µm, 2.1 ×1.50 mm) was purchased from Agilent Technologies. *Eucalyptus globulus* wood was donated by New Forest Asset Management Pty Ltd, Portland, Victoria, Australia. The soil sample was collected from the surface horizon (0-10 cm) at Willy Park, NSW, Australia. The soil was air dried, sieved (< 1.0 mm), and stored at room temperature for further use.

4.3.2.2. Preparation of Biochar and fBC

Biochar and fBC were prepared according to our previous study [244]. Details have been described in **section 4.1.2**.

4.3.2.3. Chloramphenicol Sorption on Biochar and fBC under Different pH and Different Concentrations of Humic Acid, Salt, Soil and Competitors

Interactions of biochar and fBC with chlorinated chloramphenicol in deionized water were studied in batch method at different pH (1.6 to 9) to calculate K_d. Sorption was carried out in PTFE-lined screw cap glass vials with a capacity of 50 to 100 mL. Sorbents were pre-equilibrated at a specific pH followed by adding the required amount of sorbate solution with the same pH. Batch sorption isotherm experiments were conducted at pH ranging from 4.0 to 4.5 at 25 ºC with initial chloramphenicol concentrations of 0.774 to 154.7 µM L^{-1} at room temperature using 50-60 mg L^{-1} of fBC and 100 mg L^{-1} of biochar for 40 h. These conditions made it possible to calculate the maximum sorption at different pH values. The control experiments without sorbents were also executed.

To study the effects of salts, soil and humic acid on K_d, the sorption experiments were conducted by mixing humic acid or soil or salts with chloramphenicol (3.1 µM L^{-1}) overnight, before fBC-2 (being the best sorbent) was introduced. The sorption experiments were performed at pH 4.0-4.5 and 25 ºC. Humic acid stock solution was prepared by dissolving the desired amount of humic acid in NaOH solution and stored for further use. Chloramphenicol sorption was also carried out in the presence of competitors (PABA and phenanthrene). The π-electron donor (phenanthrene) and π-electron acceptor (PABA) were chosen to unravel the possible EDA, electron acceptor-acceptor (EAA) and electron donor-donor [49] interactions mechanisms. The initial concentrations of chloramphenicol, phenanthrene and PABA were 3.1 µM L^{-1}, 1.0 mg L^{-1} and 1.0 mg L^{-1}, respectively at different pH (~1.85, 4.0-4.5 and 9.0-10.5).

Control experiments (no chloramphenicol) were also executed. The supernatant concentration of chloramphenicol and PABA were measured using HPLC with aliquots from each reactor being taken and filtered through a 0.2 μm PTFE filter. Phenanthrene concentration was measured using UV-Vis spectroscopy.

4.3.2.4. Analytical Method and Data Analysis

Chloramphenicol hydrolysis does not occur at pH 2–7 [302]. Its concentrations at different pH (1.7 to 11.0) were measured by HPLC (Jasco) equipped with an auto-sampler and UV detector at 285 nm, by 50 μL injection. A Zorbax Bonus RP C_{18} column was used for the separation. Mobile phase A was composed of acetonitrile and formic acid (v/v, 99.9: 0.1) while mobile phase B was composed of Milli-Q water and formic acid (v/v, 99.9: 0.1). The elution used 40% of A and 60% of B at a flow rate of 0.4 mL min^{-1}, which was changed to 0.3 mL min^{-1} at 0.1 min. The method run time was 7 min. The same method was used for the measurement of PABA concentration with HPLC. Phenanthrene concentration was measured using UV-Vis spectroscopy (Shimadzu, UV-1700) at ~251 nm. In addition, the concentration of Ca^{2+} and Cl^- were measured using a Merck Spectrophotometer (NOVA 60) and relevant test kits.

The adsorption data were fitted to the Langmuir and Freundlich models. The apparent sorption distribution coefficient (K_d, L kg^{-1}) is defined as the ratio of adsorbate sorbed per unit sorbent mass (Q_e, μM g^{-1}) to adsorbate concentration in solution (C_e, μM L^{-1}) at equilibrium, and was calculated using Eq. (1):

$$K_d = 1000\frac{Q_e}{C_e} = \ 1000\left(\frac{C_0 - C_e}{C_e}\right)\frac{V}{M} \qquad (4.3.1)$$

where C_o is the initial adsorbate concentration in water (μM L^{-1}), V is the solution volume (L) and M (g) is the sorbent mass.

The Langmuir and Freundlich isotherm models can be represented as follows:

$$\text{Freundlich model: } Q_e = \ K_F {C_e}^{1/n} \qquad (4.3.2)$$

$$\text{Langmuir model: } Q_e = \frac{Q_{max} K_L C_e}{1 + K_L C_e} \qquad (4.3.3)$$

where Q_{max} is the maximum adsorption capacity (μM g^{-1}), $1/n$ is a dimensionless number related to surface heterogeneity, K_F is the Freundlich capacity-affinity coefficient (μM^{1-n} L^n g^{-1}) and K_L is the Langmuir fitting parameter (L μM^{-1}). Parameters were estimated by nonlinear regression weighted by the dependent variable using above equations and fitting in Origin pro software (version 2016).

4.3.2.5. Characterizations of the Sorbents

Characterization of the prepared materials was carried out using Scanning Electron Microscope with Energy Dispersive Spectrometer (SEM-EDS) (**Table 4.3.2**), Brunauer-Emmett-Teller [127] analyzer, Raman spectroscopy and Fourier transform infrared spectroscopy (FTIR). Raman shifts measurement was done using Renishaw in Via Raman spectrometer (Gloucestershire, UK) equipped with a 17 mW Renishaw Helium-Neon Laser 633 nm and CCD array detector at 50% laser intensity. Structural analysis was conducted using FTIR (Miracle-10: Shimadzu). The spectra were obtained at 4 cm^{-1} resolutions by measuring the Antibioticsorbance from 400 to 4000 cm^{-1} using a combined 40 scans. The specific surface area and the porosity distributions were calculated using BET nitrogen adsorption-desorption isotherms and the Barrett-Joyner-Halenda (BJH) method, respectively by using a Micromeritics 3 FlexTM surface characterization analyzer at 77 K. Zeta potential was measured twice using 1.0 mM KCl solution at different pH for 48 h (Nano-ZS, Malvern). Zeta potential was measured twice for each pH.

Table 4.3.2: EDS analysis data of biochar and fBC.

Sorbent	EDS analysis (atomic percentage in each material)			
	C %	P%	N%	O%
BBC380	81.18±2.9	-		18.83±0.9
fBC-1	58.96±2.5	8.16±1.0	4.96±1.2	28.52±1.2
fBC-2	60.80±1.82	7.96±0.78	5.37±0.82	25.44±1.23

4.3.2.6. Desorption and Regeneration of fBC-2

Desorption experiments were conducted in different water matrices to calculate desorption percentage of chloramphenicol, study on fingerprinting effects and the reusability of the sorbent (fBC-2). After experiments, the supernatant was decanted and replaced with an equal volume of 50% methanol. The fBC-2 and the solution mixture were shaken on an orbital shaker for 24 h at 120 rpm and the suspension was centrifuged for 7 min at 2000 rpm. The supernatant was then filter using 0.2 μm PTFE filter paper and chloramphenicol concentration was measured using HPLC. Desorption was performed after each sorption cycle using fBC-2. The

thermal regeneration and fingerprinting ability of fBC-2 was examined by heating fBC-2 at 300 ºC.

4.3.2.7. Water and Wastewater Samples

Synthetic wastewater was prepared based on a recent study [302] and lake water was collected from Victoria Park, NSW, Australia. All water samples were filtered through 1.2 µm filter paper and stored in a fridge. The characteristics of lake water are given in **Table 4.3.3**. Deionized water, lake water and synthetic wastewater were spiked with 3.10 µM L^{-1} chloramphenicol and contacted with fBC-2 to examine sorption trends in different water. Control experiments were also conducted.

Table 4.3.3: Physicochemical properties of lake water and synthetic wastewater.

Lake water		Synthetic wastewater	
Parameter	Value	Compound	Concentration (mg L^{-1})
pH	7.20	Peptone	2.37
Temperature	19.9 ºC	Beef extract	1.8
TDS	116 mg L^{-1}	Humic acid	4.2
TOC	75.56 mg L^{-1}	Tanninc acid	4.2
Total carbon	76.72 mg L^{-1}	Arabic acid	5.0
		Sodium lignin sulphonate	2.4
		Sodium laryl sulphate	0.94
		Acacia gum powder	4.37
		Ammonium sulphate	7.1
		Potassium phosphate (KH_2PO_4)	7.0
		Magnesium sulphate ($MgSO_4.3H_2O$)	0.71

4.3.3. Results and Discussion

4.3.3.1. Sorbent Surface Properties

Surface properties of biochar and fBC were carried out using BET, EDS, FTIR, Raman and zeta potential measurement. EDS data showed that BBC380 comprised of mainly ~81% C and ~19% O% while fBC-1 comprised of 59% C, 28% O, ~5% N and ~8% P, with O/C molar ratio of 0.363. The fBC-2 was composed of 60.8% C, 25.4% O, ~5% N and ~8% P, with O/C molar ratio of 0.314 (**Table 4.3.2**). BET surface area of fBC-1 and fBC-2 were found to be 1.12 and 1.18 m^2 g^{-1}, respectively. The Langmuir surface area of fBC-1 and fBC-2 was 7.23 and 8.22, respectively. The pore size distribution of fBC-1 and fBC-2 is represented in **Figure. 4.3.1**. FTIR peak of each EDC is shown in **Figure. 4.3.2.** All biochar had alkyl –C-C- groups, aromatic -C=C- group (due to conjugated arene units), ketonic or carboxylic -C=O group and at least one hydroxyl functional group (alkyl or phenolic –OH) in its structure. The peaks around 3300-3850 cm^{-1} represents the presence of hydroxyl groups whereas peaks at 2926-2976 cm^{-1} represent the asymmetric carbon. In addition, two characteristics peaks at 1720 cm^{-1} and 1520-1594 cm^{-1} represent the presence of –C=O and -C=C- groups [55, 302].

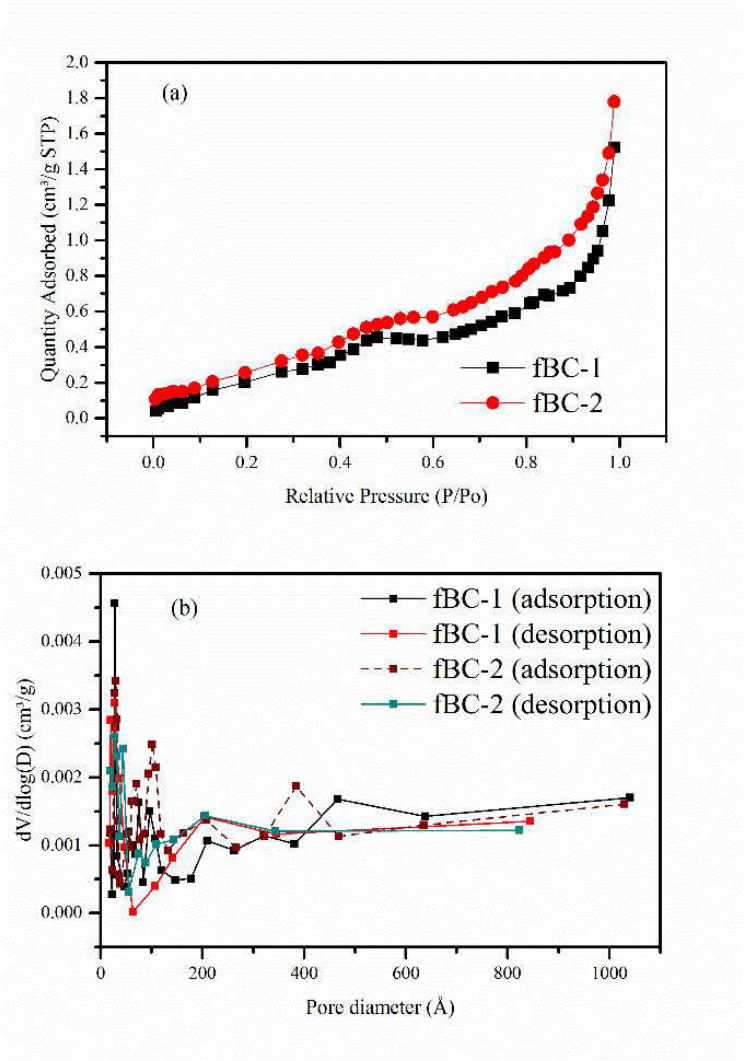

Figure 4.3.1: Nitrogen sorption isotherm for fBC-1 and fBC-2 (a). Barret-Joyner-Halenda (BJH) surface/volume mesopore analysis (adsorption/desorption) with cumulative pore size distribution of fBC-1 and fBC-2 (b).

Raman spectroscopy was also carried out to obtain further data on fBC before and after sorption. fBC showed two characteristic peaks at 1592-1597 and 1325-1345 cm^{-1} (**Figure 4.3.2b**). The two broad peaks located at ~1325-1345 cm^{-1} and ~1592-1597 cm^{-1} corresponded to the D-band (disordered structure) and G-band (graphitic structures) of sp^2-type carbon presence in fBC [344]. The sharp and relative band intensity ratio (I_G/I_D) showed the degree of functionalization in biochar. It is important to note that Raman spectra of fBC featured a strong D-band, which illustrated a slightly more amorphous character (disordered) of the carbon in fBC [344]. D-band surface defect was possible by the introduction of other elements onto carbon structure during fBC preparation.

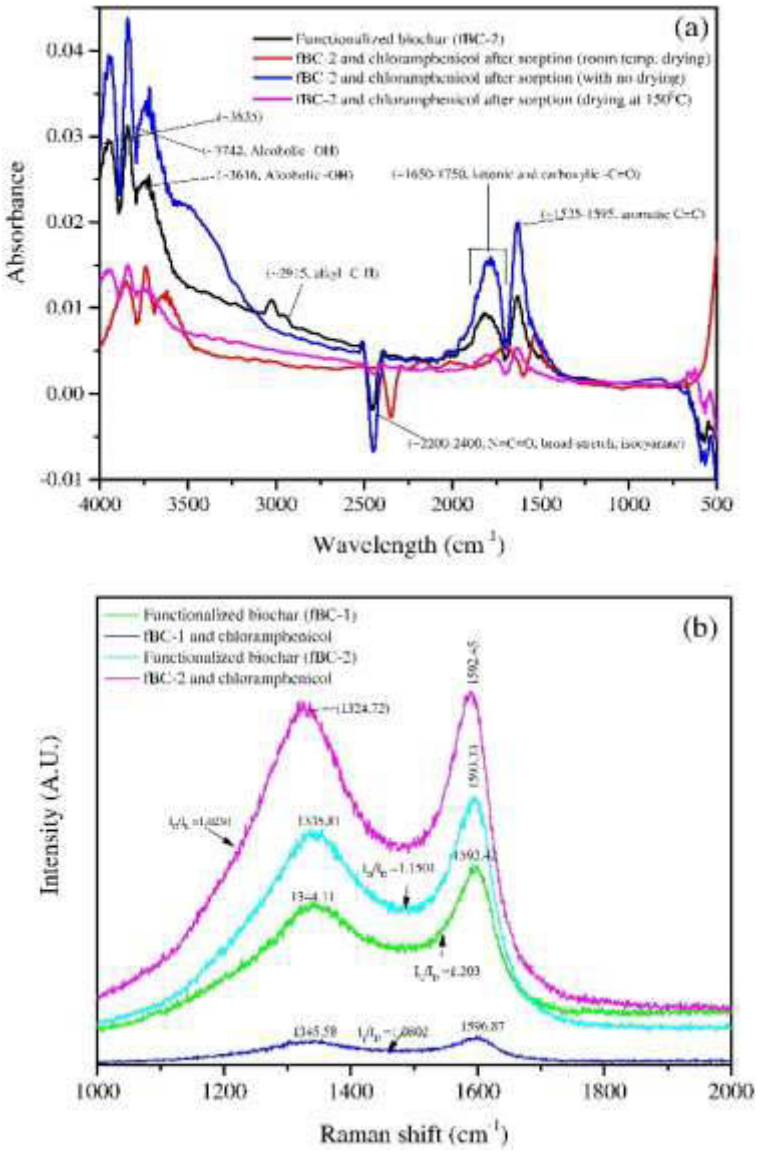

Figure 4.3.2: (a) FTIR spectra of biochar and fBC, (b) Raman spectra of fBCs (with band intensity ratio, I_G/I_D) before and after chloramphenicol sorption**.**

4.3.3.2. Chloramphenicol K_d on Biochar and fBC

Chloramphenicol sorption on biochar, fBC-1 and fBC-2 revealed pH dependence. The effect of pH on the sorption coefficient is shown in **Figure 4.3.3**. Clearly, chloramphenicol sorption was greatly governed by the electrostatic interactions between chloramphenicol and fBC surfaces. The maximum K_d value for biochar (BBC380) was found to be ~500 L kg^{-1} at pH around 4.5. Similar result was obtained for EGBC380 (data not shown). However, higher K_d values were observed for both fBC-1 and fBC-2 than biochar at all pH values studied. The finding indicated that functionalization of biochar significantly changed the biochar properties and increased its sorption capacity. The K_d values for both fBC reached their first maxima at pH ~1.6 and the maximum at approximately pH 4.5. A further increase in pH resulted in decreasing K_d values. Detailed mechanism in relation to pH values is discussed in section **4.3.3.4**. Based on the results, the maximum K_d values were found to be ~1.8×10^4 L kg^{-1} for fBC-2 and ~1.2×10^4 L kg^{-1} for fBC-1 at pH ~4.0-4.5 with initial chloramphenicol concentration of 15.5 µM L^{-1}. As fBC-2 showed a higher K_d value than fBC-1 for chloramphenicol, it was used in further sorption experiments.

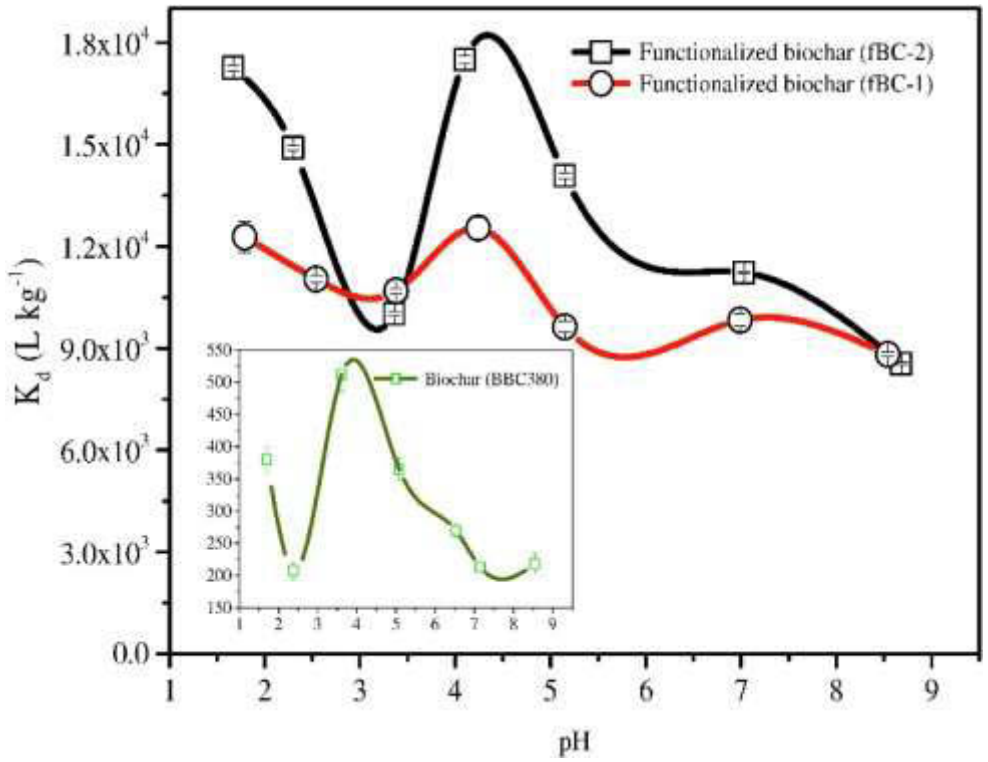

Figure 4.3.3: Effect of pH on the equilibrium K_d of chloramphenicol on biochar, fBC-1 and fBC-2 at 25 °C, using initial chloramphenicol concentration of 15.5 µM L^{-1}, 50–60 mg L^{-1} fBCs or 100 mg L^{-1} biochar. Error bars indicate the standard deviation.

4.3.3.3. Effects of Humic Acid, Salt and Soil Concentration on K_d

The effect of humic acid on K_d was studied using different concentrations of humic acid (1.0 to 40.0 mg L^{-1}). It emerged that the increase of humic acid concentration from 1.0 mg L^{-1} to 10 mg L^{-1} reduced K_d value slightly from ~2.0×10^4 to ~1.7×10^4 L kg^{-1} (**Figure 4.3.4a**). A further increase in humic acid concentration caused a significant reduction in the K_d of chloramphenicol which fell sharply to ~6.1×10^3 L kg^{-1} when humic acid concentration was raised to 40 mg L^{-1} (**Figure 4.3.4a**). In comparison, the K_d value in deionised water, in the presence of humic acid, under the same initial conditions was ~6.9×10^4 L kg^{-1} (SD, 3.7×10^3). This indicated that humic acid yielded a negative influence on the sorptive removal of chloramphenicol which can be explained by the direct competition of humic acid and fBC sorption sites for the sorption of chloramphenicol [345, 346]. Pignatello et al. (2006)[345] found that natural organic substances (e.g. humic substances) appear partially block biochar pore network and may suppress adsorption by a competitive effect at the external surface at normal temperature. The strongest suppression occurs for large molecules with reduced access to interior pores, especially when the biochar has been co-flocculated with the humic substance. Moreover, Zhou et al. (2015) [347] confirmed that pore blockage (confirmed by BET surface area measurement) as well as the more hydrophilic surface with more sorbed water molecules mainly suppressed the sorption of atrazine by biochar. In addition, hydrophobic effects and electron donor acceptor (EDA) might also be responsible for lower chloramphenicol sorption in the presence of humic acid. Hence, the presence of humic acid decreased sorption of chloramphenicol which was significant when the humic acid concentration was more than 20 mg L^{-1}.

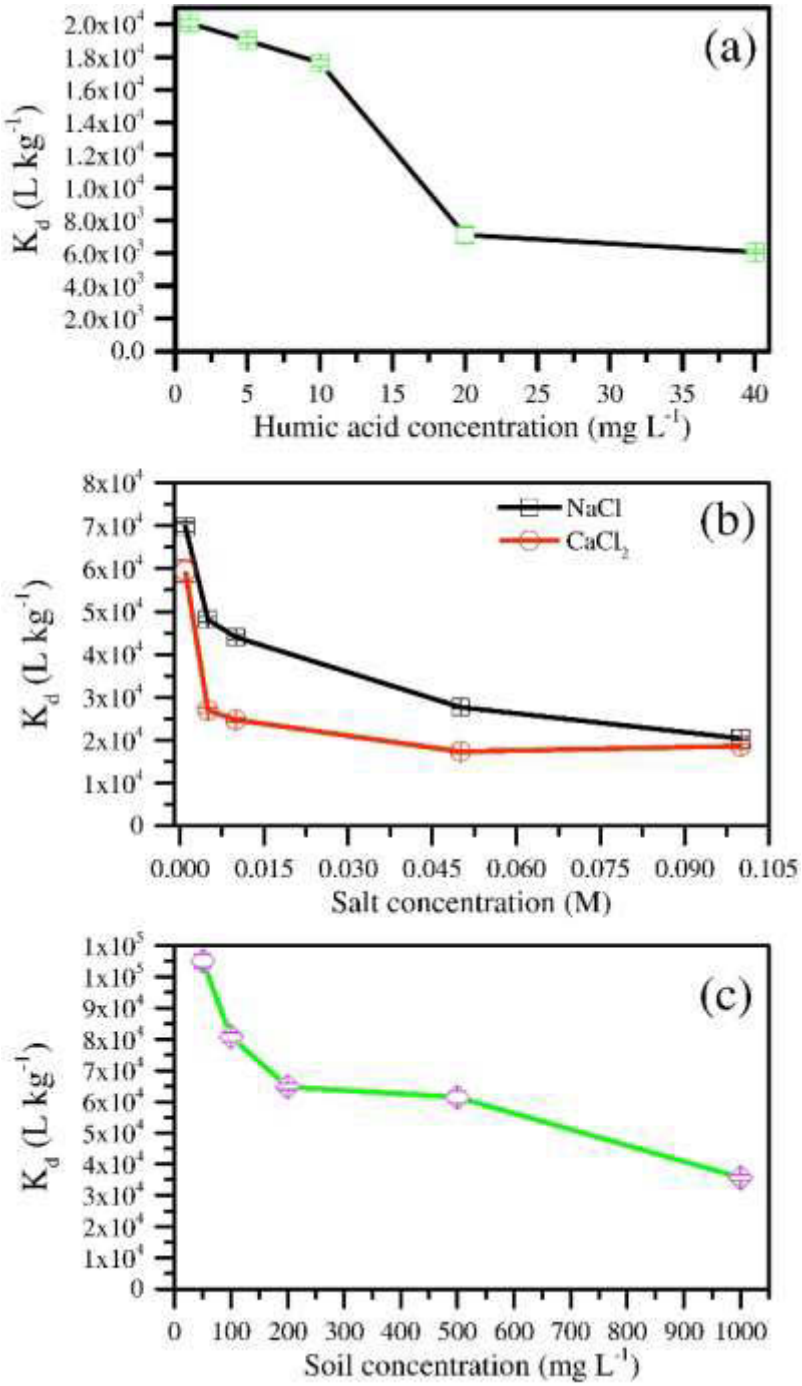

Figure 4.3.4: Effects of **(a)** humic acid concentration, **(b)** salt concentration, and **(c)** soil concentration on the equilibrium K_d of chloramphenicol at 25 °C, using 50–60 mg L^{-1} fBC-2 at pH 4.0–4.5.

The presence of lower ionic strength increased K_d slightly (**Figure 4.3.4b**). For example, in the presence of 0.001 M NaCl, K_d was found to be ~7.0×10^4 L kg^{-1} (initial chloramphenicol concentration was 3.1 μM L^{-1}), whereas it was ~6.9×10^4 L kg^{-1} in the presence of salt with the same initial chloramphenicol concentration. This effect can be

explained by the ionic mobility. Lower ionic strength increased the ionic mobility of a solution hence the ionic mobility of the fBC was increased and contributed to the overall increase in sorption [348]. However, a further increase in ionic strength (i.e. up to 0.01 M NaCl) slightly decreased the sorption distribution efficient. Further increase of NaCl concentration (0.10 M) did not have significant effect on the sorption of chloramphenicol, and the K_d was almost same. This can be explained by the saturation of biochar surface in the presence of a higher concentration of NaCl. On the other hand, in the presence of low calcium chloride concentration (0.001 M), the K_d values was almost the same as that without $CaCl_2$. Hoverer, a further increase in $CaCl_2$ concentration (up to 0.01 M) reduced the K_d values linearly, indicating that sorption of chloramphenicol in the presence of excess $CaCl_2$ salt had much higher negative influence than that of NaCl (**Figure 4.3.4b**). Control experiments with only Ca^{2+} showed that Ca^{2+} was sorbed by fBC-2 (initial Ca^{2+} concentration = 155 mg L^{-1}, final concentration = 146.5 mg L^{-1}) at pH ~4.45. Thus, it can be stated that biochar surface was highly saturated by the salt of divalent calcium ion as this ion which contributes to water hardness like magnesium.

Furthermore, K_d value was found to be significantly higher in the presence of soil, e.g. 1.06×10^5 L kg^{-1} in the presence of 5.0 mg L^{-1} of soil (50-60 mg L^{-1} of fBC-2 dosage). While in the absence of soil, chloramphenicol sorption K_d value was ~6.9×10^4 L kg^{-1} (SD 3.7×10^3). It is usual that biochar adsorbs organic contaminants significantly more than soil, and the addition of biochar to soil significantly increases sorption capacity which also depends on the type of soil [323, 349]. Soil solids consist of different minerals (e.g. quartz, calcite, montmorillonite, iron oxide) and organic matter (e.g. biopolymers, microbial and root exudates, plant litter in varying stages of degradation). Pure clay minerals and metal oxides have highly reactive surfaces, in most soils, coating/modifying of soil surfaces by organic matter profoundly modifies their sorptive character. As a result, soil organic matter fraction governs the sorption of virtually all organic molecules in soil [323]. Thus, the increase in K_d values might be due to soil organic matter and different minerals which make contribution to the overall sorption of chloramphenicol onto fBC-2. From literature it is found that, soil organic matter (π-electron acceptor site) can interact with an aromatic organic compound (with π-donor site) through π-electron donor acceptor interactions [350] which might happen in this case. Yet, the increase in soil concentration (up to 1.0 g L^{-1}) with the same dosage of fBC-2 reduced K_d values, indicating that fBC-2 dominated the overall sorption compared to soil. An increase in the amount of soil led to a decline in K_d values which may be due to partial deposition of soil particles onto biochar active surface that might block or hinder the pores of the fBC-2 as well as due to release of more organic matter including minerals in the solution (**Figure 4.3.4c**).

This aligns with the finding of different ionic strength solution discussed earlier in this section. However, chloramphenicol adsorption was still significant which was mainly due to the sorption by fBC-2 with partial contribution from soil minerals and organic fractions.

4.3.3.4. Affinity and Mechanism of Chloramphenicol Sorption by fBC

The sorption data was better fitted to the Langmuir isotherm model than the Freundlich model (**Figure 4.3.5a**). The maximum Langmuir adsorption capacities (Q_{max}) were found to be 26.2, 200.5 and 233 μM g^{-1} for biochar, fBC-1 and fBC-2, respectively. Conversely, the maximum Freundlich constant (K_F) values were 1.6, 39 and 56 $\mu M^{1-n} L^n g^{-1}$ for biochar, fBC-1 and fBC-2, respectively (**Table 4.3.3**). The higher adsorption by fBC-2 was attributed to change in the specific surface area, micropore volume, and the introduction of additional sites onto fBC through different interactions [57, 244]. Further, K_d values varied between 1.0×10^2 and 1.6×10^3; 1.35×10^3 and 8.0×10^4; and 1.6×10^3 and 1.2×10^5 L kg^{-1} for biochar, fBC-1 and fBC-2, respectively (**Figure 4.3.5b**). The isotherm showed little sign of becoming linear at lower end of the experimental concentration range for BBC380 ($1/n$ = 0.50) than that of fBC-1 ($1/n$ = 0.34) and fBC-2 ($1/n$ = 0.30), upon regressing data from 0.774 to 154.74 μM L^{-1} of chloramphenicol (**Figure 4.3.5a**). The observed values of K_d, Q_{max} and K_F for chloramphenicol were higher than reported values [298]. For example, biochar prepared at 400-700 °C from bamboo [298] had a Langmuir sorption capacity of 25.11 μM g^{-1}. The detailed sorption mechanisms at different pH are described in more detail below.

Table 4.3.4: The Freundlich and Langmuir isotherm parameters for the sorption of chloramphenicol by biochar and functionalized biochar.

Biochar	Langmuir isotherm parameter			Freundlich isotherm parameter			
	Q_{max}	K_L	r^2	K_F	n	$1/n$	r^2
BBC380	26.15±3.28	0.02±0.0059	0.970	1.62±0.59	1.99±0.32	0.502	0.932
fBC-1	200.5±10.1	0.083±.0.016	0.990	38.91±6.74	2.98±0.37	0.340	0.958
fBC-2	233±12.3	0.12±0.027	0.983	55.97±12.12	3.36±0.59	0.300	0.915

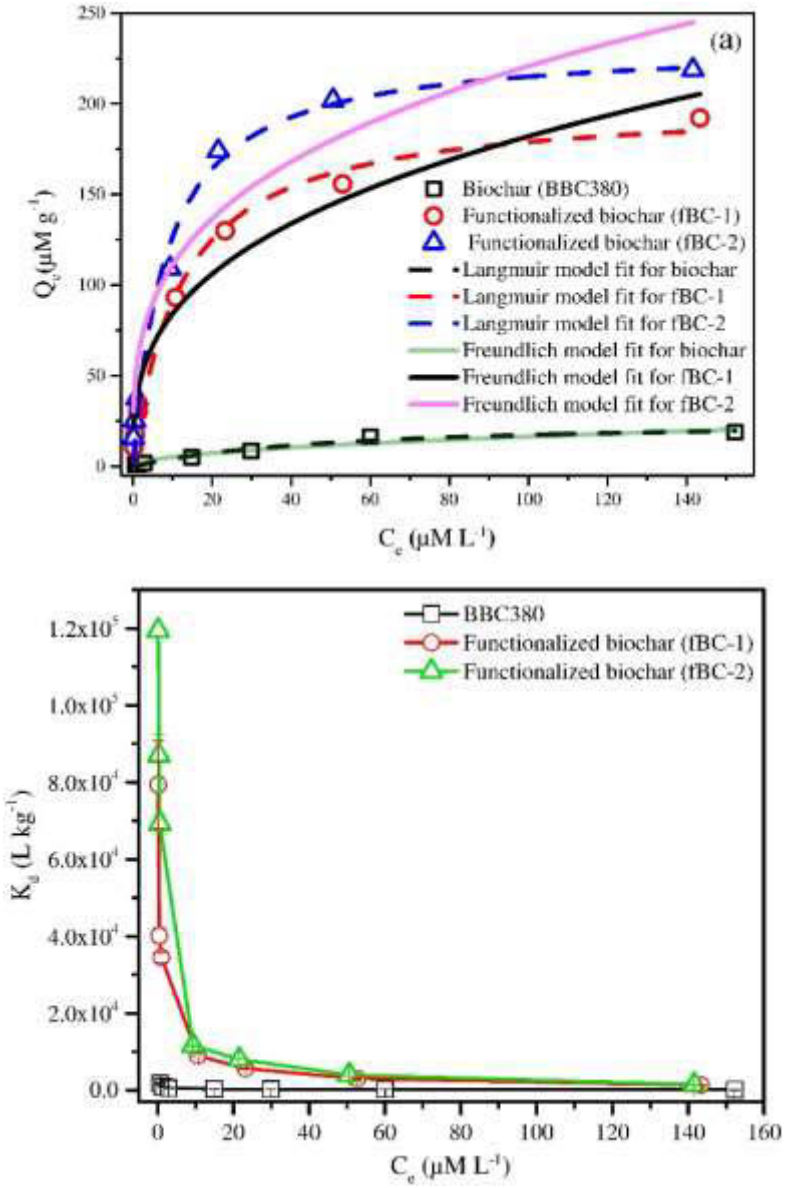

Figure 4.3.5: (a) Sorption isotherm plots and model fitting with initial chloramphenicol concentrations of 0.774–154.7 μM L^{-1} at pH 4.25, 25 °C using 50–60 mg L^{-1} fBC or 100 mg L^{-1} biochar over 40 h. **(b)** Change of K_d values (with SD as error bars) against equilibrium concentrations from isotherm studies.

At pH Below 2.0

At low pH, higher K_d values were obtained (**Figure 4.3.3**). At very low pH, proton exchange from surface functional groups (-OH and –COOH) of the biochar is not possible due to the higher *pKa* values of the surface hydroxyl group (7-10) and surface –COOH group (4.0-5.0) [351]. Thus, if solution pH could be maintained near the pK_a value, then proton exchange might contribute to the sorption process. This suggests that proton exchange is not favourable at low pH and subsequently, maximum sorption of chloramphenicol may be mostly due to EDA interactions with π-electron rich biochar and chloramphenicol surface [59, 352]. It is assumed

that stronger EDA interactions between oppositely polarized quadrupoles might be possible when the π-electron depletes aromatic rings (or regions) and π-electron rich regions (or aromatic rings) interact each other. fBC was enriched with C=C, –OH, C=O and –COOH groups (**Figure 4.3.2**) and surface zeta potential was +2.20 to +2.50 (point of zero charge) (**Table 4.3.5**). The surface functional groups of fBC may act as a strong π-electron-donor due to (i) hydroxyl groups being situated in the benzene rings (participating in resonance as a π-electron donor), and [92] strong π-electron-acceptors due to carboxyl functional groups/ ketonic functional groups on the benzene rings [244, 353-356]. Thus, when the π-electron-acceptor is positively charged and this charge lies within or resonates with an arene unit of chloramphenicol then a stabilized overall interaction is designed as π-π EDA. Resonance forms of positive species of chloramphenicol are able to form π^{+}-electron (acceptor site) and sorption affinities are mostly governed by the mechanism of π-π EDA (Case I, **Figure 4.3.6**) [244]. In addition, electron acceptor-acceptor (EAA) interactions (Case II, 1st part) may also be possible but not critical.

Table 4.3.5: Zeta potential values of fBC-1 and fBC-2.

fBC-1						
Initial pH	1.62	3.00	4.35	6.13	10.00	
Zeta potential (mV)	5.34±0.32	-3.25±0.24	-12.76±1.23	-19.6±1.15	-45.9±4.67	
fBC-2						
Initial pH	1.65	2.86	4.16	6.35	8.35	10.73
Zeta potential (mV)	4.43±0.895	-6.74±0.00	-16.4±2.47	-10.3±0.495	-27.4±7.57	-39.0±2.70

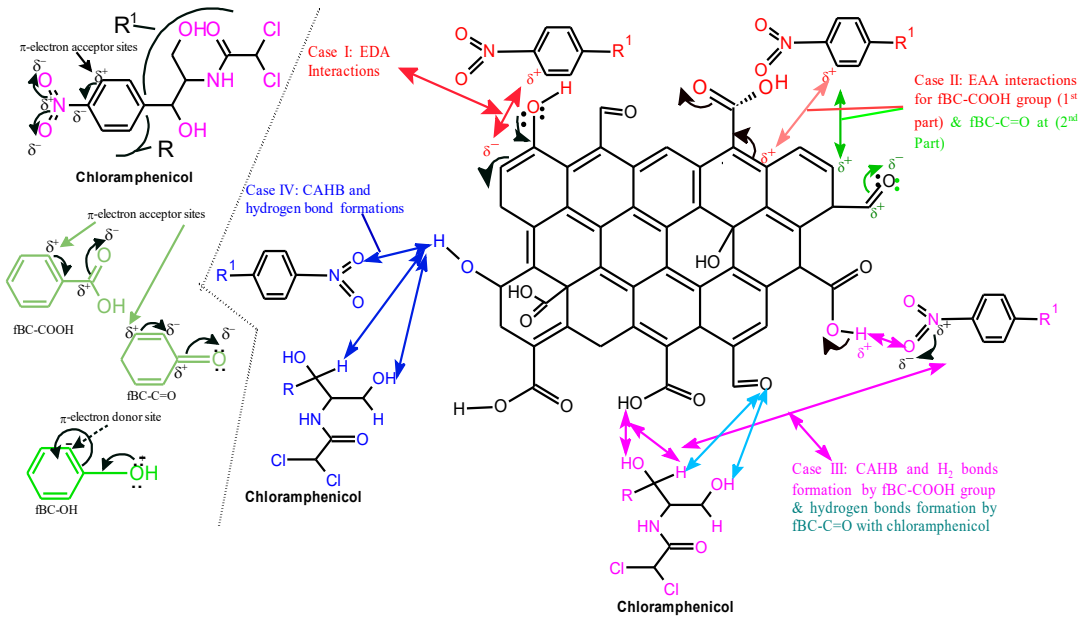

Figure 4.3.6: Proposed sorption mechanism for the removal of chloramphenicol from different water using fBC.

To test the π-π EDA hypothesis, the competitive effects of two compounds having similar affinity for the surface but opposite quadrapolarity were compared: phenanthrene, a π-electron donor by virtue of its π rich electrons (polarizable ring system) and PABA, a strong π-electron acceptor by virtue of the withdrawing capability of the acid groups. The results are presented in **Figures 4.3.7a and 4.3.8**. It can be predicted that their competitor's strengths against chloramphenicol sorption would be similar if the competitive effect was due merely to nonspecific forces, whereas PABA would be a much stronger competitor than phenanthrene if the π-electron acceptor property of chloramphenicol as well as π-electron donor property of fBC arene units were critical. **Figures 4.3.7a and 4.3.8** clearly show that PABA strongly interacted with fBC-2 (i.e. with graphene-like arene unit as π-electron donor site), suppressing chloramphenicol (acted as π-electron acceptor) adsorption significantly than phenanthrene (acted as π-electron donor). Thus. PABA is, by far, the stronger competitor than phenanthrene for chloramphenicol sorption (**Figure 4.3.7a**). This kind of interactions can be written simply as π- π EDA interactions, where EDD interactions were not as strong as EDA interaction. As the sorption of chloramphenicol was increased by ~10% (excluding SD) in the presence of phenanthrene indicating the insignificant role of EDD interactions. Similar explanation can be drawn in the absence of chloramphenicol where adsorption of PABA was higher than that in the presence of chloramphenicol (**Figure 4.3.8**). Moreover, cation exchange capacity of fBC-

2 (Ca^{2+}) in this pH range was excluded as Ca^{2+} ion adsorption capacity was found to be insignificant (data not included). We also observed, anion competitor such as PO_4^{3-} can reduce chloramphenicol sorption capacity by ~8 % at this pH range and thus anion exchange capacity of fBC-2 might be important under this condition.

Besides, the maximum K_d values can also be partially attributed to the degradation nature of chloramphenicol in excess hydrogen ions in a solution based on reaction **(4.3.4)** [357]. This increase is most logically owing to the basic character of the amide linkage (-NH-CO-), resulting in the formation of a protonated intermediate due to Lewis acid-base interaction (Eq. 4):

$$-NH-CO-\overset{H^+}{\Longleftrightarrow}-[NH=C(OH)]^+-\overset{H^+}{\Leftrightarrow}-NH(H^+)-C(OH^+)- \qquad (4.3.4)$$

Thus, this acid-degraded positive complex of chloramphenicol and positive surface of fBC (zeta potential was positive) might repel each other and sorption of this degraded product was not favorable. At low pH, different chloramphenicol K_d values were obtained for biochar, fBC-1 and fBC-2, indicating that the degradation of chloramphenicol was not pronounced but comparable (**Figure 4.3.3**). It can be concluded that sorption of chloramphenicol was mostly favoured by EDA interactions at low pH.

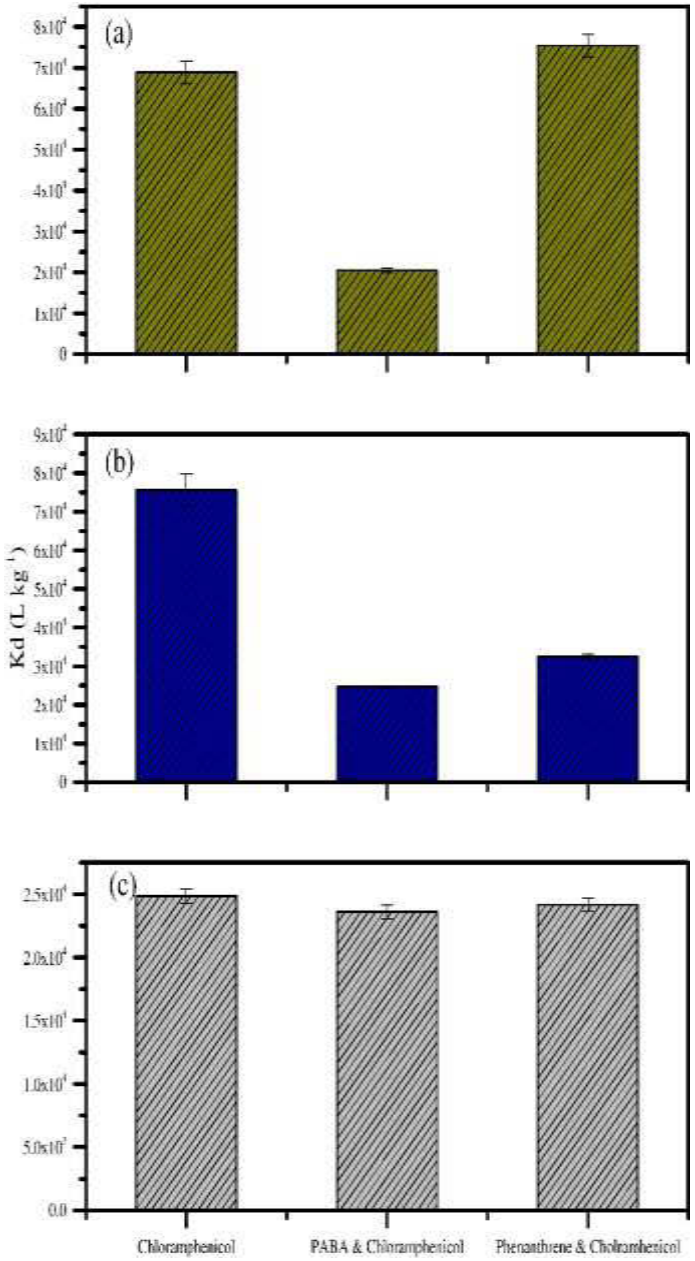

Figure 4.3.7: Effects of competitors phenanthrene and PABA on the adsorption of chloramphenicol at pH 1.82–1.85 (a), pH 4.20–4.56 (b), and pH 9.15–9.60 (c) in deionized water. Phenanthrene and PABA concentrations at 1.0 mg L^{-1}, chloramphenicol concentration at ~ 3.10 μM L^{-1}, fBC-2 dosage at 40–50 mg L^{-1}. Error bars represent the standard deviation.

At pH 4.0-4.5

Chloramphenicol has three hydrogen bond donors and five hydrogen bond acceptor groups in its structure. Aqueous solution of chloramphenicol is neutral and hydrolysis does not occur rapidly at room temperature in the pH 2 to 7 range [357]. We have carried out separate experiments for the dissociation of chloramphenicol at pH range from 1.5 to 10.0 and found that chloramphenicol concentration was almost same in all pH except only ~10% reduction at

pH ~4.5. And this was might be due to the *pKa* value of chloramphenicol. At pH 4.5, maximum K_d value is mostly due to electrostatic interactions. Proton exchange with water molecules is unfavorable (Eq. 5) by leaving the -OH group in solution, so the solution pH should increase [59, 244]. However, in our experiments, the pH shifted towards the acidic region following adsorption. The proton transfer free energy was calculated using $\Delta G^0_{H^+{}_{exch}1} = -RT\ ln(K_{a1}/K_{aw})$ and found to be +45.5 kJ mol^{-1}, where K_{aw} is the water dissociation constant for chloramphenicol. Furthermore, proton transfer is likely to be unfavorable by at least 15 kJ mol^{-1} at 293 K and pH 5 [59, 351]. Thus, the decrease in equilibrium solution pH was due to release of proton from fBC-2 surface carboxylic groups (pK_a *v*alue ~4.0-5.0) as well as from chloramphenicol functional groups (pK_a *v*alue ~5.50) although deprotonation of water molecule release –OH in the solution which might be neutralized by protons release from fBC-2 and chloramphenicol and the total interactions can be written as (Chloramphenicol O$^-$ ……H$^+$….$^-$OOC-fBC-2). Thus, overall the stabilization of the sorption complex can be obtained by releasing protons from surface functional groups and forming a strong CAHB. Hydrogen bonds among surface carboxylic groups, hydroxyl groups and quaternary nitrogen functional groups of fBC-2 and hydroxyl groups, nitro groups of chloramphenicol also play a major role in the maximum sorption at this pH (case III, reaction 4.3.6).

$$\text{Chloramphenicol} + H_2O + \text{fBC} = \text{Chloramphenicol}^+ \ldots\text{fBC} + OH^- \quad (4.3.5)$$

$$\text{Chloramphenicol} + \text{fBC} = \text{Chloramphenicol}^+ \ldots\text{fBC}^- \quad (4.3.6)$$

EAA interaction for –COOH group may not occur within this pH range as –COOH takes part in CAHB formation. Additionally, CAHB formation with the surface hydroxyl group of biochar was not possible due to higher pKa value. It is noted that maximum sorption of any organic species is observed near a pH where pK_a lies within narrow limits. To test the π-π EDA, EAA and EDD hypothesis, we also performed competitive effect on chloramphenicol sorption. The results are presented in **Figures 4.3.7b and 4.3.8**. It is noticeable that, fBC-2 surface functional groups such as –COOH (due to matched pK_a value of surface –COOH groups) and C=O can act as π-electron acceptor sites whereas arene unit can act as π-electron donor site (**Figure 4.3.6**). Thus, in this case, both interactions are preferable at this pH range if solutions are provided with both acceptor and donor competitors. **Figure 4.3.7b** clearly shows that PABA and phenanthrene strongly interacted with fBC-2 by suppressing chloramphenicol adsorption significantly. However, PABA was found to have comparative highly competitors than phenanthrene. This kind of interactions can be written simply as π- π EDA interactions due to following reasons: PABA as acceptor and fBC-2 arene unit as donor; phenanthrene as

donor and fBC-2 surface carboxylic groups and C=O groups as acceptor; π- π EAA interactions due to PABA as acceptor and fBC-2 surface carboxylic groups and C=O as acceptor; and finally, π-π EDD interactions due to phenanthrene as donor and fBC-2 arene unit as donor. However, EDA interactions was the main reason with hydrogen bonds formations which can be confirmed from **Figure 4.3.8**, which shows the strong adsorption of PABA and phenanthrene with fBC-2 due to EDA interactions that clearly support the previous explanations. Moreover, electrostatic attraction with opposite charged quadrupoles (fBC-2 as negative and Ca^{2+} as positive) were also observed as sorption of chloramphenicol reduce nearly ~18% in presence of 0.005 M L^{-1} $CaCl_2$ in the solution while presence of anion ($PO4^{3-}$) in solution did not bring any significance chloramphenicol sorption reduction.

Moreover, based on Raman spectra, it was found that the D to G band peak intensity ratio (I_D/I_G) significantly decreased after sorption (**Figure 4.3.2b**). This clearly indicated strong interaction among surface functional groups and chloramphenicol molecules. FTIR peak shifted to a point where C=O (~1720 cm^{-1}) or –COOH functional groups (~1028 cm^{-1}) as well as –OH groups (3400-3800 cm^{-1}) were located due to sorption of chloramphenicol onto functionalized biochar surfaces (**Figure 4.3.2a**). Thus, maximum sorption of chloramphenicol in this pH range was due to the formation of CAHB and weak hydrogen bonds along with mainly EDA interactions in fBC.

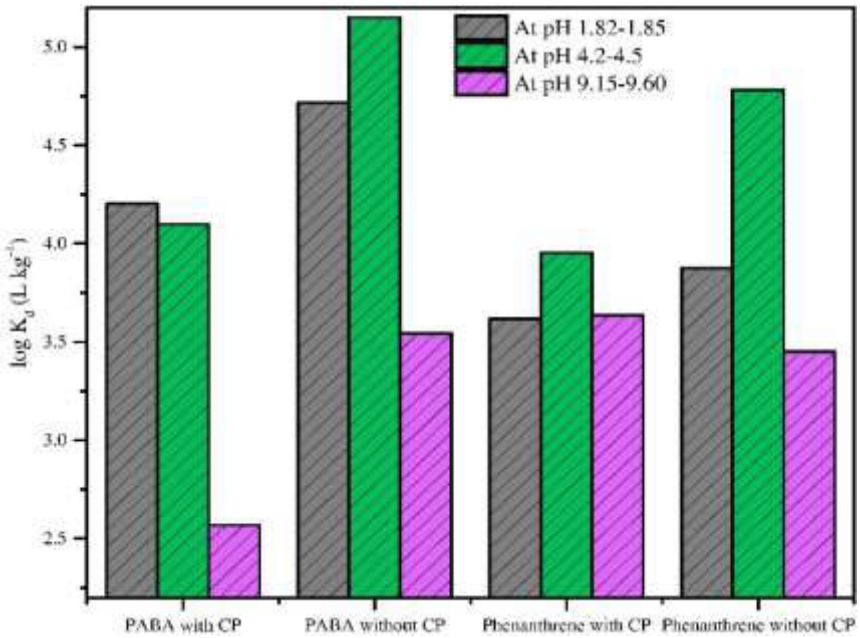

Figure 4.3.8: Sorption of PABA and phenanthrene in the presence or absence of chloramphenicol [65] in deionized water at different pH values. Solution compositions: phenanthrene and PABA concentrations at 1.0 mg L^{-1}, CP concentration at ~ 3.10 μM L^{-1}, fBC-2 dosage at 40–50 mg L^{-1}. Error bars represent the standard deviation.

At pH Above 7.0

At pH above 7.0, K_d values decreased when the pH of the solution was increased. However, the negatively charged biochar surface (zeta potential was highly negative) could still sorb chloramphenicol. This was mainly due to the formations of CAHB and weak hydrogen bonds among surface hydroxyl groups of biochar, aromatic nitro group and hydroxyl groups in chloramphenicol. The pK_a value of the surface hydroxyl group in carbon-based sorbents lay within 7-10. The only possible way was to form CAHB (Case IV, **Figure 4.3.6**). EDA was not favorable at this pH since the hydroxyl group was deprotonated. In addition, EAA could be possible due to unchanged –COOH groups on the biochar surface (Case II, 1st part). To elucidate the EDA, EAA and EDD interaction mechanisms, competitors were introduced into solution at this pH range, and results (**Figures 4.3.7c and 4.3.8**) clearly showed that PABA and phenanthrene had an insignificant effect on the overall sorption of chloramphenicol. Hence, EDA, EAA and EDD interactions would have insignificant influence at this pH due to the fact that both surface hydroxyl groups of fBC-2 and phenanthrene acted as π-electron donor. Thus, their repulsive force was stronger than attractive forces. On the other hand, fBC-2 arene unit might function as π-electron donor site whereas chloramphenicol and PABA act as π-electron acceptor sites hence sorption of chloramphenicol remains stable (**Figure 4.3.7c**). Interestingly, PABA sorption was significant in the presence of chloramphenicol. Hence, EDA might play a role in the overall sorption rather than EAA and EDD interactions. Moreover, the presence of anion (PO_4^{3-}) in solution did not bring any significant increase in chloramphenicol sorption compared to without competitors. However, the presence of Ca^{2+} in solution caused a reduction in the sorption of chloramphenicol to some extent indicating the role of electrostatic attraction to oppositely charged ions (data not presented).

Based on the results of FTIR, chloramphenicol interacted with surface –OH which led to the increase of absorbance indicating the formations of hydrogen bonds. Moreover, the Raman spectra intensity band ratio (I_D/I_G) also decreased suggesting that the –OH group played a major role in the sorption of chloramphenicol. As well, at high pH, chloramphenicol might also produce chloride ions in solution through hydrolysis (**Eq. 4.3.7**) [358].

$$-NH-CO-CHCl_2 \overset{-OH}{\Longleftrightarrow} -NH-CO-CH(OH)_2 \qquad (4.2.7)$$

Thus, chloramphenicol sorption at this pH range mainly occurred through hydrogen bond formation with little contribution from EDA interactions.

4.3.3.5. Application in Different Water at Environmentally Relevant Concentrations

The fBC-2 was applied to remove chloramphenicol (3.10 μM L^{-1}) from different water types. Pronounced differences in the removal efficiencies were observed for different water types in the sorption of chloramphenicol (**Figure 4.3.9a**). However, synthetic wastewater had a highly negative influence on the overall removal of chloramphenicol by fBC-2 followed by lake and deionized water. This might be due to the presence of different species (inorganic and organic) that were unfavorable for the comparative faster sorption of chloramphenicol from synthetic wastewater. For example, the presence of humic substances (discussed earlier) had negative influence on chloramphenicol sorption. Synthetic wastewater used in this study contained different organic materials (such as peptone, beef extract, humic acid, tannic acid, arabic acid, sodium lignin sulphonate, acacia gum powder) and inorganic (KH_2PO_4 and $MgSO_4.3H_2O$) species. Thus, it was assumed that similar kinds of interactions with humic acid could happen in the case of synthetic wastewater. In addition to this, we have separately carried out chloramphenicol sorption experiments in the presence of sodium lignin sulphonate and acacia gum powder using the same synthetic wastewater composition and same conditions, and observed that the presence of these substances significantly hindered the sorption of chloramphenicol by ~50%. In comparison with deionized water, the removal of same amount of chloramphenicol from synthetic wastewater required a higher dosage of fBC-2 and also longer contact time (**Figure 4.3.9a**). Control experiments in the absence fBC with different water matrices showed that there was no loss of chloramphenicol. On the other hand, fBC-2 needed less contact time and at a low dosage for the complete removal of chloramphenicol from lake water than synthetic wastewater. This indicated that lake water may contain fewer competitive ions or species than synthetic wastewater. In the case of deionized water, the removal of chloramphenicol was most effective which needed the least dosage of biochar. This is because deionized water does not contain any competitive species whether organic or inorganic. Hence the sorption of chloramphenicol was high and lower dosage of biochar was required. The trend for removing environmentally relevant concentrations of chloramphenicol followed the order: deionized water > lake surface water > synthetic wastewater. However, the removal of chloramphenicol from different water matrices can be improved by using higher concentration of biochar and by employing longer contact time (~48-60 h). Hence, fBC-2 can be successfully applied for the removal of environmentally relevant concentrations of chloramphenicol from water and wastewater.

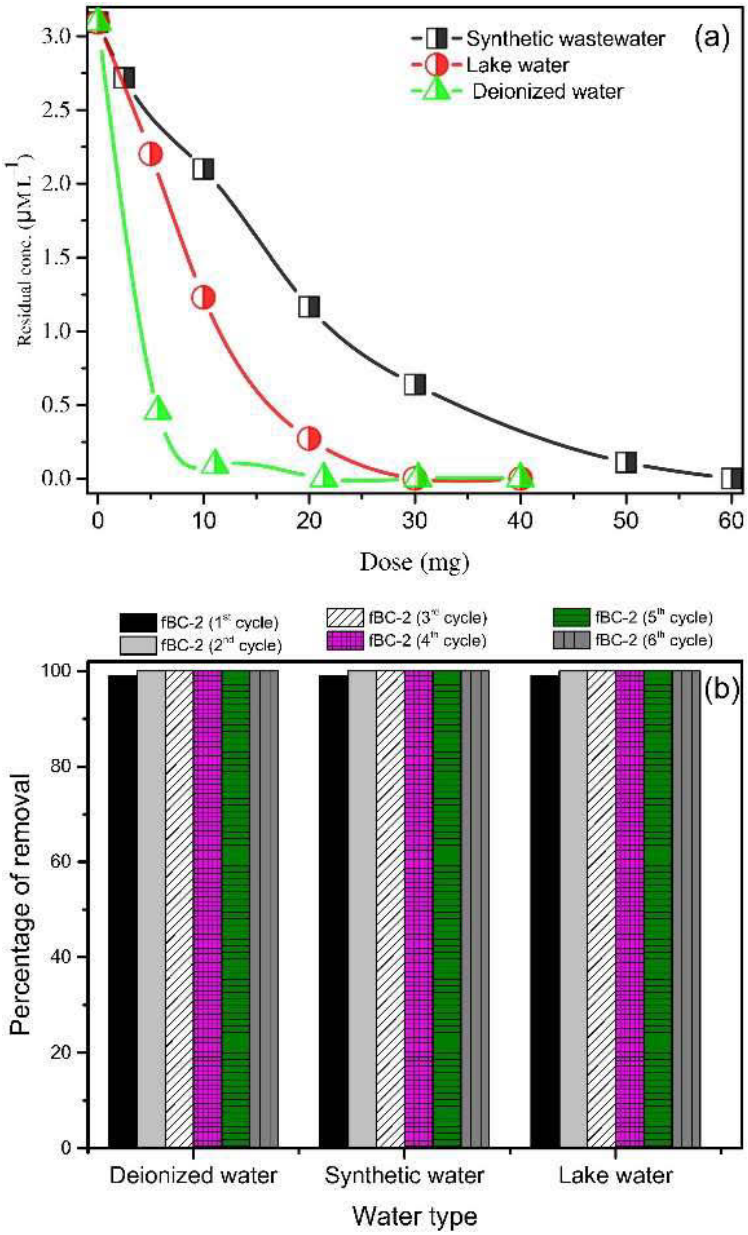

Figure 4.3.9: (a) Sorption of chloramphenicol (initial concentration 3.10 μM L^{-1}) from deionized water, lake water and synthetic wastewater at different dosages of fBC-2 against residual concentrations at pH 4.0–4.5, 25 °C (contact time was 18 h). **(b)** Reusability of fBC-2 (on percentage basis) for the removal of chloramphenicol under the same condition from different water samples.

4.3.3.6. Molecular Imprinting Effect, Regeneration and Reusability of fBC-2

Chloramphenicol that was sorbed onto fBC-2 surface was desorbed using methanol as a solvent to regenerate fBC-2. The percentage of chloramphenicol desorption by methanol (two cycles on average) from fBC-2 was found to be ~ 91%, ~ 86% and ~ 89.2% for deionised water, synthetic wastewater and lake water, respectively (**Figure 4.3.10**). The results indicated that fBC-2 had specific sites or specific functional groups on its surface that interacted with

chloramphenicol repeatedly, which clearly indicated a kind of "molecular imprinting effect" [359]. The successful cycles of application and desorption of chloramphenicol using fBC-2 showed almost the same results as those of virgin fBC-2.

This molecular imprinting effect can be confirmed by the thermal regeneration studies of fBC-2. For this reason, fBC-2 was thermally regenerated and tested under the same conditions as freshly prepared fBC-2. Regeneration ability was repeated for six cycles, and it emerged that fBC-2 can maintain excellent reusability with undiminished removal efficiencies (almost 100% under same contact time and same dosages) up to the 6^{th} cycle of application (**Figure 4.3.9b**). It is evident that due to thermal regeneration, chloramphenicol antibiotic was sorbed onto specific sites or with specific functional groups (− OH, -COOH or –C=O groups confirmed by Raman spectra) of fBC-2. This can be explained by two facts. Firstly, chloramphenicol molecules that were sorbed onto the fBC-2 surface or functional groups had to emerge during thermal treatment and leave the functional groups or surface intact as they were before. Therefore, further application of regenerated fBC-2 for chloramphenicol sorption was accelerated. Secondly, thermal regeneration of fBC-2 at 300 °C might have created some new binding sites which may have accelerated the sorption process. However, this kind of outcome might not be significant since the functionalization of biochar was carried out at 600 °C and an increase in surface porosity theoretically may not be feasible below that temperature. Furthermore, no significant change in biochar weight was noticed after regeneration. It can be suggested that chloramphenicol sorption on fBC-2 was highly site-specific producing a molecular imprinting effect, which was favourable for chloramphenicol removal and subsequent regeneration for repeatable applications.

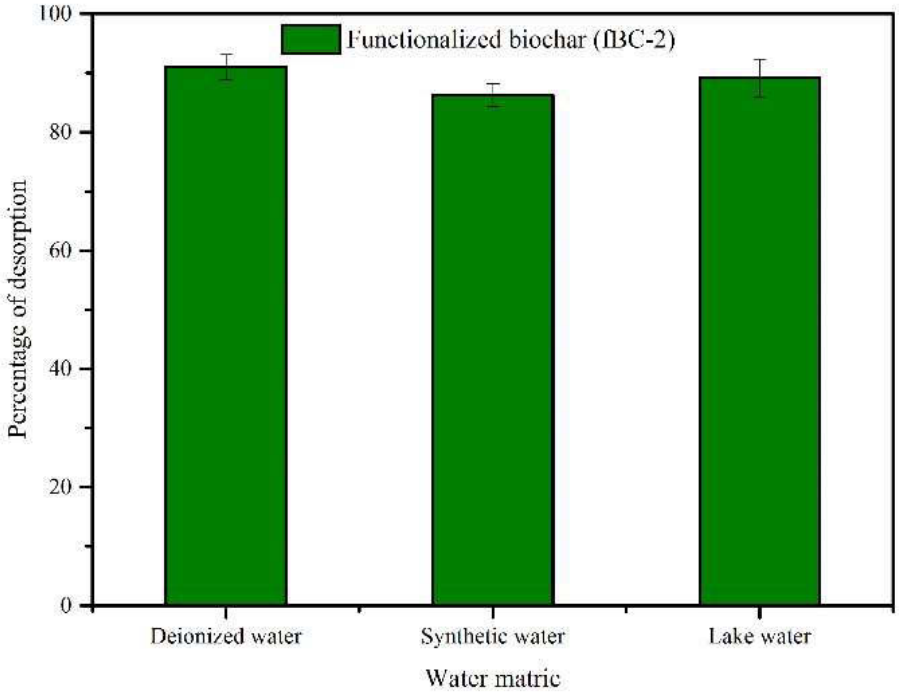

Figure 4.3.10: Percentage of regeneration of chloramphenicol.

From the findings it can be stated that fBC-2 can be successfully regenerated and reused for complete sorption of chloramphenicol. This type of functionalization of different carbonaceous materials is very efficient for the removal of organic contaminants from water and wastewater. Previous study also confirmed the efficient removal of three sulfonamide antibiotics in single and competitive modes [244] using fBC. In addition, fBC-2 or the functionalization of other carbonaceous materials utilizing the same method can generate more costeffective sorbents for the removal of different types of emerging organic contaminants.

4.3.4. Concluding Remarks

The sorptive removal of chloramphenicol by fBC was very effective in different water types. The removal of chloramphenicol was pH dependent, and maximum sorption occurred in the pH 4.0-4.5 range. The removal of chloramphenicol was described better by the Langmuir isotherm model than the Freundlich isotherm model. Sorption of chloramphenicol onto fBC-2 was significantly influenced by humic acid, salt concentration and different water properties. The removal of chloramphenicol was higher in deionized water followed by lake water and synthetic wastewater. K_d was decreased by ~70% when humic acid concentration was increased

from 0.5 to 40 mg L^{-1}. The presence of low concentration of salts and soil resulted in increasing K_d values while high concentration of salts and soil led to decreasing K_d values. The sorption of chloramphenicol onto fBC involved mainly EDA interactions at pH < 2.0; formation of CAHB and hydrogen bonds in addition to EDA in the pH 4.0-4.5; and CAHB and EDA interactions at pH > 7.0. fBC-2 can be regenerated with excellent reusability up to many cycles for the efficient removal of chloramphenicol due to creating the fingerprint effect onto specific sites of fBC-2. Finally, fBC-2 or functionalization of other carbonaceous materials with the same method can potentially generate better sorbents for the removal of similar organic contaminants in a sustainable manner.

4.4. Nano-Fe^0 immobilized onto Functionalized Biochar Gaining Excellent Stability During Sorption and Reduction of Chloramphenicol via Transforming to Reusable Magnetic Composite

4.4.1. Introduction

In the last two decades, many studies have demonstrated that ZVI (redox potential, $E^o = -0.44$ V) and several other zero-valent metals (e.g. Sn^0, Zn^0, Al^0 and Mn^0) can serve as efficient reducing agents for the remediation of chlorinated organic compounds, nitro-aromatic compounds, heavy metals, nitrate, dyes and phenolic compounds from groundwater and wastewater [65, 277-283]. ZVI is non-toxic, abundant, cheap and easy to produce, and its reduction process requires little maintenance [280]. To date, most of the studies have focused on using ZVI to remove chlorinated hydrocarbons from water [62, 281, 284, 285] due to dechlorinative reduction nature of ZVI. However, ZVI can be easily oxidized in the presence of oxygen. Powder state unstable nanosized ZVI and its intrinsic characteristics to react with surrounding media or agglomerate during preparatory processes as well as during application hinder its direct application and reduce its reactivity with poor mobility and transport for the continuous *in situ* environmental remediation [286]. These phenomena leading to ZVI applications in fixed bed column or other dynamic flow systems result in high-pressure drop and restriction of nZVI for field scale applications [286]. Attempts have been proposed to enhance the nZVI transport in natural subsurface environments with common objective of stabilizing the colloidal suspensions. nZVI has already been coated/impregnated with polymeric materials such as polystyrene sulfonate, polyacrylic acid, and carboxymethylcellulose, combined with resin, biochar [287], activated carbon [288, 289], multi-walled carbon nanotube [290], clay mineral supported (kaolinite, zeolite, clay, montmorillonite, rectorite, palygorskite, and bentonite) [291-296], and modified with hydrophilic carbon, and embedded in a silica matrix to obtain a stable nZVI suspension [297]. It was reported that nZVI particles modified by covalently binding with carboxymethylcellulose exhibited high transport potential in packed beds of glass, beads, sand and soil [297]. All these researchers reported that nZVI-composites materials were applied once for contaminant removal, with repetitive applications being rare. In addition, the fate of these nZVI-composites for further stage of application in repeatable manner is not clear. Theoretically and practically, nZVI particles in composite materials lose their reductive nature

during application when in contact with the contaminants and eventually produce different species either in solution or in composite by releasing and reacting loosely bonded surface ZVI and along in composite surface. The questions that arise are: what is the transformed ZVI-composite material? Is it stable and useable for further and repetitive applications? What are its unique characteristics in terms of chemical structure and interfacial properties? Thus to shed light on nZVI and its composite, we have synthesized nZVI from scrap materials and immobilized on fBC, which were tested for the removal of a chlorinated antibiotic chloramphenicol [(2,2-dichloro-N-[1,3-dihydroxy-1-(4-nitrophenyl)propan-2-yl]acetamide)] over repetitive cycles.

Of global concern today are antibiotics that are widely manufactured and used to treat the diseases caused by microorganisms. They are unique as they can selectively act on bacteria and pathogens by leaving the human cells and tissues unchanged, but prolonged exposure to antibiotics may develop antibiotic resistance genes [44, 57, 71, 298, 299]. Chloramphenicol as an antibiotic can cause geno-toxic and other side effects such as aplastic agranulocytosis, anaemia, and leukopenia [299]. Low removal efficiencies of chloramphenicol from wastewater has been reported using biological treatment technologies as it does not degrade in the metabolic system and thus, has been frequently detected in surface water, groundwater, and even in drinking water [16, 44]. The removal of chloramphenicol from wastewater has been reported using different physicochemical methods [284, 300, 301], among which ZVI has been widely applied [62, 284, 285]. Moreover, different studies reported different reduction products [62, 284, 285, 299], and so far no study has been conducted using ZVI and ZVI-carbonaceous composite for removing chloramphenicol except from deionized water. Hence, the application of ZVI and its composite for removing chloramphenicol from different water and the identification of byproducts are of great importance. In addition, such kind of composite may possess simultaneous sorption and reduction which has not been reported. Thus the calculation of the amount of sorption and reduction is necessary to differentiate the role of each in such composite materials.

Therefore, this study aimed to use nZVI-fBC as well as ZVI (for comparative purpose) with emphasizing given on the stability of nZVI-fBC composite along with focusing on the transformed magnetic composite (i.e. nFe_3O_4-fBC) for repeatable applications. In addition, the role of nZVI and nZVI-fBC composite for the reductive dechlorination and sorption of chloramphenicol with detailed mechanisms was investigated. Furthermore, the reduced products of chloramphenicol using nZVI and nZVI-fBC composite were identified. The effect of regeneration of the magnetized composite for repeatable application for chloramphenicol

removal was assessed up to six cycles. Finally, nFe_3O_4-fBC composite was applied (6 cycles of application) for the removal of methylene blue to assess its suitability for reuse.

4.4.2. Materials and Methods

4.4.2.1. Chemicals and Sorbent

The standards of chloramphenicol, methylene blue and organic solvents (methanol, acetonitrile, formic acid) of HPLC grade were purchased from Sigma-Aldrich, Australia. Humic acid, tannic acid, arabic acid, acacia gum powder, ammonium sulfate, beef extract, peptone, sodium lignin sulfonate, Na-laryl sulfate, K_2HPO_4, ammonium bicarbonate, magnesium sulfate, potassium chloride, sulfuric acid (~98%), nitric acid (~68), and sodium borohydrate ($NaBH_4$) were of analytical-grade. Iron oxide (Fe_3O_4) nano particles (<50 nm) were also purchased from Sigma Aldrich.

Eucalyptus globulus wood derived biochar was prepared by heating the wood particles at 380 °C for 2 h in a reactor under continuous nitrogen gas supply, and functionalization of this biochar was carried out according to a previous method [244]. Biochar and fBC were used for the sorption of chloramphenicol. Based on preliminary experiments it was found that fBC was much more effective for the immobilization of ZVI than biochar itself. Hence fBC was chosen for the nZVI-fBC composite preparation for the maximum immobilization of ZVI on fBC surface. fBC (75 μm to 1.0 mm) is the biochar containing different functional groups such as -COOH, -OH, C=O and C=C on its surface.

4.4.*2.2. nZVI Synthesis and Preparation of nZVI-fBC Composite*

Details of nZVI synthesis and preparation of nZVI-fBC composite can be found in **Chapter Three, section 3.2.1.3.**

4.4.2.3. Sorption Experiments, Chemical Analysis and Data Fitting

The interactions of biochar, fBC, nZVI, nZVI-fBC composite, and nFe_3O_4-fBC composite i.e. magnetic-fBC (converted composite during chloramphenicol removal and regeneration) with chloramphenicol solution were carried out at pH 4.0–4.5, 25 °C, based on previous study [284], in order to get maximum removal of chloramphenicol. nZVI, nZVI-fBC and magnetic-fBC were applied in different water types to determine their sorption and reduction nature of

chloramphenicol. The supernatant concentration was measured using HPLC (Jasco) with aliquots from each reactor being taken and filtered through a 0.2 μm PTFE filter followed by 50 μL of sample injection. HPLC equipped with an auto-sampler, a UV detector at 285 nm, and a Zorbax Bonus RP C_{18} column (5.0 μm, 2.1 × 1.50 mm, Agilent Technologies) was used for separation. Mobile phase A was composed of acetonitrile and formic acid (99.9: 0.1) while mobile phase B was composed of Milli-Q water and formic acid (99.9: 0.1). The elution used 40% of A and 60% of B at a flow rate of 0.4 mL min^{-1}, which was changed to 0.3 mL min^{-1} at 0.1 min. The method was run over 7 min.

Chloramphenicol and its reduced products were identified by LC-MS/QTOF in positive mode, on an Agilent Poroshell 120 EC-C_{18} column (2.7 μm, 4.6 mm × 50 mm). The elution began with 95% pure water and 5% methanol, ending with 1% pure water and 99% methanol within 9 min at a flow rate of 0.35 mL min^{-1}. Following elution, the mobile phase was changed to 95% water and 5% methanol. The total run time was 13 min.

Stock solution of methylene blue (1.0 g L^{-1}) was diluted to different initial concentrations. The nFe_3O_4-fBC composite was added without adjustment of the solution pH at a dosage of 0.5 g L^{-1} for methylene blue solution. The mixture was shaken on an orbital shaker at 120 rpm for 24 h at 25 °C. The methylene blue concentration was measured by UV–visible spectroscopy (Shimadzu). The sorption capacities of biochar, fBC, nFe_3O_4 and nFe_3O_4-fBC for chloramphenicol and methylene blue were calculated, and modelled using the Langmuir and Freundlich isotherms.

The Langmuir and Freundlich isotherm models can be represented as follows:

Freundlich model: $q_e = K_F C_e^{1/n}$ (4.4.1)

Langmuir model: $q_e = \frac{q_{max} K_L C_e}{1+K_L C_e}$ (4.4.2)

where c_e is the equilibrium concentration of chloramphenicol, q_e equilibrium concentration of chloramphenicol in solid phase, q_{max} is the maximum adsorption capacity (μM g^{-1}), n is a dimensionless number related to surface heterogeneity, K_F is the Freundlich affinity coefficient (μM^{1-n} L^n g^{-1}) and K_L is the Langmuir fitting parameter (L mg^{-1}).

4.4.*2.4. Characterizations of fBC, nZVI, nZVI-fBC and nFe_3O_4-fBC Composite*

Scanning electron microscopy (SEM) with energy dispersive spectrometer (EDS) was used to determine the morphological and chemical composition of the materials (Zeiss Evo-SEM). XRD analysis of the samples was carried out using a Bruker D8 Discover diffractometer using Cu Kα radiation, in the scattering angle 2θ range 20°–80°. Fourier transform infrared

spectroscopy (FTIR) (Miracle-10: Shimadzu) was used to determine surface functional groups. The spectra were obtained at 4 cm^{-1} resolution by measuring the absorbance from 400 to 4000 cm^{-1} using a combined 40 scans. Raman shifts measurement was carried out using Renishaw in via Raman spectrometer (Gloucestershire, UK) equipped with a Leica DMLB microscope (Wetzlar, Germany), 17 mW at 633 nm Renishaw helium-neon laser source and CCD array detector using 50% laser intensity. The abundance of surface functional groups on nZVI-fBC was obtained by using X-ray Photoelectron Spectroscopy (XPS) (Thermoscientific, UK). Iron concentration was determined using microwave plasma atomic emission spectroscopy (4100-MP-AES, Agilent Technologies). Zeta potential values of nZVI and nFe_3O_4-fBC composite were measured with 0.1 M KCl background solution (for constant ionic strength) using a Nano-ZS Zeta-seizer (Malvern, Model: ZEN3600). Zeta potential values were measured at different pH values (**Table 4.4.1**). Particle size distribution of nZVI was also measured using the same instrument.

Table 4.4.1: Zeta potential values (mV) of Fe_3O_4-fBC composite and nZVI.

Fe_3O_4-fBC composite							
Initial pH	1.56	2.58	3.50	4.80	6.50	8.45	10.85
Final pH	1.77	3.65	5.23	5.98	6.33	6.75	7.22
Zeta potential	-4.42±0.54	-20.3±1.13	-30.1±2.19	-40.0±0.57	-41.7±2.33	-42.6±1.56	-42.6±1.41
nZVI							
Initial pH	1.56	2.58	3.50	4.80	6.50	8.45	10.85
Final pH	1.63	2.63	3.79	5.22	5.71	6.54	10.11
Zeta potential	28.6±0.71	35.8±2.19	30.0±0.21	10.8±0.28	8.02±0.50	-2.02±0.22	-19.0±3.32

4.4.*2.5. Comparative Study in Different Water Samples*

Lake surface water (pH 7.2, temperature 19.9 °C, total dissolved solids 116 mg L^{-1}, total organic carbon 75.56 mg L^{-1}, total carbon 76.72 mg L^{-1}) was collected from the Victoria Park, NSW, Australia and was filtered through 1.2 µm filter paper before being stored at 4 °C. Synthetic wastewater was prepared based on a recent study [360] (**Table 4.4.2**). Deionized water, lake surface water and synthetic wastewater were spiked with 3.10 µM $L^{-1}$of

chloramphenicol before contact with nZVI, nZVI-fBC and magnetic-fBC composite to assess the extent of sorption in different water types.

Table 4.4.2: Chemical composition of synthetic wastewater.

Compound	Concentration (mg L^{-1})
Peptone	2.37
Beef extract	1.8
Humic acid	4.2
Tanninc acid	4.2
Arabic acid	5.0
Sodium lignin sulphonate	2.4
Sodium lauryl sulphate	0.94
Acacia gum powder	4.37
Ammonium sulphate	7.1
Potassium phosphate (KH_2PO_4)	7.0
Magnesium sulphate ($MgSO_4.3H_2O$)	0.71

4.4.*2.6. Desorption and Regeneration of Magnetic-fBC Composite*

Desorption of chloramphenicol was carried out to calculate and differentiate the reduction and sorption percentage of chloramphenicol using nZVI-fBC (after application in the 1stcycle) and magnetic-fBC composite (2nd to further cycles). After experiments, the supernatant was decanted and replaced with an equal volume of 50% methanol solution as solvent (solvent regeneration). After 24 h, the suspension was centrifuged for 7 min at 2000 rpm, and chloramphenicol concentration was measured directly by HPLC. Desorption was performed up to 2nd cycle. The thermal regeneration of magnetic-fBC (after 1st cycle application, nZVI-fBC transformed to magnetic-fBC composite) was carried out in an oven by heating at a pre-set temperature 300 °C for 1 h.

4.4.3. Results and Discussion

4.4.*3.1. Material Structure and Composition*

The morphologies of nZVI, nZVI-fBC composite, and nFe_3O_4-fBC composite were analyzed by SEM, EDS, XRD, XPS and Raman spectra. SEM images of unsupported fBC, nZVI-fBC and magnetic-fBC composite are shown in **Figures 4.4.1 and 4.4.2**. In the case of nZVI-fBC, the fBC surface was partially covered by the loaded nZVI particles **(Figure 4.4.1b**) and

appeared to be uneven whereas bare fBC surface was smooth in appearance (**Figure 4.4.1a**). Even after six cycles of application the SEM image (**Figure 4.4.1c**) shows the presence of nanosized iron oxide particles on fBC surface indicating that iron oxide particles were successfully incorporated with fBC by forming a stable magnetic-fBC composite. It also found some portion of nZVI in the nZVI-fBC composite was loosely bonded with fBC surface, which was confirmed by the analysis of iron content in nZVI-fBC. The iron content in the nZVI-fBC composite (7.8%) was determined by digesting of the composite in nitric acid solution (3%, v/v) followed by MP-AES analysis. In order to validate the composition of iron oxides formed on nZVI-fBC, EDS analysis was performed with nZVI-fBC composite (**Table 4.4.3**) and ~8.3% iron content was obtained.

Table 4.4.4: EDS of fBC, nZVI and nZVI-fBC.

Sample	EDS analysis (atomic percentage)				
	C (%)	P (%)	N (%)	Fe (%)	O (%)
fBC	60.80±1.82	7.96±0.78	5.37±0.82		25.44±1.23
nZVI/nFe^0				95.05±2.05	3.95±1.20
nZVI-fBC	58.90±1.5	0.82±0.20	6.56±1.20	8.3±0.30	26.20±0.9
nZVI-fBC after 1^{st} cycle application	62.30±0.56	1.04±0.20	7.32±1.20	5.48±1.32	23.68±1.78

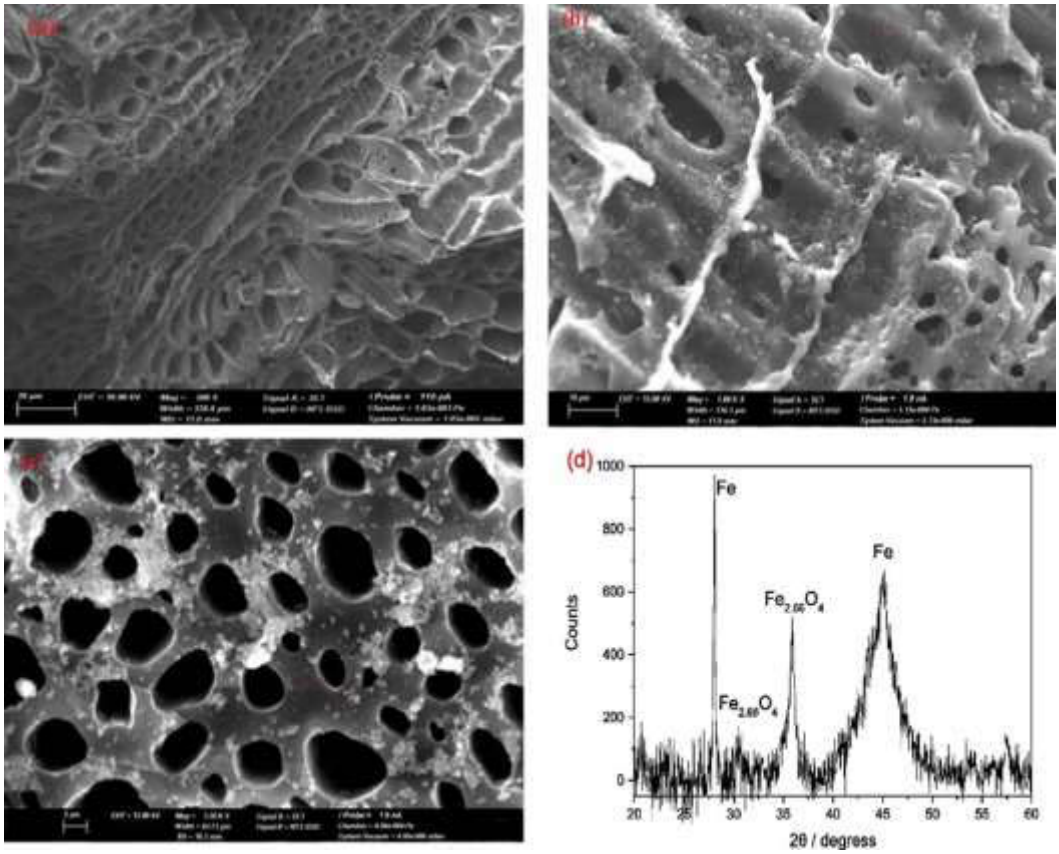

Figure 4.4.1: SEM cross-sectional images of fBC, nZVI-fBC and nFe_3O_4-fBC composite (after application of nZVI-fBC), respectively (a–c) using scanning electron microscope (SEM) with energy dispersive spectrometer (EDS) and XRD pattern of nZVI (d).

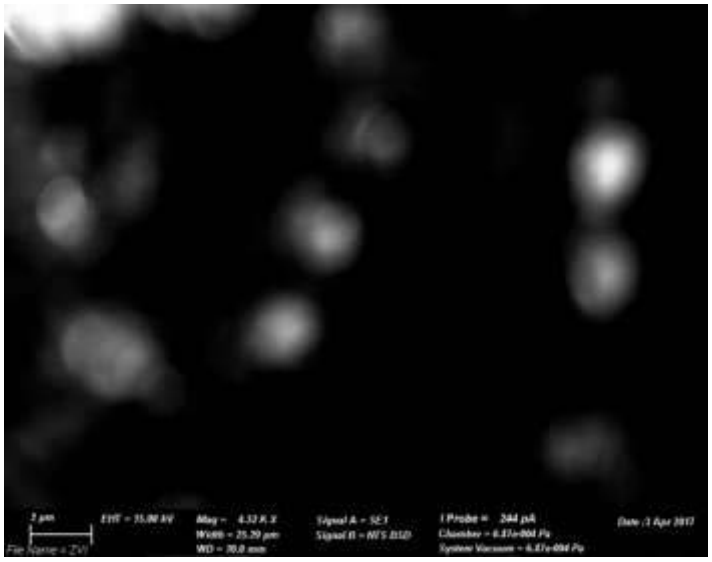

Figure 4.4.2: SEM image of nZVI.

XRD studies of nZVI showed the crystalline domain size of ZVI nanoparticles (**Figure 4.4.1d**). The crystalline scattering domain size of nFe^{o} was found at 2θ = ~45° and ~28° [279]. Particle size distribution data showed that nZVI had particle sizes in the range of 220.2 nm (77.9%) and 190.1 nm (22.1%). In addition, iron oxide was also present in ZVI due to the oxidation of a small portion of nZVI during measurement, preparatory processes or even in drying processes. EDS data showed that nZVI comprised around 92–95% of nFe^{o} with the rest being oxidized to $FeOOH/Fe_2O_3/Fe_3O_4$ particles (**Table 4.4.3 and Figure 4.4.3**). XPS analysis of nZVI-fBC showed that C1s spectra surface of this composite composed of aromatic carbon in the form of C=C (284.4 eV), C-O (286.4 eV), C=O (287.6 eV) and -COOH (289 eV) functional groups (**Figure 4.4.4a**), while O1s spectra showed that oxygen content mostly in the form of organic carbon (at 533.45 and 532.12 eV). A peak at ~530.7 eV (O1s) indicated the presence of metal oxide in the composite [in the form of Fe_2O_3/Fe_3O_4 Fe(OH)O] and this might possible due to the oxidation of surface nZVI to Fe_2O_3/Fe_3O_4 and by the interaction with surface -COOH and –C=O group to form -COOFe/-OFe (**Figure 4.4.4b**) [361-364]. Two intense peaks were observed for iron at ~711 eV (for 2p3/2) due to the formation of $Fe/Fe_2O_3/Fe_3O_4$/Fe(OH)O [361-364] and at ~725 eV (for 2p1/2) due to $FeOOH/Fe_2O_3$ (**Figure 4.4.4c**) [365]. Thus, XPS results indicated that iron was successfully immobilized onto fBC surface which might form different species such as - BC-COO-Fe-OOC-BC, BC-O-Fe-O-BC, and BC-iron/iron oxide particles. However, XRD result of nFe_3O_4-fBC after reaction with chloramphenicol only showed the presence of Fe_3O_4 in the composite (**Figure 4.4.5a**) [366].

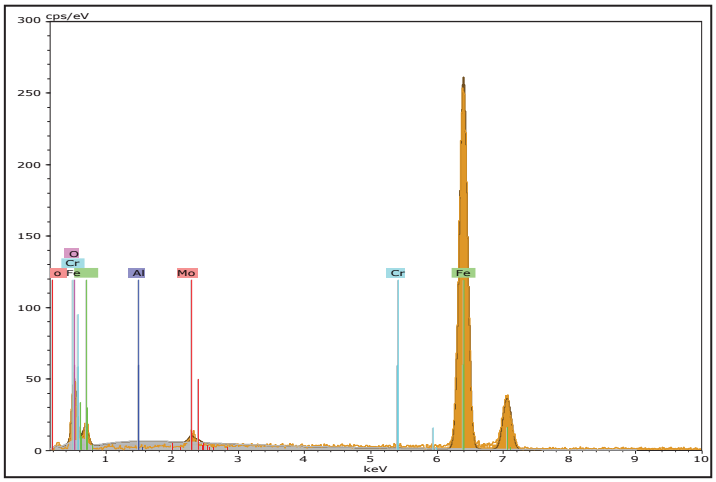

Figure 4.4.3: EDS plot of nZVI.

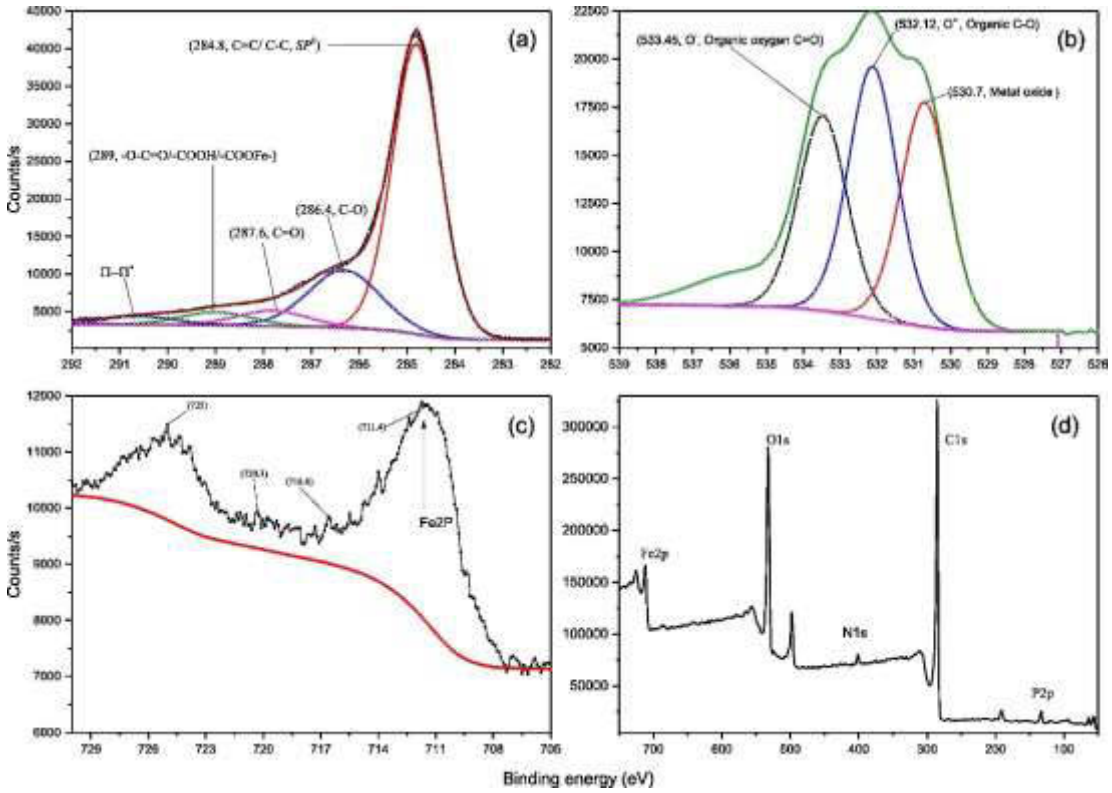

Figure 4.4.4: XPS analysis of nZVI-fBC composite before sorption experiments. Spectra were obtained by plotting counts against binding energy for C1s (a), O1s (b), Fe2p (c) and overall survey (d) in a wide scan.

FTIR spectra of nZVI-fBC showed similar functional groups present on nZVI-fBC composite, with peaks at 3400–3800 cm^{-1} (-OH/-OFe-), ~1720 cm^{-1} (C=O), 1523–1595 cm^{-1} (C=C), and ~1020–2028 cm^{-1} (-COOH/-COOFe-) (**Figure 4.4.5**). Additionally Raman spectroscopy was carried out to obtain deeper insight into the crystalline structure of the ZVI and nZVI-fBC. Bare ZVI showed bands [284] at 215.7, 278, 392, 483, 590 cm^{-1} and maximum peak at 1282.5 cm^{-1} (**Figure 4.4.6**). In the case of ZVI, the three peaks at ~215, ~278 and ~483 cm^{-1} were assigned to hematite. These results are well supported by Raman values reported for α-Fe_2O_3 in the literature [367]. A peak at ~394.7 cm^{-1} indicated both α-FeOOH and γ-FeOOH [368]. Another peat at ~483 cm^{-1} indicated α-FeOOH presence along with ZVI [368]. Raman spectra of nZVI-fBC showed three characteristic peaks at 1595.62, 1340.97 and 680 cm^{-1}. The two broad peaks located at 1340 cm^{-1} and 1595 cm^{-1}corresponded to the D-band and G-band of graphitic structures presence in nZVI-fBC. The band intensity ratio (I_G/I_D) showed the degree of functionalization in fBC. In addition, the peaks at ~680 cm^{-1} were due to the presence of magnetite Fe_3O_4 and FeO on the surface of nZVI-fBC [365, 367, 369, 370]. From literature, it is found that the Raman spectra of a freshly fractured Fe_3O_4 showed peaks at ~300, ~532 and ~661 cm^{-1} [367].

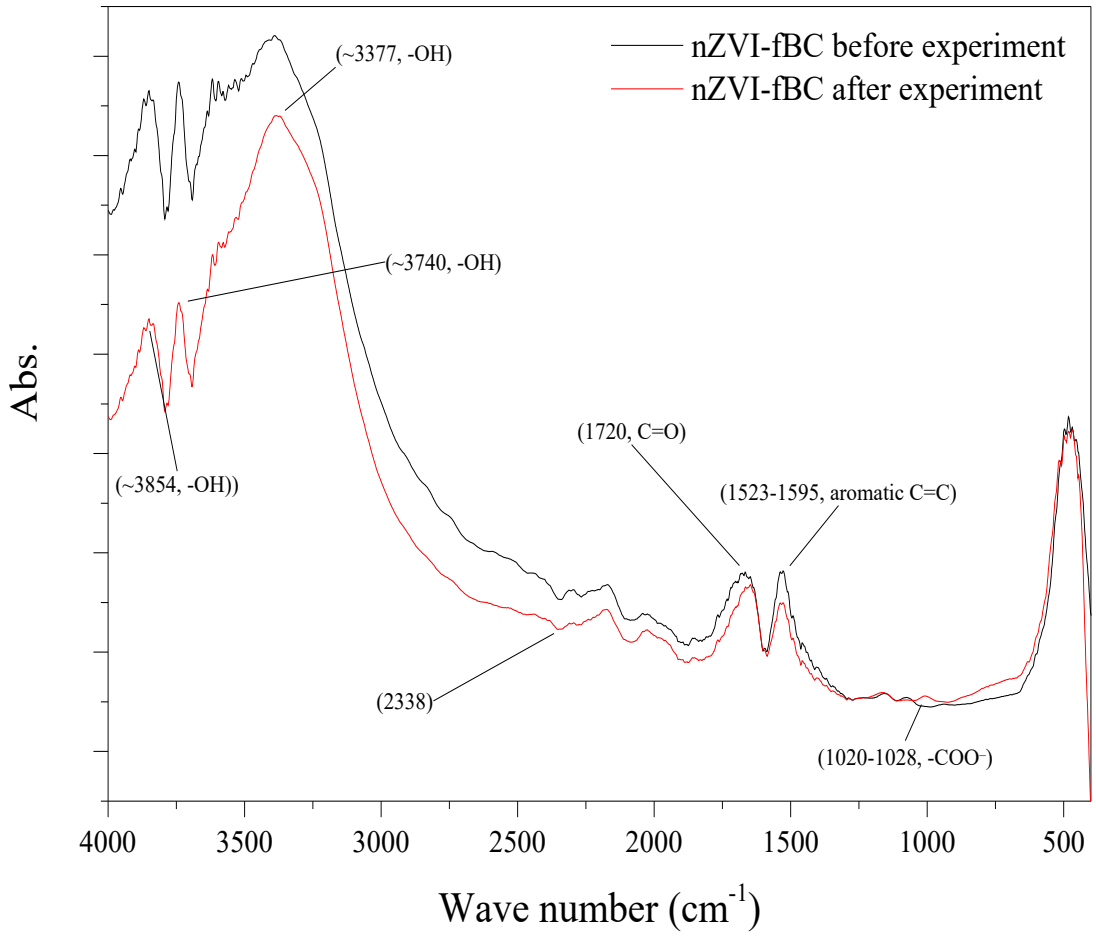

Figure 4.4.5: FTIR spectroscopy of nZVI-fBC composite before and after the sorption of chloramphenicol.

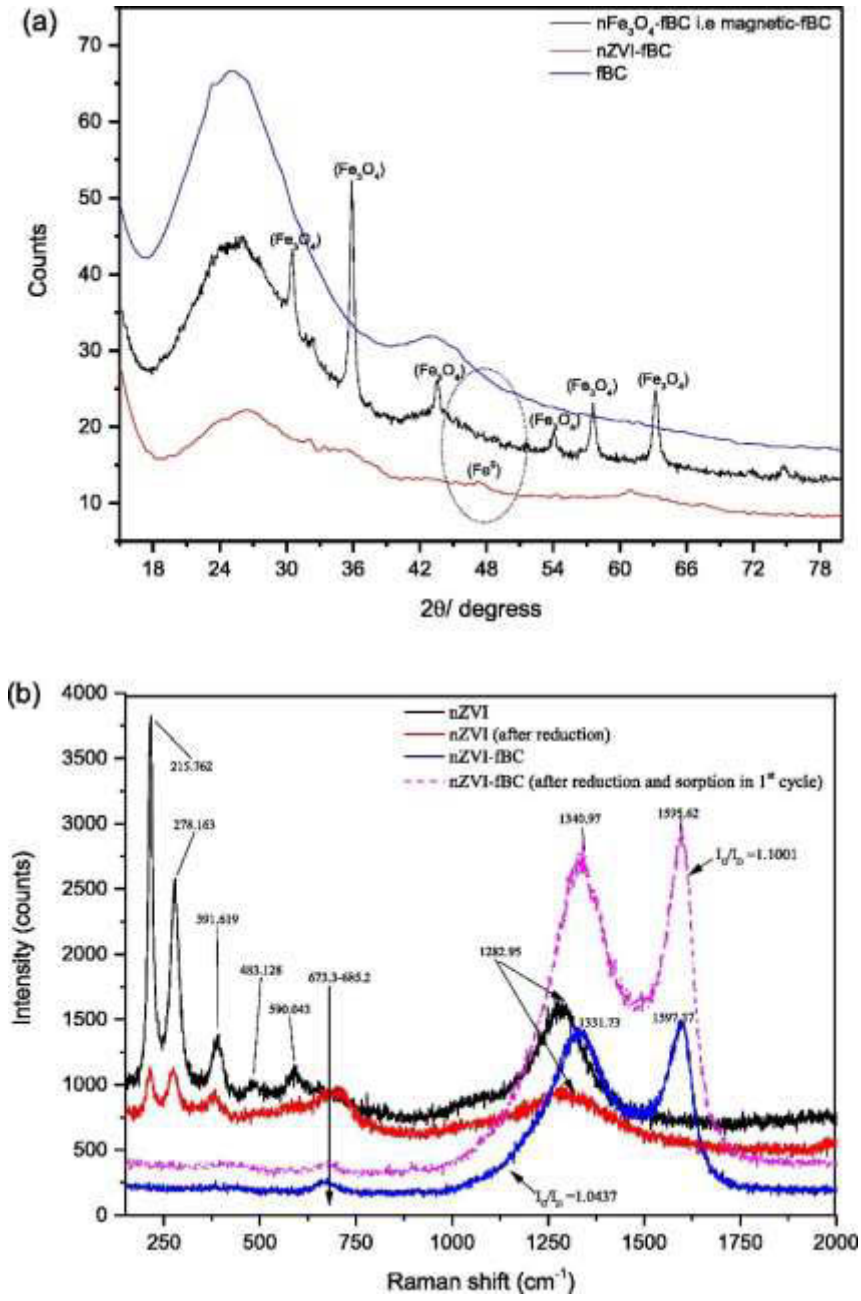

Figure 4.4.6: XRD pattern of fBC, nZVI-fBC and nFe_3O_4-fBC (a). Raman spectra of nZVI and nZVI-fBC composite (with band ratio, I_G/I_D) for the removal of chloramphenicol before and after experiments (b).

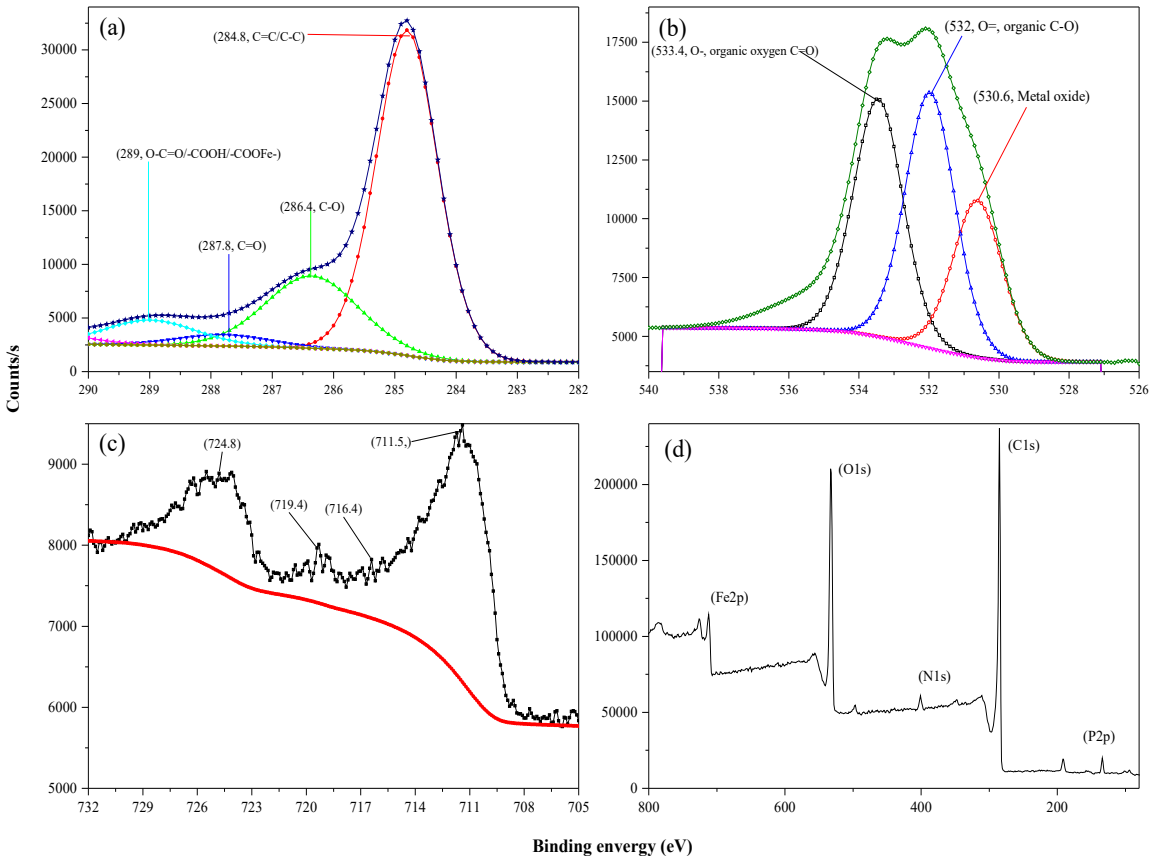

Figure 4.4.7: XPS analysis of nZVI-fBC (after 1st cycle). Spectra were obtained by plotting counts against binding energy for C1s (a), O1s (b), Fe2p (c) and overall survey (d) in a wide scan.

4.4.*3.2. Application of nZVI for Chloramphenicol Reduction*

nZVI was applied for the removal of chloramphenicol from different water types. nZVI could completely reduce 3.10 μM L^{-1} of chloramphenicol within 5–6 h depending on the water types. No pronounced difference was observed in the complete reduction and dechlorination of chloramphenicol between different water types (**Figure 4.4.8a**), although synthetic wastewater had slightly positive influence on the overall reduction of chloramphenicol followed by lake and deionized water. This is possibly due to the presence of different species that were favorable for the faster reduction of chloramphenicol in synthetic wastewater. In addition, species in synthetic wastewater might increase the ionic mobility of chloramphenicol towards nZVI particles resulted in strong interactions. However, lake water might contain less ionic species than synthetic wastewater but more than deionized water, resulting in moderate reduction of chloramphenicol. Furthermore, control experiments in the absence of nZVI with different water types showed that there was no loss of chloramphenicol. This indicated that

there was no adsorption/accumulation of chloramphenicol by organics present in synthetic wastewater.

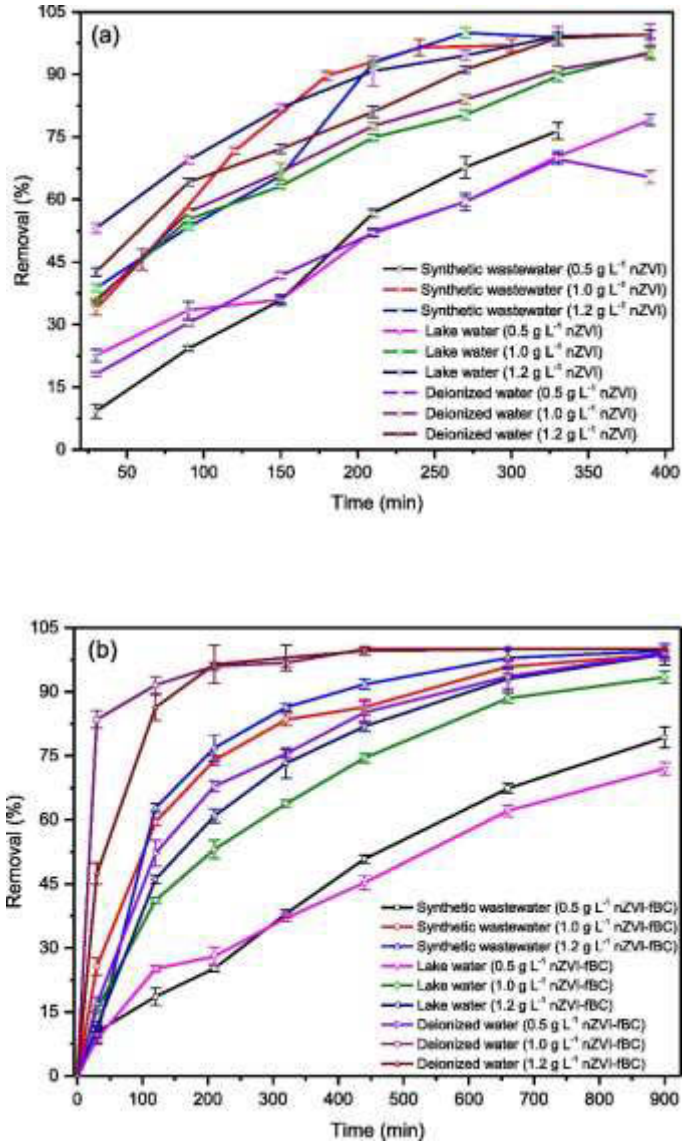

Figure 4.4.8: Percentage removal (±standard deviation) of chloramphenicol with time using nZVI (a) and nZVI-fBC composite (b). The initial concentration of chloramphenicol was 3.10 μM L^{-1}, pH 4.0–4.5, 25 °C from different water matrices with different dosages of nZVI and nZVI-fBC composite.

The rate constant (k, min^{-1}) for chloramphenicol reduction was calculated using $C_t/C_o = e^{-kt}$, where C_o and C_t are chloramphenicol concentrations at time zero and any time, respectively. From the beginning to 3 h, the reduction rate of chloramphenicol by nZVI was fast possibly due to initial surface interactions [284]. The reduction nature of nZVI particles became slow with increasing time due to surface passivation of nZVI particles by reacting with surrounding environment. In terms of complete chloramphenicol reduction by nZVI particles,

the reduction rate constant followed the order of deionized water < lake water < synthetic wastewater (**Table 4.4.5**). The detailed mechanism of chloramphenicol reduction by nZVI is presented in **Section 4.4.3.5**.

Table 4.4.5: Reduction kinetic parameters of chloramphenicol in different water types using nZVI.

Amount	Synthetic wastewater		Lake water		Deionized water	
(g L^{-1})	k (min^{-1})	r^2	k (min^{-1})	r^2	k (min^{-1})	r^2
0.50	0.0041	0.963	0.0037	0.953	0.0036	0.987
1.0	0.0127	0.990	0.0071	0.942	0.0071	0.980
1.2	0.0168	0.84	0.0132	0.950	0.0115	0.910

4.4.*3.3. nZVI-fBC Application and Its Transformation to Magnetic-fBC Composite During Chloramphenicol Removal*

The nZVI-fBC composite showed simultaneous reduction and sorption in the 1st stage of application. Sorption was dominant over reduction and followed an opposite trend of nZVI i.e. deionized water > lake surface water > synthetic wastewater (**Figure 4.4.8b**). As sorption was dominant over reduction, hence different organic and inorganic species in lake water and synthetic wastewater may interact with the fBC surface functional groups as well, competing with chloramphenicol; thus more time was needed than by nZVI for the complete removal of chloramphenicol. In the case of deionized water, there was no competitor of chloramphenicol, hence, sorption was faster. Initially, fast reduction of chloramphenicol using nZVI-fBC was observed by the loosely bonded surface nZVI following sorption by strongly bonded nZVI onto biochar surface. A small portion of loosely bonded surface nZVI was released into the solution during the application of nZVI-fBC composite in the 1st cycle. This was confirmed through the analysis of iron concentration in the supernatant by MP-AES and percentage of iron content on the nZVI-fBC surface by EDS. From these results, it was found that 0.15% of iron content was lost from nZVI-fBC composite (initially 7.8%) and likely released into solution. The properties of nZVI-fBC composite were the main reason to take additional time than nZVI itself (∼5–6 h, reduction was faster than sorption) and nZVI-fBC to be transformed into magnetic-fBC composite for complete removal of the same amount of chloramphenicol (**Figure 4.4.8b**). Furthermore, in the 2nd cycle application of nZVI-fBC composite after transformation to magnetic-fBC, chloramphenicol reduction was negligible. Additionally no iron content was found in the solution. Thus the 2nd to 7th stage applications of nZVI-fBC showed that only

sorption was dominant indicating that nZVI-fBC was transformed into magnetic biochar composite (i.e. nFe_3O_4-fBC). Some reactions might happen during the application and transformation of nZVI-fBC composite as proposed by Liu et al. [371]:

$$Fe^0(\text{in ZVI-fBC})+2H_2O \rightarrow Fe^{2+}+H_2+2OH^- \quad (4.4.3)$$

$$2Fe^0+O_2+2H_2O \rightarrow 2Fe^{2+}+4OH^- \quad (4.4.4)$$

$$6Fe^{2+}+O_2+6H_2O \rightarrow 2Fe_3O_4(s)+12H^+ \quad (44.5)$$

FTIR spectra of nZVI-fBC after experiments shifted to lower absorbance peaks at 3400–3800 cm^{-1} (-OH/-OFe-), and at 1020 cm^{-1} (-COOH/-COOFe-) [244]. These might be due to the partial release of loosely bonded iron (-OFe/-COOFe or loosely bonded ZVI) from surface functional groups (-COOH/-OH) of fBC. Hence surface functional groups of fBC became free and showed lower absorbance at different positions (**Figure 4.4.6**). EDS (**Table 4.4.1**) and MP-AES measurement already confirmed that after the 1st cycle application of nZVI-fBC, iron was released into the solution. Thus, during the first cycle, nZVI-fBC showed partial reduction followed by maximum sorption of chloramphenicol. As the sample was exposed to air during measurement, dissolved oxygen could cause partial oxidation of nZVI in nZVI-fBC composite forming iron oxygenated species (-COOFe-/-OFe/FeO/Fe_2O_3/Fe_3O_4) during the tests (**Figures 4.4.1d, 4.4.4b, and 4.4.7)** [299, 372]. Raman spectra of nZVI-fBC showed that band intensity ratio (I_G/I_D) increased after the application of nZVI-fBC composite in the 1st cycle. This information clearly indicated that surface functional groups (C=O and C=C) in nZVI-fBC became free by participating in reduction process. Hence, surface ZVI (loosely bonded) and –COOFe- or –O-Fe- lost their iron content for the reduction of chloramphenicol due to the reaction with air (in particular dissolved oxygen). In addition, a stable peak for magnetite Fe_3O_4 at 673.3–685.2 cm^{-1} remained the same after experiment. From literature, it is found that the Raman spectra of fresh Fe_3O_4 showed peaks at ~300, ~532 and ~661 cm^{-1} [367]. Our XRD and magnetization test results after reaction also indicated the presence of magnetic Fe_3O_4 particles on the composite (Figure 3a). Thereby, nZVI-fBC composite was fully transformed into magnetic-fBC (**Eqs. (4.4.4)–(4.4.6)**). In addition, in comparison with nZVI, nZVI-fBC composite material did not show any extra peaks like nZVI indicating no FeOOH, Fe_2O_3 i.e. hematite presence in the composite. However, C=O groups such as -COOH and –C=O might still associate with iron in the form of –COOFe- and C=O-Fe-. On the other hand, XPS spectra of O1s showed that the peak intensity of metal in oxide form (~530.6 eV), decreased to some extent which also indicated that loosely bonded iron took

part in the reduction and stable metal oxide remained in the composite (**Figures 4.4.4b, 4.4.4c, 4.4.7b and 4.4.7c**). Moreover, Fe2p peak intensity also significantly decreased by forming some stable iron oxide. According to Tian et al. [365], the peaks at ~530.6 eV (for O1s), ~711 (for 2p3/2) and ~725 eV (for 2p1/2) were found before and after application indicating the presence of Fe_2O_3/Fe_3O_4/Fe(OH)O in the composite (**Figures 4.4.4 and 4.4.7**). Besides, Raman spectra only indicated the presence of Fe_3O_4 and Fe(OH)O in the composite materials. Fe_3O_4 indicated the presence of magnetic particles in the composite while Fe(OH)O indicated the presence of iron species by forming bonds with the functional groups of fBC. The results showed that nZVI-fBC composite was transformed to stable magnetic (nFe_3O_4-fBC) composite during the application in the 1st cycle.

4.4.*3.4. Comparative Study among Biochar, fBC, nFe_3O_4 and nFe_3O_4-fBC for Chloramphenicol Removal*

Comparative study on the removal of chloramphenicol using biochar, nFe_3O_4-fBC, fBC and nFe_3O_4 was conducted to assess the synergistic effect. The results showed that nFe_3O_4could remove only ~3.57% of chloramphenicol whereas biochar (eucalyptus biochar, 2.0 g L^{-1}) showed 57.5% removal (after 3 days of interactions). On the other hand, fBC and nFe_3O_4-fBC showed 100% removal. In addition, the sorption isotherm study showed that the maximum Langmuir sorption capacities were 258.95 μM g^{-1} and 406.77 μM g^{-1}, respectively for fBC and nFe_3O_4-fBC composite. The results indicated that transformed magnetic composite (nFe_3O_4-fBC) had synergistic effect with an increased sorption capacity of ~57% than fBC alone (**Figure 4.4.9 and Table 4.4.6**).

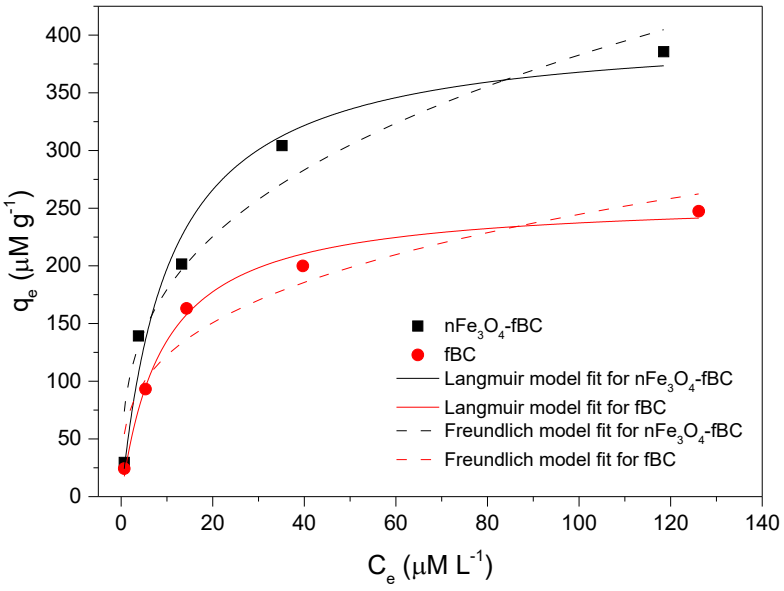

Figure 4.4.9: Sorption of chloramphenicol by fBC and Fe3O4-fBC composite with the Freundlich and Langmuir model fit.

Table 4.4.6: The Freundlich and Langmuir isotherm parameters for the sorption of chloramphenicol using fBC and Fe_3O_4-fBC.

Biochar	Langmuir isotherm			Freundlich isotherm		
	Q_{max}	K_L	r^2	K_F	n	r^2
fBC	258.95±9.52	0.110±0.02	0.991	61.25±15.0	3.33±0.67	0.909
Fe_3O_4-fBC	406.77±30.35	0.095±.026	0.968	84.26±18.2	3.04±0.50	0.940

4.4.3.5. Chloramphenicol Reduction Mechanisms and By-Products

Fresh nZVI showed bands at 215.7, 278, 392, 483, 590 and 1282.5 cm^{-1}. The intensity of most of these peaks decreased significantly after reduction [284]. nZVI (nFe^o) showed maximum peak at ~1283 cm^{-1} and the peak intensity significantly decreased and slightly shifted to 1331.7 cm^{-1} at the end of the experiments. The result from the Raman spectra clearly indicated that nZVI particles took part in the reduction processes and peak intensity reduced significantly at different points **(Figure 4.4.5).** Hematite (agglomerate particles), FeOOH and free nFe^o took

part in the reduction process, and the peak intensity was reduced significantly. This was also confirmed by the final solution pH being increased to ~8.6 from initial 4.0–4.5.

$$Fe^0+H_2O \rightarrow Fe^{2+}+H_2+OH^- \quad (4.4.6)$$

$$Fe^0+R\text{-}Cl+H^+ \rightarrow Fe^{2+}+R\text{-}H+Cl^- \quad (4.4.7)$$

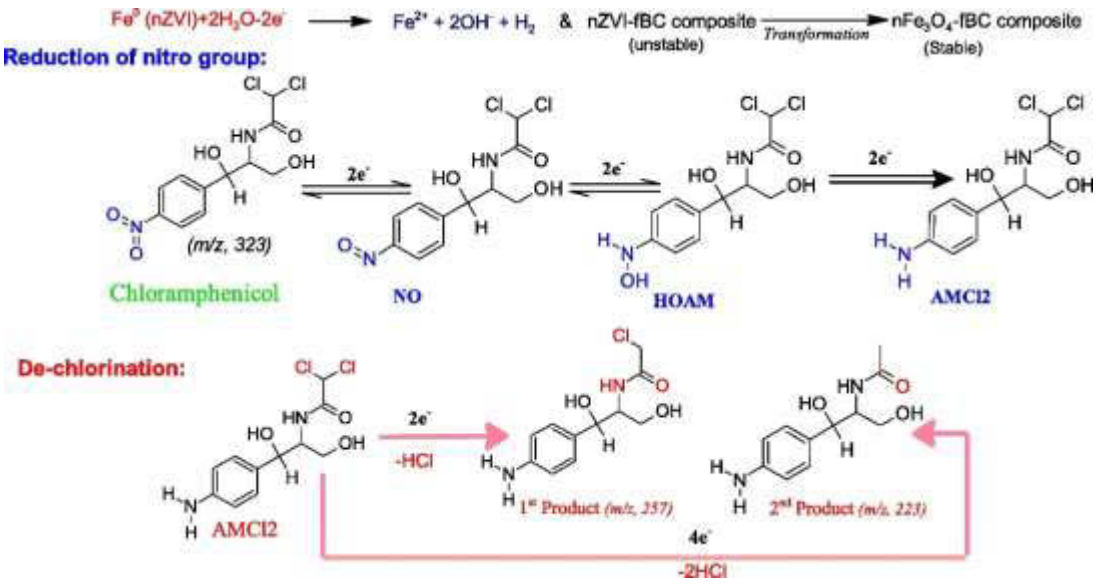

Figure 4.4.10: Proposed reduction and dechlorination mechanisms for the removal of chloramphenicol from water and wastewater.

Again, when chloramphenicol interacted with nZVI and nZVI-fBC (1st cycle), the amino group was formed rapidly by reducing nitro group due to release of electrons by nFe^0 and oxidized in the presence of water or dissolved oxygen (**reaction 4.4.6**) [373, 374]. Some of the additional intermediates were quickly produced during reduction of nitro groups turned into firstly, nitroso (NO), secondly, hydroxylamino (HOAM) and thirdly, amine (AMCl2) products of chloramphenicol (**Figure 4.4.10**). In the second stage of reduction and dechlorination, AMCl2 was transformed into two by-products namely 2-chloro-N-[1,3-dihydroxy-1-(4-aminophenyl)propan-2-yl]acetamide (1st product *m/z* 257) and dechlorinated N-[1,3-dihydroxy-1-(4-aminophenyl)propan-2-yl]acetamide (2nd product *m/z* 223) (**Reaction 4.4.7, Figures 4.4.11, 4.4.12 and 4.4.13)**. The identification of by-products was confirmed using LC-MS-QTOF. During the first cycle application of nZVI-fBC, it was found that the loss of chloramphenicol was mostly due to reduction within first few hours and later stages once the surface of nZVI-fBC was transformed, the decrease in chloramphenicol concentration was mainly due to sorption onto nZVI-fBC surface. Moreover, negligible quantities of reduced

products were detected in the solution after 18 h application of nZVI-fBC indicating that these by-products could have been sorbed by nFe_3O_4-fBC composite **(Figure 4.4.13)**. Furthermore, the 2ndcycle experiment showed minor reduction of chloramphenicol indicating that nZVI-fBC surface had been transformed to nFe_3O_4-fBC composite which gained only sorption properties (**Figure 4.4.14**).

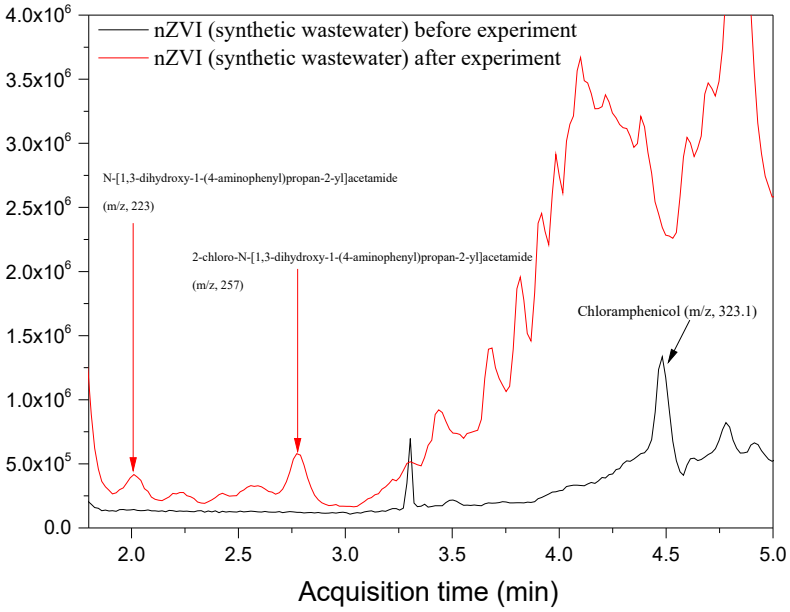

Figure 4.4.11: Reduced products of chloramphenicol as identified by LC-MS/QTOF from deionized water, synthetic wastewater and lake water using nZVI only (sample collected after 8 h).

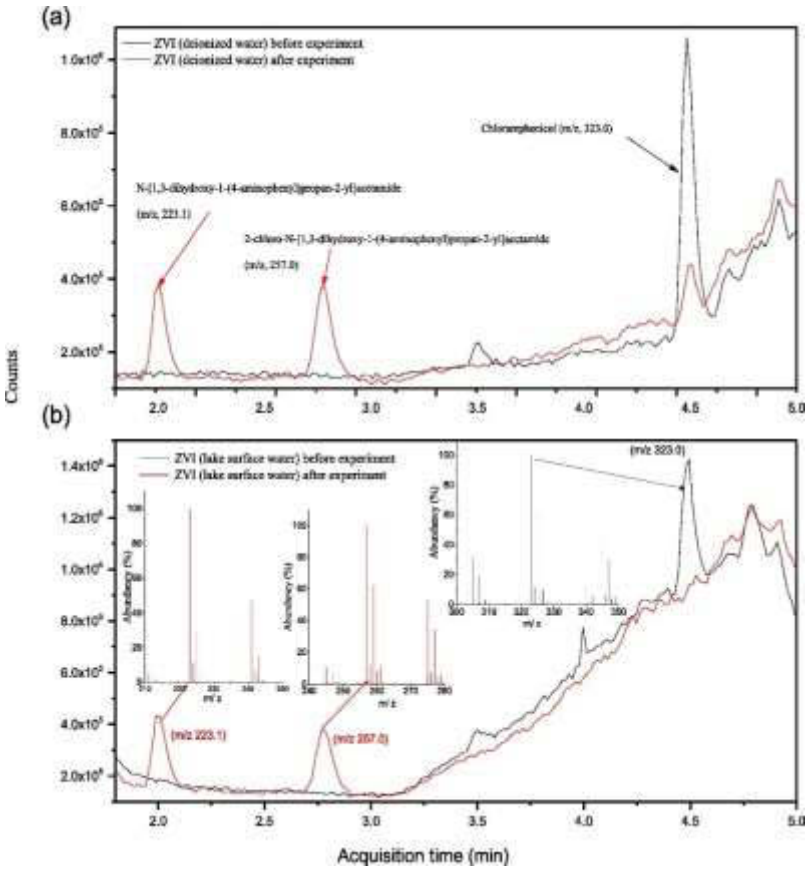

Figure 4.4.12: Chloramphenicol transformation by-products identified by their retention times (2.1 min, 2.7 min) in LC and mass spectra by LC-MS/QTOF from deionized water (a) and lake water (b) using nZVI only (sample collected after 8 h). LC-MS/QTOF method run for 13 min and data plotted up to 5 min.

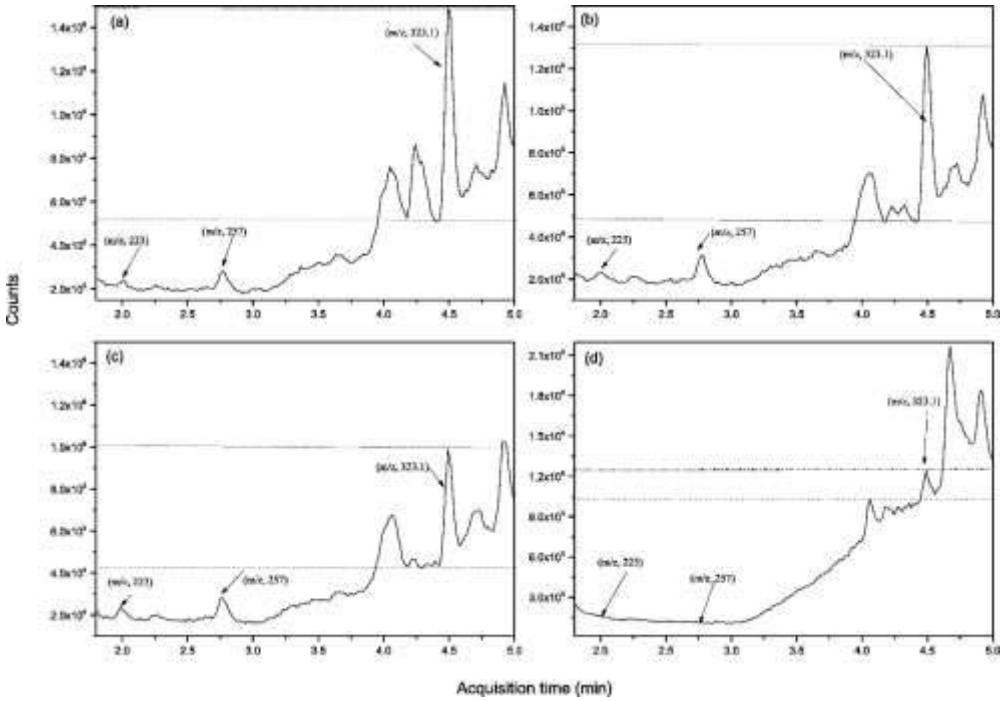

Figure 4.4.13: Chloramphenicol transformation products highlighted by their retention times after 10 min (a), 30 min (b), 150 min (c), and 12 h (d) using nZVI-fBC in synthetic wastewater during the 1st cycle application. LC-MS/QTOF method run for 13 min and data plotted up to 5 min.

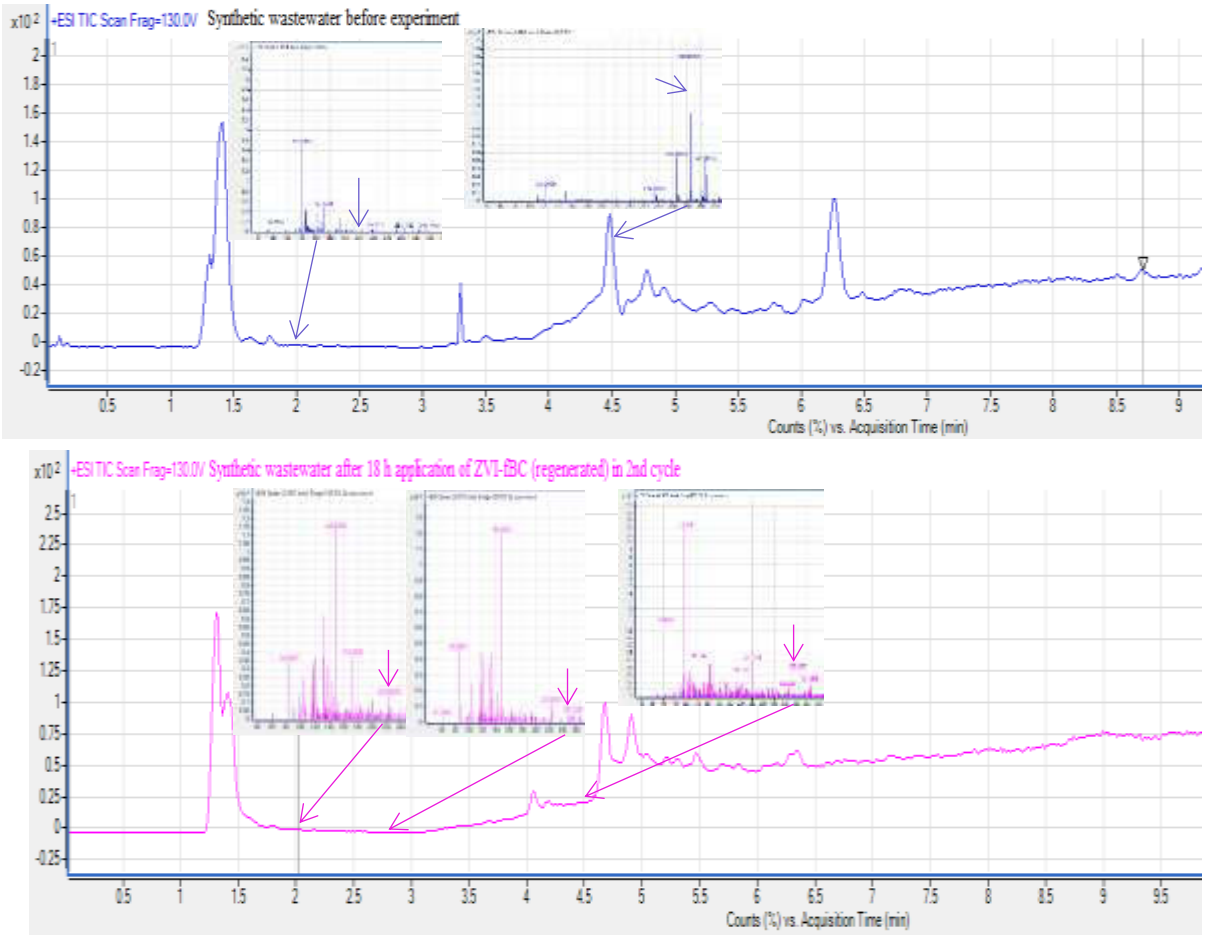

Figure 4.4.14: The 2nd cycle application of nZVI-fBC (nZVI-fBC transformed to nFe_3O_4-fBC) for the removal of chloramphenicol from synthetic wastewater. Small fraction of reduced product indicates that sorption was dominating in the 2nd and subsequent cycles.

4.4.3.6. *Mechanism of Chloramphenicol Sorption by nZVI-fBC and nFe_3O_4-fBC Composite at pH 4.0–4.5*

The removal ability of chloramphenicol by nZVI-fBC composite can be considered as two processes namely sorption (by both magnetic iron oxide and fBC) and reduction (by surface nZVI). The reduction mechanism has already been discussed in **Section 4.4.3.5**. Chloramphenicol has hydrogen bond donors and acceptors groups according to its chemical structure. The application of nZVI-fBC composite was conducted at pH around 4.0–4.5 and the sorption mechanism can be discussed below. FTIR, Raman spectra, XPS and EDS analysis of nZVI-fBC confirmed the presence of different free functional groups (e.g. C=C, –COOH, –OH and π-π*) and iron particles (such as BC-COO-Fe-OOC-BC, BC-O-Fe-O-BC, fBC-iron/iron oxide) (**Figures 4.4.4, 4.4.5, 4.4.6 and 4.4.7**). Chloramphenicol is non-ionisable compound and hydrolysis does not occur at pH 2–7 [358]. Thus, in the pH range of 4.0–4.5,

proton exchange with water molecules is unfavorable (chloramphenicol + H_2O + fBC = Chloramphenicol$^+$ …fBC + OH^-) [244]. Generally, any carbonaceous surface -COOH group has pK_a value of ~3.0–5.0[59, 351] and chloramphenicol has a pK_a value of ~5.5. So chloramphenicol could form hydrogen bonds at pH below 5.5 among fBC surface free functional groups (mostly -COOH) and nitro group present in chloramphenicol. This kind of chemical bonds are called charge assisted hydrogen bond (CAHB) (chloramphenicol-NO_2 -----HOOC- BC). Hydrogen bonds between surface carboxylic groups of fBC and hydroxyl groups in chloramphenicol also played a major role for the maximum sorption at this pH (chloramphenicol-OH-----HOOC-fBC). Strong electron donor-acceptor (EDA) interactions were favourable at the pH range 4.0–4.5 [21]. fBC surface is abundant with C=C aromatic carbon along with -OH groups (arene-OH) which can act as a π-electron donor (arene units as δ^- due to resonance effect of -OH groups), while chloramphenicol has nitro groups in its arene units which can act as π-electron acceptors (arene unit as δ^+ site in chloramphenicol due to resonance effect in the presence of sorbent) due to stronger EDA interactions (**Figure 4.4.15).** Electron-acceptor-acceptor (EAA) interaction might also be possible between fBC surface free C=O groups (BC-C=O) and chloramphenicol arene units at this pH range although such interactions may not be strong. EAA interactions for -COOH/-COOFe- groups in fBC may not occur within this pH range as -COOH takes part in CAHB formation. Additionally, CAHB formation with surface hydroxyl groups (pK_a > 7.5) of biochar was not possible due to higher pK_a value. Moreover, based on Raman spectra, it was found that the G and D band peak intensity ratio (I_G/I_D) significantly decreased after sorption (**Figure 4.4.5**). This clearly indicated strong interaction among surface functional groups and chloramphenicol molecules. FTIR peak shifted to a point where C=O (~1720 cm^{-1}) or -COOH functional groups (~1028 cm^{-1}) as well as -OH groups (3600–3800 cm^{-1}) locate due to the sorption of chloramphenicol onto biochar surfaces (**Figure 4.4.6**) [55]. Thus, maximum sorption of chloramphenicol in this pH range was due to formation of CAHB and weak hydrogen bonds along with stronger EDA and EAA interactions in fBC surface free functional groups.

In addition, nZVI-fBC surface contains iron species in different forms such as BC-COO-Fe-OOC-BC, BC-O-Fe-O-BC and fBC-iron oxide particles. After application in the 1st stage, I_G/I_D ratio increased compared to initial nZVI-fBC implied that fBC functional groups became free and the intensity ratio increased (**Figure 4.4.5**). XPS O1s spectra also indicated that stable magnetic Fe_3O_4 produced during the 1st cycle of application (**Figure 4.4.7**). The

results clearly implied that functional groups (-COOH/-OH/C=O) of fBC were distributed through different iron species on nZVI-fBC surface. Thus, sorption was fast through quick interaction of iron containing functional groups with nitro and hydroxyl functional groups of chloramphenicol. The formation of these bonds was stronger and faster compared to CAHB due to higher electron affinity of iron or iron oxides or, cation exchange capacity of iron towards chloramphenicol than carboxylic group hydrogen on biochar surface. Hence, sorption using nZVI-fBC required less time (∼12–15 h) for the complete removal of the same amount of chloramphenicol. Separate experiments on the sorption of chloramphenicol using only fBC found that it took over 24 h for the complete sorption of the same amount of chloramphenicol at the same conditions. Further applications of this composite fully turned it into a stable magnetic-fBC composite, and sorption was accelerated due to formation of iron-oxide complex with chloramphenicol:

BC-COOFe-/-OFe- or, fBC-iron oxide → fBC-iron-oxygen complex (–NO_2 in chloramphenicol) or, BC-iron-hydroxyl complex (–OH in chloramphenicol) (4.4.8)

4.4.*3.7. Percentage Sorption and Reduction of Chloramphenicol and Reusability of the Materials*

The amount of reduction and sorption of chloramphenicol using nZVI-fBC composite was calculated, with ∼28% reduction and ∼70% sorption for deionized water, ∼32.5% reduction and ∼67.5% sorption for synthetic wastewater, and ∼31% reduction and ∼69% sorption for lake water, respectively (**Figure 4.4.16a**). The results clearly indicated that nZVI-fBC composite had simultaneous sorption and reduction capability. After 2nd cycle application of nFe_3O_4-fBC composite (nZVI-fBC transformed to nFe_3O_4-fBC), desorption amount increased significantly up to ∼91.5%, ∼90.9% and ∼88.2% for deionized water, synthetic wastewater and lake water, respectively. These values confirmed that the application of nFe_3O_4-fBC composite from 2nd cycle onwards was solely due to sorption process (**Figure 4.4.16**). Therefore, the reductive nature of nZVI-fBC composite was fully turned into sorptive nature from the transformation of nZVI-fBC to nFe_3O_4-fBC composite. Further sorption/desorption experiments confirmed that the nFe_3O_4-fBC composite can be regenerated thermally in a repetitive manner up to six cycles, and can maintain excellent reusability with ∼100% chloramphenicol removal up to > 7 cycles of applications (**Figure 4.4.16b**).

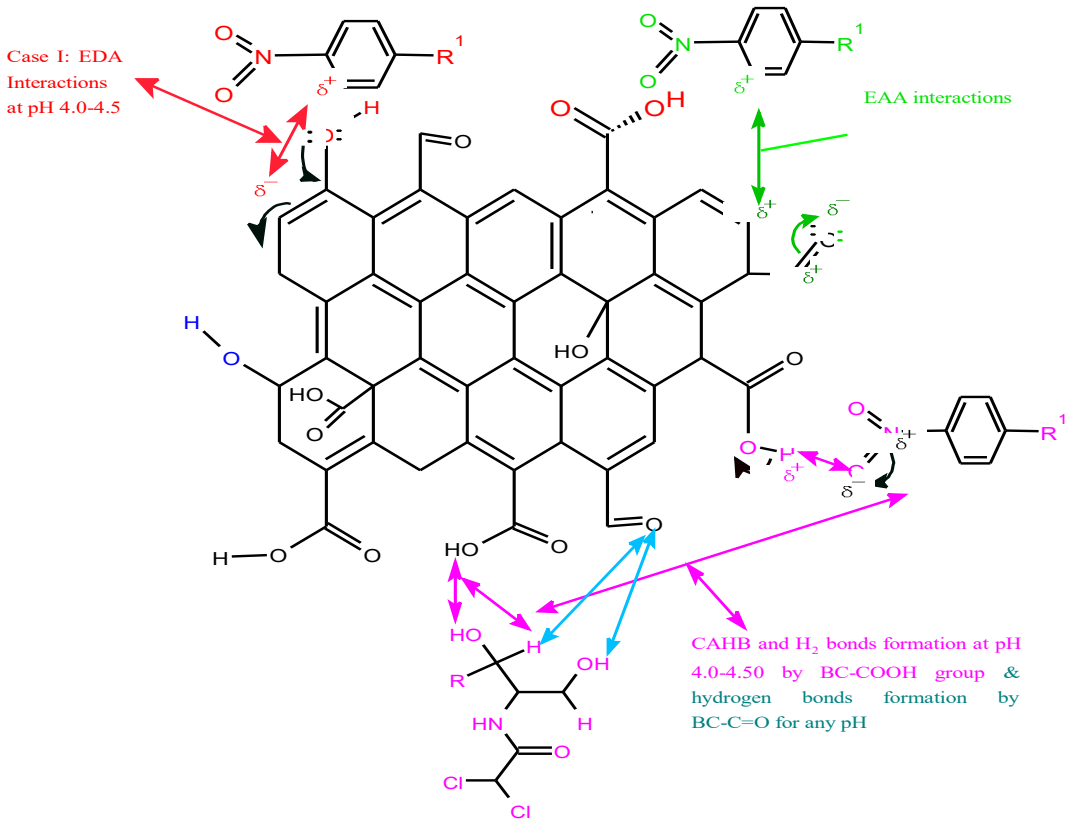

Figure 4.4.15: Chloramphenicol sorption mechanisms at pH 4.0-4.5.

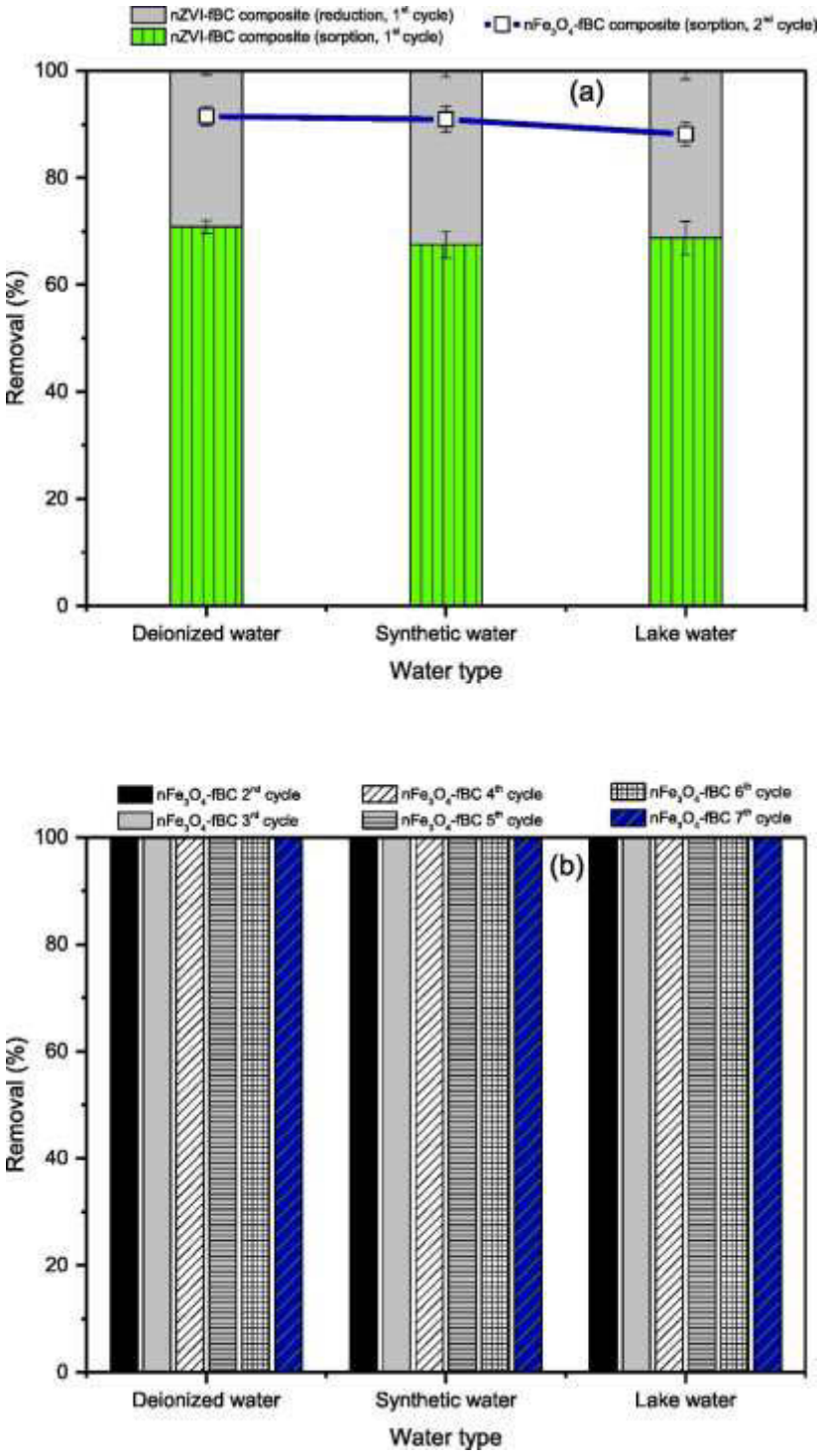

Figure 4.4.16: Percentage of sorption and reduction (cumulative basis, after excluding the amount of recoverable chloramphenicol) using nZVI-fBC composite (in the 1st cycle) followed by sorption only onto nFe_3O_4-fBC composite (a). Reusability of nFe_3O_4-fBC composite for the repetitive applications (up to 7th cycle) for the removal of chloramphenicol (3.10 μM L^{-1} initial concentration) at pH 4.0–4.5, 25 °C from different water (b).

4.4.*3.8. Application of nFe$_3$O$_4$-fBC Composite to Remove Methylene Blue*

After six cycles of application for the removal of chloramphenicol, the nFe$_3$O$_4$-fBC composite was used for the sorption of methylene blue. The results indicated that the magnetic composite took ~90 min, ~140 min and ~210 min for the complete removal of 2.5, 5.0 and 10.0 mg L^{-1} methylene blue, respectively. In addition, the maximum Langmuir sorption capacity of nFe$_3$O$_4$-fBC composite for sorption of methylene blue was found to be 285.25 mg g^{-1} with high r^2 (0.981). Maximum Freundlich sorption constant value was found to be 82.06 mg^{1-n} L^n g^{-1} (**Figures 4.4.17 and 4.4.18**). The sorption capacity was higher than reported values of 64.7–270 mg g^{-1} using different carbon materials such as activated carbon, graphene and carbon nanotube [375-377]. Thus, nFe$_3$O$_4$-fBC composite showed high sorption capability of methylene blue even after six cycles of application in chloramphenicol removal.

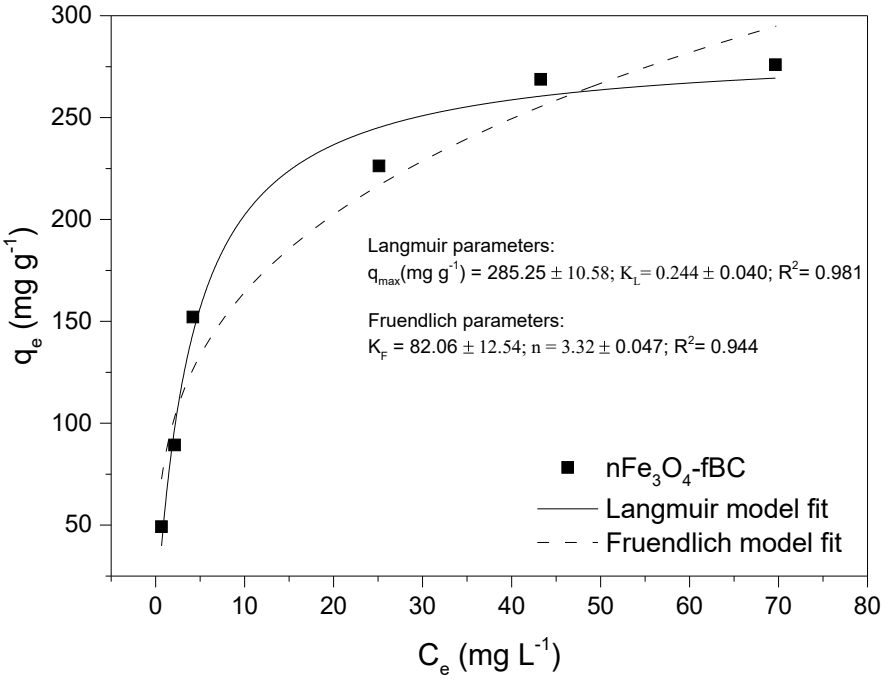

Figure 4.4.17: Sorption of methylene blue by nFe3O4-fBC with the Langmuir and Freundlich model fit.

Figure 4.4.18: Use of a magnet bar to demonstrate easy separation of nFe_3O_4-fBC composite after experiments.

4.4.4. Concluding Remarks

The interactions of nZVI and nZVI-fBC composite with chloramphenicol were very effective even in different water types. nZVI showed fast reduction capability. Although successfully immobilized, the nZVI-fBC composite quickly changed into magnetic-biochar composite (nFe_3O_4-fBC) during the 1st stage of application, within a few hours, possessing simultaneous reduction (29–32.5%) and sorption (67.5–70.5%) capabilities. Further interactions leading to sorptive behavior of newly formed nFe_3O_4-fBC composite and sorption had accelerated to next stage of applications with synergistic effect for chloramphenicol than fBC only. The removal of chloramphenicol was almost similar with different water types. Thermal regeneration of the magnetic composite showed excellent performance up to seven cycles, which can further remove methylene blue subsequently. Therefore, the results demonstrate further research is needed on nZVI immobilization onto biochar due to the instability of the immobilized nZVI-fBC composite. Overall, the transformed magnetized composite can serve as a powerful sorbent for chloramphenicol, methylene blue and other similar organic contaminants from water and wastewater.

UNIVERSITY OF TECHNOLOGY SYDNEY

Faculty of Engineering and Information Technology

CHAPTER: FIVE

ENDOCRINE DISRUPTORS REMOVAL BY FUNCTIONALIZED BIOCHAR: MECHANISMS AND APPLICATIONS IN WASTEWATER TREATMENT

CHAPTER FIVE: ENDOCRINE DISRUPTORS REMOVAL BY FUNCTIONALIZED BIOCHAR: MECHANISMS AND APPLICATIONS IN WASTEWATER TREATMENT

5.1. Sorptive Removal of Phenolic Endocrine Disruptors by Functionalized Biochar: Competitive Interaction Mechanism, Removal Efficacy and Application in Wastewater

5.1.1. Introduction

EDCs can cause adverse effects due to exogenous endocrine disruption in the reproductive, sexual differentiation, neurological and immune systems even at low concentrations (ng L^{-1} to μg L^{-1}), and have attracted increasing attention [27, 43]. Phenolic structure based compounds such as the natural estrogens 17β-estradiol (E2), estriol (E3) and estrone (E1), synthetic estrogen 17α-ethynylestradiol (EE2), and industrial compounds such as octylphenol, nonylphenol, 4-tert-butyl phenol (*4t*BP) and bisphenol A (BPA), are the most potent EDCs. EDCs are poorly removed in sewage treatment plants [26, 28, 43, 44] and are a primary source of their discharge and occurrence in surface water, groundwater, seawater and sediment [26, 45]. EDCs are relatively hydrophobic organic compounds according to their octanol-water partition coefficient (K_{ow}) values and have only one pK_a value. The chemical structures and physicochemical properties of the EDCs are shown in **Figure 2.2 and Table 2.2**, respectively.

Many separation processes such as coagulation, flocculation and precipitation have been used for the removal of EDCs from different water [28, 44]. Conventional biological processes such as activated sludge, constructed wetlands, bio-filtration have shown limited removal of EDCs [28, 44], while advanced treatment processes such as granular activated carbon, photolysis, photocatalysis, ferrate [26] free radical oxidation, Fenton oxidation, sonolysis, membrane separation, chlorination and ozonation have shown more satisfying results [28, 34, 44, 46]. Some hybrid systems such as membrane bioreactor (MBR) followed by ultrafiltration/nanofiltration/reverse osmosis, flocculation followed by activated sludge and ultrafiltration can also remove EDCs efficiently from water and wastewater [44, 47]. However, a major problem of hybrid systems is the high capital investment and operation cost. Physical separation processes such as activated carbon adsorption, membrane filtration and ion exchange usually show superior removal efficiencies of the EDC [29, 48]. Adsorption of EDCs on carbonaceous materials has been studied using activated carbon [49-51] black carbon,

single- or multi-walled carbon nanotubes (SWCNT, MWCNT) [52, 53] and biochar [26, 54, 55]. Biochar is a low-cost sorbent for the efficient removal of many hydrophilic and hydrophobic organic contaminants [56, 57]. Sorption of EDCs has also been studied using alumina, silica and hydrophobic medium [58].

So far, the sorption of EDCs has been studied using single compound, although there are reports on using membrane-based processes for mixture removal. Although carbonaceous materials such as CNT, graphene, activated carbon and biochar may have natural properties to sorb different organic contaminants simultaneously from water, such data, especially on EDCs, is scarce. Little is known about their sorptive behaviour, mechanism, affinities and distribution coefficient in the competitive mode using carbonaceous materials. Therefore, this study was focused on the competitive removal of six EDCs namely E1, E2, E3, EE2, BPA and *4t*BP using functionalized biochar (fBC). The objectives were to study (i) the competitive sorption of EDCs using fBC, [92] the detailed mechanism of EDCs' sorption, (iii) the trend of EDCs' removal by fBC, and (iv) the removal efficiency of EDCs from synthetic wastewater and MBR sewage effluent for practical applications.

5.1.2. Experimental

5.1.2.1. Chemicals and fBC Sorbent

E1 (99%), E2 (>98%), E3 (>97%), EE2 (98%), BPA (99%), and *4t*BP (99%), and organic solvents such as methanol, acetonitrile of HPLC grade were purchased from Sigma-Aldrich, Australia. Formic acid was of 99.9% purity. Potassium chloride (≥99.0%) and sodium chloride (≥99.5%) were of analytical grade. *Eucalyptus globulus* was donated by New Forest Asset Management Pty Ltd, Portland, Victoria, Australia.

First 30 g of *Eucalyptus globulus* wood particles (0.425–1.00 mm size) were pyrolyzed to obtain biochar at 400 °C under flowing nitrogen at 2.5 psi for 2 h. The biochar yield was 34.0–35.0%. The activation of biochar was carried out following a method described previously [244]. Briefly, biochar was activated by soaking in 50% *ortho*phosphoric acid (*o*H_3PO_4) with the impregnation ratio 1:1 (w/v, taking *o*H_3PO_4 as 100%) for 3 h at 50 °C followed by heating at 600 °C for another 2 h. Prepared material was cooled in the reactor, washed several times with distilled water, and the pH was adjusted to ~7, followed by drying overnight at 100 °C. After activation, ~15–20% weight loss (activated burn off) was observed. The average particle size of activated biochar was in the range 75–600 µm. As the activated biochar was enriched with different functional groups such as -COOH, -OH, C=O and C=C on

its surface, (based on X-ray Photoelectron Spectroscopy (XPS) characterization) the prepared activated biochar was termed as fBC-2.

5.1.2.2. EDCs Sorption on fBC-2 in Different Water

Competitive sorption experiments of EDCs on fBC-2 were conducted in 50 mL glass vials with Teflon-lined screw caps at 25 °C in duplicate. EDCs were dissolved in methanol to prepare the stock solution of 1.0 g L^{-1}. The final methanol content in the sorption system was <0.5% (v/v) to avoid the co-solvent effect. To study the effect of pH, the interaction of pre-equilibrated fBC-2 (20 mL of solution at the same solution pH) with EDC mixture in solution (25 mL) was carried out at different pH values (1.86, 3.1, 4.0, 5.1, 5.96, 7.85, 9.0 and 10.85) for 42 h at 25 °C. The initial concentration of each EDC in the mixture was adjusted to ~500 µg L^{-1}. Competitive sorption isotherm and kinetics experiments of EDCs in duplicate were also performed on an orbital shaker at 110 rpm, 25 °C for 48 h at pH ~ 3.0–3.25. Constant ionic strength was maintained using 0.01 M NaCl. The solid phase sorption (q_s, µg g^{-1}) and sorption distribution coefficient (K_d, L kg^{-1}) were calculated. The initial concentrations of each EDC were in the range ~250 µg L^{-1} to ~3000 µg L^{-1} in the mixture solution. The control experiments without sorbents were also performed. The sorbent dosage was selected for 15–95% sorption of each EDC at different concentrations. After equilibrium, the pH was measured, and the solution was filtered through a 0.2 µm PTFE filter and analyzed by high-performance liquid chromatography (HPLC). Raw biochar showed low removal efficiency. Hence, the discussion on the results obtained with unmodified biochar is not presented here.

The removal of EDCs spiked to synthetic wastewater, and MBR effluent (collected from Central Park, Sydney, Australia) were also studied. The chemical composition of synthetic wastewater is as follows: peptone (2.37 mg L^{-1}), beef extract (1.8 mg L^{-1}), humic acid (4.2 mg L^{-1}), tannic acid (4.2 mg L^{-1}), sodium lignin sulphonate (2.4 mg L^{-1}), Na-lauryl sulphate (0.94 mg L^{-1}), acacia gum powder (4.37 mg L^{-1}), arabic acid (5.0 mg L^{-1}), ammonium sulphate (7.1 mg L^{-1}), K_2HPO_4 (7.0 mg L^{-1}) and $MgSO_4 \cdot 3H_2O$ (0.71 mg L^{-1}) [378]. MBR effluent was filtered (1.2 µm) before being stored at 4 °C. MBR effluent and synthetic wastewaters were spiked with ~500 µg $L^{-1}$of each EDC in the mixture before interaction with fBC-2 for 44–64 h at pH 3.0–3.25, (maximum sorption-based on the pH study) at 25 °C. Different dosages of fBC-2 were used to study the removal of EDCs in competitive mode. The concentrations of the target EDCs in the MBR effluent were lower than the limit of detection (LOD). Hence EDCs were spiked to MBR effluent. Synthetic wastewater and MBR effluent

were used to examine the effect of different constitutes (organics and inorganics) present in these waters, on the removal of EDCs. The physicochemical properties of MBR sewage effluent and synthetic wastewater are listed in **Table 5.1.1**.

Table 5.1.1: Physicochemical characteristics of synthetic wastewater and MBR sewage effluent.

Parameter	Synthetic wastewater	MBR effluent
pH	7.41	7.55
Conductivity (μS cm^{-1})	56.3	621.0
Dissolved organic carbon, DOC (mg L^{-1})	5.4	8.0
Inorganic carbon (mg L^{-1})	3.71	39.23
Turbidity (NTU)	1.79	0.40
UV_{254} (cm^{-1})	0.325	0.191
Alkalinity (mg $CaCO_3$ L^{-1})	6.0	27.5
Chemical oxygen demand, COD (mg L^{-1})	23.6	26.2
Dissolved oxygen, DO (mg L^{-1})	8.5	5.2
Cl^- (mg L^{-1})	1.47	32.68
Br^- (mg L^{-1})	0.65	0.54
NO_3^- (mg L^{-1})	0.34	35.30
NO_2^- (mg L^{-1})	0.04	0
PO_4^{3-} (as P) (mg L^{-1})	3.82	0.21
SO_4^{2-} (mg L^{-1})	6.95	33.03
Na^+ (mg L^{-1})	3.04	103.88
K^+ (mg L^{-1})	2.25	21.82
Ca^{2+} (mg L^{-1})	0.18	19.99
Mg^{2+} (mg L^{-1})	0.15	4.95
Fe^{3+} (mg L^{-1})	0.08	0.10
Al^{3+} (mg L^{-1})	0	0.05

Table 5.1.2: Limit of detection (LOD) of EDCs by HPLC equipped with UV and fluorescence detectors.

EDC	LOD ($\mu g\ L^{-1}$)	Detector
E3	3.33	Fluorescence detector
BPA	6.97	Fluorescence detector
4TBP	6.65	Fluorescence detector
E2	4.60	Fluorescence detector
E1	25.80	UV detector
EE2	3.80	Fluorescence detector

5.1.2.3. Characterization of fBC-2

Microscopic analysis of fBC-2 before and after EDC sorption was carried out using scanning electron microscope (SEM) (Zeiss Evo-SEM). Brunauer-Emmett-Teller [127] nitrogen adsorption-desorption isotherms and Barrett-Joyner-Halenda (BJH) method were used to calculate specific surface area and the porosity of fBC-2 using a Micromeritics 3 FlexTM surface characterization analyzer at 77 K. The bulk elemental analysis (C, H, O, N, P) of fBC-2 was determined using Oxford energy dispersive X-ray spectroscopy (EDS) and XPS (Thermo Scientific, UK). A Renishaw inVia Raman spectrometer (Gloucestershire, UK) equipped with a Leica DMLB microscope (Wetzlar, Germany) and a 17 mW Renishaw helium-neon laser source at 633 nm (with 50% of the laser intensity) with CCD array detector was used for Raman spectroscopy. The fBC-2 was added to 0.01 M KCl solution at eight different pH values for 46 h to measure its zeta potential (Nano-ZS, Malvern).

5.1.2.4. Analyses of EDCs

EDCs were analyzed by HPLC with an auto-sampler and a reverse-phase Zorbax Bonus RP C_{18} column (5.0 µm, 2.1 × 1.50 mm, Agilent Technologies), with an injection volume of 100 µL. Mobile phase "A" was composed of acetonitrile and formic acid (99.9: 0.1) while mobile phase "B" consisted of Milli-Q water and formic acid (99.9: 0.1). The elution used 40% of "A" and 60% of "B" at a flow rate of 0.4 mL min^{-1}, which was changed to 0.3 mL min^{-1} at 0.1 min and maintained until 9.0 min. After 9 min, the flow rate was changed to 0.2 mL min^{-1} and maintained up to 24 min. EDCs were analyzed with a UV detector at 285 nm

and a fluorescence detector at 280 nm (excitation wavelength) and 310 nm (excitation wavelength). Fluorescence and UV wavelength were kept unchanged throughout the analysis. The method LOD for each EDC is given in **Table 5.1.2**.

5.1.2.5. Modelling of Sorption Kinetics, Thermodynamics and Isotherms

The sorption data were fitted to four kinetic models, namely pseudo first-order (PFO), pseudo second-order [306], the Weber–Morris intra-particle diffusion model [17] and the external mass transfer models as follow:

PFO: $q_t = q_s(1 - e^{-K_1 t})$ (5.1.1)

PSO: $q_t = \frac{K_2 q_s^2 t}{1+K_2 q_s t}$ (5.1.2)

IDM: $q_t = K_i t^{\frac{1}{2}} + C$ (5.1.3)

$[\frac{d(C_t/C_o)}{dt}]_{t=0} = -\beta S$ (5.1.4)

where K_i is the apparent diffusion rate constant (g μg^{-1} min$^{-1/2}$), q_t (μg g^{-1}) is the sorbed mass at time t, q_s (μg g^{-1}) is the equilibrium sorbent mass, K_1 (min^{-1}) is the PFO kinetic rate constant, K_2 (μg g^{-1} min^{-1}) is the PSO kinetic rate constant, and C is a constant (μg g^{-1}) that provides the thickness of the boundary layer [244]. C_0 and C_t (μg L^{-1}) represent the concentrations of EDCs in solution at the beginning and at time t, respectively, β (cm min^{-1}) is the external mass transfer coefficient, and S (cm^{-1}) is the specific surface of fBC-2 for external mass transfer. the βS value was calculated from the slope of the C_t/C_0 versus t plot [28].

Gibbs free energy (ΔG°, kJ mol^{-1}) of EDCs sorption onto fBC-2 at 25 °C was estimated with different concentrations using **Eq. (**5.1.**5)** [28]:

$\Delta G^0 = -RT\ lnK_d$ (5.1.5)

where K_d (L kg^{-1}) is the apparent individual sorption distribution coefficient and can be defined by the ratio of sorbed EDC concentration (q_s, μg g^{-1}) to aqueous EDC concentration (C_w, μg L^{-1}), using **Eq.** 5.1.6:

$K_d = 1000 \times \frac{q_s}{C_w} = 1000 \times \left(\frac{C_0 - C_w}{C_w}\right)\frac{V}{M}$ (5.1.6)

where V (L) is the solution volume, and M (g) is the sorbent mass.

The sorption data were also fitted to the Langmuir isotherm model which is represented below [378]:

Langmuir model: $q_s = \frac{q_{max} K_L C_w}{1+K_L C_w}$ (5.1.7)

where q_{max} is the maximum adsorption capacity (μg g^{-1}) and K_L is the Langmuir fitting parameter (L μg^{-1}). Parameters were estimated by nonlinear regression weighted by the dependent variable.

The sorption data obtained were used to calculate the total competitive sorption capacities using summarized Langmuir sorption **(Eqs. (**5.1.**8) and (**5.1.**9))**. Since all the competitive solutes interact and compete for the same sorption sites in fBC-2, the overall maximum sorption capacity of fBC-2 can be estimated by the additive contribution of each EDC's maximum sorption capacity [244]. The combined Langmuir model for six EDCs in competitive mode can be written as:

$$q_{total} = \frac{q_{max1}K_{L1}C_{s1}}{1+K_{L1}C_{s1}} + \frac{q_{max2}K_{L2}C_{s2}}{1+K_{L2}C_{s2}} + \frac{q_{max3}K_{L3}C_{s3}}{1+K_{L3}C_{s3}} + \frac{q_{max4}K_{L4}C_{s4}}{1+K_{L4}C_{s4}} + \frac{q_{max5}K_{L5}C_{s5}}{1+K_{L5}C_{s5}} + \frac{q_{max6}K_{L6}C_{s6}}{1+K_{L6}C_{s6}} \quad (5.1.8)$$

$$q_{max.(total)} = q_{max1} + q_{max2} + q_{max3} + q_{max4} + q_{max5} + q_{max6} \quad (5.1.9)$$

where q_{max1},q_{max2}, q_{max3}, q_{max4},q_{max5} and q_{max6} are the maximum Langmuir sorption capacity for E1, E2, E3, EE2, BPA and 4*t*BP, respectively. $q_{max.(total)}$ is the total maximum Langmuir sorption capacity of the fBC-2 for EDC mixtures, estimated by the summation of individual EDC's maximum sorption capacities.

5.1.3. Results and Discussion

5.1.3.1. Characterization of fBC-2 and EDCs

The structure of the carbon network in fBC-2 was analyzed by SEM, BET, XPS, FTIR and Raman spectra. SEM images of fBC-2 after sorption experiments showed the development of flakes like structure on the fBC-2 surface (**Figure 5.1.1**).

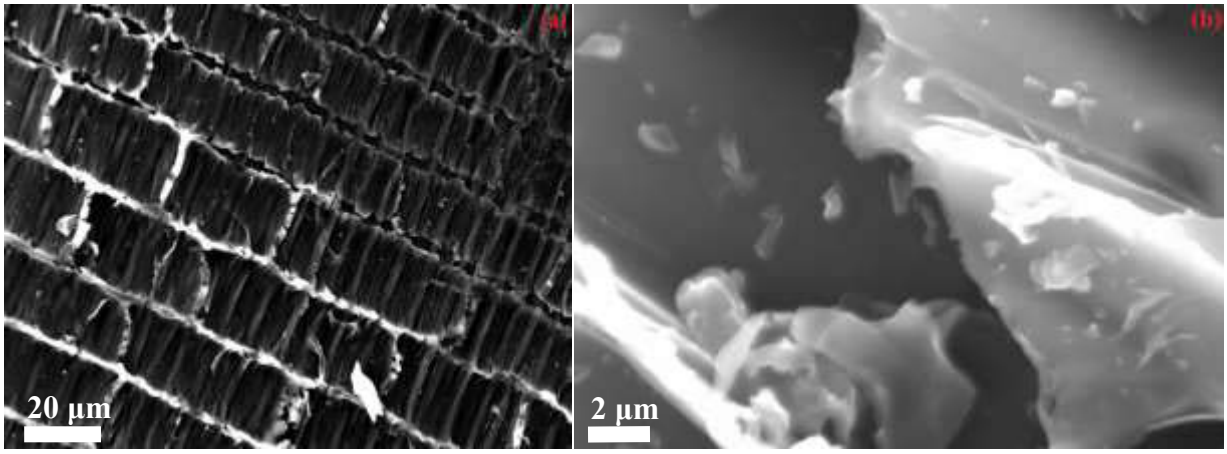

Figure 5.1.1: SEM image of fBC before (a) and after (b) sorption of EDCs.

Figure 5.1.2a represents the nitrogen adsorption-desorption isotherm plot of fBC-2. This clearly indicates that isotherm plot was found to be type II isotherm. This isotherm features N_2-uptake increment up to a relative pressure of 0.5 then slightly reduced followed by an increment of N_2 adsorption (relative pressure up to 1.0) to reach a plateau. This result suggested the existence of mesopore (2–50 nm) and macrospore (>50 nm) structure of fBC-2 and the isotherm indicate unrestricted monolayer-multilayer adsorption [379, 380]. More clearly, the arrow (**Figure 5.1.2a**) point, the beginning of the most linear middle section of the isotherm indicating the point at which monolayer coverage is complete and multilayer adsorption is about to begin. On the other hand, **Figure 5.1.2b** shows the presence of mesopores (~2–50 nm) in fBC-2 core structure which has been calculated from the adsorption branch of the isotherm by the BJH method [381]. Thus, the fBC-2 mostly contained meso and macroporous structures and tis indicated that the activation method did not lead to the development of microporous (<2.0 nm) structures. Also, BET and Langmuir surface area were found to be 1.18 and 8.22 $m^2 g^{-1}$, respectively which was much lower than the reported values [382]. The BJH adsorption cumulative surface area of pores was also found to be 1.37 $m^2 g^{-1}$ and Dubinin-Astakov micropore surface area was found to be 0.52 $m^2 g^{-1}$ (**Table 5.1.3**).

Table 5.1.3: Summary of BET and BJH physical parameters for fBC-2.

Parameter	Value
Single point surface area at P/Po = 0.30	1.05 $m^2 g^{-1}$
BET Surface Area	1.18 $m^2 g^{-1}$
Langmuir Surface Area	8.22 $m^2 g^{-1}$
t-Plot Micropore Area	1.84 $m^2 g^{-1}$
t-Plot External Surface Area	1.84 $m^2 g^{-1}$
BJH Adsorption cumulative surface area of pores between 17 Å and 3000 Å diameter	1.37 $m^2 g^{-1}$
BJH Desorption cumulative surface area of pores between 17 Å and 3000 Å diameter	1.54 $m^2 g^{-1}$
Pore Volume	

BJH Adsorption cumulative volume of pores between 17 Å and 3000 Å diameter	2.74 $cm^3\ kg^{-1}$
BJH Desorption cumulative volume of pores between 17 Å and 3000 Å diameter	2.55 $cm^3\ g^{-1}$
Dubinin-Astakov	
Micropore surface area	0.52 $m^2\ g^{-1}$
Limiting micropore volume	0.24 $cm^3\ kg^{-1}$
Pore Size	
BJH Adsorption average pore diameter (4V/A)	79.69 Å i.e. 7.97 nm
BJH Desorption average pore diameter (4V/A)	66.20 Å i.e. 6.62 nm
D-H Adsorption average pore diameter (4V/A)	75.69 Å i.e. 7.57 nm
D-H Desorption average pore diameter (4V/A)	68.603 Å i.e. 6.86 nm

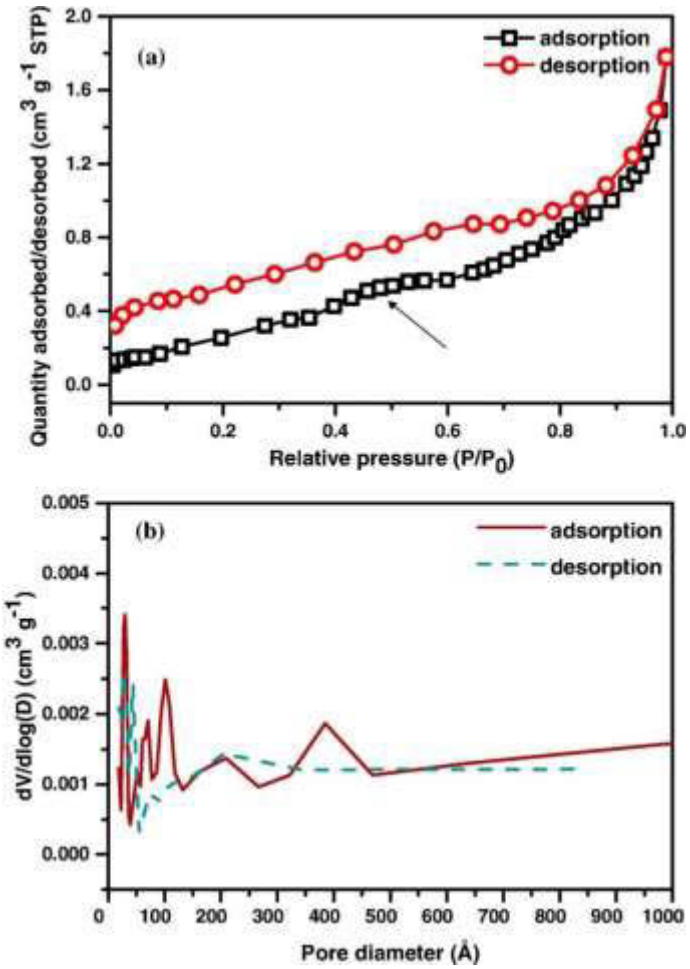

Figure 5.1.2: Nitrogen adsorption–desorption isotherm for fBC-2: Barret-Joyner-Halenda (BJH) surface/volume mesopore analysis (a), and cumulative pore size distribution (b).

The Raman spectroscopy on fBC-2 showed two characteristic peaks at 1341 and 1588 cm^{-1} (**Figure 5.1.3**), which correspond to the D-band (disordered structure) and G-band (graphitic structures) of sp^2-type carbon present in fBC-2 [244, 344]. The relative band intensity ratio (I_G/I_D) is 1.04 (>1), demonstrated the functionalization in fBC-2. It is important to note that Raman spectra of fBC-2 featured a strong D-band, which illustrated a slightly more amorphous character (disordered) of the carbon in fBC-2 owing to more oxygenated functional groups on its structure as functionalization of biochar was carried out using acid. D-band surface defect was possible by the introduction of other elements onto carbon structure during fBC-2 preparation.

XPS results indicated that fBC-2 was rich in different functional groups especially –C=C-, -C=O and –O-C=O [383]. Carbon (C1s) spectra of fBC-2 showed that fBC-2 surface was composed of aromatic carbon mostly –C=C- (284.8 eV) due to long chain arene unit, -C=O (286.3 eV), -C=O (287.8 eV), -COOH (289 eV) and π-π* (292.35 eV) due to functional groups

(**Figure 5.1.4a**). Also, fBC-2 surface contained oxygenated and phosphorous-based functional groups/complexes. O1s spectra showed that oxygen content was mostly in the form of organic carbon (at 533.3 and 531.62 eV) (**Figure 5.1.4b**) [384]. The P2p XPS spectrum of fBC-2 showed a peak at 133.79 eV in the form pentavalent tetra coordinated phosphorus (PO_4 i.e. C-O-PO_3), as in polyphosphates and/or phosphates (**Figure 5.1.4c**) [385]. The survey peaks showed the same results (**Figure 5.1.4d**). The elemental composition of fBC-2 was found to be 81.76% C, 13.32% O, 0.8% N and 2.3% P from XPS.

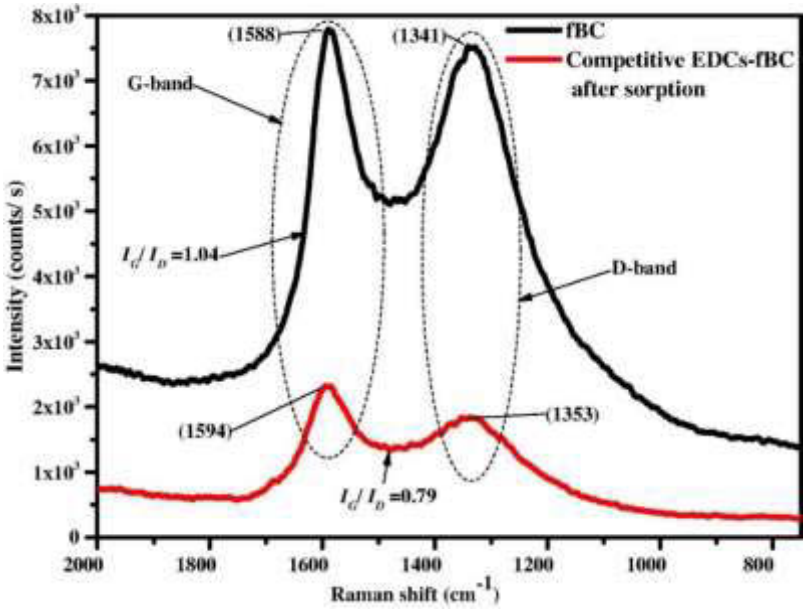

Figure 5.1.3: Raman spectra for fBC-2 before and after sorption experiments. Raman shifts measurement was carried out using Renishaw inVia Raman spectrometer equipped with a 17 mW Renishaw Helium-Neon Laser 633 nm and CCD array detector at 50% laser intensity.

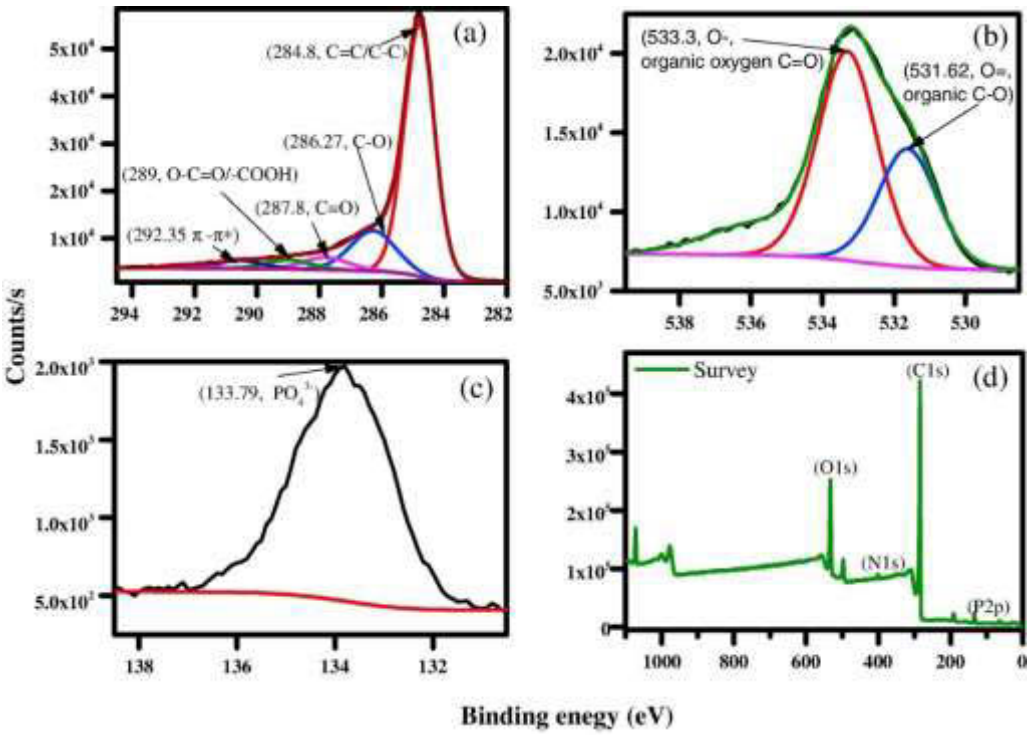

Figure 5.1.4: XPS analysis of fBC-2. Spectra were obtained by plotting counts against binding energy in a wide scan for C1s (a), O1s (b), P 2p(c) and overall survey (d).

5.1.*3.2. Effect of pH on Competitive Sorption of EDCs*

The effect of pH for competitive EDCs' sorption against the solid-phase concentration of each EDC is shown in **Figure 5.1.5a**. The sorption of individual EDC by fBC-2 was highly pH dependent and was found to be moderate at very low pH ~ 1.85 (where fBC-2 became positive). At this pH, q_s values of all EDCs were found to be low, which might be due to the repulsion between the positively charged fBC-2 (zeta potential value was positive) and protonated EDCs (**Figure 5.1.5b**). However, the EDC sorption at this pH might be due to the electron-donor–acceptor (EDA) interactions between oppositely charged arene units. Increase in pH from 1.85 to 3.5 increased the sorption capacity significantly. The q_{max}values of individual EDCs were ~4110, ~3356, ~3333, ~3350, ~2765 and ~2725 $\mu g\, g^{-1}$for E1, E2, EE2, BPA, 4tBP and E3, respectively. The maximum sorption of EDCs could be due to EDA interactions along with strong hydrogen bonds formation [302, 378]. Further increase in pH from 3.5 to pH 5.0 led to a significant reduction of the sorption of each EDC. However, when pH was increased above 5.0, another high q_s value for EDC was observed at pH near 8.0. This was due to pK_a values (pH = pK_a + log[salt/acid]) of each EDC and surface hydroxyl groups on fBC-2, which were responsible for the formation of strong hydrogen bonds together with EDA interactions with the fBC-2 surface functional groups. Further pH increases up to 10.85 caused

a decrease of q_s value of each EDC because of the highly repulsion between the negatively charged fBC-2 and the EDCs. Hydrogen bond formations, as well as EDA interactions, were not strong as solution pH was above the pK_avalues of the EDCs. The E1 sorption was the highest among the EDCs studied. This was mainly due to the presence of C=O functional group on its structure which might help in EDA interactions. Thus, q_{max} values for all EDCs in mixture mode were obtained at pH 3.0–3.5 where significant EDC interactions with fBC-2 occurred. Detailed sorption mechanism at different pH is discussed in **Section 5.1.3.5**.

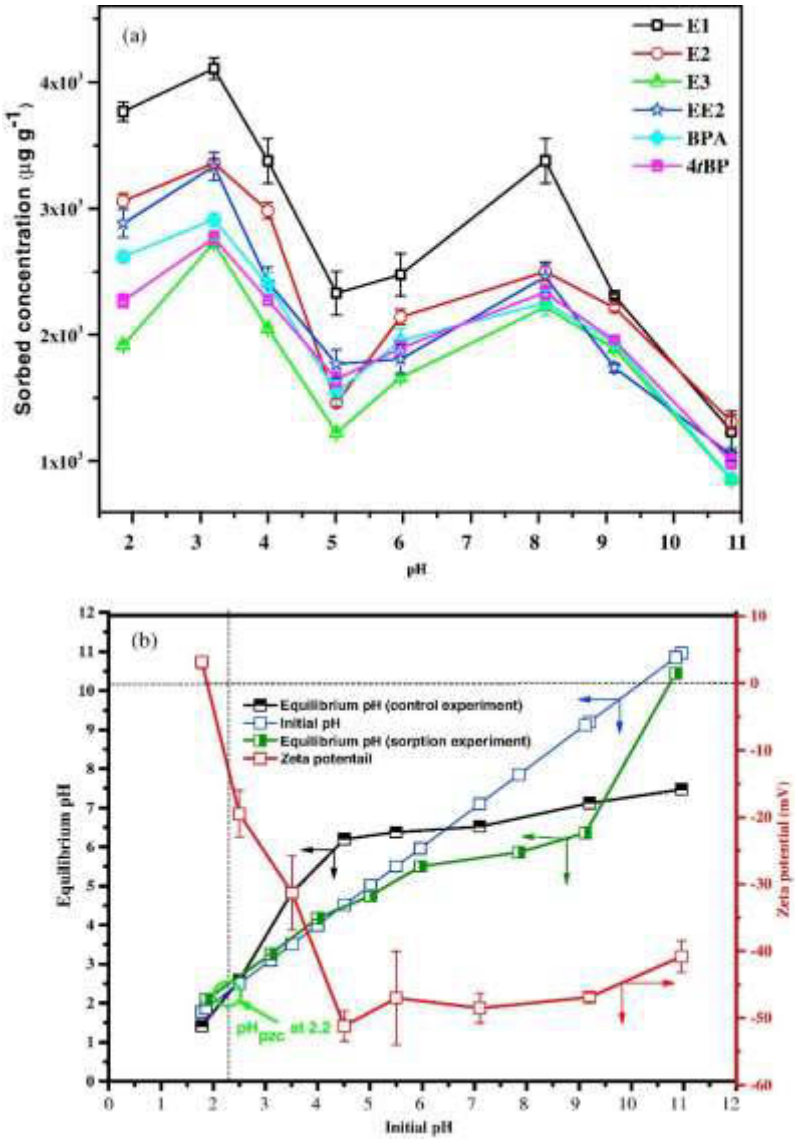

Figure 5.1.5: Effect of pH on solid phase concentration (μg g^{-1}) during EDCs sorption in competitive mode using fBC-2 at a dosage of 80 mg L^{-1} at 25 °C (a). Zeta potential values of fBC-2 using 0.01 M KCl solution at different pH with fBC-2 dosage of 400 mg L^{-1} together with initial and equilibrium pH values (b).

5.1.*3.3. EDC Sorption Kinetics*

The kinetics of the competitive sorption of EDCs onto fBC-2 is shown in **Figure 5.1.6**, with the apparent adsorption equilibrium reaching within ~42 h. Based on linear regression coefficient, the PSO model adequately described the kinetic data at 95% confidence level, compared to PFO kinetic model (data not tabulated for PFO model). From the PSO model, the q_s values were found to be 7642, 5439, 4403, 5469, 4749 and 4431 µg g^{-1} for E1, E2, E3, EE2, BPA and 4tBP, respectively (**Table 5.1.4**).

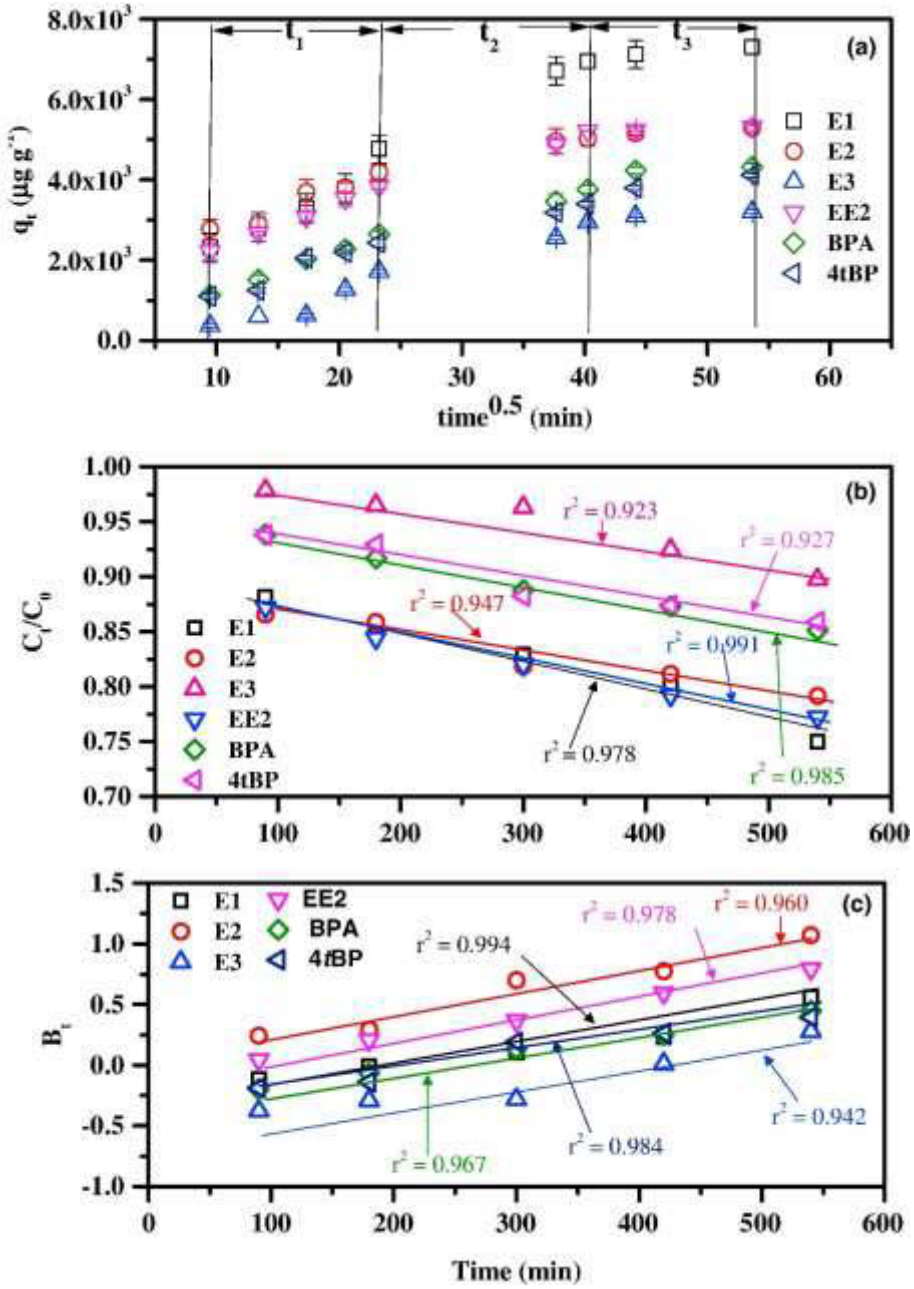

Figure 5.1.6: Kinetic model fit for EDCs adsorption on fBC-2 at 25 °C. (a) Weber-Morris plots, (b) external mass transfer plots, and (c) Boyd plots.

Table 5.1.4: Kinetic parameters calculated from the PSO and Waber-Morris kinetic models for the sorption of EDCs on fBC-2 at 25 ^{0}C.

	PSO at 25 ± 0.5 °C			Initial linear portion			2nd linear portion			3rd linear portion		
EDC	q_s (μg g^{-1})	K_2 (μg g^{-1} min^{-1})	r^2	C_1 (μg g^{-1})	K_{i1} (μg g^{-1} $min^{-0.5}$)	r^2	C_2 (μg g^{-1})	K_{i2} (μg g^{-1} $min^{-0.5}$)	r^2	C_3 (μg g^{-1})	K_{i3} (μg g^{-1} $min^{-0.5}$)	r^2
E1	7642±476	2.56E-7±5.7E-8	0.969	592±402	167±23	0.930	1735±192	131±6	0.996	5959±261	25±6	0.905
E2	5439±306	1.05E-6±3.03E7	0.933	1646±266	108±15	0.926	3002±99	51±3	0.994	4355±186	18±4	0.905
E3	4403±409	1.88E-7±5.3E-8	0.979	685±386	96±22	0.816	170±251	66±7	0.969	2629±171	11±4	1.000
EE2	5468±188	8.33E-7±1.36E-7	0.978	1079±61	119±4	0.996	2040±239	77±7	0.984	4995±64	8±1	0.937
BPA	4749±188	4.82E-7±7.67E-8	0.984	71±75	110±4	0.994	1176±288	63±8	0.965	3812±12	9±1	1.000
4*t*BP	4431±198	5.52E-7±1.02E-7	0.978	32±270	105±15	0.919	960±269	62±7	0.960	2276±20	34±0	1.000

To further evaluate the competitive sorption, the kinetic data were fitted with external mass transfer and intraparticle diffusion models as they play a major role in sorption process (**Figure 5.1.6, Table 5.1.4**). For intra-particle diffusion model, piecewise linear regression analysis of each EDC showed that q_t vs $t^{0.5}$ plots had three distinct regions. The first linear portion included the sorption period of 9.43 to 23.24 $min^{0.5}$ which represents external mass transfer and binding of EDCs by active sites on the outer surface of the fBC-2. The second linear portion included the sorption period of 23.24 to 40.24 $min^{0.5}$ represents intra-particle diffusion and binding of EDCs by active sites on macro and mesopores. The third linear portions included the period of 40.24–53.67 $min^{0.5}$, which denoted the establishment of the equilibrium [28]. The third step was very slow, thus, could not be treated as a rate-accelerating step. In addition, linear regression coefficient values were significant ($r^2 > 0.90$). The linear regression fittings for individual EDC did not pass through the origin, i.e. deviating from the origin or near saturation. This might be due to the difference in the mass transfer rate of the EDCs in the initial and final stages of sorption. From intercept (C) data it was found that the intra-particle diffusion was not the sole rate-limiting step [28]. The external mass transfer also played an important role in controlling the sorption rate. The regression coefficients ($r^2 > 0.950$) of all EDCs showed that the competitive sorption of EDCs could be represented by the external mass transfer model (**Figure 5.1.6b**).

The Boyd plot **(Eq. (**5.1.**10))** was used to explore whether intra-particle and external mass transfer processes exerted any significant influence on the sorption rate of EDCs [28]:

$$B_t = -\ln\left(1 - \frac{q_t}{q_s}\right) - 0.4977 \qquad (5.1.10)$$

From the Boyd plot, it can be observed that none of the sorption data lines pass thorough the origin (**Figure 5.1.6c**), indicating that the external mass transfer governed the sorption of EDCs on fBC-2. This finding is consistent with the previous study for BPA sorption using MWCNT where the external mass transfer was solely responsible for the sorption of BPA [28]. Thus, the sorption kinetics of EDCs could be described by PSO and external mass transfer models.

5.1.3.4. Competitive Sorption of EDCs and Gibbs Free Energy

The variations of solid phase concentration of EDCs with aqueous equilibrium concentration are represented in **Figure 5.1.7**. The isotherm data for competitive sorption of EDCs were fitted with Langmuir isotherm model. The Langmuir q_{max} were found to be 7588, 5126, 4217, 5115, 4764 and 4567 μg $g^{-1}$for E1, E2, E3, EE2, BPA and *4t*BP, respectively with regression coefficient >0.940 for all EDCs (**Figure 5.1.8** and **Table 5.1.5**). The total sorption capacity of

fBC-2 was found to be ~31375 µg g^{-1} based on the summarized Langmuir model for selected EDCs. Since the solutes competed for the same fBC-2 surface during sorption, the solute (EDC) with the highest interactions led to the highest sorption. The competitive sorption affinities followed the order: E1 > E2 ≥ EE2 > BPA > *4t*BP > E3.

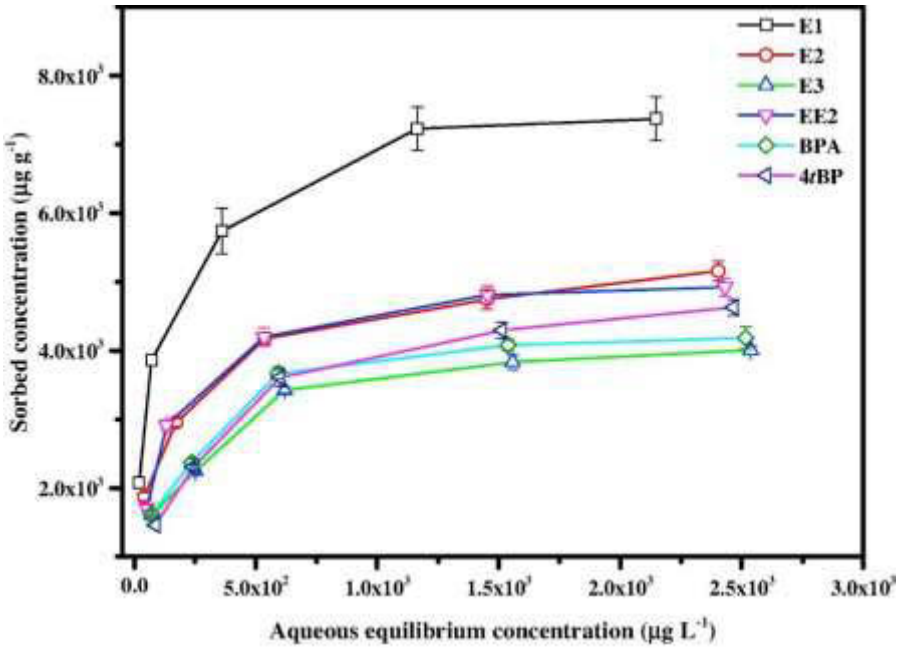

Figure 5.1.7: Solid phase concentration vs. aqueous concentration at equilibrium for the sorption of EDCs using 100 mg L−1 of fBC-2 at 25 °C.

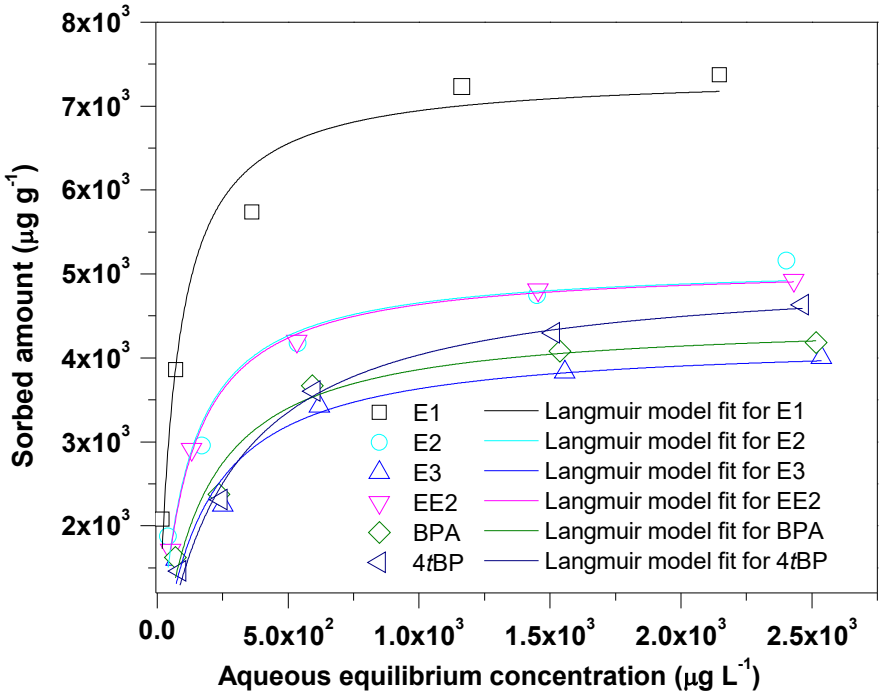

Figure 5.1.8: The Langmuir isotherm model fits for sorption of EDCs onto fBC-2.

The higher solid phase concentration of EDCs could be attributed to the functionalization of the biochar, which resulted in the formation of additional sorption sites with increased functional groups and an increase in specific surface area and micro pore volume [244]. The observed interactions were comparable with reports for sorption of various solutes by different carbon nanomaterials such as SWCNT, MWCNT and fullerene [52]. For example, carbon nanomaterials were applied for the sorption of BPA and EE2 (seperately) and it was observed that the solid phase concentrations (1×10^4– 1×10^5 µg g^{-1}) were within the range observed in this study for competitive sorption, if the same initial EDC concentration was maintained [52]. This implies that mixture of EDCs did not have adverse effect on the sorption of individual EDC using fBC-2. In comparison, limestone sediment was found less effective for the sorption interactions with BPA, E2, EE2, 4-*tert*-octylphenol and 4-n-nonylphenol, with the Freundlich constant values being significantly lower with prolonged interaction time than in this study [43]. Ying et al. [43] found the concentrations in sediment were 45, 70, 80 and 1750 µg kg^{-1} for BPA, E2, EE2, 4-*tert*-octylphenol, respectively. Similarly, lower Langmuir and Freundlich isotherm parameters were reported for BPA and EE2 interactions with sewage sludge [166]. Lorphensri et al. [58] also found EE2 removal using alumina, silica and a hydrophobic medium (porapak P) was significantly lower than in this study. Furthermore, there was a significant linear relationship between log K_d and

log C_w ($r^2 > 0.98$) (**Figure 5.1.9**). Increase in EDCs concentration reduced $K_d$value of each EDC which resulted in a decrease in removal efficiency. This was due to the gradual saturation of fBC-2 surface at higher solute concentrations, leading to lower removal efficiencies.

Table 5.1.5: Summary of the Langmuir isotherm parameters for EDCs sorption on fBC-2 at 25±0.5 ^{0}C.

EDC	q_{max}	K_L	r^2
E1	7588±308	0.0157±0.0033	0.967
E2	5126±251	0.0099±0.0024	0.946
E3	4217±233	0.0062±0.0015	0.940
EE2	5116±48	0.0096±0.0004	0.998
BPA	4765±219	0.0064±0.0014	0.954
4*t*BP	4568±157	0.0039±0.0005	0.988

The sorption spontaneity of EDCs at different concentrations (~250 to 3000 µg L^{-1}) onto fBC-2 was examined and Gibbs free energy was calculated (**Table 5.1.6**). The ΔG^0 values ranged from −29.01 to −20.17, −26.57 to −19.01, −24.78 to −18.25, −25.77 to −18.86, −24.91 to −18.38, and −24.09 to −18.68 kJ $mole^{-1}$for E1, E2, E3, EE2, BPA and 4*t*BP, respectively, when each EDC concentration was increased from ~250 to 3000 µg L^{-1}. Thus, the negative ΔG^0 values showed the spontaneous nature of the sorption of EDCs onto fBC-2.

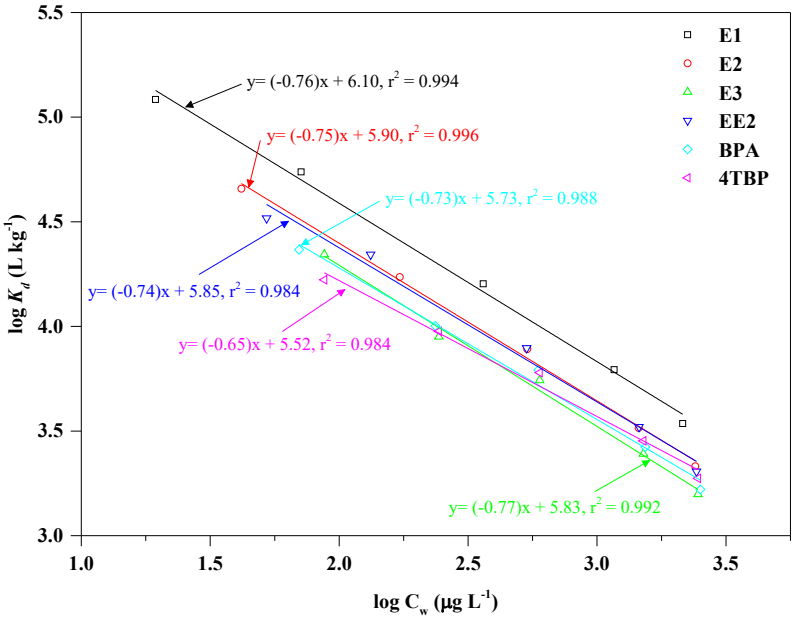

Figure 5.1.9: Logarithm plot of distribution coefficient (K_d) vs aqueous equilibrium concentration for the sorption of EDCs using 100 mg L-1 of fBC-2 at 25 ºC.

Table 5.1.6: Calculated ΔG^0 (kJ $mole^{-1}$) values for EDCs at 25 ^0C with initial concentrations of each EDC at 250-3000 µg L^{-1}. K_d values were taken as L kg^{-1}.

EDC	ΔG^0	EDC	ΔG^0
E1	-29.01	EE2	-25.77
	-27.03		-24.78
	-23.98		-22.23
	-21.64		-20.08
	-20.17		-18.86
E2	-26.57	BPA	-24.91
	-24.16		-22.83
	-22.20		-21.64
	-20.05		-19.53
	-19.01		-18.38
E3	-24.78	4*t*BP	-24.09
	-22.54		-22.69
	-21.35		-21.56
	-19.35		-19.70
	-18.25		-18.68

5.1.*3.5. Competitive Sorption Mechanism*

Interaction mechanism of each EDC with fBC-2 can be explained based on experimental findings. fBC-2 core structure consisted of meso- and macro-pores. The BET surface area and Dubinin-Astakov micropore surface area were 1.183 and 0.516 $m^2 g^{-1}$, respectively. BJH adsorption average pore diameter of fBC-2 was ~8.0 nm which might enough for diffusion of EDCs onto fBC-2 pores as the apparent molecular size of EDCs molecules was well below the average pore diameter of fBC-2 (**Table 2.2**). However, from the kinetics study, it was found that both external mass transfer (sorption by active sites) and PSO (multilayer sorption) model parameters satisfactory described sorption kinetic behaviour of EDCs on fBC-2, suggesting the role of surface functional groups present in fBC-2 for EDCs sorption. The mechanism of EDCs sorption by surface functional groups of fBC-2 is described below at different pH conditions.

Figure 5.1.3 shows the Raman spectra after sorption of a mixture of EDCs in competitive mode. The graphitic structure G-bands (mainly –C=C- arene unit) intensity was reduced significantly after sorption of EDCs in competitive mode. It suggested π-π interactions among EDCs and fBC-2 (mostly in arene unit of biochar), whereas surface defect D band (due to defect structure) was decreased greatly indicating the role of surface functional groups.

These functional groups were mostly oxygenated as confirmed by the XPS data. The decreases of peak intensity clearly suggested that hydrogen bond formation with the fBC-2 functional groups as well as with EDCs' functional groups were the main interaction mechanisms. The I_G/I_D ratio also decreased significantly indicating strong interactions between fBC-2 surface functional groups and EDCs.

Varying pH can affect the protonation-deprotonation transition of functional groups on any carbonaceous materials and change the chemical speciation for ionisable organic compounds [28]. The zeta potential values of fBC-2 suspension in aqueous solution at various pH were determined, and point of zero charge was found to be 2.2 (**Figure 5.1.5b**). Lower sorption of any compound at this pH was highly expected. At pH below 2.2, the zeta potential value of fBC-2 was found to be the positive indicating surface of fBC-2 was protonated under highly acidic conditions. EDCs molecules might also become protonated at pH 1.85 (e.g. due to hydroxyl or ketonic groups in EDCs). Hence, electrostatic repulsion of the same charge of quadruples might lead to lower sorption of EDCs at pH < 2.2. However, highly acidic condition (at pH 1.85) was still favourable to sorb EDCs by fBC-2 to some extent. The EDA interactions can explain the sorption of EDCs at this pH. Chemical structures of all EDCs contain at least one hydroxyl group in arene unit, i.e. phenolic group, and due to resonance-effect of arene unit, nearby carbon atoms in hydroxyl group (in arene unit) could act as π-electron donor site (**Figures 2.2 and 5.1.10**). Meanwhile, fBC-2 consisted of ketonic and carboxylic –C=O functional groups in its arene units (as confirmed by XPS) which might act as π-electron acceptor site for the interactions (due to resonance) and the graphene unit in fBC-2 can act as a π-electron donor site. Thus, stronger EDA interactions (from -C=O and -COOH as π-electron acceptor while EDCs as a π-electron donor) would be the main reason for the sorption of all EDCs at this pH (**Figure 5.1.10**). The π-π electron-donor–donor (EDD) interactions between phenolic –OH of EDCs and surface –OH group and graphene unit of fBC-2 are not significant, and considered weaker than EDA interactions. Thus, EDD interactions at very low pH can be excluded. The interactions of fBC-2 and EDCs can also be predicted from pH shift tests before and after adsorption experiments. The variation of solution pH is shown in **Figure 5.1.5b**. The equilibrium pH slightly increased after sorption (from 1.86 to 2.09) indicating either release of hydroxyl ions or consumption of proton either by fBC-2 or EDCs. Moreover, hydroxyl ions might exchange proton in the solution for neutralization leading to increase the solution pH. However, proton exchange for fBC-2 at pH ~ 1.85 is not favourable for –C=O, -COOH and -OH groups as their pK_a values are higher. Hence, surface -OH groups or quaternary nitrogen groups (tiny fraction) of fBC-2 as well as EDCs functional groups such as -OH and -CH might

form hydrogen bond along with EDA interactions, i.e. excess hydrogen ions took part in hydrogen bond formations hence equilibrium pH was increased. Therefore, sorption at pH ~ 1.85 was observed due to EDA interactions and hydrogen bond formations.

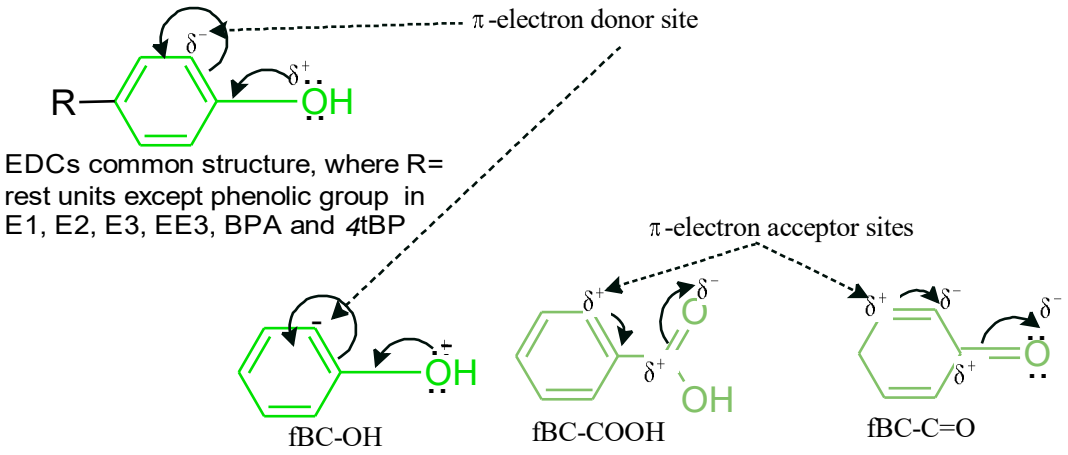

Figure 5.1.10: Resonance structures of EDCs and different functional groups in fBC-2.

The maximum solid phase concentration and K_d values of all EDCs were observed at pH 3.0–3.5 (**Figure 5.1.5a**), and the main reason might be due to the formation of strong hydrogen bonds and strong EDA interactions. Based on the pH shift study, equilibrium pH shifted slightly to higher pH (pH 3.10–4.0 to 3.25–4.18). The increase in equilibrium pH indicated hydroxyl groups released into solution, which was more significant in the control experiments than sorption experiment (**Figure 5.1.5**b). Although the pH shift seemed less significant in the sorption experiments, the release of protons from fBC-2 functional groups (e.g. -COOH) and then forming strong hydrogen bonds (-COOH in fBC-2 and phenolic –OH in EDCs) might be the main reason for resisting equilibrium pH to decrease (**Figure 5.1.5b**). Such hydrogen bonds can be proposed as charge assisted hydrogen bonds (CAHB), i.e. fBC-2-CO^{-}/COO^{-}….H^{+}…O^{-}-EDCs. Stronger hydrogen bonds might be possible with –OH groups and –CH groups in EDCs with fBC-2 surface functional groups (e.g. -COOH, -OH, C=O, C≡N groups and –C-O-PO_3 complex). However, EDA interactions could be considered the main sorption mechanism. The surface -COOH has pK_a value of ~3.0–5.0 [59, 244, 355]. Functional groups -COOH and C=O could act as strong π-electron acceptor while the phenolic group in EDCs and graphene unit of fBC-2 could act as π-electron donor site (**Figure 5.1.10**). Thus, stronger EDA interactions could be the main sorption mechanism. EDD interactions might not be significant as graphene surface could act as π-electron donor site as well as EDCs could act as π-electron donor. Hence, EDA interactions were the main mechanism for higher

sorption of EDCs with additional contribution from the CAHB formations. Zhang et al. [28] studied the separation of BPA using MWCNT and proposed the π-π stacking interactions between the bulk π-system of MWCNT surface and BPA molecule in a wide pH range of 4.0 to 10.0 [28]. They also mentioned that MWCNT could function as hydrogen bond donor to form hydrogen bonds with –OH functional groups on BPA. However, they did not mention any specific group in MWCNT responsible for π-π stacking interactions, while our observations indicated that π-π stacking interactions (EDA) only came from the surface -COOH/C=O and –C=C- groups. Also, Jung et al. [48] studied the adsorption of emerging contaminants such as EE2, BPA, sulfamethoxazole, atrazine, carbamazepine, diclofenac and ibuprofen using activated biochar at different pH (3.5, 7.0, 10.5) and suggested that maximum adsorption was mainly due to π-π interactions. Therefore, maximum interactions might be due to the formation of negative CAHB as well as strong hydrogen bonds, with the main contribution from EDA interactions leading to the higher interaction of EDCs with fBC-2.

With the increase in pH from 3.0 to 5.0, the solid phase concentration of all EDCs decreased. When pH was increased from 5.0 to 8.0, another peak interaction value for all EDCs was found although not as high as at pH ~ 3.0–3.5. All the EDCs have one pK_a value. So, near pH 8–9 proton release from any EDC is highly possible as pH = pK_a + log [salt/acid]. On the other hand, any carbonaceous surface OH group has pK_a value of ~8.0–10.0 [28, 321]. Proton exchange by EDCs molecules was calculated and found their ΔG^o values were favourable for proton exchange in solution at this condition (**Table 5.1.7**). Thus, negatively charged surfaces (zeta potential was negative, and EDCs released a proton and became negative sites) could repulse each other causing minimum interactions. However, at pH ~ 8.0 high interactions were observed for all EDCs. This might be due to the formation of strong hydrogen bonds among hydroxyl group of EDC and fBC-2 surface -OH groups, firstly, releasing the hydrogen ion from fBC-2 or EDC hydroxyl group to neutralize -OH from water molecule (splitting of water molecule) leading to shift in the equilibrium pH toward more acidic region to form CAHB (fBC-O^-….H^+…$^-$O-EDCs) (**Figure 5.1.5b**) [59, 320, 355]. In comparison with control experimental equilibrium pH, the change of equilibrium pH was also significant indicating the release of protons from surface -OH groups of fBC-2 (**Figure 5.1.5b**). The π-π EDA interactions could also play an important role under this condition. However, EDA interaction might only come from fBC-2 surface -C=O groups (π-electron acceptor), graphene unit of fBC-2 (as a π-electron donor) and EDCs (as a π-electron donor) whereas, EDA interactions might not be effective for the surface carboxylic group (pK_a value is near pH 3.0–5.0) (**Figure 5.1.10**)

[59, 320, 355]. EDD interactions might be less effective. Furthermore, at pH > 9.0, each EDC may exist as an anion, and the sorption was significantly impeded due to the electrostatic repulsive force between negatively charged fBC-2 surface and EDCs anions. The ionized forms of EDCs were the predominant fraction at pH > pK_a, and the hydrogen bonds and hydrophobic interactions between fBC-2 and each ionized EDC were much weaker than those between fBC-2 and non-ionized EDCs. Besides, both EDC and fBC-2 were negatively charged, and the electrostatic repulsion between them can also weaken their adsorption to some extent at pH > 10. Hence, lower sorption at pH above 9.0 was observed. In addition, the pH shift result was not significant at pH 10.85 indicating the insignificant role of the hydrogen bond formation.

Table 5.1.7: ΔG^o values calculated from water dissociation constant (K_{aw}) at 25 ^{0}C.

EDC	Temperature (K)	pK_{a1}	$K_{a1}\times10^{-11}$	$K_{aw}\times10^{-14}$	$ln\ K_{aw}$	RT ln K_{aw} (J mol^{-1})	RT ln K_{aw} (kJ mol^{-1})	RT ln K_{a1} (kJ mol^{-1})	$\Delta G^0_{H^+_{exch}1}$ (kJ mol^{-1})
E1	298	10.34	4.58	1.01	-32.23	-79858	-79.86	-59.00	-20.86
E2	298	10.46	3.47	1.01	-32.23	-79858	-79.86	-59.67	-20.19
E3	298	10.38	4.17	1.01	-32.23	-79858	-79.86	-59.22	-20.64
EE2	298	10.40	3.98	1.01	-32.23	-79858	-79.86	-59.33	-20.54
BPA	298	9.80	15.85	1.01	-32.23	-79858	-79.86	-55.91	-23.95
4*t*BP	298	10.16	6.92	1.01	-32.23	-79858	-79.86	-58.00	-21.86

- K_{aw} values were taken from http://www.chemguide.co.uk/physical/acidbaseeqia/kw.html
- R =8.314 (J K^{-1} mol^{-1}), $\Delta G^0_{H^+_{exch}1} = -RT\ ln(K_{a1}/\ K_{aw})$

5.1.*3.6. EDC Removal from Sewage Effluent vs. Synthetic Wastewater*

When fBC-2 was applied to remove a mixture of EDCs from MBR sewage effluent (spiked at 508.4, 525.9, 532.9, 534.5, 465.8, 460.5 µg L^{-1} of E3, BPA, *4t*BP, E2, E1 and EE2, respectively) at pH 3.0–3.25 and 25 °C, pronounced differences were observed for different EDCs in terms of their complete sorption onto fBC-2 (**Figure 5.1.11**). Using fBC-2 dosage of 100, 200 and 300 mg L^{-1} was not enough to remove the EDCs in mixture mode at the specified concentration of each EDC. Better removal results were obtained with a higher dose of 400 mg L^{-1} of fBC-2, achieving ~97% removal of E3 and *4t*BP. Although the complete removal of E1 (460.5 µg L^{-1}) was found at 300 mg L^{-1} of fBC-2 in competitive mode, the complete removal of EE2, E2 and BPA was obtained only at 400 mg L^{-1} of fBC-2. The results

indicated that sorption interactions of EDCs with fBC-2 were very efficient and dosage above 400 mg $L^{-1}$of fBC-2 can remove the EDCs completely in competitive mode from the MBR effluent. The removal trend was the same as obtained from isotherm, pH effect and sorption affinity data as E1 > E2 > EE2 > BPA > 4*t*BP > E3. However, MBR effluent was found to have a slightly negative influence on the overall removal of EDCs than deionized water and thus required an extra dosage of fBC-2. The main reason might be the presence of different species in MBR effluent that may compete for the fBC-2 surface and might block the surface functional groups of fBC-2, leading to reduced sorption of EDCs onto fBC-2 surface than in deionized water.

Synthetic wastewater also contains a mixture of different organic acids, organic compounds and inorganic salts (**Table 5.1.1**). The removal of EDCs from synthetic wastewater was carried out at various dosages of fBC-2 and residual concentration of each EDC was measured after 46, 50 and 64 h. Each EDC was spiked in synthetic wastewater (~500 µg L^{-1}) with individual concentration (measured after spiking) of 461.3, 486.0, 498.7, 497.0, 465.9, 460.4 µg L^{-1} of E3, BPA, 4*t*BP, E2, E1 and EE2, respectively. The fBC-2 dosage, residual concentrations and percentage removal of each EDC in mixture mode are given in **Table 5.1.8**. Approximately 94.2% of E3 was removed in 46 h, with 555 µg L^{-1} of fBC-2; when sorption time was increased to 64 h, the removal reached 100%. Similarly, complete removal of BPA was obtained within 50 h at 445 mg $L^{-1}$of fBC-2 dosage. This result indicates that BPA can be removed at any dosage above 445 mg L^{-1} of fBC-2 from a mixture ~500 µg L^{-1} of each EDC. A similar result was obtained for 4*t*BP. Slightly long duration (~64 h) was needed for 100% removal of E1, E2 and EE2 at fBC-2 dosage of 445 mg L^{-1}. The interactions of EDCs with fBC-2 in synthetic wastewater were found to have an adverse influence on the overall removal of EDCs than with deionized water or MBR effluent. **Table 5.1.1** shows that MBR effluent composition is more complicated than synthetic wastewater. The main reason for slow interactions arose from different organics in synthetic wastewater (e.g. Na-lauryl sulphate, beef extract, sodium lignin sulfonate, humic acid, tannic acid) and from inorganic sulfates and bi-phosphate. To shed light, separate competitive sorption experiments using fBC-2 was conducted in the presence of Na-laryl sulphate and acacia gum powder (same concentration as used in synthetic wastewater), and it was observed that EDC sorption was significantly suppressed by 38–50%. Also, control experiments in the absence fBC-2 showed that there was no loss of each EDC. Thus, the presence of Na-laryl sulphate and acacia gum powder in synthetic wastewater was the main cause for the reduced sorption of EDCs. Hence, an increased

fBC-2 dosage (>555 mg L^{-1}) is needed to ensure sufficient removal of EDC mixture from synthetic wastewater.

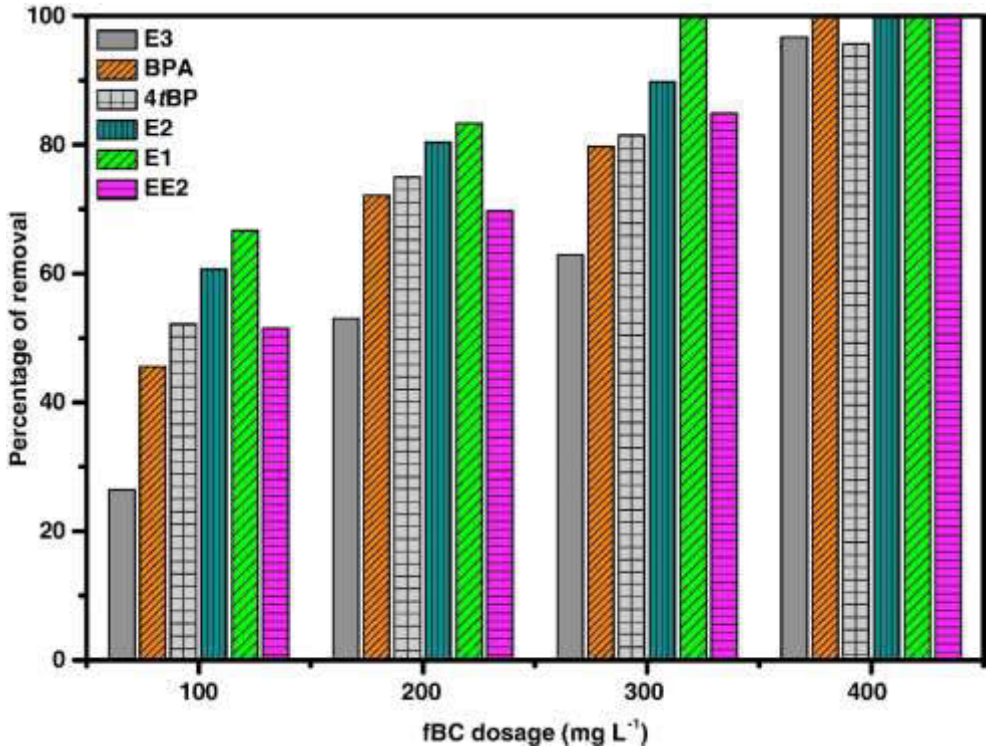

Figure 5.1.11: Sorption of EDCs in mixture mode with initial concentration of each EDC at ~500 µg L^{-1} from MBR sewage effluent at different dosages of fBC-2 at pH 3.0–3.25, 25 °C.

Table 5.1.8: EDC removal from synthetic wastewater with different dosages of fBC-2 at 46 h, 50 h and 64 h.

EDC	Initial conc. ($\mu g\ L^{-1}$)	Dosage ($mg\ L^{-1}$)	46 h		50 h		64 h	
			Residual conc. ($\mu g\ L^{-1}$)	Removal (%)	Residual conc. ($\mu g\ L^{-1}$)	Removal (%)	Residual conc. ($\mu g\ L^{-1}$)	Removal (%)
E3		110	400.0	11.9	377.1	18.2	367.0	20.4
		225	269.4	41.6	255.9	44.5	249.2	46.0
	461.3	333	208.7	54.7	202.0	56.2	178.5	61.3
		445	87.5	81.0	80.8	82.5	47.1	89.8
		555	26.9	94.2	16.8	96.4	<LOD	~100
BPA		110	419.4	13.7	392.8	19.2	352.8	35.2
		225	233.0	52.1	219.7	54.8	186.4	61.6
	486.0	333	166.4	65.8	159.8	67.1	119.8	75.3
		445	39.9	91.8	<LOD	~100	<LOD	~100
		555	<LOD	~100	<LOD	~100	<LOD	~100
4*t*BP		110	373.3	25.2	350.2	29.8	304.5	38.9
		225	159.8	67.9	152.3	69.5	125.6	74.8
	498.7	333	125.6	74.8	76.1	84.7	60.9	87.8
		445	11.4	97.7	3.8	99.2	<LOD	~100
		555	<LOD	~100	<LOD	~100	<LOD	~100
E2		110	418.1	15.9	385.5	22.4	371.6	25.2
		225	209.0	57.9	199.7	59.8	153.2	69.2
	497.0	333	102.2	79.4	88.3	82.2	74.3	85.0
		445	4.6	99.1	4.6	99.1	<LOD	~100
		555	<LOD	~100	<LOD	~100	<LOD	~100
E1		110	388.2	16.7	336.5	27.8	284.7	38.9
		225	118.1	61.1	155.3	66.7	129.4	72.2
	465.9	333	77.6	83.3	25.9	94.4	25.9	94.4
		445	25.9	94.4	<LOD	~100	<LOD	~100
		555	<LOD	~100	<LOD	~100	<LOD	~100
EE2		110	258.1	43.9	230.2	50.0	209.3	54.5
		225	244.2	47	230.2	50.0	188.4	59.1
	460.4	333	111.6	75	104.6	77.3	69.7	84.8
		445	27.9	93.9	6.9	98.5	<LOD	~100
		555	<LOD	~100	<LOD	~100	<LOD	~100

5.1.4. Concluding Remarks

In this work fBC-2 with enhanced functional groups, specific surface area, and meso and macro-pores was successfully prepared for the removal of EDC mixture from water and wastewater. The sorptive removal of EDCs by fBC-2 through competitive interactions reached equilibrium within 42 h, with the external mass transfer diffusion process as the rate-limiting step. PSO well modelled the sorption kinetics. EDC sorption was highly pH dependent, with the maximum sorption occurring at pH ~ 3.0–3.5. The sorption equilibrium followed the Langmuir isotherm model, suggesting monolayer coverage. In term of sorption mechanism, EDC sorption mainly occurred through π-π EDA interactions and by forming different hydrogen bonds. Overall, the sorption capacity and distribution coefficient values decreased as E1 > E2 ≥ EE2 > BPA > *4t*BP > E3 due to the difference in the EDCs' hydrophobicity. Water composition had a pronounced effect on EDC removal, as shown by the highest removal in deionized water, followed by MBR sewage effluent, and finally synthetic wastewater. The presence of sodium lauryl sulphonate and acacia gum in synthetic wastewater caused a significant reduction in the competitive sorption of EDCs on fBC-2. Thus, fBC-2 can be successfully applied for the removal of EDC mixtures from water and wastewater, although appropriate pre-treatment may be required to remove the interfering substances such as certain surfactants.

5.2. Sorption of Hydrophobic Organic Contaminants on Functionalized Biochar: Protagonist Role of π-π Electron-Donor-Acceptor Interactions and Hydrogen Bonds

5.2.1. Introduction

Pyrogenic carbonaceous materials (CMs) such as mesoporous carbon, biochar, activated carbon, graphene and CNTs exhibit strong sorption affinities for a wide range of organic contaminants including polycyclic aromatic hydrocarbons, benzene derivatives, phenolic compounds, and pharmaceuticals such as antibiotics, EDCs and pesticides [82, 386-391]. The interactions of such contaminants with CMs in water, sediments and soil may result in strong or weak bindings that can significantly affect the environmental fate of contaminants and their remediation rates [392-394]. The underlying physical and chemical phenomena potentially responsible for these apparent interactions of contaminants with CMs are of great importance. Further, their persistence and potential risks to aquatic life are also important. Organic contaminants comprise broad classes of chemicals, some of which are persistent in soils, sediments and water, with potential for long-term impacts. The conventional idea for ionic organic species is that they may undergo Coulombic attraction/repulsion at charged sites on the adsorbent in addition to the weak forces available to uncharged molecules, including London-van der Waals force, H-bonding, and the hydrophobic effect (solute exclusion from water) [57, 387]. However, noncovalent forces are ubiquitous between chemical interactions as they control diverse phenomena such as boiling points of liquids, solvation energies, and the structures of molecular crystals. π-π interactions constitute one of the most important classes of noncovalent interactions, contributing to biomolecular structure, chemical bonding, and the structure and properties of π-conjugated materials (such as biochar and CNTs) of interest having π-structure benzene or aromatic ring [395]. The elucidation of molecular-level interactions controlling sorption of non-ionic compounds and the influence of solution-phase composition on sorption are of considerable theoretical and practical importance. This study is therefore aimed to compare the sorptive mechanism of five non-ionic endocrine disruptor compounds (EDCs) such as E1, E2, E3, EE2 and BPA as representative HOCs on funcitionized biochar (fBC) based on their physicochemical properties (**Table** 5.2.**1)**. fBC was selected for its higher sorption capacity of organic pollutants (both in single and competitive moods) due to the presence of multifunctional groups on its surface. Also, the production and operation cost of fBC is relatively low. Further, fBC can be used repetitively after regeneration [396].

Table 5.2.1: Physicochemical Properties of Selected HOCs.

Name	Abbreviation	Chemical formula	pK_a[b]	Solubility[a] (C_s, mg L^{-1})	K_{HW}[a]	log$P$[b]
Estrone	E1	$C_{18}H_{22}O_2$	10.33	1.17	7.26 ± 0.48	4.03-4.31
17β-Estradiol	E2	$C_{18}H_{24}O_2$	10.33	2.15	2.29 ± 0.21	3.57-3.75
Estriol	E3	$C_{18}H_{24}O_3$	10.33	13.96	0.65 ± 0.02	2.54-2.67
17α-Ethynylestradiol	EE2	$C_{20}H_{24}O_2$	10.33	7.64	4.45± 0.12	3.63-3.93
Bisphenol A	BPA	$C_{15}H_{16}O_2$	9.78	313.15	0.34 ± 0.02	3.81-4.04
Phenanthrene	PHE	$C_{14}H_{10}$		1.10 [c]	17.30 ± 1.86	4.46 [c]
1,3-Dinitrobenzene	DNB	$C_6H_4N_2O_4$	13.86 [b]	185[b]	-	1.49[c]

[a]: Measured at 25 °C.
[b]: http://www.t3db.ca/toxins/T3D0782
[c]: https://pubchem.ncbi.nlm.nih.gov

The interaction mechanism of HOCs and fBC were evaluated based on theoretical, experimental and analytical findings. The magnitude of non-hydrophobic interactions was assessed by "normalizing" the hydrophobic effect. The fundamental role of non-hydrophobic interactions namely hydrogen-bond formation and π-π interaction based on adsorption-pH profiles of HOCs by fBC was examined. Further, we also identified the probes of structure-adsorption property relationships for different π-electron-donor rings of HOCs (due to –OH groups on arene units) and PHEN (as model HOC) *vs* π-electron-acceptor rings of model compounds (DNB and PABA). The potential role of π-electron-donor-acceptor domains in fBC at different pH was predicted based on equilibrium sorption distribution coefficient and sorption capacity in the π-electron-donor-acceptor systems. We also evaluated several potential causes of sorption interactions, including pH effects on sorbent hydrophobicity, π-H-bonding, effects of solution acidity on solute activity coefficient and the occurrence of π-π EDA interactions with the π-electron-acceptor and donor sites of fBC. The role of π-π interactions was assessed by solution-phase proton nuclear magnetic resonance (^{1}H NMR) and ultraviolet-visible (UV-vis) spectroscopic studies by inspecting the behaviour of π-electron-donor compounds (HOCs and PHEN) in comparison with π-electron-acceptor (DNB) systems.

5.2.2. Materials and Methods

5.2.2.1. Chemicals

E1 (99%), E2 (> 98%), E3 (> 97%), EE2 (98%), BPA (99%), phenanthrene, 1,3-dinitrobenzene, *p*-aminobenzoic acid, hexadecane, 2-nonanone (NON-2), and organic solvents such as methanol, methanol-d_4, formic acid (99.9%), and acetonitrile of HPLC grade were purchased from Sigma-Aldrich, Australia.

5.2.2.2. Materials

Eucalyptus globulus wood was used to produce biochar by heating the wood particles at 380 °C for 2 h in a reactor under continuous nitrogen gas supply and then activated using phosphoric acid according to our previous studies [25, 244, 396]. Briefly, biomass and the phosphoric acid mixture was then heated at 600 °C for 2 h under continuous nitrogen supply at 2.5 psi, cooled at room temperature, and washed with distilled water 4 times while adjusting pH to 7, followed by drying overnight at 120 °C, to obtain the activated biochar. The activated biochar product named as functionalized biochar (fBC-2) based on its surface characteristics [25, 244]. Structural analysis of carbon network showed that fBC-2 was composed of mesopore (2-50 nm) and macrospore (> 50 nm) structure. X-ray photoelectron spectroscopic (XPS) results indicated that fBC-2 surface was rich in different functional groups especially graphitic carbon (~57%), phenolic or alcoholic (C-O-, ~13.5%), carbonyl or quinone (C=O, ~4%), carboxylic or ester (COO-, ~3%), π-π* transition (~1%), quarternary nitrogen (~1%), and polyphosphates and/or phosphates (C-O-PO_3, ~1%) (**Table** 5**.2.2**). The point of zero charges for fBC-2 was pH 2.2.

Table 5.2.2: XPS Spectra Summery for fBC-2 [25, 397].

Name	Peak BE	Atomic %	Surface group	Assignment
C (1s) A	284.8	56.98	C=C	Graphitic carbon
C (1s) B	286.27	13.6	C-O-	Phenolic, alcoholic, etheric
C (1s) C	287.8	4.15	C=O	Carbonyl or quinone
C (1s) D	289	3.13	COO-	Carboxyl or ester
C (1s) E	290.54	2.77	C=O/ C=C	Carbonate, ocluded CO, p-electrons in aromatic ring
C (1s) F	292.35	1.13	π-π* transition	The transition due to conjugation
N (1s)	401.47	0.8	$C–N^{+}H-C$	Forms of quaternary nitrogen, protonated pyridinic ammonium ions, nitrogen atoms replacing carbon in graphene,
O (1s) B	533.3	8.52	C-O-	Oxygen singly bonded to carbon in aromatic rings, in phenols and ethers
O (1s) A	531.62	4.8	C=O	Oxygen doubly bonded to carbon
P (2p)	133.79	2.3	$C-O-PO_3$	Polyphosphates and/or phosphates

5.2.2.3. Batch Sorption Experiments

HOC sorption experiments in distilled water were conducted in 50 mL glass vials with Teflon-lined screw caps at 25 ^{o}C in triplicate on an orbital shaker over 48 hours using fBC-2. The sorption of HOCs using pristine biochar was not studied due to its lower sorption capacity. The effects of pH and sorption isotherm experiments of HOCs (at pH 3.0-3.5) were performed under the same conditions. The control experiments without sorbents were also conducted. The fBC-2 dosage was selected for 15-99% sorption of each HOC at different concentrations. Single sorption experiments of PHEN, NON-2; DNB and PABA were carried out at three different pH ranges, i.e. pH 1.5-1.7, 3.0-3.5, and 8.0-9.5, in triplicate. The effects of competitors such as PHEN, PABA, and DNB for HOC sorption were also carried out under the same conditions. The supernatants were filtered through a 0.45 μm PTFE filter and analyzed by high-performance liquid chromatography (HPLC) and by UV-vis spectroscopy.

HOCs were analysed by an HPLC equipment with an auto-sampler, a UV and a florescence detector. A reverse-phase Zorbax Bonus RP C_{18} column (5.0 μm, 2.1 ×1.50 mm, Agilent Technologies) was used throughout for detection and quantification of HOCs. The volume of injection was 100 μL. Mobile phase A was composed of acetonitrile and formic acid (99.9: 0.1) while mobile phase B was composed of Milli-Q water and formic acid (99.9: 0.1). The elution used 40% of A and 60% of B at a flow rate of 0.4 mL min^{-1} and maintained still 20 min. HOCs analyzed with a UV detector at 285 nm and a fluorescence detector at 280 nm (excitation wavelength) and 310 nm (excitation wavelength). Fluorescence wavelength kept

unchanged throughout the analysis. UV wavelength was changed to 240 nm at 4.10 min and maintained up to 5 min and returned to 285 nm at 5.10 min. The method time was varied based on each HOC and followed 5 min, 10 min, 12 min, 15 min and 20 min, respectively for E3 (limit of detection 3.33 μg L^{-1}) , BPA (limit of detection 6.97 μg L^{-1}), E2 (limit of detection 4.60 μg L^{-1}), E1(limit of detection 25.80 μg L^{-1}) and EE2 (limit of detection 3.80 μg L^{-1}). DNB concentration was measured using HPLC and using the same ratio of solvent and same method. The method was run for 6 minutes and using a UV wavelength of 240 nm. PHEN concentration was measured using UV-vis spectroscopy using a wavelength of 250.5 nm.

5.2.2.4. ^{1}H NMR and UV-Vis Studies for π-π EDA Interactions in Solution

UV-Vis Spectroscopic spectra of test solution of HOCs, π-donor-DNB and π-acceptor-PHEN in water were measured at room temperature using Shimadzu (UV-1700) instrument. Proton nuclear magnetic resonance (^{1}H NMR) spectra were recorded at a specific concentration of HOCs and donor-acceptor solutes at room temperature using an Agilent 500 MHz NMR instrument. Samples were prepared in methanol-d_4 and measured after 24-30 hours. The chemical shifts (δ) were recorded by internally referenced to methanol-*d4* solvent and observed proton frequency shift was calculated based on NMR instrument frequency and chemical shift.

5.2.2.5. Data Fitting

Different models employed to fit the adsorption isotherms are as follows:

$$\text{Freundlich model: } S_e = K_f\, {C_e}^n \tag{5.2.1}$$

$$\text{Polanyi-Mane model (PMM): } S_e = S_{max}^p + \left(Z \times \left(RT \ln\left(\frac{C_s}{C_e}\right)\right)^d\right) \tag{5.2.2}$$

where S_e is the solid-phase sorbed capacity (μg kg^{-1}) of HOCs, S_{max}^p is the maximum adsorption capacity (μg kg^{-1}) from PMM, n is a dimensionless number related to surface heterogeneity, and K_f is the Freundlich affinity coefficient (μg^{1-n} L^n kg^{-1}). C_e represents the aqueous-phase concentration of solute (μg L^{-1}) at 25 ^{0}C, whereas C_s (μg L^{-1}) stands for solubility of each HOC at 25 ^{0}C. Z and d are PMM adsorption fitting constants, R is universal gas constant (8.314 × 10^{-3} kJ mol^{-1} K^{-1}), and T (K) is absolute temperature. All model equations were fitted by origin-pro, with model parameters being obtained with standard coefficient of determination (r^2) and adjusted coefficient of determination (r_{adj}^2).

The single point adsorption distribution coefficient (K_d) of HOCs was calculated using Eq. (5.2.3):

Partition model: $K_d = S_e/C_e$ (5.2.3)

Where $C_e = 0.002C_s$ based on the fitting results using PMM. We used C_e/C_s ration of 0.002 to get maximum distribution coefficient.

Equilibrium sorbed volume of each HOC can be calculated based on initial and equilibrium concentrations using following equation:

$$S_v = (C_0\text{-}C_e)\ V/\ (1000\ m\ \rho_{HOC}) \quad (5.2.4)$$

where C_o and C_e (μg L^{-1}) are the initial and equilibrium concentration of HOCs; V (L) is the solution volume in the system; m (g) is the mass of fBC-2 sorbent in the system, and ρ_{HOC} (cm^3 g^{-1}) is the density of the solute.

5.2.3. Results and Discussion

5.2.3.1 Interactions of HOCs with fBC-2

The single maximum point K_d value was observed for E1 (2.90×10^6 L kg^{-1}) with the minimum for BPA (3.03×10^4 L kg^{-1}); thus, E1 was found to be adsorbed more strongly onto fBC-2 surface than other HOCs (**Figure 5.2.1a and Table 5.2.3**). The adsorption coefficient values followed the order of E1 > E2 ≥ EE2 > E3 ≈ BPA. The PMM model parameters for sorption isotherm of each HOC shows that the Polanyi theory may be useful to describe the sorption of HOCs on fBC-2, as the Polanyi theory relates to competitive sorption of organic compounds as micropore filling (**Figure 5.2.2 and Table 5.2.3**). However, we used single solute to check the viability of PMM model. At zero adsorption potential, any undeformed sorbent should have a limiting volume to the total available pores for adsorption based on Polanyi pore filling model [398]. The adsorbed volume capacities of E1, E2, E3, EE2 and BPA, calculated from their mass capacities and respective solid-phase density, were 24.0, 23.0, 15.0, 20.0, and 17.0 cm^3 kg^{-1}, respectively [387]. The Dubinin-Astakov micropore surface area of fBC-2 was 520.0 m^2 $kg^{-1,}$ and the limiting micropore volume was 0.24 (cm^3 kg^{-1}) [25]. Thus, the micropore volume of fBC was at least 63-100% less than that of the adsorbed volume capacity of HOCs. This result is contradictory with the pore-filling mechanism for un-deformable sorbents [398, 399]. Therefore, pore filling cannot be the dominant mechanism for the sorption of HOCs by fBC-2. Polanyi theory, however, is applicable for either pore-filling or flat surface adsorption and adsorption parameters correlate with the material surface defects curvatures of carbon materials, which can affect the adsorption significantly. BET surface area of fBC-2 was found to be 1.18 (m^2 g^{-1}) [25]. Thus, we hypothesize that surface adsorption of HOCs (rather than pore filling) is the dominant sorption mechanism and which came from

different functional groups of fBC-2 surface. Therefore, several factors need to be considered for surface adsorption of HOCs: (i) potential energy of adsorption sites on solute-coated sorbent surface (i.e. fBC-2) should be lower and more homogeneous than that on un-coated sorbent surface, (ii) sorbed solute molecules on the sorbent surface should have attractive forces for solute molecules, and (iii) the maximum sorption capacity depends on the sorbent surface area and its relative functional groups [398]. However, the higher solid phase concentration of HOCs could be attributed to the functionalization of biochar resulting in the formation of additional sorption sites.

Table 5.2.3: Summary of the Freundlich Isotherm Parameters for Each HOC Adsorption on fBC-2 at 25 ± 0.5 °C.

HOC	K_F	n	r^2	$Adj.\ r^2$
E1	8.76E6±2.6E6	0.17	0.935	0.920
E2	4.10E6±1.1E6	0.25	0.953	0.937
E3	2.97E6±6.7E5	0.25	0.965	0.953
EE2	5.51E6±2.32E6	0.22	0.907	0.876
BPA	2.60E6±1.2E6	0.27	0.876	0.821

Table 5.2.4: Summary of the PMM Isotherm Parameters for Each HOC Adsorption on fBC-2 at 25 ± 0.5 °C (d=1).

HOC	S^o_{max}	Z	r^2	$Adj.\ r^2$
E1	3.81E7± 4.62E6	-0.13±0.03	0.929	0.894
E2	3.55E7± 3.90E6	-0.17±0.04	0.950	0.922
E3	2.27E7± 0.92E6	-0.17±0.02	0.987	0.980
EE2	3.21E7± 2.88E6	-0.14±0.03	0.954	0.931
BPA	2.36E7± 3.72E6	-0.19±0.07	0.831	0.750

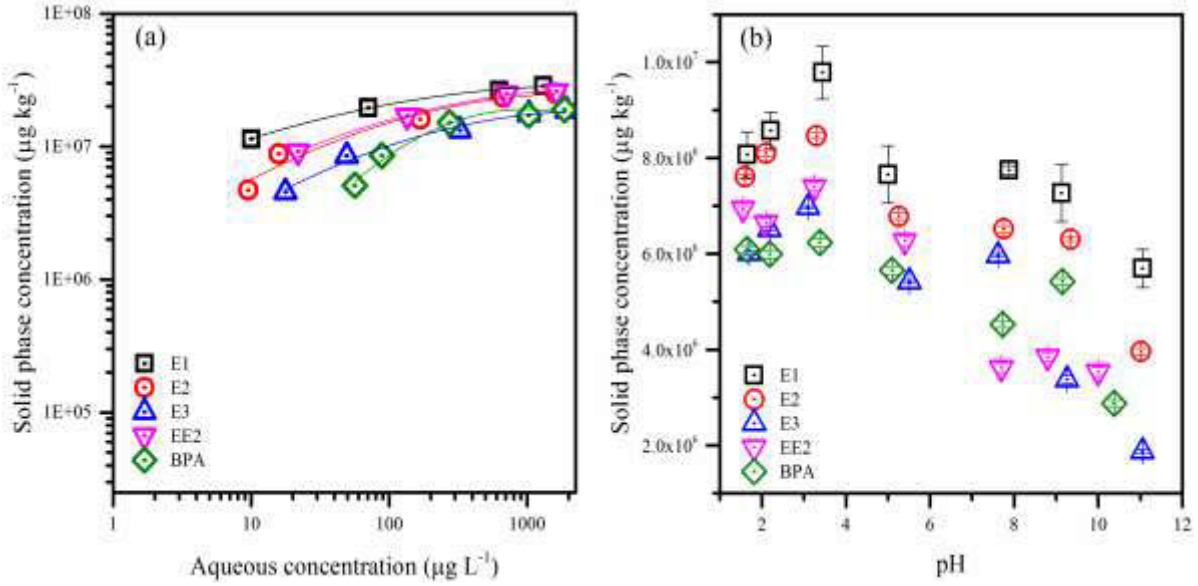

Figure 5.2.1: (a) Adsorption isotherms of estrone (E1), 17β-estradiol (E2), estriol (E3), 17α-ethynylestradiol (EE2) and bisphenol A (BPA) on fBC at pH 3.0-3.5. Solid lines are the polynomial fitting curves using PMM. (b) Effect of pH on solid phase concentration (μg kg^{-1}) during HOC sorption (initial concentration of each HOC was ~500 μg L^{-1}) by fBC with dosage of 40-60 mg L^{-1}, 25 ºC.

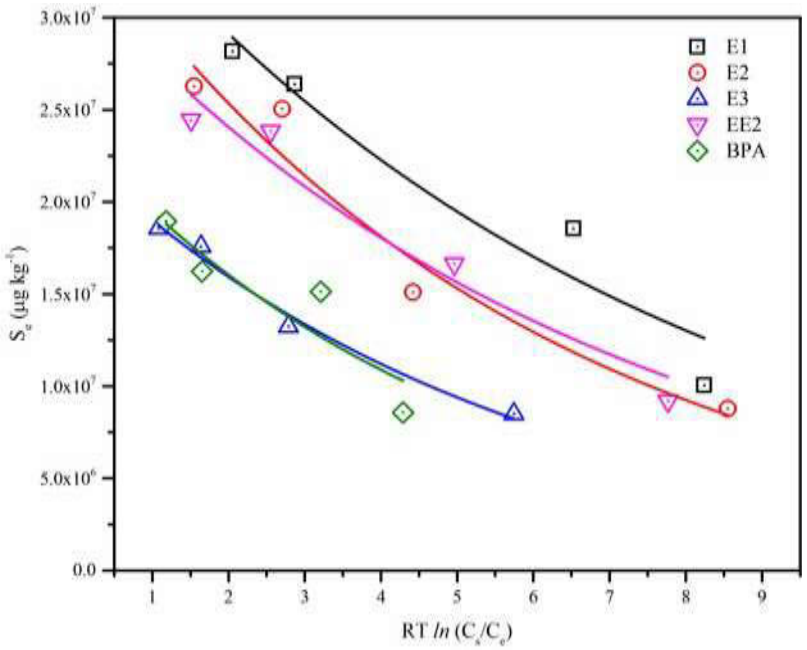

Figure 5.2.2: PMM Sorption Isotherm Fitting for HOCs. Isotherm Parameters were Normalized by the Primary Solute Solubility with b= 1, and S_e of Single-Solute Isotherms.

Freundlich isotherm r_{adj}^2 values of HOCs provided a slightly better fit than PMM isotherm r_{adj}^2 values indicating the role of surface functional groups for multilayer sorption of HOCs and the heterogeneity of the sorbent. Freundlich parameter '*n*' values of HOCs ranged from 0.17 to 0.27, and all solute isotherms were nonlinear for all HOCs indicating that favourable for multilayer adsorption and heterogeneous energy distribution of fBC-2 (**Tables 5.2.4 and 5.2.5**). Hence, the net interactive forces involving the solvent, solute, and the adsorbent are assumed to be responsible for the solute adsorption by sorbent surface activity in addition to pore filling in our fBC-2 [400]. Among different forces of attraction, van der Waals force is primarily considered the dominant force for gas or vapour adsorption onto any hydrophobic adsorbent surface (such as CNTs), which may also be significant for adsorption from the aqueous phase [400]. Considering only van der Waals forces, however, may not be applicable in cases when dipole-dipole, induced-dipole, and H-bonding or π-π donor-acceptor interactions exist, typically in the aqueous phase, where these forces can be necessary especially for chemicals and adsorbents with specific functional groups. Different possible interactions including H-bonds, hydrophobic effects, π-π bonds, covalent and electrostatic interactions can be observed and are responsible for the adsorption of organic chemicals on the surface of fBC-2. The strengths of such interactions and their and contribution to the overall sorption are a function of the properties of both organic chemicals and fBC-2 surface [400]. Based on pH effects as shown in **Figure 5.2.1b**, lower sorption of HOCs was expected below the point of zero charge of fBC-2 due to the repulsion of same charged species (i.e. positive fBC-2 surface and protonated phenolic –OH groups of HOCs). Above the point of zero charge of fBC-2, higher sorption of HOCs is expected due to oppositely charged species (negative fBC surface and neutral or deprotonated HOCs). Aside from electrostatic interactions, EDA interactions, H-bond formation and hydrophobic effects may play vital roles. Hence, at pH below 2.2, lower sorption was found, which was mainly due to EDA and hydrophobic effects. The maximum sorption of HOCs at pH 3.0-3.5 could be due to EDA interactions together with the strong H-bond formation, hydrophobic effects and electrostatic interactions. At pH 8.0-9.5, the sorption for each HOC was also slightly higher than pH 3.0-3.5, which might be due to H-bond formations and EDA interactions. Details on the noncovalent forces based on experimental findings are presented in the following subsections.

5.2.3.2. Role of H-bond and π-H bond for Sorption of HOCs

pH impacted sorption of all HOCs (**Figure 5.2.1b)**, with the most significant effect at pH range 3.0-3.5 and the least significant effect above pH 9.5. We categorized the adsorption data fall into three distinct pH ranges: pH below 2.2, pH 3.0-3.5, and pH 8.0-9.5. In general, the variations of sorption at different pH indicated that H-bond formation was involved.

To ensure that the effect of solution pH on HOC sorption was not a result of changes in the aqueous phase and solute activity coefficients, the solubilities of HOCs, PHEN and DNB were measured in three different solution pH values (**Table 5.2.1**). The fact that no significant changes in solubilities were observed indicated that the changes in sorption with pH resulted from the effects on sorbent-sorbate interactions, not solute-solvent interactions. Previously, Zhu et al. [350] studied PHEN interaction mechanisms on soil organic matter and concluded that sorption of PHEN was solely due to π-π interactions by rejecting solute hydrophobicity, H-bonding, solute co-planarity, solute activity coefficient, and mineral surface proportionating. We also observed that sorption of PHEN was high at low pH (**Figure 5.2.3a**) and the solubility of PHEN was not affected by solution pH. One may assume that the variation of K_d values at different pH for sorption of PHEN was related to H-bond formation.

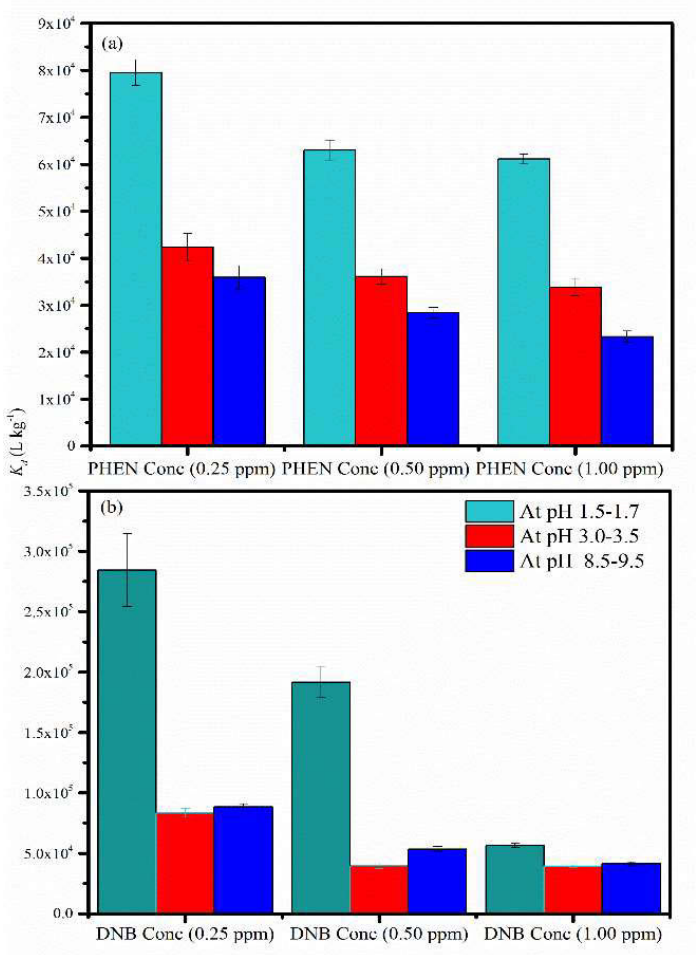

Figure 5.2.3: Individual sorption of different concentrations of (a) phenanthrene (PHEN) and (b) 1,3-dinitrobenzene (DNB) on fBC-2 at different pH, 25 ^{0}C using fBC-2 dosage of 18-25 mg L^{-1} and 40-60 mg L^{-1}, respectively for PHEN and DNB.

However, H-bond and π-H-bond formation at low pH by fBC-2 can be ruled out based on the following assumptions. NON-2 is a compound commonly known as stronger H-acceptor and non π-donor than aromatic hydrocarbons [350]. If the hypothesis was correct, plausible explanation of NON-2 sorption (at low pH) is that NON-2-sorption should increase as pH decreases. This is due to H-bond formation by a polar ketonic group of NON-2 with proton groups of sorbent, and π-H-bond formation by NON-2 with the aromatic π-system of sorbent (i.e. graphitic unit of fBC-2). However, the opposite trend where the sorption of NON-2 on fBC-2 was decreasing with pH decrease was observed (**Figure 5.2.4**). We also carried out the solubility test for NON-2 and found no changes in solubilities at pH 1.8 and pH 3.5 but at pH 8.5 solubility decreased by ~25%. Also, PHEN molecule does not have any oxygenated functional group to form H-bonds with a surface functional group of fBC-2. However, sorption of NON-2 at different pH was mainly due to hydrophobic effect. Thus, H-bonding and π-H-bonding (by the withdrawal of electron density from the ring by the H-bond) of fBC-2 cannot

explain the acid-enhanced sorption of PHEN[19]. Therefore, sorption of PHEN was mainly due to hydrophobic effects and π-π-EDA interactions between PHEN and fBC-2. On the other side, selected HOCs have at least one hydroxyl group along with other groups connected with arene units in their structure. Consequently, sorption interactions of HOCs will not be similar in all cases as PHEN. For example, a variation of solution pH indicates that H-bond formation is associated with surface functional groups on fBC-2 and HOCs. Hence, after excluding π-H-bonding, it can be concluded that the pH-dependent sorption of HOCs is undoubtedly due to their H-bonding involvement plus other interactions such as π-π EDA interactions, and hydrophobic interactions. However, the contribution of H-bonding to the overall adsorption of HOCs is unknown.

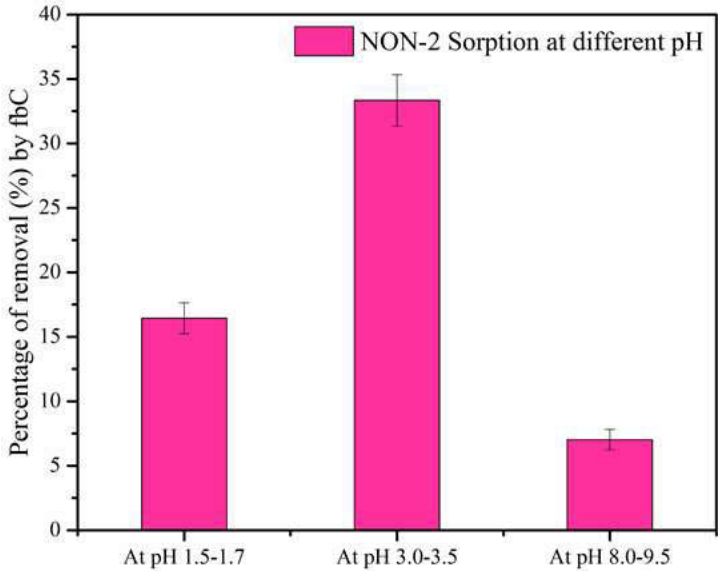

Figure 5.2.4: Removal percentage NON-2 during sorption by fBC-2 (30-35 mg L^{-1}) at different pH, highlighting the role of π-H-bonding and H-bonding with fBC-2.

5.2.3.3. Normalization to Hydrophobic Effects

The role of hydrophobic interactions was premeditated using inert solvent-n-hexadecane. Higher single point adsorption coefficient (K_d) of HOCs attributed to the higher sorption of HOCs by fBC-2. Thus, the normalization of K_d values by hexadecane-water partition coefficient (K_{HW}) could rule out the hydrophobic effect, and potential adsorption mechanism could be due to π-π interactions. We measured the hexadecane-water partition coefficient (K_{HD}) of HOCs and PHEN at 25 ºC (**Table 5.2.1**). The hydrophobicity followed the order of PHEN > E1 > E2 > EE2 > E3 > BPA. The resulting parameters are listed in **Tables 5.2.1 and 5.2.5.**

The normalized partition coefficient (K_d/K_{HD}) of HOCs showed significantly higher values than PHEN (**Figure 5.2.5a**) indicating the significant role of π-π interactions for HOCs sorption by fBC-2. Moreover, this relationship was directly related to K_d and K_{HD} of HOCs (**Figure 5.2.5b**).

Table 5.2.5: Hexadecane-Water Partition Coefficient and Sorption Coefficient Relationship.

Compound	log K_{HW}	log K_d (C_e = 0.002 C_s) at pH 3.0-3.5	K_d/K_{HW} (C_e = 0.002 C_s) at pH 3.0-3.5
E1	0.84	6.46	418934
E2	0.36	5.90	345894
E3	-0.19	5.33	331013
EE2	0.65	5.70	111964
BPA	-0.47	4.48	88645
PHE	1.251	2.96 (at pH 1.5)	51.17

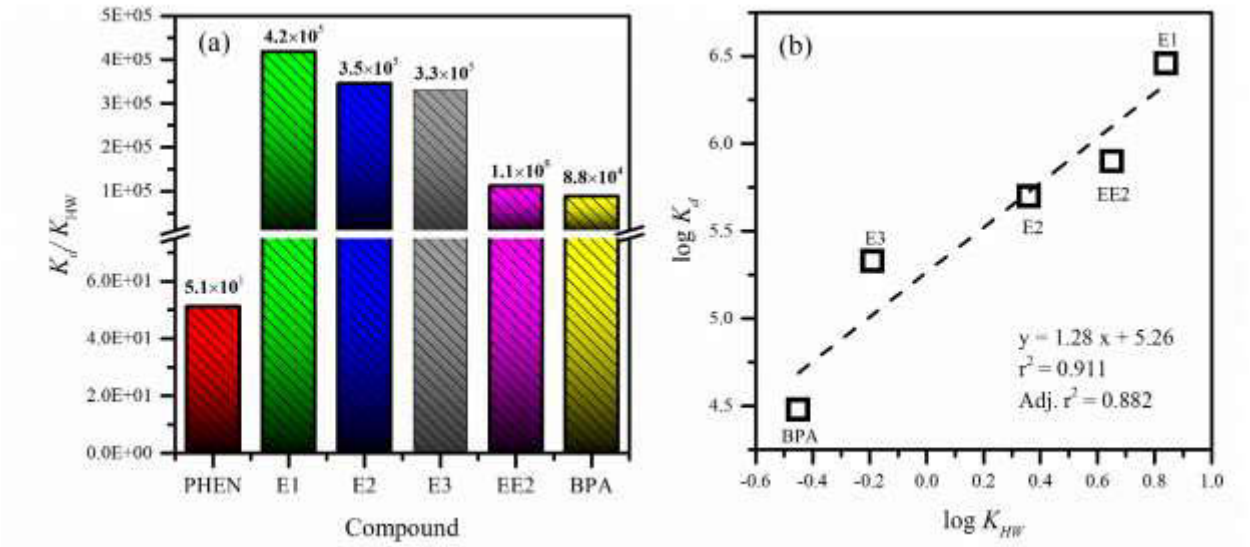

Figure 5.2.5: (a) Comparison of K_d/K_{HW} between phenanthrene (PHEN) and HOCs such as estrone (E1), 17β-estradiol (E2), estriol (E3), 17α-ethynylestradiol (EE2) and bisphenol A (BPA). K_d/K_{HW} was calculated at C_e = 0.002 C_s. The K_d/K_{HW} values of solutes were directly labelled on their respective bars due to the off-scale values. The differences among them are consistent with the explanation that π-π bonds played a major role after eliminating hydrophobic effects. The π-π bonds formed among HOCs and fBC-2 were a donor/acceptor system, and much stronger than those between PHEN and fBC-2. (b) Relationship between log K_{HW} *vs* log K_d as calculated at C_e = 0.002 C_s.

5.2.3.4. Evidence for π-π EDA Interactions

5.2.3.4.1. *Evidence from Experimental Finding*

From literature, it has been reported that the adsorption of chemical contaminants on CMs increases with increasing oxygen-containing functional groups, which is partially attributed to π-π EDA interactions [244, 388, 401]. Surface carboxylic acid, nitro, and ketonic groups of CMs can act as an electron acceptor to form π-π EDA interactions with aromatic molecules and thereby enhance sorption [402]. On the other hand, graphitic carbon like structure, hydroxyl and amine groups present in different CMs can serve as π-electron-donor site depending on the type of functionalization. The strongest π-π interactions are between oppositely charged arene units, while the weakest one is between like polarized units [402]. All HOCs used in this study have at least one hydroxyl group connected with arene unit and we hypothesis that this arene unit could act as the π-electron-donor site due to resonance effects. If the hypothesis is correct, then the presence of a competitor (π-electron acceptor) in the same solution should affect sorption capacity to some extent. Thus, to prove this concept, we provided both π-electron-donor (PHEN) and π-electron-acceptors (DNB and PABA) at different concentrations in each HOC solution at three different pH (pH 1.5-1.8, 3.0-3.5, and 8.5-9.5) individually and observed their effects.

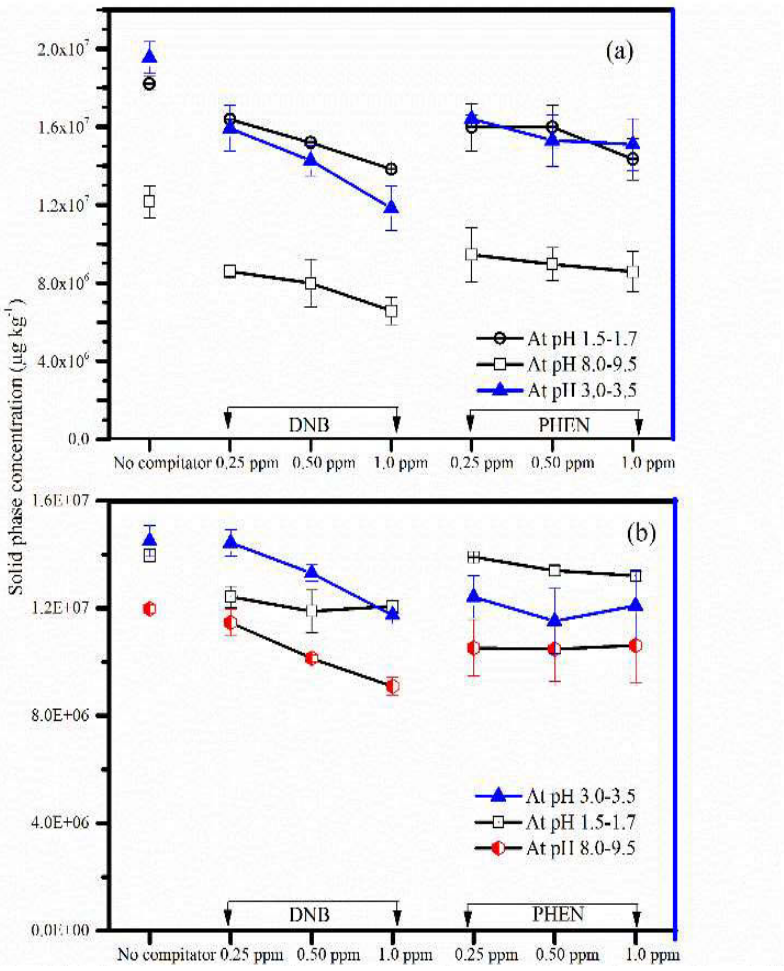

Figure 5.1.6: Sorption performance of (a) estrone (E1) and (b) bisphenol A (BPA) in the absence and presence of competitor such as π-electron-donor phenanthrene (PHEN) and π-electron-acceptor 1,3-dinitrobenzene (DNB). Their interactions indicated the role of co-solutes and the role of π-π electron-donor-donor or donor-acceptor multi-system on the sorption performance of HOCs by fBC-2. Error bar representing the standard deviation. Sorption performance of 17*β*-estradiol (E2), estrio (E3) and 17*α*-ethynylestradiol (EE2) in the absence and presence of π-electron-donor-acceptor system is represented in Figure 5.2.7. Each HOC initial concentration was ~1000 µg L^{-1} and fBC dosage was maintained 40-60 mg L^{-1}.

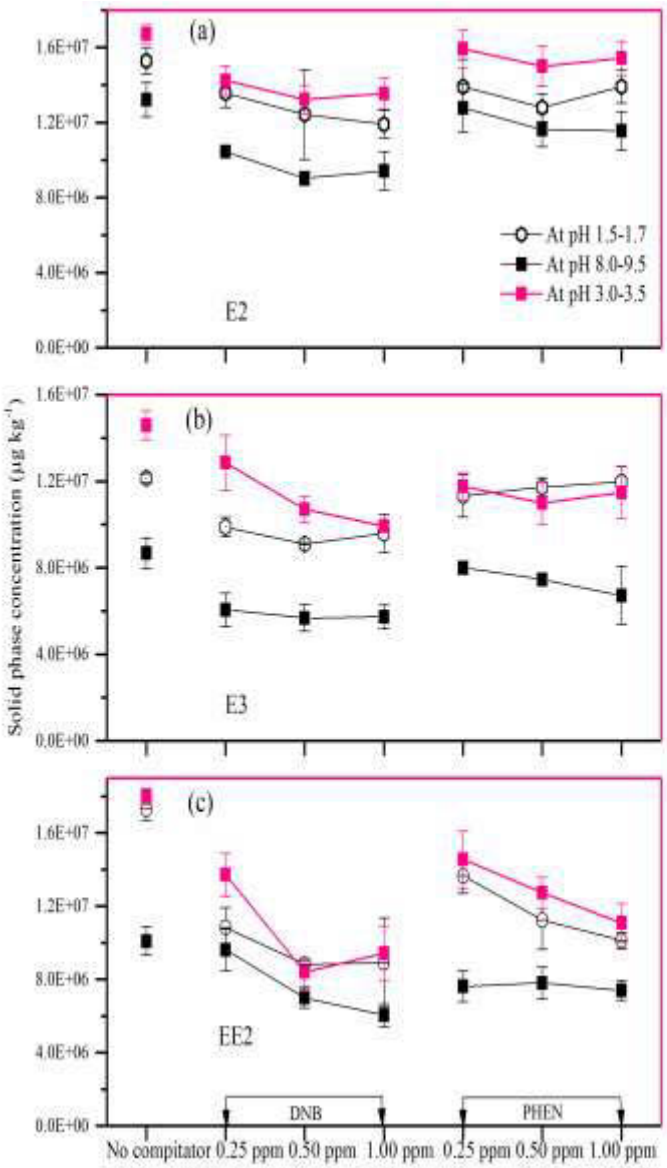

Figure 5.2.7: Sorption performance of (a) 17β-estradiol (E2), (b) estriol (E3), and (b) 17α-ethynylestradiol (EE2) in the absence and presence of competitors such as π-electron-donor phenanthrene (PHEN) and π-electron-acceptor 1,3-dinitrobenzene (DNB). Their interactions indicated the role of co-solutes and the role of π-π electron-donor-donor or donor-acceptor multi-system on the sorption performance of HOCs by fBC-2. Error bar representing the standard deviation. The initial concentration of HOC was ~1000 μg L^{-1} and fBC-2 dosage was maintained 40-60 mg L^{-1}.

Apparent view of the **Figures 5.2.6** and **5.2.7** provided an overall idea of the competitors' effects on HOC sorption. DNB has a higher influence on the reduction of sorption capacity of HOCs than PHEN. This change is high at pH 3.0-3.5 compared to other pH values. For example, in the presence of PHEN, no significant change in the solid-phase sorption capacity of BPA observed. This indicates the minor role of π-electron-donor-donor interactions as arene unit in BPA served as the π-electron-donor site. In contrast, the presence of DNB reduced the solid-phase sorption capacity of E1 and BPA by ~48% and ~25%, respectively, apparently supporting the role of EDA interactions. However, the presence of PHEN also affect sorption capacity to few extents, and this might be due to co-solute effects. Similar strong EDA interactions have also happened for E2, E3 and EE2 (**Figure 5.2.8)**. Thus, DNB had an adverse effect on the adsorption of HOCs. This result is consistent with the π-π-EDA interactions after normalizing hydrophobic effects as shown in **Figure 5.2.5a**, indicating the protagonist role of the EDA interactions in solution. Also, we also used another model π-electron-acceptor such as PABA and obtained similar results (**Figures 5.2.9 and 5.2.10**). Thereby, these findings indicated the protagonist role of EDA interactions in the sorption of EDCs by fBC-2.

Moreover, a previous study hypothesised that increasing solution pH facilitated deprotonation of the acidic functional groups (-COOH, -OH) of CMs [388]. Deprotonated functional groups (e.g. $-COO^-$ and $-O^-$) might modify the hydrophobicity and the net charge on the carbon surface, which can further promote the π-electron-donor ability of the graphene surface ($-COO^-$ is a strong electron donor), thereby enhancing π-π EDA interactions of two nitroaromatics (e.g. DNB and 1,3,5-trinitrobenzene as π-electron acceptors) [388]. They observed that sorption of nitroaromatics to single-walled CNTs increased by 2-3 times with the increase of solution pH. Thus, similar interactions may apply to the system in this study. We observed that sorption of DNB by fBC-2 was slightly increased when pH was increased from 3.0-3.5 to 8.5-9.5, indicating the role of EDA interactions between DNB and deprotonated acid functional group ($-COO^-$) of fBC (**Figure 5.2.4b**). All these results indicated that π-π-electron-donor-acceptor interaction was one of the significant forces responsible for the overall HOC-fBC-2 interactions.

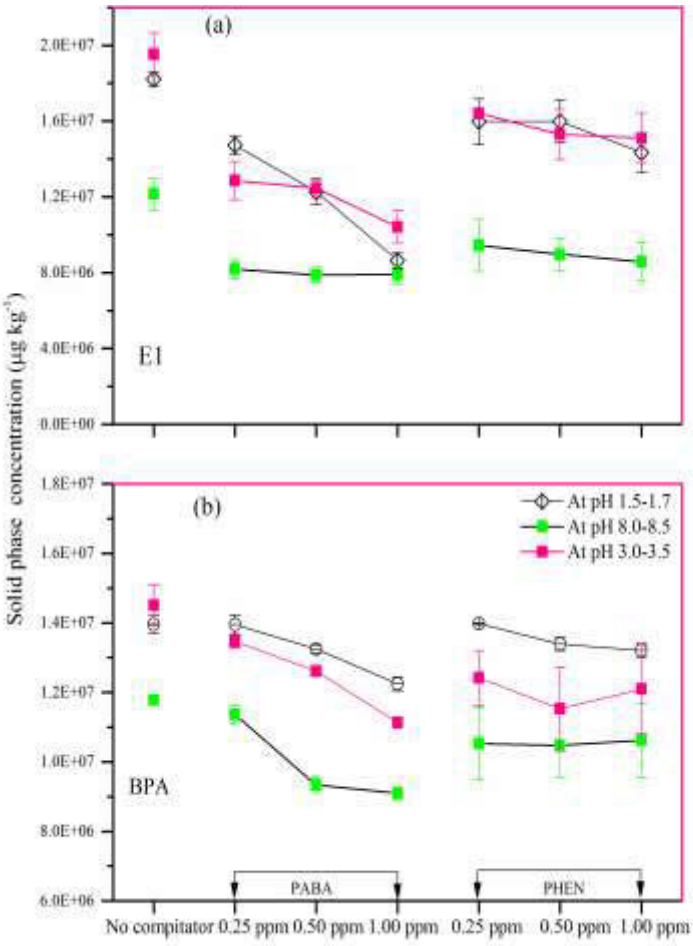

Figure 5.2.9: Sorption performance of (a) estrone (E1) and (b) bisphenol A (BPA) in the absence and presence of competitors such as π-electron-donor phenanthrene (PHEN) and π-electron-acceptor *p*-amino benzoic acid (PABA). Their interactions indicated the role of co-solutes and the role of π-π electron-donor-donor or donor-acceptor multi-system on the sorption performance of HOCs by fBC-2. Error bar representing the standard deviation. The initial concentration of HOC was ~1000 µg L^{-1} and fBC-2 dosage was maintained 40-60 mg L^{-1}.

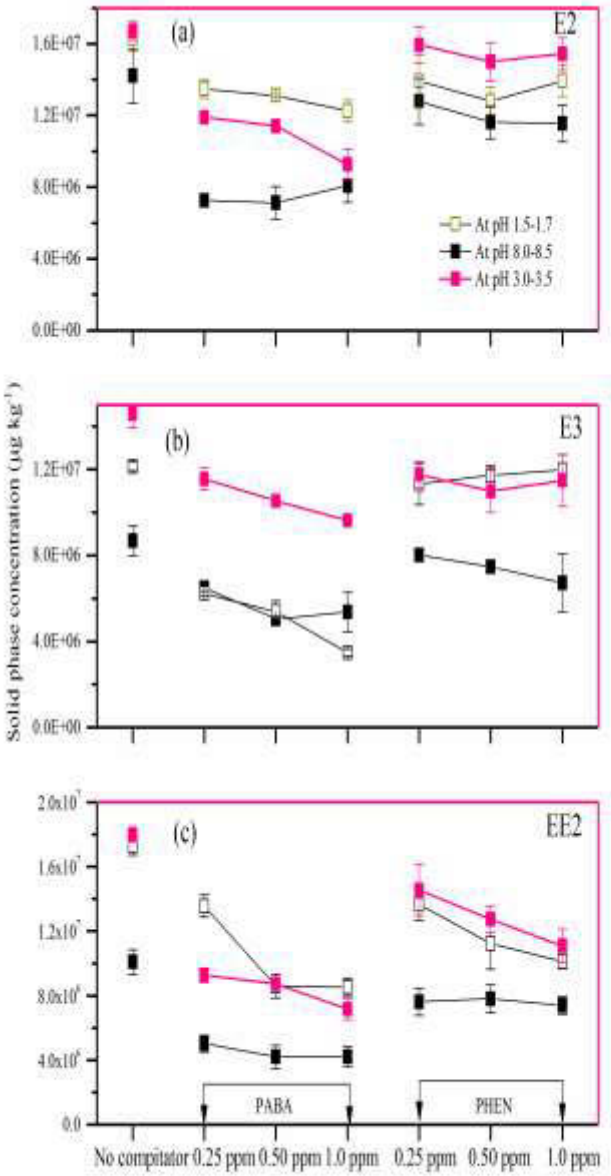

Figure 5.2.10: Sorption performance of (a) 17β-estradiol (E2), (b), estriol (E3), and (b) 17α-ethynylestradiol (EE2) in the absence and presence of competitors such as π-electron-donor phenanthrene (PHEN) and π-electron-acceptor *p*-amino benzoic acid (PABA). Their interactions indicated the role of co-solutes and the role of π-π electron-donor-donor or donor-acceptor multi-system on the sorption performance of HOCs by fBC-2. Error bar representing the standard deviation. The initial concentration of HOC was ~1000 µg L^{-1} and fBC-2 dosage was maintained 40-60 mg L^{-1}.

5.2.3.4.2. UV-Vis Spectroscopic Evidence

Figure 5.2.11 shows the presence of π-π charge-transfer absorbance band in the UV region for the mixture of DNB (as an acceptor), PHEN (as a donor) and HOCs (such as BPA, E3 and E1 as π-donor). Noteworthy deviation of adsorption intensity was observed for PHEN and DNB solutions (**Figure 5.2.5a**). A similar result was also observed for DNB and E1 or BPA interactions indicating the π-π EDA interactions took place (**Figure 5.2.5b-d**). On the other hand, no interaction (no deviation of adsorption intensity) was observed for the mixture of PHEN and E1/BPA/E3. We also increased the donor-acceptor concentration and similar result observed which indicate the EDA interactions between π-electron-donor site and π-electron-acceptor site of the selected model compounds (**Figure 5.2.5b**). Hence, we predict same interactions in solutions at different pH happened between π-electron donor and π-electron acceptor sites of fBC-2 and π-electron donor site in the target HOCs.

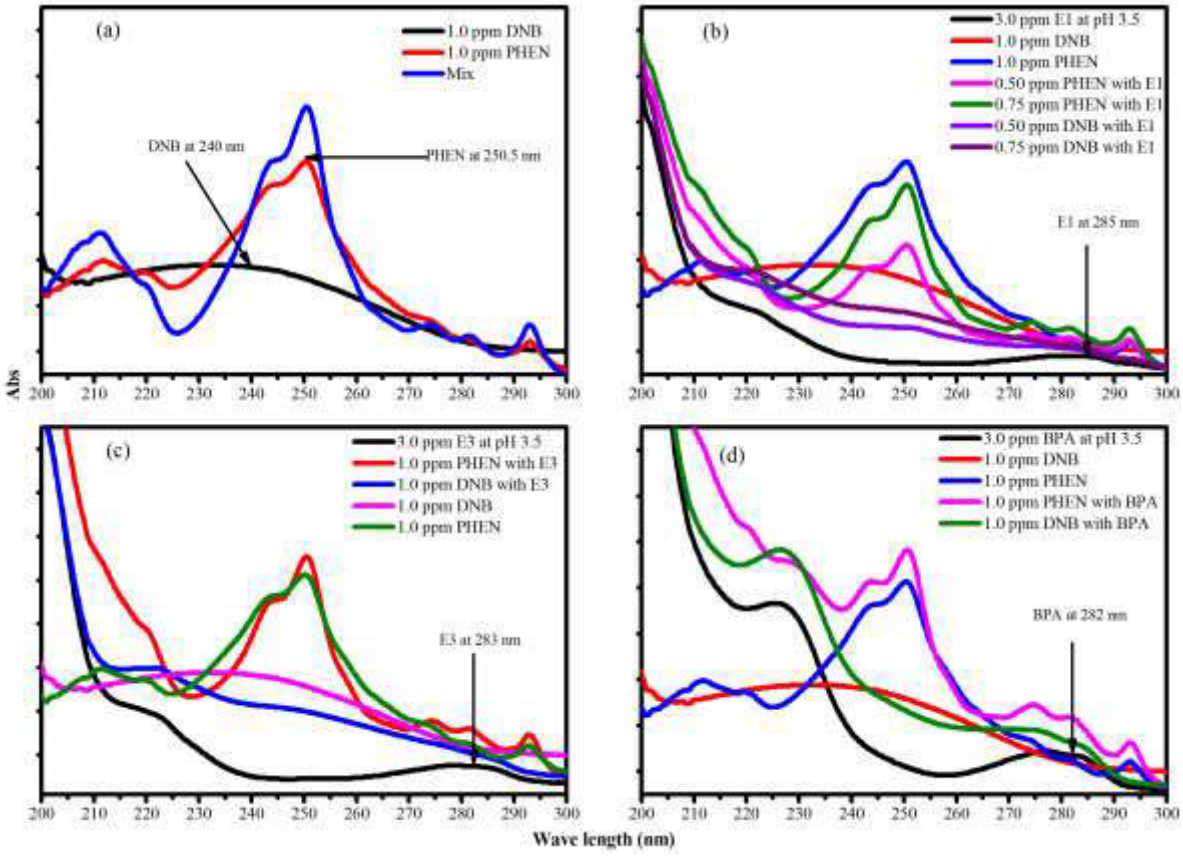

Figure 5.2.11: UV-Vis spectra difference in the acceptor-donor mixture showing the charge-transfer absorption band of π-π complexes. (a) Donor-phenanthrene (PHEN), acceptor 1,3-dinitrobenzene (DNB) and their mixing interaction, (b) Donor-PHEN, acceptor-DNB and HOC-estrone (E1) interactions, (c) Donor-PHEN, acceptor-DNB and HOC-estriol (E3) interactions, and (d) Donor- PHEN, acceptor-DNB and HOC-BPA interactions clearly indicating the difference of absorption band of π-π complexes.

5.2.3.4.3. ^{1}H NMR Spectroscopic Evidence: Specific Direction of π-π EDA Interactions

Previously, Zhu et al. [350] and Wijnja et al.[318] used ^{1}H NMR spectroscopy to examine π-π interactions in solutions among PHEN, quinones, N-heteroaromatic cations, naphthalene, pentamethylbenzene, 1,3,5-benzenetricarboxylic acid, 1,4,5,8-naphthalenetetracarboxylic acid and pyridine. In this study, we also used ^{1}H NMR tool to demonstrate molecular complexation in solution between π-electron-donor (PHEN) and π-electron-acceptor (DNB) and their effect on π-π interactions in a solution of E1 and BPA (as π-donor due), separately. We assume that π-π interactions might occur between subunits attached to fBC-2 surface due to π-electron-donor (i.e., graphitic carbon, OH, and NH_2) and/or π-electron-acceptor (e.g., COOH, C=O, C-O-PO_3) groups. Our assumption is reasonable because π-π interactions occur, in here, readily in a nonaqueous solvent (methanol-d_4) and π-π interactions have already been demonstrated in solid-liquid-phase systems based on donor-acceptor competitor experimental proof.

In ^{1}H NMR, it has long been known that placing a nucleus above or below the plane of an aromatic structure causes electronic shielding due to “ring current” effects. Moreover, placing a magnetic nucleus along the edge of an aromatic ring results in the opposite ring current effects so-called deshielding effect. Hence, because of the parallel-planner geometry of a π-π complex system, one may easily expect an upfield chemical shift (δ) of protons on one ring induced by the ring current effect of the opposing ring [388]. This has been used as a tool to identify π-π interactions in solution for different compounds [350, 388]. Similarly, our case is entirely consistent with the formation of π-π complexes as a function of interactions due to observed upfield chemical shift in complex mixtures of π-donor and π-acceptor model compounds.

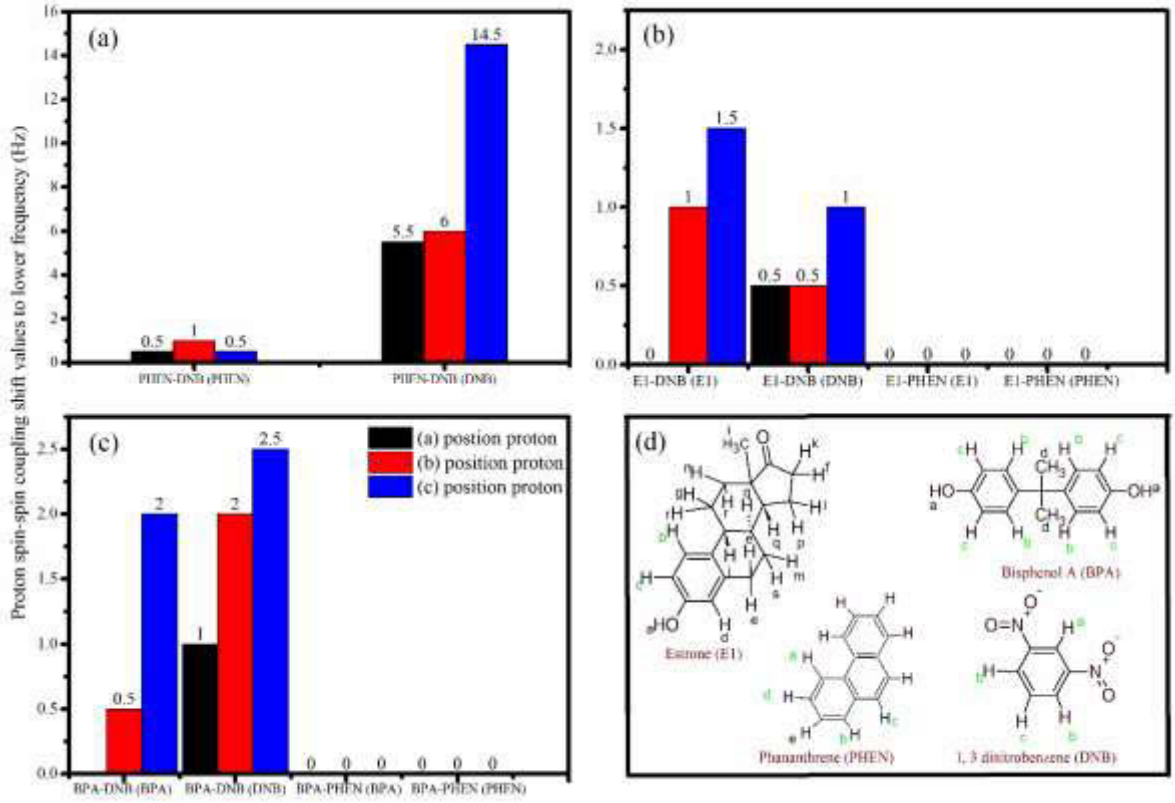

Figure 5.2.12: ^{1}H NMR observed frequency shift for different protons in specific carbon bonded protons in the respective structure of structure of E1, BPA, DNB, and PHEN (Figures a-c). ΔHz of each proton in each component in their mixture specified within first bracket. Data obtained from a series of combine mixing solution of solutes and their increased shielding by extra-nuclear electrons (i.e. increasing magnetic field at fixed frequency) from a fixed concentration of solute in methanol-d4 solvent. Observed frequency shift (ΔHz) for each solute in solution was measured by multiplying the chemical shift (δ) of each solute and spectrophotometer frequency for different proton positions (marked as green color) as shown in figure (d). Structural proton positions were labelled based on ^{1}H NMR peaks accessible at http://sdbs.db.aist.go.jp/sdbs/cgi-bin/cre_result.cgi?STSI=151281072529897. (d) Illustration of offset geometry of HOCs in which proton number lies in the structure.

Therefore, It was calculated the observed frequency shift for specific proton (in respective carbon of arene unit) in the same orientation for the respective solute. The specific direction of π-π interactions orientation was identified for each solute. Upfield shifts of protons at different positions of each solute occurred for the following combinations: (i). PHEN (positions a, b, c in **Figures 5.2.12a & d**) in a mixture solution of PHEN and DNB; (ii). DNB (positions a, b, and c in **Figures 5.2.12a & d**) in a mixture solution of PHEN and DNB; (iii). E1 (positions b, and c in **Figures 5.2.12b & d**) in the mixture solution of E1 and DNB; (iv). DNB (positions a, b, and c in **Figures 5.2.12b & d**) in the mixture solution of E1 and DNB; (v). BPA (positions b, and c in **Figures 5.2.12c & d**) in the mixture of BPA and DNB; (vi). DNB (positions a, b, and c in **Figures 5.2.12c & d**) in the mixture of BPA and DNB. No

upfield frequency changes for respective protons were observed (Hz = 0) from the interactions of E1 and BPA with PHEN (**Figure 5.2.12**).

These results show that arene unit of HOCs served as a π-electron-donor unit due to the presence of hydroxyl group. Hence, clear π-π EDA interactions observed for DNB and π-electron-donors (i.e. E1 and BPA) in solution and the interactions were specific toward defined protons in each arene unit (i.e. π-π-electron-donor-acceptor system). We predict that the similar interactions also responsible for other HOCs such as E2, EE2 and E3. As fBC-2 consists of both π-electron-donors and π-electron-acceptors groups, thereby, π-π EDA interactions happened at different pH. Also, the NMR results for different HOCs did not provide evidence of π-H-bonding, as no downfield shifts of protons were observed for different complexes indicating the insignificant involvement of π-H-bonding [350].

5.2.3.5. Role of π-Donor and π-Acceptor Domains in fBC-2 Structure at Different pH

CMs consist of graphitic sheets and different functional groups. For example, CNTs contain more than 95% graphitic carbon. Hence, the hydrophobicity of CNTs is an important factor affecting the sorption of solutes. Functionalization of CMs can introduce hydrophilic moieties to the surface of CMs and thereby affect the sorption affinity of the contaminants [55, 403]**.** For example, the introduction of O-containing moieties either increases or decreases sorption of organic contaminants and might act as π-electron-donor (e.g., OH group) and π-electron-acceptor (e.g., COOH, C=O, -COO-) sites [271, 396, 404]**.** The presence of aromatic amine groups (hetero) in the polyaromatic surface of CMs can act as π-electron-acceptor in forming π^{+}-π EDA interactions with the π-electron-rich surface of CMs [387]. XPS results of fBC-2 showed that fBC-2 consisted of 81.76% C, 13.32% O, 0.8% N and 2.3% P. Hence, fBC-2 surface was composed of C=C, –C-OH, -COOH, C=O, heteroaromatic amine and pentavalent tetra coordinated phosphorus (PO_4, i.e. C-O-PO_3) groups. These functional groups can serve as either π-electron-donor and π-electron-acceptor or both. Therefore, it can be predicted that π-π interactions were? based on solution chemistry and effects of competitors (π-donor or acceptor) at different solution pH. Thence, the presence of π-electron-donor and acceptor compounds in the solution can hamper the sorption significantly, and this result can reveal that the presence and the role of π-donor/acceptor domains in any materials.

In general, π-electron-donor site of any material binds to a π-electron acceptor compound and vice versa. At pH 8.0 to 9.5, fBC-2 surface might serve as the π-electron-acceptor site due to surface ketonic, ester, and hetero-N-cyclic aromatic groups [387]. Also, the zeta potential of

fBC-2 was found profoundly negative at this pH (-48.0 mV) indicating the presence of the deprotonated carboxylic (-COO^-, a strong electron-donor), which could serve as hydrophobic moiety and form H-bonds together with EDA interactions. The π-electron-donor ability also came from graphitic carbon; surface –OH (if not dissociate); and $–NH_2$ groups. Therefore, at this pH range, from the comparison of K_d values of PHEN and DNB, it can be concluded that π-electron-donor ability of fBC-2 is stronger than π-electron-acceptor groups (**Figure 5.2.4**). However, both groups are active for EDA interactions. Furthermore, sorption of HOCs did not change significantly in the presence of π-donor PHEN (indicating HOCs served as π-donor groups) and changed a lot in the presence of DNB and PABA (**Figures 5.2.7-11**). Therefore, we assume π-electron-donor groups dominants over π-electron-acceptor groups for EDA interactions, but this domination is not strong as like as acid enhanced sorption of HOCs; PHEN; PABA and DNB (at pH 1.5-1.7).

At pH 3.0-3.5, we predict both π-electron-donor and π-electron-acceptor domains of fBC-2 were active to form strong EDA interactions and strong H-bonds. This can be confirmed by the higher sorption of all HOCs (**Figure 5.2.1b**). Thus, maximum pH is from EDA interactions as fBC-2 surface comprises of π-electron-acceptor (e.g., COOH, C=O, hetro-N-cyclic, C-O-PO_3) and π-electron-donor (e.g. graphitic carbon of fBC-2, –OH, $–NH_2$) groups. Similar interpretation for EDA interactions can be made based on **Figure 5.2.4,** where sorption of PHEN was significance over pH 8.0-9.5. The zeta potential value of fBC-2 at this pH was -18.0 mV and deprotonation of surface –OH groups was insignificant at this pH (due to pK_a sorption at this value of surface –OH group is 8.5-10) indicating the role of H-bonds formations together with EDA interactions [59]. Also, pK_a value of each HOC is more than 10 (**Table 5.2.1**). Thus, charge-assisted H-bond formation also played an imported role for the maximum sorption of HOCs. H-bonds formation can also come from ketonic groups or ester groups of fBC-2 as the maximum sorption of NON-2 (as H-acceptor) was found at pH 3.0-3.5 indicating the role of H-bond formation. These findings indicated the role of both π-electron-donor and acceptor domains of fBC-2 surface for the sorption of HOCs, PHEN and DNB.

The sorption of PHEN, PABA and DNB were increased considerably when the solution pH was low (1.5-1.7) indicating the presence of both π-electron-donor and π-electron-acceptor groups on fBC-2 surface (**Figures 5.2.4** and **5.2.13**). Also, at pH below 1.8, fBC-2 surface became positive (+4.5 mV), indicating that the surface hydroxyl, carboxyl and amino groups of fBC-2 became protonated (i.e. $COOH_2^+$, $-OH_2^+$, $-NH_3^+$). Therefore the H-bonds formation by fBC-2 at this pH would play a minor role. Graphene surface of fBC-2 could serve as the π-electron-donor site [405], and ketonic group, ester groups, C-O-PO_3 and hetero-N-cyclic

groups of fBC-2 might serve as the π-electron-acceptor groups. Hence, EDA was the main sorption mechanism. Finally, HOC sorption in the presence of PHEN, PABA and DNB (**Figures 5.2.7-11**) also indicated the duel behaviours of fBC-2 surfaces at this pH. Hence, at this pH range, both π-electron-donor and π-electron-acceptor groups were significantly active for the sorption of opposite π-electron compounds. The EDA interactions were the strongest interactions among other interactions at this pH range. Therefore, fBC-2 surface consists of different functional groups, and their behaviours change significantly with the change of solution chemistry.

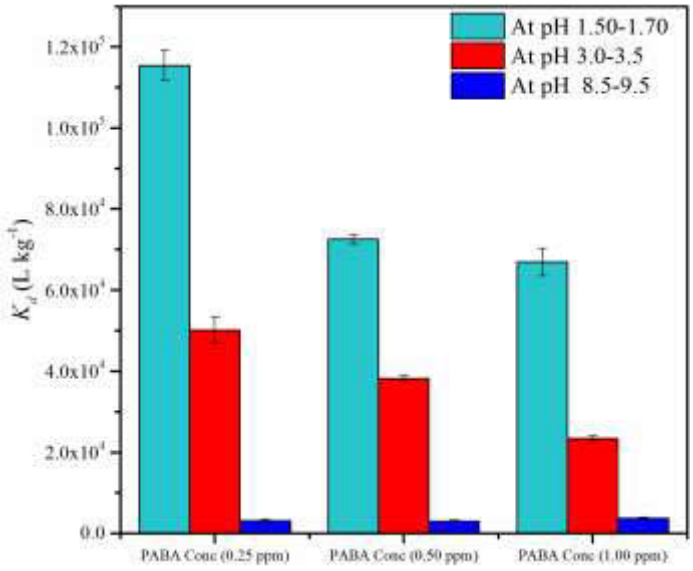

Figure 5.2.13: Sorption of PABA at different concentrations and different pH using fBC-2 dosage of 40-60 mg L^{-1}.

5.2.4. Concluding Remarks

The affinity of functinalized biochar toward hydrophobic organic contaminants sorption showed excellent results. The main causes of this affinities are π-π-EDA interactions and hydrogen bonds formation together with other sorption mechanisms such as pore filling; electrostatic attractions and hydrophobic effect. Different theoretical, instrumental and experimental proofs for a potential cause of hydrogen bonds and π-π-EDA interactions were undertaken. Most importantly, the specific direction of π-π-EDA interactions was identified. Also, π-electron-donor and π-electron-acceptor domains in fBC-2 were responsible for the different sorptive mechanism at different solution pH. Therefore, functinalized biochar has the capability for sorption of a wide range of hydrophobic organic contaminants from aqueous solution.

UNIVERSITY OF TECHNOLOGY SYDNEY

Faculty of Engineering and Information Technology

CHAPTER: SIX

CONCLUSIONS AND RECOMMENDATIONS

CHAPTER SIX: CONCLUSIONS AND RECOMMENDATIONS

6.1. Conclusions

In this study, different adsorptive materials such as biochar, fBC-1 and fBC-2, and a fBC composite were successfully prepared by the utilization of woody biomass (bamboo and eucalyptus wood) and scrap iron material (for composite sorbent). These materials were successfully applied to remove antibiotics and EDCs in single and competitive mode from water and wastewaters (e.g. lake water, MBR effluent and synthetic wastewater).

fBC was found to have good sorption capacity for removal of sulfonamide class of antibiotics (e.g. sulfamethazine (SMZ); sulfamethoxazole (SMX), sulfatiazole (STZ)), chloramphenicol class of antibiotic (e.g. chloramphenicol) and EDCs (e.g. estrone (E1), 17β-estradiol (E2), estriol (E3), 17α-ethynylestradiol (EE2), bisphenol A (BPA) and 4-*tert*-butylphenol (4*t*BP)) over pristine biochars. In this study, detailed mechanisms for removal of antibiotics and EDCs were determineed based on pH profile, speciation, ionic strength, materials charecteristics, temperature, thermodynamics, solution chemistry, and water matrixes. Different isotherm models such as the Langmuir isotherm model, Fruendlich isotherm model, and Polani-Mane model were applied to analyse the sorption data. For competitive sorption, summerized isotherm models were proposed. Several kinetic models such as pseudo first order kinetic model, pseudo second order kinetic model, intraparticle diffusion model and Boyd model were also employed. Speciall focus was given on both single and competitive effects on sorption performance based on experimental, theoretical and instrumental findings. The experimental, instrumental and theoretical findings suggested that antibiotics and EDCs sorption occurred mainly through pseudo-second order and external mass transfer diffusion processes, by forming H-bonds along with π-π EDA interactions at different pH. Other interactions such as van der walls forces, hydrophobic effect, electrostatic interactions, Lewis acid based interactions and ion exchange capacity were also studied in details. The treatment of wastewaters (e.g. synthetic wastewater, lake water and MBR effluent) was found very promising result using modified biochars in both single and competitive mode. The complete removal of antibitics and EDCs from different water decreased in the order: deionised water > MBR sewage effluent > synthetic wastewater. The presence of sodium lauryl sulphonate and acacia gum in synthetic wastewater significantly suppressed sorption affinity of antibiotcs and EDCs by 38–50%, hence requiring more fBC to maintain removal efficacy. With the regeneration of adsorbent, the applicability of biochar and fBC in water and

wastewater treatment will be economically feasible. Therefore, in this thesis, I particularly focus on the removal mechanism in detail using biochar and fBCs.

6.2. Contributions to the Field

- The successful application of novel adsorbents (fBC-1 & fBC-2) prepared from bamboo and eucalyptus wood for removing antibiotics and EDCs from aqueous solution in both single and competitive mode.
- Development of an efficient method for modifying surface of biochar helps to improve its adsorption capacities.
- Clearly addressed on details adsorptiom mechanisms based on different parameters such as pH profile, speciation, ionic strength, materials characteristics, temperature, thermodynamics, solution chemistry, and water matrices.
- Batch adsorption experiments and characterization of adsorbents improved the understandings on adsorption mechanisms of antibiotics and EDCs onto the adsorbents.
- Regeneration of adsorbent was successfully carried out.
- Successfully treated water and wastewater such as lake water, synthetic wastewater and MBR effluents.
- It was found that presence of sodium lauryl sulphonate and acacia gum in synthetic wastewater significantly suppressed sorption affinity of antibiotcs and EDCs by 38–50%.
- Advantages and disadvantages of adsorption of antibiotics and EDCs was successfully analysed based on experimental, theoretical and analytical findings.
- Prepared materials successfully applied for the treatment of 14 different organic contaminants such as antibiotics, EDCs, HOCs, and hydrophilic organic contaminants.

6.3. Recommendations for Further Research

The following recommendations are made for any future study on this important topic:

- Future research needs to explore highly efficient, low-cost adsorbents such as immobilisation of different metal-oxides onto fBC; preparation of fBC-complex for hybrid treatment technology e.g. sorption-reduction/oxidation for EC removal.
- fBC can be utilized in combination with othe chemical/biological processes e.g. MBR-fBC, fBC-photocatalysis hybrid system for EC removal.

- The majority of studies reported have been conducted in batch trials and single compound studies in synthetic waters. These trials need to be extended to continuous mode column with competitive solutes trials which have more relevance to real operating systems in natural water.
- Surface modifications of the adsorbents can be explored to increase the capacity and strength of adsorption without significantly increasing the cost of such modification.
- The technique developed in this study needs to be tested at pilot scale for commercial application of organic pollutants removal from wastewater.
- The constant discharge of antibiotics and EDCs in the aquatic environment becomes an essential part of the present life. Considering the widespread presence of these chemicals in the environment, it is essential that strategies be developed to control widespread environmental contamination of EDCs and antibiotics.
- More regeneration studies need to be done for adsorbents to reduce the costs of the water treatment process.

REFERENCES

[1] E. Diamanti-Kandarakis, J.P. Bourguignon, L.C. Giudice, R. Hauser, G.S. Prins, A.M. Soto, R.T. Zoeller, A.C. Gore, Endocrine-disrupting chemicals: an Endocrine Society scientific statement, Endocrin.e Rev. 30 (2009) 293-342.

[2] A. Sapkota, A.R. Sapkota, M. Kucharski, J. Burke, S. McKenzie, P. Walker, R. Lawrence, Aquaculture practices and potential human health risks: current knowledge and future priorities, Environ. Int. 34 (2008) 1215-1226.

[3] B. Kasprzyk-Hordern, R.M. Dinsdale, A.J. Guwy, The removal of pharmaceuticals, personal care products, endocrine disruptors and illicit drugs during wastewater treatment and its impact on the quality of receiving waters, Water Res. 43 (2009) 363-380.

[4] G. Dantas, M.O. Sommer, R.D. Oluwasegun, G.M. Church, Bacteria subsisting on antibiotics, Science 320 (2008) 100-103.

[5] A.K. Sarmah, M.T. Meyer, A.B. Boxall, A global perspective on the use, sales, exposure pathways, occurrence, fate and effects of veterinary antibiotics (VAs) in the environment, Chemosphere 65 (2006) 725-759.

[6] A.L. Batt, D.D. Snow, D.S. Aga, Occurrence of sulfonamide antimicrobials in private water wells in Washington County, Idaho, USA, Chemosphere 64 (2006) 1963-1971.

[7] R. Hirsch, T. Ternes, K. Haberer, K.L. Kratz, Occurrence of antibiotics in the aquatic environment, Sci. Total Environ. 225 (1999) 109-118.

[8] A.M. Jacobsen, B. Halling-Sørensen, F. Ingerslev, S.H. Hansen, Simultaneous extraction of tetracycline, macrolide and sulfonamide antibiotics from agricultural soils using pressurised liquid extraction, followed by solid-phase extraction and liquid chromatography–tandem mass spectrometry, J. Chromatograph. A 1038 (2004) 157-170.

[9] M.E. Lindsey, M. Meyer, E. Thurman, Analysis of trace levels of sulfonamide and tetracycline antimicrobials in groundwater and surface water using solid-phase extraction and liquid chromatography/mass spectrometry, Anal. Chem. 73 (2001) 4640-4646.

[10] S. Mompelat, B. Le Bot, O. Thomas, Occurrence and fate of pharmaceutical products and by-products, from resource to drinking water, Environ. Int. 35 (2009) 803-814.

[11] T.A. Ternes, Occurrence of drugs in German sewage treatment plants and rivers1, Water Res. 32 (1998) 3245-3260.

[12] C.G. Daughton, T.A. Ternes, Pharmaceuticals and personal care products in the environment: agents of subtle change?, Environ. Health Perspect. 107 (1999) 907.

[13] K. Ji, S. Kim, S. Han, J. Seo, S. Lee, Y. Park, K. Choi, Y.L. Kho, P.G. Kim, J. Park, Risk assessment of chlortetracycline, oxytetracycline, sulfamethazine, sulfathiazole, and erythromycin in aquatic environment: are the current environmental concentrations safe?, Ecotoxicol. 21 (2012) 2031-2050.

[14] H.T. Lai, J.H. Hou, C.I. Su, C.L. Chen, Effects of chloramphenicol, florfenicol, and thiamphenicol on growth of algae Chloella pyrenoidosa, Isochrysis galbana, and Tetraselmis chui, Ecotoxicol. Environ. Safety 72 (2009) 329-334.

[15] L. Wollenberger, B. Halling-Sørensen, K.O. Kusk, Acute and chronic toxicity of veterinary antibiotics to Daphnia magna, Chemosphere 40 (2000) 723-730.

[16] K. Chen, J. Zhou, Occurrence and behavior of antibiotics in water and sediments from the Huangpu River, Shanghai, China, Chemosphere 95 (2014) 604-612.

[17] A. Hartmann, A.C. Alder, T. Koller, R.M. Widmer, Identification of fluoroquinolone antibiotics as the main source of umuC genotoxicity in native hospital wastewater, Environ. Toxicol. Chem. 17 (1998) 377-382.

[18] M. Lee, H. Lee, P. Ryu, Public health risks: Chemical and antibiotic residues-review, Asian-Australasian J. Animal Sci. 14 (2001) 402-413.

[19] H. Chen, H. Luo, Y. Lan, T. Dong, B. Hu, Y. Wang, Removal of tetracycline from aqueous solutions using polyvinylpyrrolidone (PVP-K30) modified nanoscale zero valent iron, J. Hazard. Mater. 192 (2011) 44-53.

[20] Z. Qiang, X. Bao, W. Ben, MCM-48 modified magnetic mesoporous nanocomposite as an attractive adsorbent for the removal of sulfamethazine from water, Water Res. 47 (2013) 4107-4114.

[21] Y. Fan, B. Wang, S. Yuan, X. Wu, J. Chen, L. Wang, Adsorptive removal of chloramphenicol from wastewater by NaOH modified bamboo charcoal, Bioresour. Technol. 101 (2010) 7661-7664.

[22] F.F. Liu, J. Zhao, S. Wang, B. Xing, Adsorption of sulfonamides on reduced graphene oxides as affected by pH and dissolved organic matter, Environ. Pollut. 210 (2016) 85-93.

[23] H. Liu, G. Zhang, C.Q. Liu, L. Li, M. Xiang, The occurrence of chloramphenicol and tetracyclines in municipal sewage and the Nanming River, Guiyang City, China, J. Environ. Monitor. 11 (2009) 1199-1205.

[24] V. Homem, L. Santos, Degradation and removal methods of antibiotics from aqueous matrices–a review, J. Environ. Manage. 92 (2011) 2304-2347.

[25] M.B. Ahmed, J.L. Zhou, H.H. Ngo, M.A.H. Johir, K. Sornalingam, Sorptive removal of phenolic endocrine disruptors by functionalized biochar: Competitive interaction mechanism, removal efficacy and application in wastewater, Chem. Eng. J. 335 (2018) 801-811.

[26] J. Jiang, Q. Yin, J. Zhou, P. Pearce, Occurrence and treatment trials of endocrine disrupting chemicals (EDCs) in wastewaters, Chemosphere 61 (2005) 544-550.

[27] K. Sornalingam, A. McDonagh, J.L. Zhou, Photodegradation of estrogenic endocrine disrupting steroidal hormones in aqueous systems: Progress and future challenges, Sci. Total Environ. 550 (2016) 209-224.

[28] L. Zhang, P. Fang, L. Yang, J. Zhang, X. Wang, Rapid method for the separation and recovery of endocrine-disrupting compound bisphenol AP from wastewater, Langmuir 29 (2013) 3968-3975.

[29] D. Grover, J. Zhou, P. Frickers, J. Readman, Improved removal of estrogenic and pharmaceutical compounds in sewage effluent by full scale granular activated carbon: impact on receiving river water, J. Hazard. Mater. 185 (2011) 1005-1011.

[30] D. Belhaj, R. Baccar, I. Jaabiri, J. Bouzid, M. Kallel, H. Ayadi, J.L. Zhou, Fate of selected estrogenic hormones in an urban sewage treatment plant in Tunisia (North Africa), Sci. Total Environ. 505 (2015) 154-160.

[31] N. Klamerth, S. Malato, A. Agüera, A. Fernández-Alba, Photo-Fenton and modified photo-Fenton at neutral pH for the treatment of emerging contaminants in wastewater treatment plant effluents: a comparison, Water Res. 47 (2013) 833-840.

[32] Y. Luo, W. Guo, H.H. Ngo, L.D. Nghiem, F.I. Hai, J. Zhang, S. Liang, X.C. Wang, A review on the occurrence of micropollutants in the aquatic environment and their fate and removal during wastewater treatment, Sci. Total Environ. 473 (2014) 619-641.

[33] D. Dolar, M. Gros, S. Rodriguez-Mozaz, J. Moreno, J. Comas, I. Rodriguez-Roda, D. Barceló, Removal of emerging contaminants from municipal wastewater with an integrated membrane system, MBR–RO, J. Hazard. Mater. 239 (2012) 64-69.

[34] S. Esplugas, D.M. Bila, L.G.T. Krause, M. Dezotti, Ozonation and advanced oxidation technologies to remove endocrine disrupting chemicals (EDCs) and pharmaceuticals and personal care products (PPCPs) in water effluents, J. Hazard. Mater. 149 (2007) 631-642.

[35] J. Rivera-Utrilla, M. Sánchez-Polo, M.Á. Ferro-García, G. Prados-Joya, R. Ocampo-Pérez, Pharmaceuticals as emerging contaminants and their removal from water. A review, Chemosphere 93 (2013) 1268-1287.

[36] J.O. Tijani, O.O. Fatoba, L.F. Petrik, A review of pharmaceuticals and endocrine-disrupting compounds: sources, effects, removal, and detections, Water Air Soil Pollut. 224 (2013) 1770.

[37] M. Dunier, A.K. Siwicki, Effects of pesticides and other organic pollutants in the aquatic environment on immunity of fish: a review, Fish Shellfish Immunol. 3 (1993) 423-438.

[38] A. Watkinson, E. Murby, S. Costanzo, Removal of antibiotics in conventional and advanced wastewater treatment: implications for environmental discharge and wastewater recycling, Water Res. 41 (2007) 4164-4176.

[39] K. Košutić, D. Dolar, D. Ašperger, B. Kunst, Removal of antibiotics from a model wastewater by RO/NF membranes, Separat. Purificat. Technol. 53 (2007) 244-249.

[40] L.K. Wang, Y.-T. Hung, N.K. Shammas, Adv. Physicoche. Treat. Technol. Springer, 2007.

[41] M. Ahmaruzzaman, Adsorption of phenolic compounds on low-cost adsorbents: a review, Adv.Colloid Interface Sci. 143 (2008) 48-67.

[42] Z. Aksu, Ö. Tunç, Application of biosorption for penicillin G removal: comparison with activated carbon, Process Biochem. 40 (2005) 831-847.

[43] G.-G. Ying, R.S. Kookana, P. Dillon, Sorption and degradation of selected five endocrine disrupting chemicals in aquifer material, Water Res. 37 (2003) 3785-3791.

[44] M.B. Ahmed, J.L. Zhou, H.H. Ngo, W. Guo, N.S. Thomaidis, J. Xu, Progress in the biological and chemical treatment technologies for emerging contaminant removal from wastewater: A critical review, J. Hazard. Mater. (2016).

[45] K. Maskaoui, J.L. Zhou, Colloids as a sink for certain pharmaceuticals in the aquatic environment, Environ. Sci. Pollut. Res. 17 (2010) 898-907.

[46] A. Zhang, J. Wang, Y. Li, Performance of calcium peroxide for removal of endocrine-disrupting compounds in waste activated sludge and promotion of sludge solubilization, Water Res. 71 (2015) 125-139.

[47] R. Rosal, A. Rodríguez, J.A. Perdigón-Melón, A. Petre, E. García-Calvo, M.J. Gómez, A. Agüera, A.R. Fernández-Alba, Occurrence of emerging pollutants in urban wastewater and their removal through biological treatment followed by ozonation, Water Res. 44 (2010) 578-588.

[48] C. Jung, J. Park, K.H. Lim, S. Park, J. Heo, N. Her, J. Oh, S. Yun, Y. Yoon, Adsorption of selected endocrine disrupting compounds and pharmaceuticals on activated biochars, J. Hazard. Mater. 263 (2013) 702-710.

[49] A.M. Redding, F.S. Cannon, S.A. Snyder, B.J. Vanderford, A QSAR-like analysis of the adsorption of endocrine disrupting compounds, pharmaceuticals, and personal care products on modified activated carbons, Water Res. 43 (2009) 3849-3861.

[50] Z. Yu, S. Peldszus, P.M. Huck, Adsorption characteristics of selected pharmaceuticals and an endocrine disrupting compound—Naproxen, carbamazepine and nonylphenol—on activated carbon, Water Res. 42 (2008) 2873-2882.

[51] C. Zhang, C. Lai, G. Zeng, D. Huang, C. Yang, Y. Wang, Y. Zhou, M. Cheng, Efficacy of carbonaceous nanocomposites for sorbing ionizable antibiotic sulfamethazine from aqueous solution, Water Res. 95 (2016) 103-112.

[52] B. Pan, D. Lin, H. Mashayekhi, B. Xing, Adsorption and hysteresis of bisphenol A and 17α-ethinyl estradiol on carbon nanomaterials, Environ. Sci. Technol. 42 (2008) 5480-5485.

[53] L. Zhang, F. Pan, X. Liu, L. Yang, X. Jiang, J. Yang, W. Shi, Multi-walled carbon nanotubes as sorbent for recovery of endocrine disrupting compound-bisphenol F from wastewater, Chem. Eng. J. 218 (2013) 238-246.

[54] C. Jung, L.K. Boateng, J.R. Flora, J. Oh, M.C. Braswell, A. Son, Y. Yoon, Competitive adsorption of selected non-steroidal anti-inflammatory drugs on activated biochars: experimental and molecular modeling study, Chem. Eng. J. 264 (2015) 1-9.

[55] M.B. Ahmed, J.L. Zhou, H.H. Ngo, W. Guo, M. Chen, Progress in the preparation and application of modified biochar for improved contaminant removal from water and wastewater, Bioresour. Technol. 214 (2016) 836-851.

[56] M.B. Ahmed, J.L. Zhou, H.H. Ngo, W. Guo, Insight into biochar properties and its cost analysis, Biomass Bioenerg. 84 (2016) 76-86.

[57] M.B. Ahmed, J.L. Zhou, H.H. Ngo, W. Guo, Adsorptive removal of antibiotics from water and wastewater: progress and challenges, Sci. Total Environ. 532 (2015) 112-126.

[58] O. Lorphensri, J. Intravijit, D.A. Sabatini, T.C. Kibbey, K. Osathaphan, C. Saiwan, Sorption of acetaminophen, 17α-ethynyl estradiol, nalidixic acid, and norfloxacin to silica, alumina, and a hydrophobic medium, Water Res. 40 (2006) 1481-1491.

[59] M. Teixidó, J.J. Pignatello, J.L. Beltrán, M. Granados, J. Peccia, Speciation of the ionizable antibiotic sulfamethazine on black carbon (biochar), Environ. Sci. Technol. 45 (2011) 10020-10027.

[60] C. Chartres, J. Williams, Can Australia overcome its water scarcity problems?, J. Develop. Sustain. Agricul. 1 (2006) 17-24.

[61] O. Sköld, Antibiotics and antibiotic resistance, John Wiley & Sons2011.

[62] M. Nie, C. Yan, M. Li, X. Wang, W. Bi, W. Dong, Degradation of chloramphenicol by persulfate activated by Fe2+ and zerovalent iron, Chem. Eng. J. 279 (2015) 507-515.

[63] K. Kümmerer, A. Henninger, Promoting resistance by the emission of antibiotics from hospitals and households into effluent, Clinical Microbiol. Infect. 9 (2003) 1203-1214.

[64] N. Kemper, Veterinary antibiotics in the aquatic and terrestrial environment, Ecol. Indicat. 8 (2008) 1-13.

[65] B. Sunkara, J. Zhan, J. He, G.L. McPherson, G. Piringer, V.T. John, Nanoscale zerovalent iron supported on uniform carbon microspheres for the in situ remediation of chlorinated hydrocarbons, ACS Appl. Mater. Interface 2 (2010) 2854-2862.

[66] A.B. Boxall, D.W. Kolpin, B. Halling-Sørensen, J. Tolls, Peer reviewed: are veterinary medicines causing environmental risks?, Environ. Sci. Technol. 37 (2003) 286A-294A.

[67] X. Guo, C. Yang, Z. Dang, Q. Zhang, Y. Li, Q. Meng, Sorption thermodynamics and kinetics properties of tylosin and sulfamethazine on goethite, Chem. Eng. J. 223 (2013) 59-67.

[68] G.T. Ankley, B.W. Brooks, D.B. Huggett, Sumpter, J. P, Repeating history: pharmaceuticals in the environment, Environ. Sci. Technol. 41 (2007) 8211-8217.

[69] H. Zhao, J.L. Zhou, J. Zhang, Tidal impact on the dynamic behavior of dissolved pharmaceuticals in the Yangtze Estuary, China, Sci. Total Environ. 536 (2015) 946-954.

[70] L. Mi, G.A. Licina, S. Jiang, Nonantibiotic-based Pseudomonas aeruginosa biofilm inhibition with osmoprotectant analogues, ACS Sustain. Chem. Eng. 2 (2014) 2448-2453.

[71] C. Chen, L. Zheng, J. Zhou, H. Zhao, Persistence and risk of antibiotic residues and antibiotic resistance genes in major mariculture sites in Southeast China, Sci. Total Environ. 580 (2017) 1175-1184.

[72] H. Lu, W. Zou, P. Chai, J. Wang, L. Bazinet, Feasibility of antibiotic and sulfate ions separation from wastewater using electrodialysis with ultrafiltration membrane, J. Cleaner Product. 112 (2016) 3097-3105.

[73] C. Adams, Y. Wang, K. Loftin, M. Meyer, Removal of antibiotics from surface and distilled water in conventional water treatment processes, J. Environ. Eng. 128 (2002) 253-260.

[74] S.R. Pouran, A.A.A. Raman, W.M.A.W. Daud, Review on the application of modified iron oxides as heterogeneous catalysts in Fenton reactions, J. Cleaner Product. 64 (2014) 24-35.

[75] W.H. Organization, Pharmaceuticals in drinking-water, (2012).

[76] A. Ghauch, A. Tuqan, H.A. Assi, Antibiotic removal from water: elimination of amoxicillin and ampicillin by microscale and nanoscale iron particles, Environ. Pollut. 157 (2009) 1626-1635.

[77] K. Kümmerer, Antibiotics in the aquatic environment–a review–part I, Chemosphere 75 (2009) 417-434.

[78] M. Hernando, M. Mezcua, A. Fernández-Alba, D. Barceló, Environmental risk assessment of pharmaceutical residues in wastewater effluents, surface waters and sediments, Talanta 69 (2006) 334-342.

[79] C. Yan, Y. Yang, J. Zhou, M. Liu, M. Nie, H. Shi, L. Gu, Antibiotics in the surface water of the Yangtze Estuary: occurrence, distribution and risk assessment, Environ. Pollut. 175 (2013) 22-29.

[80] Z. Qiang, C. Adams, Potentiometric determination of acid dissociation constants (pKa) for human and veterinary antibiotics, Water Res. 38 (2004) 2874-2890.

[81] S. Thiele-Bruhn, Pharmaceutical antibiotic compounds in soils–a review, J. Plant Nutrit. Soil Sci. 166 (2003) 145-167.

[82] A.U. Rajapaksha, M. Vithanage, M. Ahmad, D.C. Seo, J.S. Cho, S.E. Lee, S.S. Lee, Y.S. Ok, Enhanced sulfamethazine removal by steam-activated invasive plant-derived biochar, J. Hazard. Mater. 290 (2015) 43-50.

[83] J. Feitosa-Felizzola, S. Chiron, Occurrence and distribution of selected antibiotics in a small Mediterranean stream (Arc River, Southern France), J. Hydrol. 364 (2009) 50-57.

[84] S.M. Mitchell, M. Subbiah, J.L. Ullman, C. Frear, D.R. Call, Evaluation of 27 different biochars for potential sequestration of antibiotic residues in food animal production environments, J. Environ. Chem. Eng. 3 (2015) 162-169.

[85] L. Rizzo, C. Manaia, C. Merlin, T. Schwartz, C. Dagot, M. Ploy, I. Michael, D. Fatta-Kassinos, Urban wastewater treatment plants as hotspots for antibiotic resistant bacteria and genes spread into the environment: a review, Sci. Total Environ. 447 (2013) 345-360.

[86] M. Mehrjouei, S. Müller, D. Möller, Energy consumption of three different advanced oxidation methods for water treatment: a cost-effectiveness study, J. Cleaner Product. 65 (2014) 178-183.

[87] R.J. Kavlock, G.P. Daston, C. DeRosa, P. Fenner-Crisp, L.E. Gray, S. Kaattari, G. Lucier, M. Luster, M.J. Mac, C. Maczka, Research needs for the risk assessment of health and environmental effects of endocrine disruptors: a report of the US EPA-sponsored workshop, Environ. Health Perspect. 104 (1996) 715.

[88] E.R. Kabir, M.S. Rahman, I. Rahman, A review on endocrine disruptors and their possible impacts on human health, Environ. Toxicol. Pharmacol. 40 (2015) 241-258.

[89] A.L. Lister, G.J. Van Der Kraak, Endocrine disruption: why is it so complicated?, Water Qual. Res. J. Canada 36 (2001) 175-190.

[90] S.D. Kim, J. Cho, I.S. Kim, B.J. Vanderford, S.A. Snyder, Occurrence and removal of pharmaceuticals and endocrine disruptors in South Korean surface, drinking, and waste waters, Water Res. 41 (2007) 1013-1021.

[91] S.A. Snyder, S. Adham, A.M. Redding, F.S. Cannon, J. DeCarolis, J. Oppenheimer, E.C. Wert, Y. Yoon, Role of membranes and activated carbon in the removal of endocrine disruptors and pharmaceuticals, Desalination 202 (2007) 156-181.

[92] A. de Wilt, A. Butkovskyi, K. Tuantet, L.H. Leal, T.V. Fernandes, A. Langenhoff, G. Zeeman, Micropollutant removal in an algal treatment system fed with source separated wastewater streams, J. Hazard. Mater. 304 (2016) 84-92.

[93] M. Grassi, G. Kaykioglu, V. Belgiorno, G. Lofrano, Removal of emerging contaminants from water and wastewater by adsorption process, Emerging compounds removal from wastewater, Springer, 2012, 15-37.

[94] N. De la Cruz, J. Giménez, S. Esplugas, D. Grandjean, L. De Alencastro, C. Pulgarin, Degradation of 32 emergent contaminants by UV and neutral photo-fenton in domestic wastewater effluent previously treated by activated sludge, Water Res. 46 (2012) 1947-1957.

[95] C. Frye, E. Bo, G. Calamandrei, L. Calza, F. Dessì-Fulgheri, M. Fernández, L. Fusani, O. Kah, M. Kajta, Y. Le Page, Endocrine disrupters: a review of some sources, effects, and mechanisms of actions on behaviour and neuroendocrine systems, J. Neuroendocrinol. 24 (2012) 144-159.

[96] M.B. Kjærstad, C. Taxvig, H.R. Andersen, C. Nellemann, Mixture effects of endocrine disrupting compounds in vitro, Int. J. Androl. 33 (2010) 425-433.

[97] A. Deegan, B. Shaik, K. Nolan, K. Urell, M. Oelgemöller, J. Tobin, A. Morrissey, Treatment options for wastewater effluents from pharmaceutical companies, International Journal of Environ. Sci. Technol. 8 (2011) 649-666.

[98] L. Prieto-Rodriguez, S. Miralles-Cuevas, I. Oller, A. Agüera, G.L. Puma, S. Malato, Treatment of emerging contaminants in wastewater treatment plants (WWTP) effluents by solar photocatalysis using low TiO2 concentrations, J. Hazard. Mater. 211 (2012) 131-137.

[99] N.H. Tran, T. Urase, H.H. Ngo, J. Hu, S.L. Ong, Insight into metabolic and cometabolic activities of autotrophic and heterotrophic microorganisms in the biodegradation of emerging trace organic contaminants, Bioresour. Technol. 146 (2013) 721-731.

[100] C. Preda, M.C. Ungureanu, C. Vulpoi, Endocrine disruptors in the environment and their impact on human health, Environ. Eng. Manage. J. 11 (2012).

[101] U. WHO, State of the science of endocrine disrupting chemicals 2012: an assessment of the state of the science of endocrine disruptors prepared by a group of experts for the United Nations Environment Programme and World Health Organization, Geneva, WHO (2013).

[102] T. Nguyen, H. Ngo, W. Guo, J. Zhang, S. Liang, Q. Yue, Q. Li, T. Nguyen, Applicability of agricultural waste and by-products for adsorptive removal of heavy metals from wastewater, Bioresour. Technol. 148 (2013) 574-585.

[103] S.A. Snyder, P. Westerhoff, Y. Yoon, D.L. Sedlak, Pharmaceuticals, personal care products, and endocrine disruptors in water: implications for the water industry, Environ. Eng. Sci. 20 (2003) 449-469.

[104] Y. Zhang, J.L. Zhou, Occurrence and removal of endocrine disrupting chemicals in wastewater, Chemosphere 73 (2008) 848-853.

[105] D. Macwan, P.N. Dave, S. Chaturvedi, A review on nano-TiO_2 sol–gel type syntheses and its applications, J. Mater. Sci. 46 (2011) 3669-3686.

[106] P.E. Stackelberg, J. Gibs, E.T. Furlong, M.T. Meyer, S.D. Zaugg, R.L. Lippincott, Efficiency of conventional drinking-water-treatment processes in removal of pharmaceuticals and other organic compounds, Sci. Total Environ. 377 (2007) 255-272.

[107] P. Westerhoff, Y. Yoon, S. Snyder, E. Wert, Fate of endocrine-disruptor, pharmaceutical, and personal care product chemicals during simulated drinking water treatment processes, Environ. Sci. Technol. 39 (2005) 6649-6663.

[108] A. Garcia-Rodríguez, V. Matamoros, C. Fontàs, V. Salvadó, The ability of biologically based wastewater treatment systems to remove emerging organic contaminants—a review, Environ. Sci. Pollut. Res. 21 (2014) 11708-11728.

[109] D.S.S. Raj, Y. Anjaneyulu, Evaluation of biokinetic parameters for pharmaceutical wastewaters using aerobic oxidation integrated with chemical treatment, Process Biochem. 40 (2005) 165-175.

[110] J. Benner, D.E. Helbling, H.-P.E. Kohler, J. Wittebol, E. Kaiser, C. Prasse, T.A. Ternes, C.N. Albers, J. Aamand, B. Horemans, Is biological treatment a viable alternative for micropollutant removal in drinking water treatment processes?, Water Res. 47 (2013) 5955-5976.

[111] J. Radjenović, M. Matošić, I. Mijatović, M. Petrović, D. Barceló, Membrane bioreactor (MBR) as an advanced wastewater treatment technology, Emerging Contaminants from Industrial and Municipal Waste, Springer, 2008, 37-101.

[112] V. Matamoros, R. Gutiérrez, I. Ferrer, J. García, J.M. Bayona, Capability of microalgae-based wastewater treatment systems to remove emerging organic contaminants: a pilot-scale study, J. Hazard. Mater. 288 (2015) 34-42.

[113] D. Sreekanth, D. Sivaramakrishna, V. Himabindu, Y. Anjaneyulu, Thermophilic treatment of bulk drug pharmaceutical industrial wastewaters by using hybrid up flow anaerobic sludge blanket reactor, Bioresour. Technol. 100 (2009) 2534-2539.

[114] G.Y. Töre, S. Meriç, G. Lofrano, G. De Feo, Removal of trace pollutants from wastewater in constructed wetlands, Emerging Compounds Removal from Wastewater, Springer, 2012, 39-58.

[115] W. Yang, N. Cicek, J. Ilg, State-of-the-art of membrane bioreactors: Worldwide research and commercial applications in North America, J. Membrane Sci. 270 (2006) 201-211.

[116] S. Malato, M.I. Maldonado, I. Oller, A. Zapata, Removal of pesticides from water and wastewater by solar-driven photocatalysis, Emerging Compounds Removal from Wastewater, Springer, 2012, 59-76.

[117] D. Barceló, M. Petrovic, Conclusions and future research needs, Comprehen. Anal. Chem. 50 (2007) 515-527.

[118] J. Zhou, Z. Zhang, E. Banks, D. Grover, J. Jiang, Pharmaceutical residues in wastewater treatment works effluents and their impact on receiving river water, J. Hazard. Mater. 166 (2009) 655-661.

[119] W. Eckenfelder, Wastewater treatment, Wiley Online Library, 2006.

[120] G.T. Daigger, J.P. Boltz, Trickling Filter and Trickling Filter-Suspended Growth Process Design and Operation: A State-of-the-Art Review, Water Environ. Res. 83 (2011) 388-404.

[121] T. Cajthaml, Z. Křesinová, K. Svobodová, M. Möder, Biodegradation of endocrine-disrupting compounds and suppression of estrogenic activity by ligninolytic fungi, Chemosphere 75 (2009) 745-750.

[122] C. Wang, J. Li, B. Wang, G. Zhang, Development of an empirical model for domestic wastewater treatment by biological aerated filter, Process Biochem. 41 (2006) 778-782.

[123] I. Naz, D.P. Saroj, S. Mumtaz, N. Ali, S. Ahmed, Assessment of biological trickling filter systems with various packing materials for improved wastewater treatment, Environ. Technol. 36 (2015) 424-434.

[124] E. McLamore, S. Sharvelle, Z. Huang, K. Banks, Simultaneous treatment of graywater and waste gas in a biological trickling filter, Water Environ. Res. 80 (2008) 2096-2103.

[125] A.Y.C. Lin, T.H. Yu, S.K. Lateef, Removal of pharmaceuticals in secondary wastewater treatment processes in Taiwan, J. Hazard. Mater. 167 (2009) 1163-1169.

[126] A. Svenson, A.-S. Allard, M. Ek, Removal of estrogenicity in Swedish municipal sewage treatment plants, Water Res. 37 (2003) 4433-4443.

[127] T.F. Silva, M.E.F. Silva, A.C. Cunha-Queda, A. Fonseca, I. Saraiva, M. Sousa, C. Gonçalves, M. Alpendurada, R.A. Boaventura, V.J. Vilar, Multistage treatment system for raw leachate from sanitary landfill combining biological nitrification–denitrification/solar photo-Fenton/biological processes, at a scale close to industrial–biodegradability enhancement and evolution profile of trace pollutants, Water Res. 47 (2013) 6167-6186.

[128] H.V. Phan, F.I. Hai, J. Kang, H.K. Dam, R. Zhang, W.E. Price, A. Broeckmann, L.D. Nghiem, Simultaneous nitrification/denitrification and trace organic contaminant (TrOC) removal by an anoxic–aerobic membrane bioreactor (MBR), Bioresour. Technol. 165 (2014) 96-104.

[129] L. Su, D. Aga, K. Chandran, W.O. Khunjar, Factors impacting biotransformation kinetics of trace organic compounds in lab-scale activated sludge systems performing nitrification and denitrification, J. Hazard. Mater. 282 (2015) 116-124.

[130] S. Suarez, J.M. Lema, F. Omil, Removal of pharmaceutical and personal care products (PPCPs) under nitrifying and denitrifying conditions, Water Res. 44 (2010) 3214-3224.

[131] D. Gerrity, S. Gamage, J.C. Holady, D.B. Mawhinney, O. Quiñones, R.A. Trenholm, S.A. Snyder, Pilot-scale evaluation of ozone and biological activated carbon for trace organic contaminant mitigation and disinfection, Water Res. 45 (2011) 2155-2165.

[132] J. Reungoat, B. Escher, M. Macova, F. Argaud, W. Gernjak, J. Keller, Ozonation and biological activated carbon filtration of wastewater treatment plant effluents, Water Res. 46 (2012) 863-872.

[133] Ç. Kalkan, K. Yapsakli, B. Mertoglu, D. Tufan, A. Saatci, Evaluation of biological activated carbon (BAC) process in wastewater treatment secondary effluent for reclamation purposes, Desalination 265 (2011) 266-273.

[134] P. Jin, X. Jin, X. Wang, Y. Feng, X.C. Wang, Biological activated carbon treatment process for advanced water and wastewater treatment, Biomass Now-Cultivation and Utilization, InTech, 2013.

[135] V. Matamoros, E. Uggetti, J. García, J.M. Bayona, Assessment of the mechanisms involved in the removal of emerging contaminants by microalgae from wastewater: a laboratory scale study, J. Hazard. Mater. 301 (2016) 197-205.

[136] F. Passos, M. Hernandez-Marine, J. Garcia, I. Ferrer, Long-term anaerobic digestion of microalgae grown in HRAP for wastewater treatment. Effect of microwave pretreatment, Water Res. 49 (2014) 351-359.

[137] W. Shi, L. Wang, D.P. Rousseau, P.N. Lens, Removal of estrone, 17α-ethinylestradiol, and 17ß-estradiol in algae and duckweed-based wastewater treatment systems, Environ. Sci. Pollut. Res. 17 (2010) 824-833.

[138] C. Cruz-Morató, L. Ferrando-Climent, S. Rodriguez-Mozaz, D. Barceló, E. Marco-Urrea, T. Vicent, M. Sarrà, Degradation of pharmaceuticals in non-sterile urban wastewater by Trametes versicolor in a fluidized bed bioreactor, Water Res. 47 (2013) 5200-5210.

[139] A. Garcia-Rodríguez, V. Matamoros, C. Fontàs, V. Salvadó, The influence of light exposure, water quality and vegetation on the removal of sulfonamides and tetracyclines: a laboratory-scale study, Chemosphere 90 (2013) 2297-2302.

[140] G. Buttiglieri, T. Knepper, Removal of emerging contaminants in wastewater treatment: conventional activated sludge treatment, Emerging Contaminants from Industrial and Municipal Waste, Springer, 2007, 1-35.

[141] Z.-h. Liu, Y. Kanjo, S. Mizutani, Removal mechanisms for endocrine disrupting compounds (EDCs) in wastewater treatment—physical means, biodegradation, and chemical advanced oxidation: a review, Sci. Total Environ. 407 (2009) 731-748.

[142] O. Braga, G.A. Smythe, A.I. Schäfer, A.J. Feitz, Fate of steroid estrogens in Australian inland and coastal wastewater treatment plants, Environ. Sci. Technol. 39 (2005) 3351-3358.

[143] Q. Sun, M. Lv, A. Hu, X. Yang, C.P. Yu, Seasonal variation in the occurrence and removal of pharmaceuticals and personal care products in a wastewater treatment plant in Xiamen, China, J. Hazard. Mater. 277 (2014) 69-75.

[144] S.L. Simonich, T.W. Federle, W.S. Eckhoff, A. Rottiers, S. Webb, D. Sabaliunas, W. De Wolf, Removal of fragrance materials during US and European wastewater treatment, Environ. Sci. Technol. 36 (2002) 2839-2847.

[145] J.-J. Yang, C.D. Metcalfe, Fate of synthetic musks in a domestic wastewater treatment plant and in an agricultural field amended with biosolids, Sci. Total Environ. 363 (2006) 149-165.

[146] A. Melo-Guimarães, F.J. Torner-Morales, J.C. Durán-Álvarez, B.E. Jiménez-Cisneros, Removal and fate of emerging contaminants combining biological, flocculation and membrane treatments, Water Sci. Technol. 67 (2013) 877-885.

[147] C. Miege, J. Choubert, L. Ribeiro, M. Eusèbe, M. Coquery, Fate of pharmaceuticals and personal care products in wastewater treatment plants–conception of a database and first results, Environ. Pollut. 157 (2009) 1721-1726.

[148] S.S. Teske, R.G. Arnold, Removal of natural and xeno-estrogens during conventional wastewater treatment, Rev. Environ. Sci. Bio-technol. 7 (2008) 107-124.

[149] G.U. Semblante, F.I. Hai, X. Huang, A.S. Ball, W.E. Price, L.D. Nghiem, Trace organic contaminants in biosolids: impact of conventional wastewater and sludge processing technologies and emerging alternatives, J. Hazard. Mater. 300 (2015) 1-17.

[150] T. Furuichi, K. Kannan, K. Suzuki, S. Tanaka, J.P. Giesy, S. Masunaga, Occurrence of estrogenic compounds in and removal by a swine farm waste treatment plant, Environ. Sci. Technol. 40 (2006) 7896-7902.

[151] N. Le-Minh, S. Khan, J. Drewes, R. Stuetz, Fate of antibiotics during municipal water recycling treatment processes, Water Res. 44 (2010) 4295-4323.

[152] A.S. Stasinakis, N.S. Thomaidis, O.S. Arvaniti, A.G. Asimakopoulos, V.G. Samaras, A. Ajibola, D. Mamais, T.D. Lekkas, Contribution of primary and secondary treatment on the removal of benzothiazoles, benzotriazoles, endocrine disruptors, pharmaceuticals and perfluorinated compounds in a sewage treatment plant, Sci. Total Environ. 463 (2013) 1067-1075.

[153] A. Joss, H. Andersen, T. Ternes, P.R. Richle, H. Siegrist, Removal of estrogens in municipal wastewater treatment under aerobic and anaerobic conditions: consequences for plant optimization, Environ. Sci. Technol. 38 (2004) 3047-3055.

[154] B. Chang, F. Chiang, S. Yuan, Anaerobic degradation of nonylphenol in sludge, Chemosphere 59 (2005) 1415-1420.

[155] J. Zhao, Y. Li, C. Zhang, Q. Zeng, Q. Zhou, Sorption and degradation of bisphenol A by aerobic activated sludge, J. Hazard. Mater. 155 (2008) 305-311.

[156] S. Yang, F.I. Hai, W.E. Price, J. McDonald, S.J. Khan, L.D. Nghiem, Occurrence of trace organic contaminants in wastewater sludge and their removals by anaerobic digestion, Bioresour. Technol. 210 (2016) 153-159.

[157] A.S. Stasinakis, Review on the fate of emerging contaminants during sludge anaerobic digestion, Bioresour. Technol. 121 (2012) 432-440.

[158] B.O. Clarke, S.R. Smith, Review of 'emerging'organic contaminants in biosolids and assessment of international research priorities for the agricultural use of biosolids, Environ. Int. 37 (2011) 226-247.

[159] T.H. Yu, A.Y.C. Lin, S.K. Lateef, C.F. Lin, P.Y. Yang, Removal of antibiotics and non-steroidal anti-inflammatory drugs by extended sludge age biological process, Chemosphere 77 (2009) 175-181.

[160] J.L. Conkle, J.R. White, C.D. Metcalfe, Reduction of pharmaceutically active compounds by a lagoon wetland wastewater treatment system in Southeast Louisiana, Chemosphere 73 (2008) 1741-1748.

[161] M. Hijosa-Valsero, V. Matamoros, J. Martín-Villacorta, E. Bécares, J.M. Bayona, Assessment of full-scale natural systems for the removal of PPCPs from wastewater in small communities, Water Res. 44 (2010) 1429-1439.

[162] V.G. Samaras, A.S. Stasinakis, D. Mamais, N.S. Thomaidis, T.D. Lekkas, Fate of selected pharmaceuticals and synthetic endocrine disrupting compounds during wastewater treatment and sludge anaerobic digestion, J. Hazard. Mater. 244 (2013) 259-267.

[163] O. Ganzenko, D. Huguenot, E.D. Van Hullebusch, G. Esposito, M.A. Oturan, Electrochemical advanced oxidation and biological processes for wastewater treatment: a review of the combined approaches, Environ. Sci. Pollut. Res. 21 (2014) 8493-8524.

[164] V.V. Pidlisnyuk, R.M. Marutovsky, K.H. Radeke, N. Klimenko, Biosorption Processes for Natural and Waste Water Treatment–Part II: Experimental Studies and Theoretical Model of a Biosorption Fixed Bed, Eng. Life Sci. 3 (2003) 439-445.

[165] L.N. Nguyen, F.I. Hai, S. Yang, J. Kang, F.D. Leusch, F. Roddick, W.E. Price, L.D. Nghiem, Removal of pharmaceuticals, steroid hormones, phytoestrogens, UV-filters, industrial chemicals and pesticides by Trametes versicolor: role of biosorption and biodegradation, Int. Biodeteriorat. Biodegrad. 88 (2014) 169-175.

[166] B. Banihashemi, R.L. Droste, Sorption–desorption and biosorption of bisphenol A, triclosan, and 17α-ethinylestradiol to sewage sludge, Sci. Total Environ. 487 (2014) 813-821.

[167] A.K. Kumar, S.V. Mohan, P. Sarma, Sorptive removal of endocrine-disruptive compound (estriol, E3) from aqueous phase by batch and column studies: kinetic and mechanistic evaluation, J. Hazard. Mater. 164 (2009) 820-828.

[168] V.M. Monsalvo, J.A. McDonald, S.J. Khan, P. Le-Clech, Removal of trace organics by anaerobic membrane bioreactors, Water Res. 49 (2014) 103-112.

[169] L.N. Nguyen, F.I. Hai, J. Kang, W.E. Price, L.D. Nghiem, Removal of emerging trace organic contaminants by MBR-based hybrid treatment processes, Int. Biodeteriorat. Biodegrad. 85 (2013) 474-482.

[170] T. Trinh, B. Van Den Akker, R.M. Stuetz, H. Coleman, P. Le-Clech, S. Khan, Removal of trace organic chemical contaminants by a membrane bioreactor, Water Sci. Technol. 66 (2012) 1856-1863.

[171] C. Abegglen, A. Joss, C.S. McArdell, G. Fink, M.P. Schlüsener, T.A. Ternes, H. Siegrist, The fate of selected micropollutants in a single-house MBR, Water Res. 43 (2009) 2036-2046.

[172] F. Meng, S.R. Chae, H.S. Shin, F. Yang, Z. Zhou, Recent advances in membrane bioreactors: configuration development, pollutant elimination, and sludge reduction, Environ. Eng. Sci. 29 (2012) 139-160.

[173] W. Luo, F.I. Hai, W.E. Price, W. Guo, H.H. Ngo, K. Yamamoto, L.D. Nghiem, High retention membrane bioreactors: challenges and opportunities, Bioresour. Technol. 167 (2014) 539-546.

[174] C. Li, C. Cabassud, C. Guigui, Evaluation of membrane bioreactor on removal of pharmaceutical micropollutants: a review, Desalin. Water Treat. 55 (2015) 845-858.

[175] J. Radjenović, M. Petrović, D. Barceló, Fate and distribution of pharmaceuticals in wastewater and sewage sludge of the conventional activated sludge (CAS) and advanced membrane bioreactor (MBR) treatment, Water Res. 43 (2009) 831-841.

[176] K.C. Wijekoon, F.I. Hai, J. Kang, W.E. Price, W. Guo, H.H. Ngo, L.D. Nghiem, The fate of pharmaceuticals, steroid hormones, phytoestrogens, UV-filters and pesticides during MBR treatment, Bioresour. Technol. 144 (2013) 247-254.

[177] S.K. Maeng, B.G. Choi, K.T. Lee, K.G. Song, Influences of solid retention time, nitrification and microbial activity on the attenuation of pharmaceuticals and estrogens in membrane bioreactors, Water Res. 47 (2013) 3151-3162.

[178] N. Klamerth, S. Malato, A. Agüera, A. Fernández-Alba, G. Mailhot, Treatment of municipal wastewater treatment plant effluents with modified photo-Fenton as a tertiary treatment for the degradation of micro pollutants and disinfection, Environ. Sci. Technol. 46 (2012) 2885-2892.

[179] J. Vymazal, Plants used in constructed wetlands with horizontal subsurface flow: a review, Hydrobiologia 674 (2011) 133-156.

[180] H.L. Song, K. Nakano, T. Taniguchi, M. Nomura, O. Nishimura, Estrogen removal from treated municipal effluent in small-scale constructed wetland with different depth, Bioresour. Technol. 100 (2009) 2945-2951.

[181] M. Hijosa-Valsero, G. Fink, M.P. Schlüsener, R. Sidrach-Cardona, J. Martín-Villacorta, T. Ternes, E. Bécares, Removal of antibiotics from urban wastewater by constructed wetland optimization, Chemosphere 83 (2011) 713-719.

[182] S.A. Hussain, S.O. Prasher, R.M. Patel, Removal of ionophoric antibiotics in free water surface constructed wetlands, Ecol. Eng. 41 (2012) 13-21.

[183] N. Park, B.J. Vanderford, S.A. Snyder, S. Sarp, S.D. Kim, J. Cho, Effective controls of micropollutants included in wastewater effluent using constructed wetlands under anoxic condition, Eecol. Eng. 35 (2009) 418-423.

[184] V. Matamoros, J. García, J.M. Bayona, Organic micropollutant removal in a full-scale surface flow constructed wetland fed with secondary effluent, Water Res. 42 (2008) 653-660.

[185] V. Matamoros, J.M. Bayona, Behavior of emerging pollutants in constructed wetlands, Emerging Contaminants from Industrial and Municipal Waste, Springer, 2007, 199-217.

[186] C. Comninellis, A. Kapalka, S. Malato, S.A. Parsons, I. Poulios, D. Mantzavinos, Advanced oxidation processes for water treatment: advances and trends for R&D, J. Chem. Technol. Biotechnol. 83 (2008) 769-776.

[187] I.A. Balcıoğlu, M. Ötker, Treatment of pharmaceutical wastewater containing antibiotics by O3 and O3/H2O2 processes, Chemosphere 50 (2003) 85-95.

[188] K. Ikehata, M. Gamal El-Din, S.A. Snyder, Ozonation and advanced oxidation treatment of emerging organic pollutants in water and wastewater, Ozone: Sci. Eng. 30 (2008) 21-26.

[189] K. Ikehata, N. Jodeiri Naghashkar, M. Gamal El-Din, Degradation of aqueous pharmaceuticals by ozonation and advanced oxidation processes: a review, Ozone: Sci. Eng. 28 (2006) 353-414.

[190] J.L. Acero, F.J. Benitez, F.J. Real, G. Roldan, Kinetics of aqueous chlorination of some pharmaceuticals and their elimination from water matrices, Water Res. 44 (2010) 4158-4170.

[191] M. Deborde, U. Von Gunten, Reactions of chlorine with inorganic and organic compounds during water treatment—kinetics and mechanisms: a critical review, Water Res. 42 (2008) 13-51.

[192] C. Noutsopoulos, D. Mamais, T. Mpouras, D. Kokkinidou, V. Samaras, K. Antoniou, M. Gioldasi, The role of activated carbon and disinfection on the removal of endocrine disrupting chemicals and non-steroidal anti-inflammatory drugs from wastewater, Environ. Technol. 35 (2014) 698-708.

[193] V. Belgiorno, L. Rizzo, D. Fatta, C. Della Rocca, G. Lofrano, A. Nikolaou, V. Naddeo, S. Meric, Review on endocrine disrupting-emerging compounds in urban wastewater: occurrence and removal by photocatalysis and ultrasonic irradiation for wastewater reuse, Desalination 215 (2007) 166-176.

[194] C. Noutsopoulos, E. Koumaki, D. Mamais, M.C. Nika, A.A. Bletsou, N.S. Thomaidis, Removal of endocrine disruptors and non-steroidal anti-inflammatory drugs through wastewater chlorination: the effect of pH, total suspended solids and humic acids and identification of degradation by-products, Chemosphere 119 (2015) S109-S114.

[195] F.J. Real, J.F. Benitez, J.L. Acero, F. Casas, Comparison between chlorination and ozonation treatments for the elimination of the emerging contaminants amitriptyline hydrochloride, methyl salicylate and 2-phenoxyethanol in surface waters and secondary effluents, J. Chem. Technol. Biotechnol. 90 (2015) 1400-1407.

[196] I.R. Bautitz, R.F.P. Nogueira, Degradation of tetracycline by photo-Fenton process—Solar irradiation and matrix effects, J. Photochem. Photobiol. A: Chem. 187 (2007) 33-39.

[197] J.L. Acero, F.J. Benitez, F.J. Real, E. Rodriguez, Elimination of selected emerging contaminants by the combination of membrane filtration and chemical oxidation processes, Water Air Soil Pollut. 226 (2015) 139.

[198] A. Rodríguez, R. Rosal, J. Perdigón-Melón, M. Mezcua, A. Agüera, M. Hernando, P. Letón, A. Fernández-Alba, E. García-Calvo, Ozone-based technologies in water and wastewater treatment, Emerging Contaminants from Industrial and Municipal Waste, Springer, 2008, 127-175.

[199] M. Maldonado, S. Malato, L. Pérez-Estrada, W. Gernjak, I. Oller, X. Doménech, J. Peral, Partial degradation of five pesticides and an industrial pollutant by ozonation in a pilot-plant scale reactor, J. Hazard. Mater. 138 (2006) 363-369.

[200] T. Garoma, S.K. Umamaheshwar, A. Mumper, Removal of sulfadiazine, sulfamethizole, sulfamethoxazole, and sulfathiazole from aqueous solution by ozonation, Chemosphere 79 (2010) 814-820.

[201] T.H. Kim, S.D. Kim, H.Y. Kim, S.J. Lim, M. Lee, S. Yu, Degradation and toxicity assessment of sulfamethoxazole and chlortetracycline using electron beam, ozone and UV, J. Hazard. Mater. 227 (2012) 237-242.

[202] H. Shemer, Y.K. Kunukcu, K.G. Linden, Degradation of the pharmaceutical metronidazole via UV, Fenton and photo-Fenton processes, Chemosphere 63 (2006) 269-276.

[203] S. Gan, E. Lau, H. Ng, Remediation of soils contaminated with polycyclic aromatic hydrocarbons (PAHs), J. Hazard. Mater. 172 (2009) 532-549.

[204] M.D.G. de Luna, M.L. Veciana, C.C. Su, M.C. Lu, Acetaminophen degradation by electro-Fenton and photoelectro-Fenton using a double cathode electrochemical cell, J. Hazard. Mater. 217 (2012) 200-207.

[205] C. Yan, M. Nie, Y. Yang, J. Zhou, M. Liu, M. Baalousha, J.R. Lead, Effect of colloids on the occurrence, distribution and photolysis of emerging organic contaminants in wastewaters, J. Hazard. Mater. 299 (2015) 241-248.

[206] A.G. Trovó, R.F. Nogueira, A. Agüera, C. Sirtori, A.R. Fernández-Alba, Photodegradation of sulfamethoxazole in various aqueous media: persistence, toxicity and photoproducts assessment, Chemosphere 77 (2009) 1292-1298.

[207] I. Arslan-Alaton, S. Dogruel, Pre-treatment of penicillin formulation effluent by advanced oxidation processes, J. Hazard. Mater. 112 (2004) 105-113.

[208] W. Song, W. Chen, W.J. Cooper, J. Greaves, G.E. Miller, Free-radical destruction of β-lactam antibiotics in aqueous solution, J. Phy. Chem. A 112 (2008) 7411-7417.

[209] S. Yu, B. Lee, M. Lee, I.H. Cho, S.W. Chang, Decomposition and mineralization of cefaclor by ionizing radiation: kinetics and effects of the radical scavengers, Chemosphere 71 (2008) 2106-2112.

[210] T. Csay, G. Rácz, E. Takács, L. Wojnárovits, Radiation induced degradation of pharmaceutical residues in water: chloramphenicol, Radiat. Phy. Chem. 81 (2012) 1489-1494.

[211] S.P. Mezyk, J.R. Peller, S.K. Cole, W. Song, B.J. Mincher, B.M. Peake, W.J. Cooper, Studies in radiation chemistry: application to ozonation and other advanced oxidation processes, Ozone: Sci.Eng. 30 (2008) 58-64.

[212] A.L. Estrada, Y.Y. Li, A. Wang, Biodegradability enhancement of wastewater containing cefalexin by means of the electro-Fenton oxidation process, J. Hazard. Mater. 227 (2012) 41-48.

[213] D. Mansour, F. Fourcade, N. Bellakhal, M. Dachraoui, D. Hauchard, A. Amrane, Biodegradability improvement of sulfamethazine solutions by means of an electro-Fenton process, Water Air Soil Pollut. 223 (2012) 2023-2034.

[214] U.I. Gaya, A.H. Abdullah, Heterogeneous photocatalytic degradation of organic contaminants over titanium dioxide: a review of fundamentals, progress and problems, J. Photochem. Photobiol. C: Photochem. Rev. 9 (2008) 1-12.

[215] A. Dirany, I. Sirés, N. Oturan, M.A. Oturan, Electrochemical abatement of the antibiotic sulfamethoxazole from water, Chemosphere 81 (2010) 594-602.

[216] D. Ghernaout, M. Naceur, Ferrate (VI): In situ generation and water treatment–A review, Desalin. Water Treat. 30 (2011) 319-332.

[217] J. Jiang, Research progress in the use of ferrate (VI) for the environmental remediation, J. Hazard. Mater. 146 (2007) 617-623.

[218] J.Q. Jiang, Z. Zhou, V. Sharma, Occurrence, transportation, monitoring and treatment of emerging micro-pollutants in waste water—a review from global views, Microchem. J. 110 (2013) 292-300.

[219] H. Roth, Y. Gendel, P. Buzatu, O. David, M. Wessling, Tubular carbon nanotube-based gas diffusion electrode removes persistent organic pollutants by a cyclic adsorption–electro-Fenton process, J. Hazard. Mater. 307 (2016) 1-6.

[220] E. Isarain-Chávez, R.M. Rodríguez, P.L. Cabot, F. Centellas, C. Arias, J.A. Garrido, E. Brillas, Degradation of pharmaceutical beta-blockers by electrochemical advanced oxidation processes using a flow plant with a solar compound parabolic collector, Water Res. 45 (2011) 4119-4130.

[221] B. Ohtani, Photocatalysis A to Z—What we know and what we do not know in a scientific sense, J. Photochem. Photobiol. C: Photochem. Rev. 11 (2010) 157-178.

[222] E.S. Elmolla, M. Chaudhuri, Photocatalytic degradation of amoxicillin, ampicillin and cloxacillin antibiotics in aqueous solution using UV/TiO_2 and UV/H_2O_2/TiO_2 photocatalysis, Desalination 252 (2010) 46-52.

[223] L. Prieto-Rodríguez, I. Oller, N. Klamerth, A. Agüera, E. Rodríguez, S. Malato, Application of solar AOPs and ozonation for elimination of micropollutants in municipal wastewater treatment plant effluents, Water Res. 47 (2013) 1521-1528.

[224] T. Yonar, G.E. Ustun, S.K.A. Solmaz, Treatment of 3-indole butyric acid with solar photo-catalytic reactor, Desalin. Water Treat. 48 (2012) 82-88.

[225] N. Miranda-García, S. Suárez, B. Sánchez, J. Coronado, S. Malato, M.I. Maldonado, Photocatalytic degradation of emerging contaminants in municipal wastewater treatment plant effluents using immobilized TiO_2 in a solar pilot plant, Appl. Catal. B: Environ. 103 (2011) 294-301.

[226] M. Panizza, G. Cerisola, Direct and mediated anodic oxidation of organic pollutants, Chem. Rev. 109 (2009) 6541-6569.

[227] C.C. Jara, D. Fino, V. Specchia, G. Saracco, P. Spinelli, Electrochemical removal of antibiotics from wastewaters, Appl. Catal. B: Environ. 70 (2007) 479-487.

[228] J.R. Domínguez, T. González, P. Palo, J. Sánchez-Martín, Anodic oxidation of ketoprofen on boron-doped diamond (BDD) electrodes. Role of operative parameters, Chem. Eng. J. 162 (2010) 1012-1018.

[229] R.P. Suri, M. Nayak, U. Devaiah, E. Helmig, Ultrasound assisted destruction of estrogen hormones in aqueous solution: effect of power density, power intensity and reactor configuration, J. Hazard. Mater. 146 (2007) 472-478.

[230] H. Andersen, H. Siegrist, B. Halling-Sørensen, T.A. Ternes, Fate of estrogens in a municipal sewage treatment plant, Environ. Sci. Technol. 37 (2003) 4021-4026.

[231] V. Naddeo, M. Landi, D. Scannapieco, V. Belgiorno, Sonochemical degradation of twenty-three emerging contaminants in urban wastewater, Desalin. Water Treat. 51 (2013) 6601-6608.

[232] J. Radjenović, M. Petrović, F. Ventura, D. Barceló, Rejection of pharmaceuticals in nanofiltration and reverse osmosis membrane drinking water treatment, Water Res. 42 (2008) 3601-3610.

[233] K.J. Choi, H.J. Son, S.H. Kim, Ionic treatment for removal of sulfonamide and tetracycline classes of antibiotic, Sci. Total Environ. 387 (2007) 247-256.

[234] C. Dickert, Ion exchange, Kirk-Othmer Encyclopedia of Chemical Technology (2000).

[235] G.E. Üstün, S.K.A. Solmaz, A. Birgül, Regeneration of industrial district wastewater using a combination of Fenton process and ion exchange—A case study, Resour. Conservation Recycling 52 (2007) 425-440.

[236] H. Tekin, O. Bilkay, S.S. Ataberk, T.H. Balta, I.H. Ceribasi, F.D. Sanin, F.B. Dilek, U. Yetis, Use of Fenton oxidation to improve the biodegradability of a pharmaceutical wastewater, J. Hazard. Mater. 136 (2006) 258-265.

[237] D.M. Ruthven, Fundamentals of adsorption equilibrium and kinetics in microporous solids, Adsorption and Diffusion, Springer, 2006, 1-43.

[238] E.K. Putra, R. Pranowo, J. Sunarso, N. Indraswati, S. Ismadji, Performance of activated carbon and bentonite for adsorption of amoxicillin from wastewater: Mechanisms, isotherms and kinetics, Water Res. 43 (2009) 2419-2430.

[239] A. Xie, J. Dai, X. Chen, T. Zou, J. He, Z. Chang, C. Li, Y. Yan, Hollow imprinted polymer nanorods with a tunable shell using halloysite nanotubes as a sacrificial template for selective recognition and separation of chloramphenicol, RSC Adv. 6 (2016) 51014-51023.

[240] F. Yu, Y. Li, S. Han, J. Ma, Adsorptive removal of antibiotics from aqueous solution using carbon materials, Chemosphere 153 (2016) 365-385.

[241] M.R. Azhar, H.R. Abid, H. Sun, V. Periasamy, M.O. Tadé, S. Wang, Excellent performance of copper based metal organic framework in adsorptive removal of toxic sulfonamide antibiotics from wastewater, J. Colloid Interface Sci. 478 (2016) 344-352.

[242] D.M. Pavlović, L. Ćurković, D. Blažek, J. Župan, The sorption of sulfamethazine on soil samples: Isotherms and error analysis, Sci. Total Environ. 497 (2014) 543-552.

[243] A. Veksha, H. McLaughlin, D.B. Layzell, J.M. Hill, Pyrolysis of wood to biochar: Increasing yield while maintaining microporosity, Bioresour. Technol. 153 (2014) 173-179.

[244] M.B. Ahmed, J.L. Zhou, H.H. Ngo, W. Guo, M.A.H. Johir, K. Sornalingam, Single and competitive sorption properties and mechanism of functionalized biochar for removing sulfonamide antibiotics from water, Chem. Eng. J. 311 (2017) 348-358.

[245] Y. Yao, B. Gao, H. Chen, L. Jiang, M. Inyang, A.R. Zimmerman, X. Cao, L. Yang, Y. Xue, H. Li, Adsorption of sulfamethoxazole on biochar and its impact on reclaimed water irrigation, J. Hazard. Mater. 209 (2012) 408-413.

[246] F. Lian, B. Sun, Z. Song, L. Zhu, X. Qi, B. Xing, Physicochemical properties of herb-residue biochar and its sorption to ionizable antibiotic sulfamethoxazole, Chem. Eng. J. 248 (2014) 128-134.

[247] F. Wang, X. Ren, H. Sun, L. Ma, H. Zhu, J. Xu, Sorption of polychlorinated biphenyls onto biochars derived from corn straw and the effect of propranolol, Bioresour. Technol. 219 (2016) 458-465.

[248] C. Stoquart, P. Servais, P.R. Bérubé, B. Barbeau, Hybrid membrane processes using activated carbon treatment for drinking water: a review, J. Membrane Sci. 411 (2012) 1-12.

[249] C. Ávila, J.M. Bayona, I. Martín, J.J. Salas, J. García, Emerging organic contaminant removal in a full-scale hybrid constructed wetland system for wastewater treatment and reuse, Ecol. Eng. 80 (2015) 108-116.

[250] M.F.N. Secondes, V. Naddeo, V. Belgiorno, F. Ballesteros Jr, Removal of emerging contaminants by simultaneous application of membrane ultrafiltration, activated carbon adsorption, and ultrasound irradiation, J. Hazard. Mater. 264 (2014) 342-349.

[251] M. Ibáñez, E. Gracia-Lor, L. Bijlsma, E. Morales, L. Pastor, F. Hernández, Removal of emerging contaminants in sewage water subjected to advanced oxidation with ozone, J. Hazard. Mater. 260 (2013) 389-398.

[252] W. Czekała, K. Malińska, R. Cáceres, D. Janczak, J. Dach, A. Lewicki, Co-composting of poultry manure mixtures amended with biochar–The effect of biochar on temperature and C-CO_2 emission, Bioresour. Technol. 200 (2016) 921-927.

[253] D. Klinar, Universal model of slow pyrolysis technology producing biochar and heat from standard biomass needed for the techno-economic assessment, Bioresour. Technol. 206 (2016) 112-120.

[254] M. Kwiatkowski, Application of fast multivariant identification technique of adsorption systems to analyze influence of production process conditions on obtained microporous structure parameters of carbonaceous adsorbents, Micropor. Mesopor. Mater. 115 (2008) 314-331.

[255] Y. Ma, W.J. Liu, N. Zhang, Y.S. Li, H. Jiang, G.P. Sheng, Polyethylenimine modified biochar adsorbent for hexavalent chromium removal from the aqueous solution, Bioresour. Technol. 169 (2014) 403-408.

[256] D.H.K. Reddy, S.M. Lee, Magnetic biochar composite: facile synthesis, characterization, and application for heavy metal removal, Colloid Surf. A: Physicochem. Eng. Aspect. 454 (2014) 96-103.

[257] C. Gan, Y. Liu, X. Tan, S. Wang, G. Zeng, B. Zheng, T. Li, Z. Jiang, W. Liu, Effect of porous zinc–biochar nanocomposites on Cr (vi) adsorption from aqueous solution, RSC Adv. 5 (2015) 35107-35115.

[258] J.J. Pan, J. Jiang, W. Qian, R.K. Xu, Arsenate adsorption from aqueous solution onto Fe (III)-modified crop straw biochars, Environ. Eng. Sci. 32 (2015) 922-929.

[259] S. Wang, B. Gao, Y. Li, A. Mosa, A.R. Zimmerman, L.Q. Ma, W.G. Harris, K.W. Migliaccio, Manganese oxide-modified biochars: preparation, characterization, and sorption of arsenate and lead, Bioresour. Technol. 181 (2015) 13-17.

[260] Y. Xue, B. Gao, Y. Yao, M. Inyang, M. Zhang, A.R. Zimmerman, K.S. Ro, Hydrogen peroxide modification enhances the ability of biochar (hydrochar) produced from hydrothermal carbonization of peanut hull to remove aqueous heavy metals: batch and column tests, Chem. Eng. J. 200 (2012) 673-680.

[261] G.X. Yang, H. Jiang, Amino modification of biochar for enhanced adsorption of copper ions from synthetic wastewater, Water Res. 48 (2014) 396-405.

[262] X. Tan, Y. Liu, G. Zeng, X. Wang, X. Hu, Y. Gu, Z. Yang, Application of biochar for the removal of pollutants from aqueous solutions, Chemosphere 125 (2015) 70-85.

[263] Y. Wu, P. Zhang, H. Zhang, G. Zeng, J. Liu, J. Ye, W. Fang, X. Gou, Possibility of sludge conditioning and dewatering with rice husk biochar modified by ferric chloride, Bioresour. Technol. 205 (2016) 258-263.

[264] M. Irfan, Q. Chen, Y. Yue, R. Pang, Q. Lin, X. Zhao, H. Chen, Co-production of biochar, bio-oil and syngas from halophyte grass (Achnatherum splendens L.) under three different pyrolysis temperatures, Bioresour. Technol. 211 (2016) 457-463.

[265] M. Zhang, B. Gao, S. Varnoosfaderani, A. Hebard, Y. Yao, M. Inyang, Preparation and characterization of a novel magnetic biochar for arsenic removal, Bioresour. Technol. 130 (2013) 457-462.

[266] J. Lee, J. Kim, T. Hyeon, Recent progress in the synthesis of porous carbon materials, Adv. Mater. 18 (2006) 2073-2094.

[267] W. Shen, Z. Li, Y. Liu, Surface chemical functional groups modification of porous carbon, Recent Patents Chem. Eng. 1 (2008) 27-40.

[268] D. Mohan, A. Sarswat, Y.S. Ok, C.U. Pittman Jr, Organic and inorganic contaminants removal from water with biochar, a renewable, low cost and sustainable adsorbent–a critical review, Bioresour. Technol. 160 (2014) 191-202.

[269] A.E. Creamer, B. Gao, S. Wang, Carbon dioxide capture using various metal oxyhydroxide–biochar composites, Chem. Eng. J. 283 (2016) 826-832.

[270] M. Jia, F. Wang, X. Jin, Y. Song, Y. Bian, L.A. Boughner, X. Yang, C. Gu, X. Jiang, Q. Zhao, Metal ion–oxytetracycline interactions on maize straw biochar pyrolyzed at different temperatures, Chem. Eng. J. 304 (2016) 934-940.

[271] X.R. Jing, Y.Y. Wang, W.J. Liu, Y.K. Wang, H. Jiang, Enhanced adsorption performance of tetracycline in aqueous solutions by methanol-modified biochar, Chem. Eng. J. 248 (2014) 168-174.

[272] K.K. Shimabuku, J.P. Kearns, J.E. Martinez, R.B. Mahoney, L. Moreno-Vasquez, R.S. Summers, Biochar sorbents for sulfamethoxazole removal from surface water, stormwater, and wastewater effluent, Water Res. 96 (2016) 236-245.

[273] H. Zheng, Z. Wang, J. Zhao, S. Herbert, B. Xing, Sorption of antibiotic sulfamethoxazole varies with biochars produced at different temperatures, Environ. Pollut. 181 (2013) 60-67.

[274] L. Ji, W. Chen, S. Zheng, Z. Xu, D. Zhu, Adsorption of sulfonamide antibiotics to multiwalled carbon nanotubes, Langmuir 25 (2009) 11608-11613.

[275] L. Ji, Y. Wan, S. Zheng, D. Zhu, Adsorption of tetracycline and sulfamethoxazole on crop residue-derived ashes: implication for the relative importance of black carbon to soil sorption, Environ. Sci. Technol. 45 (2011) 5580-5586.

[276] S. Teixeira, C. Delerue-Matos, L. Santos, Removal of sulfamethoxazole from solution by raw and chemically treated walnut shells, Environ. Sci. Pollut. Res. 19 (2012) 3096-3106.

[277] I. Dror, O.M. Jacov, A. Cortis, B. Berkowitz, Catalytic transformation of persistent contaminants using a new composite material based on nanosized zero-valent iron, ACS Appl. Mater. Interface 4 (2012) 3416-3423.

[278] J. Xu, X. Liu, G.V. Lowry, Z. Cao, H. Zhao, J.L. Zhou, X. Xu, Dechlorination mechanism of 2, 4-dichlorophenol by magnetic MWCNTs supported Pd/Fe nanohybrids: rapid adsorption, gradual dechlorination, and desorption of phenol, ACS Appl. Mater. Interface 8 (2016) 7333-7342.

[279] Y.P. Sun, X.Q. Li, J. Cao, W.X. Zhang, H.P. Wang, Characterization of zero-valent iron nanoparticles, Adv. Colloid Interface Sci. 120 (2006) 47-56.

[280] F. Fu, D.D. Dionysiou, H. Liu, The use of zero-valent iron for groundwater remediation and wastewater treatment: a review, J. Hazard. Mater. 267 (2014) 194-205.

[281] H. Khalil, D. Mahajan, M. Rafailovich, M. Gelfer, K. Pandya, Synthesis of zerovalent nanophase metal particles stabilized with poly (ethylene glycol), Langmuir 20 (2004) 6896-6903.

[282] M. Liu, Y. Wang, L. Chen, Y. Zhang, Z. Lin, $Mg(OH)_2$ supported nanoscale zero valent iron enhancing the removal of Pb (II) from aqueous solution, ACS Appl. Mater. Interface. 7 (2015) 7961-7969.

[283] H. Sun, G. Zhou, S. Liu, H.M. Ang, M.O. Tadé, S. Wang, Nano-Fe^0 encapsulated in microcarbon spheres: synthesis, characterization, and environmental applications, ACS Appl. Mater. Interface. 4 (2012) 6235-6241.

[284] S. Xia, Z. Gu, Z. Zhang, J. Zhang, S.W. Hermanowicz, Removal of chloramphenicol from aqueous solution by nanoscale zero-valent iron particles, Chem. Eng. J. 257 (2014) 98-104.

[285] W. Chu, S. Ding, T. Bond, N. Gao, D. Yin, B. Xu, Z. Cao, Zero valent iron produces dichloroacetamide from chloramphenicol antibiotics in the absence of chlorine and chloramines, Water Res. 104 (2016) 254-261.

[286] Y. Zou, X. Wang, A. Khan, P. Wang, Y. Liu, A. Alsaedi, T. Hayat, X. Wang, Environmental remediation and application of nanoscale zero-valent iron and its composites for the removal of heavy metal ions: a review, Environ. Sci. Technol. 50 (2016) 7290-7304.

[287] S. Wang, B. Gao, Y. Li, A.E. Creamer, F. He, Adsorptive removal of arsenate from aqueous solutions by biochar supported zero-valent iron nanocomposite: batch and continuous flow tests, J. Hazard. Mater. 322 (2017) 172-181.

[288] J. Xiao, B. Gao, Q. Yue, Y. Sun, J. Kong, Y. Gao, Q. Li, Characterization of nanoscale zero-valent iron supported on granular activated carbon and its application in removal of acrylonitrile from aqueous solution, J. Taiwan Inst. Chem. Eng. 55 (2015) 152-158.

[289] J. Xiao, B. Gao, Q. Yue, Y. Gao, Q. Li, Removal of trihalomethanes from reclaimed-water by original and modified nanoscale zero-valent iron: characterization, kinetics and mechanism, Chem. Eng. J. 262 (2015) 1226-1236.

[290] G. Sheng, A. Alsaedi, W. Shammakh, S. Monaquel, J. Sheng, X. Wang, H. Li, Y. Huang, Enhanced sequestration of selenite in water by nanoscale zero valent iron immobilization on carbon nanotubes by a combined batch, XPS and XAFS investigation, Carbon 99 (2016) 123-130.

[291] Ç. Üzüm, T. Shahwan, A.E. Eroğlu, K.R. Hallam, T.B. Scott, I. Lieberwirth, Synthesis and characterization of kaolinite-supported zero-valent iron nanoparticles and their application for the removal of aqueous Cu^{2+} and Co^{2+} ions, Appl. Clay Sci. 43 (2009) 172-181.

[292] S.A. Kim, S. Kamala-Kannan, K.J. Lee, Y.-J. Park, P.J. Shea, W.H. Lee, H.M. Kim, B.-T. Oh, Removal of Pb (II) from aqueous solution by a zeolite–nanoscale zero-valent iron composite, Chem. Eng. J. 217 (2013) 54-60.

[293] S. Bhowmick, S. Chakraborty, P. Mondal, W. Van Renterghem, S. Van den Berghe, G. Roman-Ross, D. Chatterjee, M. Iglesias, Montmorillonite-supported nanoscale zero-valent iron for removal of arsenic from aqueous solution: Kinetics and mechanism, Chem. Eng. J. 243 (2014) 14-23.

[294] N. Yuan, G. Zhang, S. Guo, Z. Wan, Enhanced ultrasound-assisted degradation of methyl orange and metronidazole by rectorite-supported nanoscale zero-valent iron, Ultrason. Sonochem. 28 (2016) 62-68.

[295] Z.X. Chen, X.Y. Jin, Z. Chen, M. Megharaj, R. Naidu, Removal of methyl orange from aqueous solution using bentonite-supported nanoscale zero-valent iron, J. Colloid Interface Sci. 363 (2011) 601-607.

[296] Y. Li, W. Cheng, G. Sheng, J. Li, H. Dong, Y. Chen, L. Zhu, Synergetic effect of a pillared bentonite support on SE (VI) removal by nanoscale zero valent iron, Appl. Catal. B: Environ. 174 (2015) 329-335.

[297] J. Fatisson, S. Ghoshal, N. Tufenkji, Deposition of carboxymethylcellulose-coated zero-valent iron nanoparticles onto silica: roles of solution chemistry and organic molecules, Langmuir 26 (2010) 12832-12840.

[298] P. Liao, Z. Zhan, J. Dai, X. Wu, W. Zhang, K. Wang, S. Yuan, Adsorption of tetracycline and chloramphenicol in aqueous solutions by bamboo charcoal: a batch and fixed-bed column study, Chem. Eng. J. 228 (2013) 496-505.

[299] W. Guo, M. Geng, H. Song, J. Sun, Removal of chloramphenicol and simultaneous electricity generation by using microbial fuel cell technology, Int. J. Electrochem. Sci 11 (2016) 5128-5139.

[300] D. Wu, Y. Chen, Z. Zhang, Y. Feng, Y. Liu, J. Fan, Y. Zhang, Enhanced oxidation of chloramphenicol by GLDA-driven pyrite induced heterogeneous Fenton-like reactions at alkaline condition, Chem. Eng. J. 294 (2016) 49-57.

[301] G. Lofrano, G. Libralato, R. Adinolfi, A. Siciliano, P. Iannece, M. Guida, M. Giugni, A.V. Ghirardini, M. Carotenuto, Photocatalytic degradation of the antibiotic chloramphenicol and effluent toxicity effects, Ecotoxicol. Environ. Safety 123 (2016) 65-71.

[302] M.B. Ahmed, J.L. Zhou, H.H. Ngo, W. Guo, M.A. Johir, K. Sornalingam, D. Belhaj, M. Kallel, Nano-Fe^0 immobilized onto functionalized biochar gaining excellent stability during sorption and reduction of chloramphenicol via transforming to reusable magnetic composite, Chem. Eng. J. 322 (2017) 571-581.

[303] M. Seifrtová, L. Nováková, C. Lino, A. Pena, P. Solich, An overview of analytical methodologies for the determination of antibiotics in environmental waters, Anal. Chimica Acta 649 (2009) 158-179.

[304] Y. Li, X. Wu, Z. Li, S. Zhong, W. Wang, A. Wang, J. Chen, Fabrication of CoFe2O4–graphene nanocomposite and its application in the magnetic solid phase extraction of sulfonamides from milk samples, Talanta 144 (2015) 1279-1286.

[305] S. Wan, Z. Hua, L. Sun, X. Bai, L. Liang, Biosorption of nitroimidazole antibiotics onto chemically modified porous biochar prepared by experimental design: Kinetics, thermodynamics, and equilibrium analysis, Process Safety Environ. Protection 104 (2016) 422-435.

[306] J.-D. Mao, R. Johnson, J. Lehmann, D. Olk, E.G. Neves, M. Thompson, K. Schmidt-Rohr, Abundant and stable char residues in soils: implications for soil fertility and carbon sequestration, Environ. Sci. Technol. 46 (2012) 9571-9576.

[307] M. Xie, W. Chen, Z. Xu, S. Zheng, D. Zhu, Adsorption of sulfonamides to demineralized pine wood biochars prepared under different thermochemical conditions, Environ. Pollut. 186 (2014) 187-194.

[308] S. Fukahori, T. Fujiwara, R. Ito, N. Funamizu, pH-dependent adsorption of sulfa drugs on high silica zeolite: modeling and kinetic study, Desalination 275 (2011) 237-242.

[309] Z. Pei, S. Yang, L. Li, C. Li, S. Zhang, X.Q. Shan, B. Wen, B. Guo, Effects of copper and aluminum on the adsorption of sulfathiazole and tylosin on peat and soil, Environ. Pollut. 184 (2014) 579-585.

[310] H. Zhao, X. Liu, Z. Cao, Y. Zhan, X. Shi, Y. Yang, J. Zhou, J. Xu, Adsorption behavior and mechanism of chloramphenicols, sulfonamides, and non-antibiotic pharmaceuticals on multi-walled carbon nanotubes, J. Hazard. Mater. 310 (2016) 235-245.

[311] F. Wang, W. Sun, W. Pan, N. Xu, Adsorption of sulfamethoxazole and 17β-estradiol by carbon nanotubes/CoFe2O4 composites, Chem. Eng. J. 274 (2015) 17-29.

[312] B. Sun, F. Lian, Q. Bao, Z. Liu, Z. Song, L. Zhu, Impact of low molecular weight organic acids (LMWOAs) on biochar micropores and sorption properties for sulfamethoxazole, Environ. Pollut. 214 (2016) 142-148.

[313] M.K. Richter, M. Sander, M. Krauss, I. Christl, M.G. Dahinden, M.K. Schneider, R.P. Schwarzenbach, Cation binding of antimicrobial sulfathiazole to leonardite humic acid, Environ. Sci. Technol. 43 (2009) 6632-6638.

[314] M. Kahle, C. Stamm, Time and pH-dependent sorption of the veterinary antimicrobial sulfathiazole to clay minerals and ferrihydrite, Chemosphere 68 (2007) 1224-1231.

[315] X. Zhang, W. Guo, H.H. Ngo, H. Wen, N. Li, W. Wu, Performance evaluation of powdered activated carbon for removing 28 types of antibiotics from water, J. Environ. Manage. 172 (2016) 193-200.

[316] W. Chen, L. Duan, L. Wang, D. Zhu, Adsorption of hydroxyl-and amino-substituted aromatics to carbon nanotubes, Environ. Sci. Technol. 42 (2008) 6862-6868.

[317] S. Zhang, Z. Min, H.L. Tay, M. Asadullah, C.Z. Li, Effects of volatile–char interactions on the evolution of char structure during the gasification of Victorian brown coal in steam, Fuel 90 (2011) 1529-1535.

[318] H. Wijnja, J.J. Pignatello, K. Malekani, Formation of π–π complexes between phenanthrene and model π-acceptor humic subunits, J. Environ. Qual. 33 (2004) 265-275.

[319] D. Zhang, B. Pan, H. Zhang, P. Ning, B. Xing, Contribution of different sulfamethoxazole species to their overall adsorption on functionalized carbon nanotubes, Environ. Sci. Technol. 44 (2010) 3806-3811.

[320] J. Ni, J.J. Pignatello, B. Xing, Adsorption of aromatic carboxylate ions to black carbon (biochar) is accompanied by proton exchange with water, Environ. Sci. Technol. 45 (2011) 9240-9248.

[321] P. Gilli, L. Pretto, V. Bertolasi, G. Gilli, Predicting Hydrogen-Bond Strengths from Acid− Base Molecular Properties. The p K a Slide Rule: Toward the Solution of a Long-Lasting Problem, Accounts Chem. Res. 42 (2008) 33-44.

[322] F. Yang, L. Zhao, B. Gao, X. Xu, X. Cao, The Interfacial Behavior between Biochar and Soil Minerals and Its Effect on Biochar Stability, Environ. Sci. Technol. 50 (2016) 2264-2271.

[323] J. Lehmann, S. Joseph, Biochar for environmental management: science, technology and implementation, Routledge, 2015.

[324] I.T. Carvalho, L. Santos, Antibiotics in the aquatic environments: a review of the European scenario, Environ. Int. 94 (2016) 736-757.

[325] E. Cui, Y. Wu, Y. Zuo, H. Chen, Effect of different biochars on antibiotic resistance genes and bacterial community during chicken manure composting, Bioresour. Technol. 203 (2016) 11-17.

[326] A.U. Rajapaksha, M. Vithanage, M. Zhang, M. Ahmad, D. Mohan, S.X. Chang, Y.S. Ok, Pyrolysis condition affected sulfamethazine sorption by tea waste biochars, Bioresour. Technol. 166 (2014) 303-308.

[327] B. Wang, Y.S. Jiang, F.Y. Li, D.Y. Yang, Preparation of biochar by simultaneous carbonization, magnetization and activation for norfloxacin removal in water, Bioresour. Technol. 233 (2017) 159-165.

[328] V. Calisto, G. Jaria, C.P. Silva, C.I. Ferreira, M. Otero, V.I. Esteves, Single and multi-component adsorption of psychiatric pharmaceuticals onto alternative and commercial carbons, J. Environ. Manage. 192 (2017) 15-24.

[329] L. Nielsen, T.J. Bandosz, Analysis of the competitive adsorption of pharmaceuticals on waste derived materials, Chem. Eng. J. 287 (2016) 139-147.

[330] P. Devi, A.K. Saroha, Synthesis of the magnetic biochar composites for use as an adsorbent for the removal of pentachlorophenol from the effluent, Bioresour. Technol. 169 (2014) 525-531.

[331] D. Chen, X. Yu, C. Song, X. Pang, J. Huang, Y. Li, Effect of pyrolysis temperature on the chemical oxidation stability of bamboo biochar, Bioresour. Technol. 218 (2016) 1303-1306.

[332] J. Tang, H. Lv, Y. Gong, Y. Huang, Preparation and characterization of a novel graphene/biochar composite for aqueous phenanthrene and mercury removal, Bioresour. Technol. 196 (2015) 355-363.

[333] Z. Zhu, J. Xie, M. Zhang, Q. Zhou, F. Liu, Insight into the adsorption of PPCPs by porous adsorbents: Effect of the properties of adsorbents and adsorbates, Environ. Pollut. 214 (2016) 524-531.

[334] L. Qin, Z. Zhou, J. Dai, P. Ma, H. Zhao, J. He, A. Xie, C. Li, Y. Yan, Novel N-doped hierarchically porous carbons derived from sustainable shrimp shell for high-performance removal of sulfamethazine and chloramphenicol, J. Taiwan Inst. Chem. Eng. 62 (2016) 228-238.

[335] J. Dai, J. He, A. Xie, L. Gao, J. Pan, X. Chen, Z. Zhou, X. Wei, Y. Yan, Novel pitaya-inspired well-defined core–shell nanospheres with ultrathin surface imprinted nanofilm from magnetic mesoporous nanosilica for highly efficient chloramphenicol removal, Chem. Eng. J. 284 (2016) 812-822.

[336] J. Chen, D. Zhang, H. Zhang, S. Ghosh, B. Pan, Fast and slow adsorption of carbamazepine on biochar as affected by carbon structure and mineral composition, Sci. Total Environ. 579 (2017) 598-605.

[337] Z. Dai, X. Zhang, C. Tang, N. Muhammad, J. Wu, P.C. Brookes, J. Xu, Potential role of biochars in decreasing soil acidification-A critical review, Sci. Total Environ. 581 (2017) 601-611.

[338] O. Das, A.K. Sarmah, The love–hate relationship of pyrolysis biochar and water: a perspective, Sci. Total Environ. 512 (2015) 682-685.

[339] A. Mandal, N. Singh, T. Purakayastha, Characterization of pesticide sorption behaviour of slow pyrolysis biochars as low cost adsorbent for atrazine and imidacloprid removal, Sci. Total Environ. 577 (2017) 376-385.

[340] G. Sorrenti, C.A. Masiello, B. Dugan, M. Toselli, Biochar physico-chemical properties as affected by environmental exposure, Sci. Total Environ. 563 (2016) 237-246.

[341] W. Suliman, J.B. Harsh, N.I. Abu-Lail, A.-M. Fortuna, I. Dallmeyer, M. Garcia-Pérez, The role of biochar porosity and surface functionality in augmenting hydrologic properties of a sandy soil, Sci. Total Environ. 574 (2017) 139-147.

[342] L. Ji, W. Chen, L. Duan, D. Zhu, Mechanisms for strong adsorption of tetracycline to carbon nanotubes: a comparative study using activated carbon and graphite as adsorbents, Environ. Sci. Technol. 43 (2009) 2322-2327.

[343] M. Taheran, M. Naghdi, S. Brar, E. Knystautas, M. Verma, A. Ramirez, R. Surampalli, J. Valero, Adsorption study of environmentally relevant concentrations of chlortetracycline on pinewood biochar, Sci. Total Environ. 571 (2016) 772-777.

[344] B. Peng, L. Chen, C. Que, K. Yang, F. Deng, X. Deng, G. Shi, G. Xu, M. Wu, Adsorption of Antibiotics on Graphene and Biochar in Aqueous Solutions Induced by π-π Interactions, Sci. Report. 6 (2016).

[345] J.J. Pignatello, S. Kwon, Y. Lu, Effect of natural organic substances on the surface and adsorptive properties of environmental black carbon (char): attenuation of surface activity by humic and fulvic acids, Environ. Sci. Technol. 40 (2006) 7757-7763.

[346] M. Zhang, L. Shu, X. Guo, X. Shen, H. Zhang, G. Shen, B. Wang, Y. Yang, S. Tao, X. Wang, Impact of humic acid coating on sorption of naphthalene by biochars, Carbon 94 (2015) 946-954.

[347] F. Zhou, H. Wang, W. Zhang, R. Qiu, Pb (II), Cr (VI) and atrazine sorption behavior on sludge-derived biochar: role of humic acids, Environ. Sci. Pollut. Res. 22 (2015) 16031-16039.

[348] S. Park, K.-S. Lee, G. Bozoklu, W. Cai, S.T. Nguyen, R.S. Ruoff, Graphene oxide papers modified by divalent ions—enhancing mechanical properties via chemical cross-linking, ACS Nano 2 (2008) 572-578.

[349] G. Cornelissen, Ö. Gustafsson, Importance of unburned coal carbon, black carbon, and amorphous organic carbon to phenanthrene sorption in sediments, Environ. Sci. Technol. 39 (2005) 764-769.

[350] D. Zhu, S. Hyun, J.J. Pignatello, L.S. Lee, Evidence for π− π electron donor−acceptor interactions between π-donor aromatic compounds and π-acceptor sites in soil organic matter through pH effects on sorption, Environ. Sci. Technol. 38 (2004) 4361-4368.

[351] B. Pan, B. Xing, Adsorption mechanisms of organic chemicals on carbon nanotubes, Environ. Sci. Technol. 42 (2008) 9005-9013.

[352] X. Ma, S. Agarwal, Adsorption of emerging ionizable contaminants on carbon nanotubes: advancements and challenges, Molecules 21 (2016) 628.

[353] M. Sander, J.J. Pignatello, Characterization of charcoal adsorption sites for aromatic compounds: insights drawn from single-solute and bi-solute competitive experiments, Environ. Sci. Technol. 39 (2005) 1606-1615.

[354] M. Keiluweit, M. Kleber, Molecular-level interactions in soils and sediments: the role of aromatic π-systems, Environ. Sci. Technol. 43 (2009) 3421-3429.

[355] C. Lattao, X. Cao, J. Mao, K. Schmidt-Rohr, J.J. Pignatello, Influence of molecular structure and adsorbent properties on sorption of organic compounds to a temperature series of wood chars, Environ. Sci. Technol. 48 (2014) 4790-4798.

[356] D. Zhu, J.J. Pignatello, Characterization of aromatic compound sorptive interactions with black carbon (charcoal) assisted by graphite as a model, Environ. Sci. Technol. 39 (2005) 2033-2041.

[357] T. Higuchi, C.D. Bias, The kinetics of degradation of chloramphenicol in solution: I. A study of the rate of formation of chloride ion in aqueous media, J. Pharmaceut. Sci. 42 (1953) 707-714.

[358] T. Higuchi, A.D. Marcus, The kinetics of degradation of chloramphenicol in solution: III. The nature, specific hydrogen ion catalysis, and temperature dependencies of the degradative reactions, J. Pharmaceut. Sci. 43 (1954) 530-535.

[359] S. Zhang, X. Song, W. Zhang, N. Luo, L. Cai, Determination of low urinary 8-hydroxy-2-deoxyguanosine excretion with capillary electrophoresis and molecularly imprinted monolith solid phase microextraction, Sci. Total Environ. 450 (2013) 266-270.

[360] M. Johir, M. Pradhan, P. Loganathan, J. Kandasamy, S. Vigneswaran, Phosphate adsorption from wastewater using zirconium (IV) hydroxide: kinetics, thermodynamics and membrane filtration adsorption hybrid system studies, J. Environ. Manage. 167 (2016) 167-174.

[361] R. Li, Y. Wang, C. Zhou, C. Wang, X. Ba, Y. Li, X. Huang, J. Liu, Carbon-stabilized high-capacity ferroferric oxide nanorod array for flexible solid-state alkaline battery–supercapacitor hybrid device with high environmental suitability, Adv. Funct. Mater. 25 (2015) 5384-5394.

[362] X. Qiu, Z. Fang, B. Liang, F. Gu, Z. Xu, Degradation of decabromodiphenyl ether by nano zero-valent iron immobilized in mesoporous silica microspheres, J. Hazard. Mater. 193 (2011) 70-81.

[363] Ç. Üzüm, T. Shahwan, A.E. Eroğlu, I. Lieberwirth, T.B. Scott, K.R. Hallam, Application of zero-valent iron nanoparticles for the removal of aqueous Co^{2+} ions under various experimental conditions, Chem. Eng. J. 144 (2008) 213-220.

[364] C.T. Wu, K.M.K. Yu, F. Liao, N. Young, P. Nellist, A. Dent, A. Kroner, S.C.E. Tsang, A non-syn-gas catalytic route to methanol production, Nature Commun. 3 (2012) 1050.

[365] Q. Tian, Q. Wang, Q. Xie, J. Li, Aqueous Solution Preparation, Structure, and Magnetic Properties of Nano-Granular $Zn_xFe_{3-x}O_4$ Ferrite Films, Nanoscale Res. Letter. 5 (2010) 1518.

[366] X. Zhang, Y. Niu, X. Meng, Y. Li, J. Zhao, Structural evolution and characteristics of the phase transformations between α-Fe_2O_3, Fe_3O_4 and γ-Fe_2O_3 nanoparticles under reducing and oxidizing atmospheres, CrystEngComm 15 (2013) 8166-8172.

[367] D. De Faria, S. Venâncio Silva, M. De Oliveira, Raman microspectroscopy of some iron oxides and oxyhydroxides, J. Raman Spectros. 28 (1997) 873-878.

[368] D.K. Padhi, K. Parida, Facile fabrication of α-FeOOH nanorod/RGO composite: a robust photocatalyst for reduction of Cr (VI) under visible light irradiation, J. Mater. Chem. A 2 (2014) 10300-10312.

[369] C. Ban, Z. Wu, D.T. Gillaspie, L. Chen, Y. Yan, J.L. Blackburn, A.C. Dillon, Nanostructured Fe3O4/swnt electrode: binder-free and high-rate li-ion anode, Adv. Mater. 22 (2010).

[370] C. Wang, G. Shao, Z. Ma, S. Liu, W. Song, J. Song, Constructing Fe_3O_4@ N-rich carbon core-shell microspheres as anode for lithium ion batteries with enhanced electrochemical performance, Electrochimica Acta 130 (2014) 679-688.

[371] A. Liu, J. Liu, J. Han, W.X. Zhang, Evolution of nanoscale zero-valent iron (nZVI) in water: microscopic and spectroscopic evidence on the formation of nano-and micro-structured iron oxides, J. Hazard. Mater. 322 (2017) 129-135.

[372] J.A. Mielczarski, G.M. Atenas, E. Mielczarski, Role of iron surface oxidation layers in decomposition of azo-dye water pollutants in weak acidic solutions, Appl. Catal. B: Environ. 56 (2005) 289-303.

[373] B. Liang, H.Y. Cheng, D.Y. Kong, S.-H. Gao, F. Sun, D. Cui, F.Y. Kong, A.J. Zhou, W.Z. Liu, N.Q. Ren, Accelerated reduction of chlorinated nitroaromatic antibiotic chloramphenicol by biocathode, Environ. Sci. Technol. 47 (2013) 5353-5361.

[374] Y.C. Huo, W.W. Li, D. Min, D.D. Wang, H.Q. Liu, Q. Kong, T.C. Lau, R.J. Zeng, Zero-valent iron nanoparticles with sustained high reductive activity for carbon tetrachloride dechlorination, RSC Adv. 5 (2015) 54497-54504.

[375] Y. Li, Q. Du, T. Liu, X. Peng, J. Wang, J. Sun, Y. Wang, S. Wu, Z. Wang, Y. Xia, Comparative study of methylene blue dye adsorption onto activated carbon, graphene oxide, and carbon nanotubes, Chem. Eng. Res. Design 91 (2013) 361-368.

[376] Y. Yao, F. Xu, M. Chen, Z. Xu, Z. Zhu, Adsorption behavior of methylene blue on carbon nanotubes, Bioresour. Technol. 101 (2010) 3040-3046.

[377] T. Liu, Y. Li, Q. Du, J. Sun, Y. Jiao, G. Yang, Z. Wang, Y. Xia, W. Zhang, K. Wang, Adsorption of methylene blue from aqueous solution by graphene, Colloid Surface. B: Biointerface. 90 (2012) 197-203.

[378] M.B. Ahmed, J.L. Zhou, H.H. Ngo, W. Guo, M.A.H. Johir, D. Belhaj, Competitive sorption affinity of sulfonamides and chloramphenicol antibiotics toward functionalized biochar for water and wastewater treatment, Bioresour. Technol. 238 (2017) 306-312.

[379] M. Khalfaoui, S. Knani, M. Hachicha, A.B. Lamine, New theoretical expressions for the five adsorption type isotherms classified by BET based on statistical physics treatment, J. Colloid Interface Sci. 263 (2003) 350-356.

[380] Z.A. ALOthman, A review: fundamental aspects of silicate mesoporous materials, Materials 5 (2012) 2874-2902.

[381] S. Storck, H. Bretinger, W.F. Maier, Characterization of micro-and mesoporous solids by physisorption methods and pore-size analysis, Appl. Catal. A: General 174 (1998) 137-146.

[382] X. Dong, J. Fu, X. Xiong, C. Chen, Preparation of hydrophilic mesoporous carbon and its application in dye adsorption, Mater. Letter. 65 (2011) 2486-2488.

[383] T. Okpalugo, P. Papakonstantinou, H. Murphy, J. McLaughlin, N. Brown, High resolution XPS characterization of chemical functionalised MWCNTs and SWCNTs, Carbon 43 (2005) 153-161.

[384] V. Datsyuk, M. Kalyva, K. Papagelis, J. Parthenios, D. Tasis, A. Siokou, I. Kallitsis, C. Galiotis, Chemical oxidation of multiwalled carbon nanotubes, Carbon 46 (2008) 833-840.

[385] A. Puziy, O. Poddubnaya, R. Socha, J. Gurgul, M. Wisniewski, XPS and NMR studies of phosphoric acid activated carbons, Carbon 46 (2008) 2113-2123.

[386] X. Zhang, B. Gao, A.E. Creamer, C. Cao, Y. Li, Adsorption of VOCs onto engineered carbon materials: A review, J. Hazard. Mater. 338 (2017) 102-123.

[387] F. Xiao, J.J. Pignatello, π^+–π Interactions between (Hetero) aromatic amine cations and the graphitic surfaces of pyrogenic carbonaceous materials, Environ. Sci. Technol. 49 (2015) 906-914.

[388] J. Chen, W. Chen, D. Zhu, Adsorption of nonionic aromatic compounds to single-walled carbon nanotubes: effects of aqueous solution chemistry, Environ. Sci. Technol. 42 (2008) 7225-7230.

[389] M. Tagliavini, F. Engel, P.G. Weidler, T. Scherer, A.I. Schäfer, Adsorption of steroid micropollutants on polymer-based spherical activated carbon (PBSAC), J. Hazard. Mater. 337 (2017) 126-137.

[390] F. Reguyal, A.K. Sarmah, W. Gao, Synthesis of magnetic biochar from pine sawdust via oxidative hydrolysis of $FeCl_2$ for the removal sulfamethoxazole from aqueous solution, J. Hazard. Mater. 321 (2017) 868-878.

[391] D. Shan, S. Deng, T. Zhao, B. Wang, Y. Wang, J. Huang, G. Yu, J. Winglee, M.R. Wiesner, Preparation of ultrafine magnetic biochar and activated carbon for pharmaceutical adsorption and subsequent degradation by ball milling, J. Hazard. Mater. 305 (2016) 156-163.

[392] M.T. Jonker, A.A. Koelmans, Sorption of polycyclic aromatic hydrocarbons and polychlorinated biphenyls to soot and soot-like materials in the aqueous environment: mechanistic considerations, Environ. Sci. Technol. 36 (2002) 3725-3734.

[393] J. Zhou, R. Liu, A. Wilding, A. Hibberd, Sorption of selected endocrine disrupting chemicals to different aquatic colloids, Environ. Sci. Technol. 41 (2007) 206-213.

[394] L. Joseph, Q. Zaib, I.A. Khan, N.D. Berge, Y.G. Park, N.B. Saleh, Y. Yoon, Removal of bisphenol A and 17α-ethinyl estradiol from landfill leachate using single-walled carbon nanotubes, Water Res. 45 (2011) 4056-4068.

[395] C.D. Sherrill, Energy component analysis of π interactions, Account. Chem. Res. 46 (2012) 1020-1028.

[396] M.B. Ahmed, J.L. Zhou, H.H. Ngo, W. Guo, M.A.H. Johir, K. Sornalingam, M.S. Rahman, Chloramphenicol interaction with functionalized biochar in water: sorptive mechanism, molecular imprinting effect and repeatable application, Sci. Total Environ. 609 (2017) 885-895.

[397] A.P. Terzyk, The influence of activated carbon surface chemical composition on the adsorption of acetaminophen (paracetamol) in vitro: Part II. TG, FTIR, and XPS analysis of carbons and the temperature dependence of adsorption kinetics at the neutral pH, Colloid Surface. A: Physicochem. Eng. Aspect. 177 (2001) 23-45.

[398] K. Yang, X. Wang, L. Zhu, B. Xing, Competitive sorption of pyrene, phenanthrene, and naphthalene on multiwalled carbon nanotubes, Environ. Sci. Technol. 40 (2006) 5804-5810.

[399] Z. Yu, W. Huang, Competitive sorption between 17α-ethinyl estradiol and naphthalene/phenanthrene by sediments, Environ. Sci. Technol. 39 (2005) 4878-4885.

[400] K. Yang, B. Xing, Adsorption of organic compounds by carbon nanomaterials in aqueous phase: Polanyi theory and its application, Chem. Rev. 110 (2010) 5989-6008.

[401] H. Peng, D. Zhang, B. Pan, J. Peng, Contribution of hydrophobic effect to the sorption of phenanthrene, 9-phenanthrol and 9, 10-phenanthrenequinone on carbon nanotubes, Chemosphere 168 (2017) 739-747.

[402] J. Pignatello, W.A. Mitch, W. Xu, Activity and reactivity of pyrogenic carbonaceous matter toward organic compounds, Environ. Sci. Technol. 51 (2017) 8893-8908.

[403] K. Balasubramanian, M. Burghard, Chemically functionalized carbon nanotubes, Small 1 (2005) 180-192.

[404] X. Wang, Y. Liu, S. Tao, B. Xing, Relative importance of multiple mechanisms in sorption of organic compounds by multiwalled carbon nanotubes, Carbon 48 (2010) 3721-3728.

[405] Z. Pei, L. Li, L. Sun, S. Zhang, X.Q. Shan, S. Yang, B. Wen, Adsorption characteristics of 1, 2, 4-trichlorobenzene, 2, 4, 6-trichlorophenol, 2-naphthol and naphthalene on graphene and graphene oxide, Carbon 51 (2013) 156-163.